PHYTOCHEMICAL INVESTIGATION AND BIOLOGICAL ACTIVITIES OF GENUS *CORYDALIS*

A THESIS SUBMITTED TO THE

CENTRAL DEPARTMENT OF CHEMISTRY

INSTITUTE OF SCIENCE AND TECHNOLOGY

TRIBHUVAN UNIVERSITY

NEPAL

FOR THE AWARD OF

DOCTOR OF PHILOSOPHY

IN CHEMISTRY

BY

BINITA MAHARJAN

DECEMBER 2024

PHYTOCHEMICAL INVESTIGATION AND BIOLOGICAL ACTIVITIES OF GENUS *CORYDALIS*

A THESIS SUBMITTED TO THE

CENTRAL DEPARTMENT OF CHEMISTRY

INSTITUTE OF SCIENCE AND TECHNOLOGY

TRIBHUVAN UNIVERSITY

NEPAL

FOR THE AWARD OF

DOCTOR OF PHILOSOPHY

IN CHEMISTRY

BY

BINITA MAHARJAN

DECEMBER 2024

TRIBHUVAN UNIVERSITY

Institute of Science and Technology

DEAN'S OFFICE

Kirtipur, Kathmandu, Nepal

Reference No.:

Institute of Science & Technology
Dean's Office
Kirtipur 2045

EXAMINERS

The Title of Ph.D. Thesis: "Phytochemical Investigation and Biological Activities of Genus *Corydalis* "

Name of Candidate: Binita Maharjan

Internal Examiner:

Dr. Achyut Adhikari
Central Department of Chemistry
Tribhuvan University, NEPAL

External Examiners:

(1) Prof. Dr. Rajendra Gyawali
Kathmandu University
Dhulikhel, NEPAL

(2) Prof. Dr. Somobrata Acharya
Indian Association for the Cultivation of Science
Kolkata, INDIA

(3) Dr. Kentaro TASHIRO
National Institute for Materials Science
Tsukuba, JAPAN

31 December, 2024

(Dr. Surendra Kumar Gautam)
Asst. Dean

DECLARATION

Thesis entitled **"Phytochemical investigation and biological activities of genus *Corydalis*"** which is being submitted to the Central Department of Chemistry, Institute of Science and Technology (IOST), Tribhuvan University, Nepal, for the award of the degree of Doctor of Philosophy (Ph.D.), is a research work carried out by me under the supervision of Assoc. Prof. Dr. Ram Lal (Swagat) Shrestha of Department of Chemistry, Amrit Campus, Tribhuvan University and co-supervised by Prof. Dr. Lok Kumar Shrestha, and Dr. Jonathan Patrick Hill of National Institute for Materials Science (NIMS), Japan.

This research is original and has not been submitted earlier in part or whole in this or any other form to any university or institute, here or elsewhere, for the award of any degree.

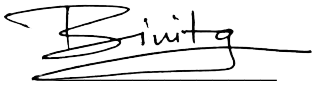

Binita Maharjan

RECOMMENDATION

This is to recommend that **Ms. Binita Maharjan** has carried out research entitled **"Phytochemical investigation and biological activities of genus *Corydalis*"** for the award of Doctor of Philosophy (Ph.D.) in **Chemistry** under our supervision. To our knowledge, this work has not been submitted for any other degree.

She has fulfilled all the requirements laid down by the Institute of Science and Technology (IOST), Tribhuvan University, Kirtipur, for the submission of the thesis for the award of a PhD degree.

Dr. Ram Lal (Swagat) Shrestha
Supervisor
Associate Professor
Department of Chemistry
Amrit Campus, Tribhuvan University
Lainchaur, Kathmandu, Nepal

Prof. Dr. Lok Kumar Shrestha
Co-supervisor
Principal Researcher
Research Center for Materials Nanoarchitectonics (MANA)
National Institute for Materials Science (NIMS)
1-1 Namiki, Tsukuba Ibaraki, Japan

Dr. Jonathan Patrick Hill
Co-supervisor
Group Leader and Chief Researcher
Research Center for Materials Nanoarchitectonics (MANA)
National Institute for Materials Science (NIMS)
1-1 Namiki, Tsukuba Ibaraki, Japan

December 2024

त्रिभुवन विश्वविद्यालय
TRIBHUVAN UNIVERSITY
विज्ञान तथा प्रविधि अध्ययन संस्थान
Institute of Science and Technology
रसायन शास्त्र केन्द्रीय विभाग
CENTRAL DEPARTMENT OF CHEMISTRY
कीर्तिपुर, काठमाडौं, नेपाल
Kirtipur, Kathmandu, NEPAL

पत्र संख्या:
Ref. No.:

LETTER OF APPROVAL

Date: 31st December 2024

On the recommendation of **Assoc. Prof. Dr. Ram Lal (Swagat) Shrestha, Prof. Dr. Lok Kumar Shrestha** and **Dr. Jonathan Patrick Hill**, this PhD thesis submitted by **Ms. Binita Maharjan**, entitled **"Phytochemical investigation and biological activities of genus *Corydalis*"** is forwarded by Central Department Research Committee (CDRC) to the Dean, IOST, T.U.

Dr. Jagadeesh Bhattarai
Professor
Head
Central Department of Chemistry
Tribhuvan University
Kirtipur, Kathmandu, Nepal

Tel.: 977-1-4332034, Fax No.: +977-1-4330537, http://www.cdctu.edu.np e-mail: head@cdc.tu.edu.np

ACKNOWLEDGEMENTS

I am deeply honored and delighted to express my gratitude to my supervisor, **Assoc. Prof. Dr. Ram Lal (Swagat) Shrestha, Department of Chemistry, Amrit Campus, Lainchaur, Kathmandu, Nepal**. His unwavering support and invaluable guidance have been instrumental throughout this research study. Not only did he provide me the opportunity to work under his mentorship, but his continual encouragement and warmth have been a significant source of motivation in my academic journey. I appreciate him and express a heartfelt gratitude.

I would also like to sincerely thank my co-supervisors, **Prof. Dr. Lok Kumar Shrestha** and **Dr. Jonathan Patrick Hill** from NIMS, Japan, for their co-supervision and for providing the necessary laboratory facilities to complete this research. I also appreciate **Dr. Katsuhiko Ariga** and **Dr. Daniel Tony Payne** from NIMS, Japan, for their valuable insights and support. I am incredibly thankful to **Dr. Stefano Dall'Acqua** and **Dr. Stefania Sut** from Padova University for their assistance with laboratory facilities and spectral analysis and to **Dr. Nicola Ferri** and his team for his support in biological activity tests. I would also like to thank **Dr. Jhashanath Subin Adhikari**, for his support in computational studies.

I am also very grateful for valuable encouragement and mentorship of **Prof. Dr. Jagadeesh Bhattarai**, **Head of Central Department of Chemistry, Kirtipur, Kathmandu, Nepal, Prof. Dr. Ram Chandra Basnet, Prof. Dr. Kedar Nath Ghimire, Prof. Dr. Megh Raj Pokhrel, Prof. Dr. Niranjan Parajuli, Assoc. Prof. Dr. Surya Kant Kalauni, Assoc. Prof. Dr. Achyut Adhikari, Dr. Bishnu Marasini, Dr. Shyam Sharan Shrestha** and all others who have supported this work directly or indirectly.

I wish to acknowledge **Prof. Dr. Daman Raj Gautam, Assoc. Prof. Dr. Bhushan Shakya, Assoc. Prof. Shree Dhar Gautam, Asst. Prof. Dr. Deval Prasad Bhattarai,** and all others from **Chemistry Department at Amrit Campus, Lainchour, Kathmandu, Nepal**, for providing the research labs necessary for this study. I also extend my gratitude to the **Research Center for Materials Nanoarchitectonics (MANA), National Institute for Materials Science (NIMS), Tsukuba, Japan** and **Department of Pharmaceutical and Pharmacological Sciences, University of**

Padova, Padova, Italy, for aiding with compound isolation, spectral work and biological activity tests. I extend my gratitude to **Department of Plant Resources, Ministry of Forests and Environment, Government of Nepal, Thapathali, Kathmandu, Nepal, Research Institute for Bioscience and Biotechnology, Chyasal, Lalitpur, Nepal, Himalayan Research Centre, Radhe Radhe, Bhaktapur, Nepal** for bioactivities of extracts. My sincere thanks to the **University Grants Commission** for the **Ph.D. Fellowship and Research Support**.

I am very grateful to **Mr. Ganga Datt Bhatt** from the **National Herbarium and Plant Research Division, Godawari, Lalitpur, Nepal**, for his assistance with plant taxonomy. I sincerely appreciate **Mani Raj Budhathoki, Nanda K. Manandhar,** and my colleagues at Amrit Campus for their continuous encouragement and help.

I reserve the highest respect and gratitude for my beloved parents, **Mr. Bunukaji Maharjan** and **Mrs. Dandevi Maharjan,** who have been my constant source of encouragement and strength. Their unwavering support, sacrifices, and faith in me have been the pillars of my success. I am equally grateful to my brother, **Mr. Dipesh Maharjan,** for his help with lab work and to all my relatives for their love and support.

A special note of appreciation goes to **Mrs. Sangita Shrestha, Principal of Kathmandu Valley School & College, Syuchatar, Kalanki, Kathmandu**, for her encouragement and for providing laboratory facilities. I am also grateful to **Shubhadra Shrestha, Susmita K.C., Dhan Awatar Bal (Sujal Tamang), Top Bahadur Gharti, and Ashmita Gharti** for their assistance with lab and administrative tasks.

I am indebted to **Babita Shrestha** and **Sushila Shrestha** for their continuous support. I give special thanks to my friends **Timila Shrestha** and **Samjhana Bharati**, who supported me throughout this journey for laboratory and other administrative work.

Lastly, I again want to express my profound appreciation and love to all my family, friends, and mentors. Their enduring encouragement and unwavering belief in me supported me through this research and guided me toward a positive and fulfilling life path.

Binita Maharjan

December 2024

शोध सार

नेपालको हिमाली क्षेत्रका उच्च भू-भागमा पाइने वनस्पतिहरू जैविक सक्रिय यौगिकहरूले भरिपूर्ण छन् । यी यौगिकहरूले महत्वपूर्ण औषधीय मूल्य राख्दछन् र परम्परागत रूपमा विभिन्न रोगहरूको उपचारका लागि प्रयोग हुँदै आएका छन् । *Corydalis* प्रजातिले जैविक सक्रियता देखाउनुका साथै यसमा आइसोक्विनोलिन एल्कालोइडहरू प्रचुर मात्रामा पाईन्छन् । नेपालबाट सङ्कलित *Corydalis chaerophylla, C. govaniana* र *C. casimiriana* को नमूनाहरूमा हेक्जेन, मिथानोल, र क्लोरोफर्म जस्ता घोलकको प्रयोग गरी सार तत्वहरु सङ्कलित गरियो । *C. chaerophylla* का हेक्जेन, मिथानोल, र क्लोरोफर्मका एक्सट्राक्टहरूलाई LC-DAD-MS^n विश्लेषण द्वारा १५ विभिन्न प्रकारका एल्कालोइडहरू पहिचान गरियो ।

मिथानोल र क्लोरोफर्म एक्सट्राक्टहरूले चार प्रकारका जीवाणु र एक ढुसी विरुद्ध महत्वपूर्ण गतिविधि देखाए, जसमा क्लोरोफर्म एक्सट्राक्टले उच्च फिनोलिक सामग्री (११३ mg GAE/g) र DPPH Assay मा उत्कृष्ट एन्टिअक्सिडेन्ट क्षमता (IC_{50} २६१.५ µg/mL) देखायो। मिथानोल एक्सट्राक्टले अल्फा-एमाइलेज अवरोध (IC_{50} ५१.५२ µg/mL) र कम विषाक्तता (LC_{50} १९६ µg/mL) देखायो, तर इन भिभो टक्सिसिटी परीक्षणले मिथानोल र क्लोरोफर्मका LD_{50} क्रमशः १०००.३६ र ५१५ mg/kg BW रहेको देखायो।

तीनवटै बिरुवाहरूका क्लोरोफर्म एक्सट्राक्टहरूलाई क्रोमाटोग्राफिक विधिबाट १३ विभिन्न शुद्ध एल्कालोइडहरू अलग गरियो, जसमा *Corydalis chaerophylla* बाट चार नयाँ एल्कालोइडहरू पत्ता लगाइयो । यी नयाँ यौगिकहरूको संरचना 1D र 2D स्पेक्ट्रोस्कोपी र मास स्पेक्ट्रोमेट्री प्रयोग गरी व्याख्या गरियो । यी चार यौगिकहरूको ऊर्जा र बल न्यूनतम आणविक संरचनाहरू B3LYP कार्यात्मक र 6-31G* आधार DFT स्तरमा सेट प्रयोग गरेर क्वान्टम मेकानिकल गणनाहरूबाट प्राप्त गरियो । तिनीहरूलाई क्रमशः Chaeronepaline-A (**१**), Chaeronepaline-B (**२**), Chaeronepaline-

C (३), Chaeronepaline-D (४) नाम दिइयो । यस्तै, *C. chaerophylla* बाट bicuculline (५), corydalmine (६), 8-hydroxydihydrosanguinarine (७), dihydrosanguinarine (८), scoulerine (९) जस्ता ज्ञात यौगिकहरू अलग गरिएको थियो, भने *C. govaniana* बाट govaniadine (१०) अलग गरी पहिचान गरिएको थियो र stylopine (११), adlumine (१२), तथा adlumidine (१३) लाई *C. casimiriana* बाट पहिचान गरिएको थियो ।

Berberine, californidine र govaniadine ले LDLR वृद्धि गर्ने गुण देखायो, जुन Simvastatine को तुलनामा लगभग समान थियो । Californidine र berberine ले PCSK9 को प्रभाव कम गरे, जबकि govaniadine ले स्टाटिन-जस्तै प्रभाव देखायो । नयाँ एल्कालोइडहरू (१-४) लाई Huh7 कोषहरूमा LDLR र PCSK9 को एक्सप्रेशन र कोलेस्ट्रोल बायोसिन्थेसिसमा तिनीहरूको प्रभाव मूल्याङ्कन गर्न परीक्षण गरियो । परिणामले यौगिक २ र ३ ले LDLR वृद्धि गरेको र कोलेस्ट्रोल संश्लेषण रोक्ने प्रतिक्रिया देखियो । यौगिक २ ले PCSK9 को स्राव पनि घटायो, जसले यसलाई सम्भावित हाइपोक्लोलेस्टेरोलिमिक एजेन्टको रूपमा संकेत गऱ्यो । यी निष्कर्षहरूले *Corydalis* एल्कलॉइडहरूको चिकित्सीय सम्भावनालाई प्रकाश पार्छ, जसले थप *in vivo* अनुसन्धानको आवश्यकता देखाउँछ।

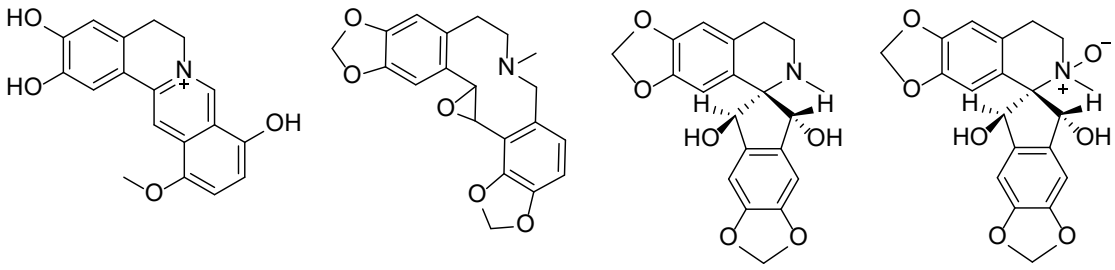

१ २ ३ ४

मुख्य शब्दहरूः *Corydalis - एक्स्ट्याक्सन - जैविक क्रियाकलापहरू - आइसोलेसन - पहिचान - आइसोक्विनोलिन एल्कलॉइडहरू - कोलेस्ट्रोल नियन्त्रण*

ABSTRACT

The Himalayan region in Nepal is home to high-altitude flora known for their rich bioactive compounds. These compounds hold significant medicinal value and have been traditionally used to treat a variety of diseases. Among these, species of the *Corydalis* genus are recognized for their abundance of isoquinoline alkaloids, known for their diverse bioactivities. The three species, *Corydalis chaerophylla*, collected from Phulchowki, Lalitpur and *C. govaniana*, and *C. casimiriana,* collected from Langtang, Rasuwa, Nepal were extracted sequentially with hexane, methanol, and chloroform.

The extracts of *C. chaerophylla* were subjected to liquid chromatography diode array detection multiple stage mass spectrometry (LC-DAD-MS^n) analysis, resulting in the identification of fifteen alkaloids. Antimicrobial testing of extracts revealed significant inhibition with methanol and chloroform extracts, supported by high phenolic content (113 mg GAE/g in chloroform) and antioxidant activity (IC_{50} = 261.5 μg/mL in the DPPH assay). The methanol extract exhibited strong α-amylase inhibitory activity (IC_{50} = 51.52 μg/mL), highlighting its potential as an antidiabetic agent, but was less toxic in brine shrimp lethality analysis (LC_{50} = 196 μg/mL) compared to the chloroform extract. However, in vivo acute oral toxicity studies showed toxic effects for methanol (LD_{50} = 1000.36 mg/kg BW) and chloroform (LD_{50} = 515 mg/kg BW) extracts, requiring careful dose optimization for therapeutic applications.

Chromatographic separation of chloroform extracts of different *Corydalis* species led to the isolation of thirteen pure alkaloids, including four new compounds from whose structures were elucidated by 1D and 2D NMR spectroscopy and mass spectrometry. The energy and force minimized molecular structures of these four compounds were obtained from quantum mechanical calculations using Becke, 3-parameter, Lee–Yang–Parr (B3LYP) functional and 6-31G* basis set at the density functional theory (DFT) level. The new identified compounds were named as Chaeronepaline-A (**1**), Chaeronepaline-B (**2**), Chaeronepaline-C (**3**), and Chaeronepaline-D (**4**), respectively, owing to the *C. chaerophylla* species from Nepal. Additionally, known alkaloids such as bicuculline (**5**), corydalmine (**6**), 8-hydroxydihydrosanguinarine (**7**), dihydrosanguinarine (**8**), and scoulerine (**9**) were isolated from *C. chaerophylla*, while

govaniadine (**10**), was isolated and characterized from *C. govaniana* and stylopine (**11**), adlumine (**12**), and adlumidine (**13**) were identified from *C. casimiriana*.

In a first set of experiment, berberine, californidine, and govaniadine demonstrated low-density lipoprotein receptor (LDLR) induction in human hepatocyte model similar to 2.5 μM simvastatin. Californidine and berberine decreased proprotein convertase subtilisin/kexin type 9 (PCSK9) expression, contrasting with simvastatin, which increased PCSK9. Govaniadine showed a statin-like effect by increasing both LDLR and PCSK9 levels. Further testing in the hepatocyte model showed that berberine, californidine, and govaniadine reduced total cholesterol levels, suggesting a promising hypocholesterolemic effect. Also, in the second set, the newly isolated alkaloids (**1-4**) were also evaluated in Huh7 cells to examine their impact on LDLR and PCSK9 expression and cholesterol biosynthesis for potential hypocholesterolemic activity. Results indicated that compounds **2** and **3** increased LDLR expression and inhibited cholesterol synthesis, with compound **2** additionally reducing PCSK9 secretion in Huh7 cells.

Thus, this study identified and characterized bioactive alkaloids from *Corydalis* species, with compound **2** (chaeronepaline-B) demonstrating significant hypocholesterolemic potential by modulating LDLR, PCSK9, and cholesterol biosynthesis pathways. These findings highlight the therapeutic promise of *Corydalis* alkaloids, warranting further *in vivo* validation.

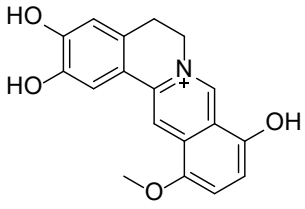

1

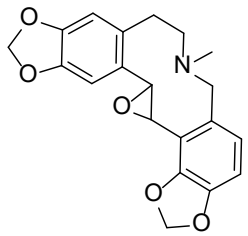

2

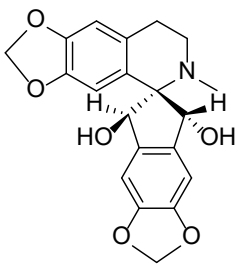

3

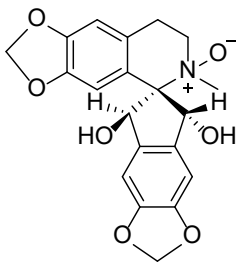

4

Keywords: *Corydalis – Extraction – Bioactivities – Isolation – Characterization – Isoquinoline Alkaloids – Anticholesterol*

LIST OF ACRONYMS AND ABBREVIATIONS

^{13}C-NMR	:	Carbon-13 Nuclear Magnetic Resonance
1D-NMR	:	One-Dimensional Nuclear Magnetic Resonance Spectroscopy
^{1}H-NMR	:	Proton Nuclear Magnetic Resonance
2D-NMR	:	Two-Dimensional Nuclear Magnetic Resonance Spectroscopy
ABTS	:	2,2-Azino-Bis-3-Ethylbenzothiazoline-6-Sulphonic Acid
AIA	:	Adjuvant-Induced Arthritis
APCI	:	Atmospheric Pressure Chemical Ionization
aPKCs	:	Atypical Protein Kinase C
ATCC	:	American Type Culture Collection
B3LYP	:	Becke, 3-parameter, Lee–Yang–Parr
BCA	:	Bicinchoninic Acid Assay
BIAs	:	Benzylisoquinoline Alkaloids
Bio-Rad	:	Biochemicals and Radiochemicals
BSA	:	Bovine Serum Albumin
BSLA	:	Brine Shrimp Lethality Assay
BW	:	Body Weight
CC	:	Column Chromatography
CD	:	Circular Dichroism
CE	:	*Corydalis edulis*
CID	:	Collision-Induced Dissociation
COSY	:	Correlation Spectroscopy
COX-2	:	Cyclooxygenase-2
cPKCs	:	Conventional Protein Kinase C
CVD	:	Cardiovascular Disease
DAD	:	Diode-Array Detection
DAPI	:	4′,6-Diamidino-2-Phenylindole
DCM	:	Dichloromethane
DEPT	:	Distortionless Enhancement by Polarization Transfer
DFT	:	Density Functional Theory
DMEM	:	Dulbecco's Modified Eagle Medium

DMSO	:	Dimethyl Sulfoxide
DNA	:	Deoxyribonucleic Acid
DNSA	:	Dinitrosalicylic Acid
DPPH	:	2,2-Diphenyl-1-Picrylhydrazyl
ECD	:	Electronic Circular Dichroism
ECL	:	Electrochemiluminescence
EDTA	:	Ethylenediamine Tetraacetic Acid
ELISA	:	Enzyme-Linked Immunosorbent Assay
ESI	:	Electrospray Ionization
FBS	:	Fetal Bovine Serum
FCS	:	Fluorescence Correlation Spectroscopy
FRAP	:	Ferric Reducing Antioxidant Power
FTIR	:	Fourier-Transform Infrared Spectroscopy
GAE	:	Gallic Acid Equivalents
GAPDH	:	Glyceraldehyde-3-Phosphate Dehydrogenase
GHS	:	Globally Harmonized System
GSH	:	Glutathione
GST	:	Glutathione S-Transferase
HDL-C	:	High-Density Lipoprotein Cholesterol
HEK	:	Human Embryonic Kidney
HeLa	:	Henrietta Lacks
HepG2	:	Hepatoblastoma Cell Line
HETCOR	:	Heteronuclear Correlation
HIT	:	Heparin-Induced Thrombocytopenia
HMBC	:	Heteronuclear Multiple Bond Correlation
HMG-CoA	:	Hydroxymethylglutaryl-Coenzyme A
HNF1a	:	Hepatocyte Nuclear Factor-1 Alpha
HPLC	:	High-Performance Liquid Chromatography
HPLC-DAD	:	High-Performance Liquid Chromatography Diode Array Detector
HR-ESI-MS	:	High Resolution Electrospray Ionization Mass Spectrometry
HR-MS	:	High-Resolution Mass Spectrometry
HSQC	:	Heteronuclear Single Quantum Coherence

IC_{50}	:	Half-Maximal Inhibitory Concentration
IR	:	Infrared
LB	:	Luria-Bertani
LC	:	Liquid Chromatography
LC_{50}	:	Lethality Concentration 50%
LC-APCI-MS	:	Liquid Chromatography Atmospheric Pressure Chemical Ionization Mass Spectrometry
LC-DAD	:	Liquid Chromatography Diode-Array Detection
LC-DAD-MS	:	Liquid Chromatography Diode-Array Detection Mass Spectrometry
LC-DAD-MS^n	:	Liquid Chromatography Diode Array Detection Multiple Stage Mass Spectrometry
LC-MS	:	Liquid Chromatography-Mass Spectrometry
LD_{50}	:	Median Lethal Dose
LDL	:	Low-Density Lipoprotein
LDLC	:	Low-Density Lipoprotein Cholesterol
LDLR	:	Low-Density Lipoprotein Receptor
LPS	:	Lipopolysaccharides
m/z	:	Mass to Charge Ratio
MAE	:	Microwave-Assisted Extraction
MALDI	:	Matrix-Assisted Laser Desorption/Ionization
MCF-10A	:	Mammary Epithelial Cell Line
MCF-7	:	Michigan Cancer Foundation-7
MEM	:	Minimum Essential Medium
Me-N	:	Methyl Attached with Nitrogen
MeOD	:	Deuterated Methanol
MeOH	:	Methanol
MHA	:	Mueller-Hinton Agar
MHz	:	Megahertz
MIC	:	Minimum Inhibitory Concentration
mRNA	:	Messenger Ribonucleic Acid
MS	:	Mass Spectrometry
mTOR	:	Mammalian Target of Rapamycin
NMR	:	Nuclear Magnetic Resonance

NOESY	:	Nuclear Overhauser Effect Spectroscopy
nPKCs	:	Novel Protein Kinase C
NPRL	:	Natural Product Research Laboratory
OECD	:	Organization For Economic Cooperation and Development
PARP1	:	Poly [ADP-Ribose] Polymerase 1
PBS	:	Phosphate Buffered Saline
PCSK9	:	Proprotein Convertase Subtilisin/Kexin Type 9
PEDA	:	Photoenolization/Diels−Alder
PES	:	Polyethersulfone
PKC	:	Protein Kinase C
PMID	:	Pubmed Identifier
ppm	:	Parts Per Million
PTLC	:	Preparative Thin Layer Chromatography
PVDF	:	Polyvinylidene Fluoride
QE	:	Quercetin Equivalents
QTof	:	Quadrupole Time-of-Flight
ROS	:	Reactive Oxygen Species
S.N.	:	Serial Number
SAR	:	Structure-Activity Relationships
SBC18	:	Stable Bond Sb-C18
SCF	:	Self-Consistent Field
SD	:	Standard Deviation
SDS-PAGE	:	Sodium Dodecyl-Sulfate Polyacrylamide Gel Electrophoresis
SFE	:	Supercritical Fluid Extraction
SMs	:	Secondary Metabolites
SRB	:	Sulforhodamine B
SREBP	:	Sterol Regulatory Element Binding Proteins
T2DM	:	Type 2 Diabetes Mellitus
TBS-T20	:	Tris-Buffered Saline Tween 20
TDDS	:	Time-Dependent Data System
TFC	:	Total Flavonoid Content
TLC	:	Thin-Layer Chromatography
TPC	:	Total Phenolic Content

UAE	:	Ultrasonic-Assisted Extraction
UFF	:	Universal Force Field
UV	:	Ultravoilet
UV-VIS	:	Ultra Violet-Visible Spectroscopy
XDB	:	Extra Densely Bonded
ZOI	:	Zone of Inhibition

LIST OF SYMBOLS

α	:	Alpha
β	:	Beta
δ	:	Chemical Shift
%	:	Percentage
μ	:	Micro
°C	:	Degree Celsius
J	:	Coupling Constant
o	:	Ortho
p	:	Para

LIST OF TABLES

Page No.

LIST OF FIGURES

Page No.

LIST OF SCHEMES

Page No.

TABLE OF CONTENTS

Page No.

CHAPTER 1

1. INTRODUCTION

1.1. Background

1.1.1. Natural Products and Secondary Metabolites

Natural products derived from plants, more specifically secondary metabolites (SMs), have proven to be one of the most effective drug sources across a variety of therapeutic fields, particularly in the treatment of cancer and analgesy (Cragg *et al.*, 2005; Grothaus *et al.*, 2010; Newman & Cragg, 2009). Plant produce such compounds for defense against herbivores and pathogens as well as a reaction against environmental stresses. Fewer than 10% of the world's biodiversity has been investigated for potential biological activity, suggesting that several advantageous naturally occurring lead compounds await to be discovered. The challenge lies in figuring out how to acquire this natural chemical diversity (Dias *et al.*, 2012; Ramakrishna & Ravishankar, 2011). Natural healthcare was the exclusive method for the treatment and prevention of human ailments for thousands of years. Traditional Ayurveda, Unani, Chinese medicine, Kampo and Korean medicine have all been practiced around the world and have developed into well-organized, controlled medical systems (Yuan *et al.*, 2016; Zhang *et al.*, 2018).

Nature serves as a distinctive repository of bioactive natural compounds, whose structural diversity, complexity, and biological activity underscore their crucial role as sources of pharmacophores and lead molecules in medicinal chemistry, ultimately contributing to the development of clinical medications (Chen *et al.*, 2015; Kingston, 2011; Marques *et al.*, 2016). Newmann and Cragg (2016) have claimed that natural products continue to exhibit a prominent influence in the identification of lead compounds for the advancement of pharmaceuticals targeting human diseases. The significant and undeniable impact of natural products on the development of chemotherapeutic treatments remains apparent, even when excluding other categories. There is still a significant amount of unexplored tiny molecules in Nature's vast collection, with a particular emphasis on the marine and microbial ecosystems (Newman & Cragg, 2016). In 2020, they reiterated that natural products remain the most promising sources for identifying novel agents or active templates, which, when

developed in conjunction with synthetic chemists and biologists, present the potential for discovering new structures that may yield effective treatments for various human diseases (Newman & Cragg, 2020). Synthesis and accumulation of SMs are very complicated processes that are affected by a wide variety of factors, some of which are internal developmental genetic circuits (such as regulated genes and enzymes) and some of which are external environment factors (such as light, temperature, water, salinity, etc.) (Barthwal & Mahar, 2024; Li *et al.*, 2020; Pant *et al.*, 2021).

There are around 100,000 SMs found in the plant kingdom, each of which is unique to a particular taxonomic group. Based on the biochemical process, there are three primary categories of secondary metabolites found in plants. These categories comprise phenolic chemicals (like, flavonoids and phenylpropanoids), terpenes (such as isoprenoids), and nitrogen-containing compounds (including cyanogenic glycosides, alkaloids, and glucosinolates)(Al-Khayri *et al.*, 2023; Li *et al.*, 2020). Among them, alkaloids are a large cluster of compounds that can be discovered in Mother Nature across the globe. There are various types of alkaloids, but the indole, tropasne, and isoquinoline alkaloids are particularly significant. Alkaloids continue to hold a significant amount of potential for the development of novel medicines since they might eventually reveal new chemical compounds and a wide variety of pharmacological features. In addition to carbon, nitrogen, or hydrogen, alkaloids may also contain sulphur and, on extremely rare occasions, bromine, phosphorus, or chlorine. According to reports that have been published up to this instance, higher plant species that belong to the groups Amaryllidaceae, Berberidaceae, Leguminaceae, Liliaceae, Ranunculaceae, Solanaceae and Papaveraceae are notably abundant in alkaloids, which are mainly extracted through acid-base extraction process (Bhambhani *et al.*, 2021; Dey *et al.*, 2020). In this research we have considered Genus *Corydalis* from Papaveraceae family for the extraction and isolation of isoquinoline alkaloids.

1.1.2. Natural Products Originated Medicines

Natural product-originated medicines have been pivotal in drug discovery and development, providing a vast reservoir of pharmacologically active compounds with unique chemical diversity. Derived from secondary metabolites of plants, microorganisms, and marine organisms, these compounds exhibit diverse bioactivities, including anticancer, antimicrobial, anti-inflammatory, and cardiovascular effects.

Their structural complexity and biological activity often surpass synthetic counterparts, making them invaluable in modern medicine. For instance, paclitaxel, derived from the Pacific yew tree (*Taxus brevifolia*), remains a cornerstone in chemotherapy, while artemisinin, isolated from *Artemisia annua*, revolutionized malaria treatment (Newman & Cragg, 2020). Other examples include morphine, extracted from *Papaver somniferum* (opium poppy), which remains a gold standard for pain management, and aspirin, originally derived from salicylic acid in willow bark (*Salix* species), now widely used for its anti-inflammatory and anticoagulant properties. Recent research highlights the anti-cancer, anti-diabetic, and neuroprotective properties of plant-derived alkaloids, flavonoids, and terpenoids, reaffirming the therapeutic potential of natural products (Olofinsan *et al.*, 2023).

In recent years, the U.S. Food and Drug Administration (USFDA) has approved several drugs derived from natural products, underscoring their significance in addressing unmet medical needs. For example, the anti-cancer drug galunisertib, derived from natural alkaloid frameworks, was approved for treating hepatocellular carcinoma in 2021. Similarly, plitidepsin, a marine-derived compound, has shown efficacy against COVID-19 and multiple myeloma (Banday *et al.*, 2024). Plant-derived drugs like ingenol mebutate (from *Euphorbia* species) for actinic keratosis and cannabidiol (CBD) for epilepsy further highlight the diverse applications of natural products in pharmacology (Shilpha *et al.*, 2018). Commonly used natural product-derived drugs include quinine and its derivatives for malaria, digoxin from *Digitalis* for heart conditions, and vincristine from *Catharanthus roseus* for leukemia (Shukla *et al.*, 2024; Triska *et al.*, 2023; Virginia *et al.*, 2023). As advancements in genomic and analytical technologies continue to expand our ability to isolate and characterize natural compounds, these medicines remain central to developing innovative therapies for complex diseases.

1.1.3. Genus Corydalis

The genus *Corydalis*, belonging to the Papaveraceae family, is one of the most diverse groups within the subfamily Fumarioideae. It comprises over 470 species primarily distributed across the temperate regions of the Northern Hemisphere, including Eurasia and North America. Nepal alone hosts 57 distinct species, underscoring the genus's significant presence in the Himalayan region. The diversity and adaptability of

Corydalis species are reflected in their ability to thrive in various habitats, including high-altitude terrains and temperate climates (Dar *et al.*, 2011).

The Papaveraceae family, which houses *Corydalis*, is economically and medicinally important, comprising approximately 42 genera and 775 species globally, with 5 genera and 29 species identified in Nepal. Species like *Papaver somniferum* are renowned for producing alkaloids such as morphine and codeine, which are widely used in pain management and sedatives. Similarly, *Corydalis* species are celebrated for their rich isoquinoline alkaloid content, which exhibits a variety of bioactivities, including antimicrobial, analgesic, and anticancer properties (Egan *et al.*, 2024; Wikipedia contributors, 2024; Yashasvi, 2024).

The genus *Corydalis* demonstrates remarkable diversity in its morphology and bioactive compound profiles. Species within this genus have been utilized in traditional medicine systems across China, Nepal, and other parts of Asia to treat various ailments. The evolutionary relationships within the Papaveraceae family and the unique bioactive properties of *Corydalis* species position this genus as a subject of immense pharmacological and ecological significance. They possess a significant abundance of alkaloids, specifically isoquinoline alkaloids, which exhibit diverse biological properties. These compounds play a crucial role in chemical defense mechanisms against a wide range of microorganisms and herbivores (Majak *et al.*, 2003; Schmeller *et al.*, 1997). Traditionally, certain species of *Corydalis* have been widely employed in China, Korea, Japan, and other Eastern Asian nations for the curative treatment of various medical conditions (Li *et al.*, 2006; Ma *et al.*, 2008; Wangchuk *et al.*, 2012) attributed to their significant antibacterial, antiviral, and anticancer effects (Liu *et al.*, 2019; Tian *et al.*, 2020; Zhang *et al.*, 2016). Each year, new alkaloid structures, along with the biological activities that are associated with them, are reported from plants belonging to this genus. Certain alkaloids possess biological and pharmacological features that have significant potential for treating severe conditions such as Alzheimer's disease, cancer, and microbial infections. Despite the fact that isoquinoline alkaloids have been found in a wide variety of plants and even in other biological sources, the diversity of structures found in *Corydalis* alkaloids has proven to be particularly fascinating to natural product researchers (Iranshahy *et al.*, 2014). Various alkaloids derived from *Corydalis* have been documented to exhibit hepatoprotective

properties (Jahan *et al.*, 2021), inhibit urease activity (Shrestha *et al.*, 2013), possess leishmanicidal activity (Callejon *et al.*, 2014), demonstrate pharmacokinetic characteristics (Marques *et al.*, 2016), possess analgesic properties (Muhammad *et al.*, 2015), induce apoptosis (Sivakumaran *et al.*, 2018), and exert cytotoxic effects on human cancerous cell lines (Marques *et al.*, 2020).

In this research, *C. chaerophylla* DC., *C. govaniana* Wall., and *C. casimiriana* Duthie & Prain ex Prain, acquired from Nepal, are glabrous herbs located in the alpine regions across Nepal, India, and Pakistan. They thrive in humid, shaded conditions found at elevations between 2400-4800 meters. They have served as remedies for ailments like diarrhea, dysentery, syphilis, and scrofula (Sivakumaran *et al.*, 2018).

1.1.4. Corydalis chaerophylla DC.

The glabrous herb *Corydalis chaerophylla* DC. (*C. chaerophylla*), commonly called Okhare Jhar in Nepali, thrives in the elevated regions of Nepal, India, and Pakistan. They survive in wet, shadowy conditions in forests and clearings, often close to running water at elevations ranging from 1800–5500 metres (Lidén, 2012; Sivakumaran *et al.*, 2018). In conventional medicine, the root juice of *C. chaerophylla* was used to treat fever, indigestion and peptic ulcers. *C. chaerophylla* juice was traditionally used for peptic ulcers, with a recommended intake of around four teaspoons, three times per day. A dosage of approximately 6 teaspoons, administered three times day, of the root juice was advised for the treatment of dyspepsia. This medicinal approach requires blending the root juice with an equivalent portion of root juice from *Cyathula capitate* Moq. N. Kuro (Manandhar, 1993). Previous scientific investigations on the aforementioned species have resulted in the identification and isolation of numerous alkaloids. These alkaloids have demonstrated inhibitory properties against hepatitis virus, amoeba, tumours, and liver cancer. Additionally, they have shown potential in enhancing sedative effects and improving immunological function (Jeong *et al.*, 2012; Khodorova *et al.*, 2013; Muhammad *et al.*, 2015).

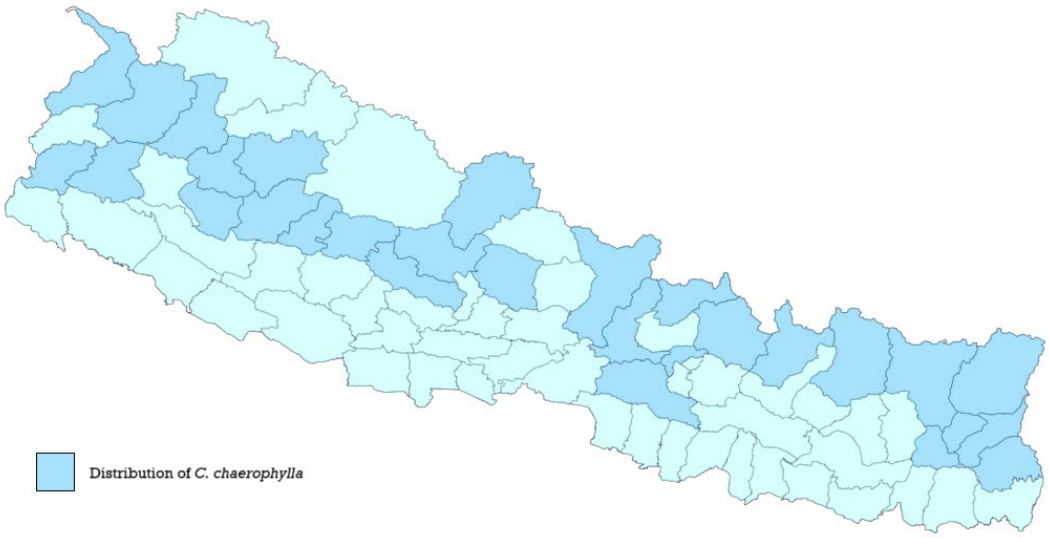

Figure 1: Distribution of *C. chaerophylla* in Nepal

The height of these perennial herbs ranges from 0.6 to 1.3 metres. The thick rootstock exhibits remnants of scales from past years' growth at the apex. The stem is upright, covered in leaves, and branches in the upper portion. The radical leaves are sparse and resemble ferns, with petioles of 10-30 cm in length. They have a triangular shape and measure 13-20 cm in length and 10-20 cm in width. The petioles of the cauline leaves are 2-6 cm. The cauline leaves are green on the upper side and glaucous on the below side, measuring 7–15 x 5–12 cm. The leaflets are strongly dentate to pinnatifid, forming acute lobes. The upper leaves are attached directly to the stem, they are smaller in size, have a triangular shape, and are divided into two leaflets. The racemes are 5-15 cm long, arranged in a thick, spike-like manner, with flowers positioned on one side, ranging from 10 to 40 in number, occasionally with branching. The bracts are elongated and have a narrow, obovate shape, measuring 4-5 mm. The pedicels measure 4-5 mm and bend backwards when the fruit is formed. The sepals are 1-1.5 × 1 mm and have toothed edges, occasionally ending in a pointed tip. The colour of the Corolla is typically a pale yellow, sometimes exhibiting a tinge of brown or green. The outer petals are typically lacking or have a short crest, and they are pointed at the tip. The top petal measures 15-20 mm and has a cylindrical spur that is straight or slightly curved, measuring 8-12 mm. The nectary is about half to three quarters as long as the spur. The lower petal is boat-shaped and not swollen, and its distal section is often not bent backwards. The length of the inner petals is 7-9 millimetres. The stigma is square and flat, with four simple papillae at the apex. The inner papillae are small and distinct,

while the outer ones are broad and scattered. There are also geminate papillae on the sides and basal lobes. The capsule is pendant, obovoid in shape, measuring 8-10 mm. It contains 5-10 seeds and opens explosively to release them. The size of the style is between 2 and 2.5 millimetres. The size of the seeds ranges from 0.9 to 1.4 millimetres. The flowering season is April to September and the fruiting season is from May to November (Lidén, 2012).

Classification:

Kingdom	:	Plantae
Clade	:	Tracheophytes
Clade	:	Angiosperms
Clade	:	Eudicots
Order	:	Ranunculales
Family	:	Papaveraceae
Subfamily	:	Fumarioideae
Tribe	:	Fumarieae
Subtribe	:	Corydalinae
Genus	:	*Corydalis*
Species	:	*chaerophylla*
Binomial name	:	*Corydalis chaerophylla* DC.
Synonym	:	*Capnodes chaerophyllum* (DC.) Kuntze
Common name	:	Okhare Jhar

Figure 2: *Corydalis chaerophylla* plant

1.1.5. Corydalis govaniana Wall.

Corydalis govaniana Wall. (*C. govaniana*), is a noteworthy perennial herb that flourishes in the high-altitude regions of the Himalayas, spanning across Nepal, Pakistan, and India. It holds various local names, such as "Bhutkesh" in Nepal, "Inderajatta" in Jammu and Kashmir, "Cheri pawa" in Urdu, and "Ralchhat nagpo" in Ladakh. This plant thrives in damp, shady environments found between elevations of 2,400 and 4,800 meters, typically on grassy hilltops, making it a resilient species well-adapted to its mountainous habitat.

Botanically, *C. govaniana* is characterized by its compact, caespitose form, standing at a height ranging from 15 to 50 cm. Its dark green, glabrous or slightly puberulent stems

arise from a thick, fibrous rootstock that is densely crowned with the remnants of old leaf sheaths. The plant has several radical leaves, each borne on petioles that measure between 5 and 10 cm long. The leaves themselves are triangular-ovate in shape, deeply pinnate with 4-5 pairs of pinnae, and can grow up to 14 cm long. Smaller, vaginate cauline leaves may also be present. The racemes, which contain clusters of 10 to 35 yellow flowers, stand atop tall pedicels and are distinctive in their elongated, lanceolate, and deeply divided bracts.

The bright yellow corolla, with petals that taper into delicate spurs measuring 8-12 mm, is a striking feature of this plant. The flower's structure is complex, with square stigmas and distinctive papillae, contributing to its specialized pollination mechanism. The plant blooms and bears fruit from June onwards, with the capsules containing smooth seeds arranged in two rows.

C. govaniana holds significant ethnomedical value, particularly in traditional medicine systems of the Himalayan region. For centuries, the roots of this herb have been employed in the treatment of a variety of ailments. Historical records suggest its use in treating syphilis, scrofula (a form of tuberculosis affecting the lymph nodes), and various cutaneous infections. It has also been used to alleviate gastrointestinal issues such as diarrhea and dysentery, highlighting its versatile role in local herbal remedies.

Phytochemical studies have identified several tetrahydroprotoberberine-type alkaloids within *C. govaniana*, which are thought to contribute to its medicinal properties. These alkaloids, first reported by researchers like Mukhopadhyay and Mehra in the late 20th century, have garnered attention for their potential pharmacological benefits. The plant’s significance in traditional and modern medicine, combined with its distinctive botanical features, make *C. govaniana* an important species in both ecological and medicinal research across its native range.

C. govaniana is not only a beautiful herb native to the Himalayas but also a valuable source of traditional medicine. Its complex botanical structure, resilience in high-altitude environments, and longstanding medicinal uses demonstrate its ecological importance and cultural significance in the regions where it grows (Lidén, 2012).

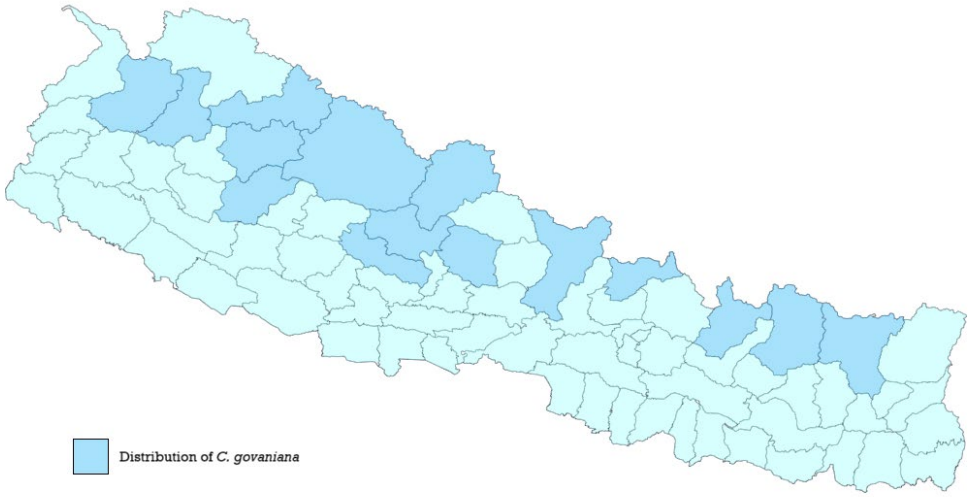

Figure 3: Distribution of *C. govaniana* in Nepal

C. govaniana is highly regarded for its wide range of local medicinal uses across the Himalayan regions, where it grows naturally. The root of the plant holds a prominent place in traditional herbal medicine, often used as an antiperiodic, appetizer, diuretic, and skin tonic. One of its most important applications is in the treatment of syphilis and various cutaneous affections. In addition, it is utilized to treat poisoning, limb swelling, and gastrointestinal pain caused by worm infestations (Shaheen *et al.*, 2012; Ur-Rahman *et al.*, 2019).

The juice extracted from the plant has a diuretic effect, making it useful for treating urinary issues, while the powdered flowers are employed in addressing eye diseases (Khan *et al.*, 2013). Moreover, applying the juice of the flowers externally on the forehead is believed to relieve headaches. In veterinary medicine, the roots are given to cattle to treat dysentery and digestive disorders, while the floral shoots are utilized for ophthalmic problems in both humans and animals (Hamayun *et al.*, 2006). The plant also serves as a laxative, and its extracts are commonly used to combat fevers, liver disorders, and eye infections (Kayani *et al.*, 2015; Singh *et al.*, 2017).

In addition to its local medicinal uses, *C. govaniana* is recognized in traditional Chinese medicine (Liu *et al.*, 2016; Wu, 2005). The plant has been used to treat various respiratory conditions, including asthma, chest infections, whooping cough, and other respiratory disorders. It is also known for its antipyretic and febrifuge properties,

effectively reducing fever and easing muscular pain, gastric disorders, and other gastrointestinal issues (Gairola *et al.*, 2014).

The medicinal versatility of this herb extends to veterinary practices as well. The entire plant or flowers are boiled and used to treat stomach aches and abdominal bloating in livestock such as cows, sheep, and goats. Furthermore, the cooked portions of the plant are applied to assist in placental retention in cows, improving reproductive health in animals (Ballabh & Chaurasia, 2007). The plant has ceremonial purposes as well (Kayani *et al.*, 2015).

In summary, *C. govaniana* has a long-standing history of medicinal use for a variety of ailments ranging from skin diseases and fever to gastrointestinal disorders and respiratory infections. Its applications in both human and veterinary medicine underscore its importance as a valuable plant in traditional healing systems across the Himalayan regions and beyond.

Classification:

Kingdom	:	Plantae
Clade	:	Tracheophytes
Clade	:	Angiosperms
Clade	:	Eudicots
Order	:	Ranunculales
Family	:	Papaveraceae
Subfamily	:	Fumarioideae
Tribe	:	Fumarieae
Subtribe	:	Corydalinae
Genus	:	*Corydalis*
Species	:	*govaniana*
Binomial name	:	*Corydalis govaniana* Wall
Synonym	:	*Corydalis swatensis* Kitam.
Common name	:	Bhutkesh

Figure 4: *Corydalis govaniana* plant

1.1.6. *Corydalis casimiriana* Duthie and Prain ex Prain

Corydalis casimiriana Duthie & Prain (*C. casimiriana*), a non-hairy herb, is native to the Himalayan areas spanning Nepal, Bhutan, China, and India. It can be either an annual or short-lived perennial, typically growing between 20 to 70 cm tall. The plant is slender and weak-stemmed, with much branching starting at the base and many leaves that contribute to its delicate appearance. The leaves are bi- or tri-ternate, glaucous on the underside, with lobules that are deeply divided and obovate, giving the foliage a finely divided, feathery look.

The racemes of *C. casimiriana* bear 4 to 12 yellow flowers, which are tipped with a unique blackish-purple coloration on the inner petals. The flowers are narrow and acute, with the upper petal measuring 9 to 11 mm in length. The spur of the flower is often up-curved and slender, while the nectary extends halfway along the length of the spur. One of the plant's most striking features is its pendent capsule, which contains 6 to 10 seeds and is explosively dehiscent, meaning the seeds are dispersed forcefully upon maturation.

C. casimiriana is adapted to high-altitude environments, growing in open grassy slopes, pastures, and areas that have recently been burned, as well as in the understories of open subalpine coniferous forests. It thrives at altitudes ranging from 2,800 to 4,700 meters, making it a common sight in the mountainous regions of the Himalayas. The plant is known for its ability to colonize disturbed environments such as burned areas, highlighting its resilience in challenging conditions.

Despite its widespread distribution, there has been limited phytochemical research on *C. casimiriana*. While its relatives in the *Corydalis* genus are often studied for their medicinal properties, this particular species has not been extensively examined for potential therapeutic uses. However, like other *Corydalis* species, it may hold untapped medicinal or ethnobotanical value, particularly in the high-altitude regions where it grows. Further research into its phytochemistry could reveal new insights into its potential benefits.

In conclusion, *C. casimiriana* is a delicate and widely distributed herb in the Himalayas, growing in high-altitude, open habitats. Its ability to thrive in harsh, disturbed environments and its distinctive floral features make it an interesting plant both

ecologically and botanically, even though its medicinal or chemical properties have yet to be fully explored (Lidén, 2012).

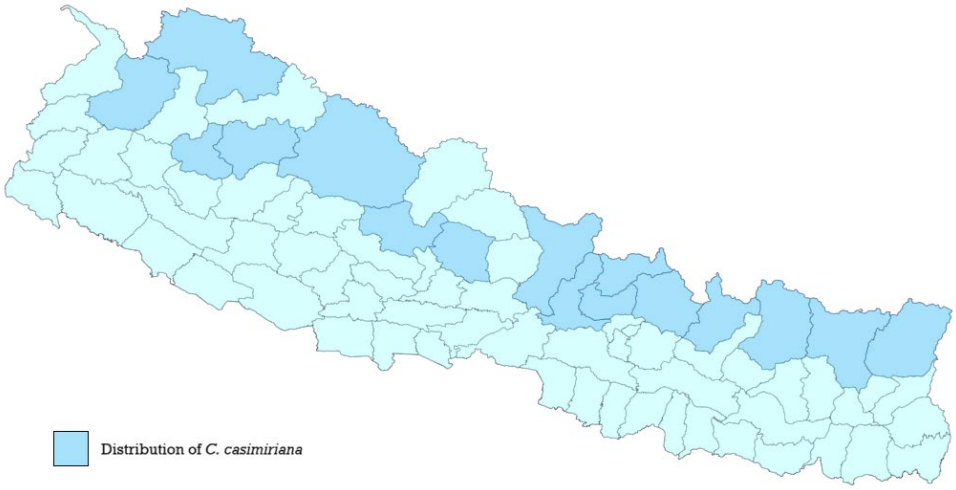

Figure 5: Distribution of *C. casimiriana* in Nepal

Classification:

Figure 6: *Corydalis casimiriana* plant

Kingdom	:	Plantae
Clade	:	Tracheophytes
Clade	:	Angiosperms
Clade	:	Eudicots
Order	:	Ranunculales
Family	:	Papaveraceae
Subfamily	:	Fumarioideae
Tribe	:	Fumarieae
Subtribe	:	Corydalinae
Genus	:	*Corydalis*
Species	:	*casimiriana*
Binomial name	:	*Corydalis casimiriana* Duthie and Prain ex Prain
Synonym	:	*Corydalis prainiana* Kanodia & Mukh.
Common name	:	Not available

1.1.7. The Advancement in Natural Product Extraction

The extraction process of natural products involves isolating bioactive compounds from plant or other natural sources, a fundamental step in natural product chemistry that has been used for centuries to obtain medicinal and aromatic compounds. This process typically begins with drying and grinding the raw material, such as plant roots, leaves, seeds, or entire plants, to increase the surface area and facilitate the extraction of bioactive constituents. Solvent selection plays a crucial role, as different compounds require solvents of varying polarity to dissolve effectively. Common solvents include hexane, methanol, ethanol, chloroform, and water, depending on the solubility of the target compounds (Azwanida, 2015). Solvents are selected depending on the polarity of the compounds being targeted—polar solvents like water and methanol are often used for hydrophilic compounds (e.g., flavonoids), while non-polar solvents like chloroform target lipophilic compounds (e.g., alkaloids, terpenoids) (Harborne, 1998). Cold percolation, maceration, Soxhlet extraction, and ultrasonic-assisted extraction are among the most widely used extraction methods. Cold percolation and maceration are traditional methods where plant material is left to soak in solvent over several hours or days, relying on passive diffusion to extract compounds, making these methods suitable for thermolabile compounds (Handa *et al.*, 2008).

Soxhlet extraction, a more intensive method developed in the 19th century, involves continuous cycles of solvent vaporization and condensation over plant material, ensuring the extraction of both volatile and non-volatile compounds. This method is often faster and more exhaustive than maceration and percolation, but it can degrade heat-sensitive compounds due to extended exposure to high temperatures (Azmir *et al.*, 2013). Ultrasonic-assisted extraction (UAE) has gained popularity for its efficiency and is widely applied for both polar and nonpolar compounds. UAE involves using ultrasound waves to create cavitation bubbles in the solvent, which collapse and release energy, disrupting cell walls and enhancing compound release. This method is advantageous for rapid extraction and can be conducted at lower temperatures, preserving heat-sensitive compounds. Recent advancements also include microwave-assisted extraction (MAE) and supercritical fluid extraction (SFE), which use microwave energy or supercritical CO_2 as the extraction medium, enabling precise

temperature control and efficient extraction with minimal solvent use, aligning with the principles of green chemistry (Mustafa & Turner, 2011).

The concentration and purification of extracted compounds are essential following extraction, often involving solvent evaporation using a rotary evaporator or similar devices under reduced pressure. Subsequent purification techniques, such as column chromatography (CC) or preparative thin-layer chromatography (PTLC), allow for the isolation of specific compounds based on their physical and chemical properties. Depending on the complexity of the extract and the target compounds, further analyses, such as nuclear magnetic resonance (NMR) spectroscopy, mass spectrometry (MS), or high-performance liquid chromatography (HPLC), are employed to confirm compound identity and purity (Ncube *et al.*, 2008). Thus, the extraction process, carefully designed to accommodate different natural product classes, remains a critical step in the study of bioactive natural compounds and drug discovery research.

1.1.8. Bioassay Guided Isolation of Natural Products

Bioassay-guided isolation is a systematic and iterative approach used to identify and isolate bioactive compounds from natural sources, such as plants, fungi, and marine organisms, based on their biological activity. This method combines extraction, fractionation, and bioassay testing to ensure that the compounds isolated exhibit the desired biological activity, thus aiding in the discovery of new therapeutic agents. The process begins with a crude extract prepared from the natural source, which is then screened for biological activity using relevant *in vitro* or *in vivo* assays. Active extracts are subsequently fractionated, often by partitioning with solvents of different polarities or by chromatography, to separate the mixture into smaller, manageable portions. Each fraction is then re-evaluated using the bioassay, a crucial step that allows researchers to track the bioactivity and pinpoint which fractions contain active compounds. This process is repeated multiple times, narrowing down the fractions until individual bioactive constituents are isolated and purified (Cos *et al.*, 2006).

A variety of chromatographic techniques, including liquid-liquid extraction, column chromatography, and high-performance liquid chromatography (HPLC), are often employed to separate compounds based on their chemical properties, such as polarity, size, or charge. Thin-layer chromatography (TLC) is also frequently used for initial

profiling of fractions and for quick, visual detection of bioactive compounds with indicator assays. Once isolated, compounds undergo structural elucidation, often using advanced spectroscopic methods like nuclear magnetic resonance (NMR) and mass spectrometry (MS), which provide insight into the chemical structure and functional groups present in the active compounds (Harvey, 2000). This iterative approach is especially valuable for complex natural mixtures, where bioassay-guided fractionation ensures that bioactive compounds are not overlooked during the isolation process.

Bioassay-guided isolation not only maximizes the efficiency of natural product research but also helps identify novel compounds with potential pharmaceutical applications. For example, quinine, paclitaxel, and artemisinin were all discovered through bioassay-guided approaches, highlighting the technique's effectiveness in drug discovery (Kinghorn *et al.*, 2009). In addition, bioassay-guided isolation is adaptable to various bioassays, including antimicrobial, anticancer, antioxidant, and enzyme inhibition assays, making it versatile across a wide range of therapeutic targets. Given the ongoing interest in natural products as sources of new drugs, bioassay-guided isolation remains a cornerstone methodology in pharmacognosy and natural product chemistry, driving the discovery of structurally diverse and bioactive natural compounds.

1.1.9. Phytochemical Screening of Natural Products

Phytochemical screening is a preliminary and essential process in natural product research, involving the qualitative analysis of plant extracts to identify the presence of various bioactive compounds, such as alkaloids, flavonoids, saponins, tannins, terpenoids, and phenolics. This initial screening helps to determine the phytochemical profile of a plant, guiding subsequent isolation and bioassay-guided fractionation studies. The process typically involves solvent extraction, where plant materials are subjected to solvents like methanol, ethanol, or water to obtain crude extracts that contain different classes of phytochemicals based on solubility (Edeoga *et al.*, 2005).

Qualitative tests are conducted to detect specific classes of phytochemicals. For example, alkaloids can be identified by treating extracts with reagents such as Dragendorff's or Mayer’s, which produce a characteristic precipitate. Flavonoids are often tested using the lead acetate test, which produces yellow precipitates, or the ferric chloride test, which gives a color change indicating the presence of phenolics. Tannins

are detected using the ferric chloride test, which yields a blue-black color when tannins are present. Saponins can be identified through the froth test, where persistent frothing in an aqueous solution indicates their presence, while terpenoids are often detected by the Salkowski test, which yields a reddish-brown coloration when terpenoids are present. This set of simple, qualitative tests provides a quick and efficient way to determine the presence of various bioactive compounds in plant materials (Reynolds & Sofowora, 1984).

Phytochemical screening is significant in ethnopharmacology, where traditional medicinal plants are studied for bioactive compounds based on traditional usage. By identifying the classes of compounds present in a plant, researchers can prioritize plants for further investigation in pharmacological studies. For example, tannins and flavonoids are often associated with antioxidant properties, while alkaloids are frequently linked with antimicrobial and analgesic activities (Parekh & Chanda, 2010). As a result, phytochemical screening serves as a valuable tool in narrowing down bioactive compounds with potential therapeutic applications and is a critical step in the field of drug discovery from natural sources.

1.1.10. Total Phenolic and Flavonoid Content Studies

The evaluation of phenolic and flavonoid contents in plant extracts is important for gauging their antioxidant strength and potential health-promoting effects. Phenolics and flavonoids are secondary metabolites widely known for their bioactive properties, including antioxidant, anti-inflammatory, antimicrobial, and anticancer effects (Dai & Mumper, 2010). To determine total phenolic content (TPC), the Folin-Ciocalteu method is commonly employed, where the Folin-Ciocalteu reagent reacts with phenolic compounds to produce a blue complex measurable at 765 nm. This assay expresses TPC results in gallic acid equivalents (GAE), facilitating comparative studies across various plant extracts (Singleton *et al.*, 1999). The total flavonoid content (TFC), on the other hand, is often measured by the aluminum chloride colorimetric method, where flavonoids form a yellow complex with aluminum ions that can be quantified at 415 nm. The TFC values are typically expressed in terms of quercetin equivalents (QE), allowing for standardized reporting of flavonoid levels in plant samples (Chang *et al.*, 2002). Both phenolics and flavonoids are highly influenced by extraction techniques and solvent choice. Studies have demonstrated that polar solvents, particularly

methanol and ethanol, are effective for extracting these compounds due to their compatibility with phenolic and flavonoid structures, often resulting in higher yields from dried plant material (Sultana *et al.*, 2009). The significance of phenolics and flavonoids lies not only in their ability to neutralize free radicals and reduce oxidative stress but also in their role in promoting overall health. For example, a high concentration of phenolic content has been correlated with increased antioxidant activity, as shown by assays like DPPH (2,2-diphenyl-1-picrylhydrazyl) and FRAP (Ferric Reducing Antioxidant Power), which are commonly used to evaluate the radical-scavenging abilities of plant extracts (Re *et al.*, 1999). Given the broad range of biological activities associated with phenolics and flavonoids, TPC and TFC assessments are not only critical for identifying plants with high therapeutic potential but also serve as preliminary steps for isolating specific bioactive compounds, thereby advancing research in natural product chemistry and pharmacology.

1.1.11. Antimicrobial Activities

The antimicrobial activities of crude plant extracts play an essential role in bioassay-guided isolation, a method widely used to identify bioactive compounds from natural sources. Crude extracts provide a complex matrix of metabolites, many of which may exhibit synergistic effects that contribute to their antimicrobial properties. In the initial stages of bioassay-guided isolation, crude extracts are screened for activity against specific microbial strains, often using assays such as disk diffusion, broth dilution, and minimum inhibitory concentration (MIC) determination. These tests help prioritize extracts with potent antimicrobial effects for further fractionation (Cos *et al.*, 2006; Ríos & Recio, 2005). The effectiveness of crude extracts against pathogens, including antibiotic-resistant bacteria and fungi, has generated significant interest, as these extracts may contain a diverse array of bioactive compounds—such as alkaloids, flavonoids, terpenoids, and saponins—that act on multiple microbial targets. This complex composition can prevent the rapid development of resistance that often occurs with single-compound antibiotics (Abreu *et al.*, 2012). Bioassay-guided fractionation involves progressively separating the crude extract into smaller fractions, each tested for antimicrobial activity to identify the specific compounds responsible for observed effects. The repetitive process of separation and testing continues until pure active compounds are isolated, such as alkaloids and flavonoids, which have demonstrated

potent antimicrobial effects in various studies (Scazzocchio *et al.*, 2001). The use of crude extracts in antimicrobial bioassays has additional advantages, as the diverse compounds within an extract can exert different antimicrobial mechanisms, such as disrupting cell membranes, inhibiting enzymes, or interfering with microbial DNA (Cowan, 1999). This multi-target approach is particularly valuable for overcoming resistant strains, which are a growing global health concern. Furthermore, crude extracts can reveal compounds that might be ineffective alone but demonstrate significant antimicrobial effects in combination with other compounds within the extract, a phenomenon that can be lost in pure-compound testing (Wagner & Ulrich-Merzenich, 2009). Thus, the study of crude extract antimicrobial activity provides a foundation for bioassay-guided isolation, leading to the discovery of novel antimicrobial agents that could address urgent needs in infectious disease treatment.

1.1.12. Antioxidant Activities

The antioxidant activities of crude extracts are crucial in bioassay-guided isolation, where the goal is to identify specific compounds with significant antioxidant potential. Antioxidants play a key role in scavenging free radicals and preventing oxidative stress, which is associated with various chronic diseases, including cancer, cardiovascular diseases, and neurodegenerative disorders (Halliwell & Gutteridge, 1985). Crude plant extracts offer a broad spectrum of phytochemicals—such as phenolics, flavonoids, tannins, and terpenoids—that contribute to their antioxidant activity through mechanisms such as hydrogen atom donation, electron transfer, and metal ion chelation (Gülçin, 2012). The initial screening of crude extracts using assays like the DPPH (2,2-diphenyl-1-picrylhydrazyl) radical scavenging, ABTS (2,2′-azino-bis[3-ethylbenzothiazoline-6-sulphonic acid]) radical cation decolorization, and ferric reducing antioxidant power (FRAP) assays helps to pinpoint extracts with high antioxidant potential.

The DPPH radical scavenging assay is a widely used method to evaluate antioxidant activity in natural compounds, based on the ability of antioxidants to reduce the DPPH radical, resulting in a colour change from purple to yellow, which is measured spectrophotometrically (Brand-Williams *et al.*, 1995).

The ABTS radical cation decolorization assay similarly measures antioxidant activity, where antioxidants quench the $ABTS^{\bullet+}$ radical cation, leading to a decrease in absorbance, which can be quantified to assess antioxidant potency (Re *et al.*, 1999).

The FRAP assay evaluates antioxidant power by measuring the reduction of ferric (Fe^{3+}) to ferrous (Fe^{2+}) ions in the presence of antioxidants; the formation of a blue-coloured complex is measured spectrophotometrically, with higher absorbance indicating stronger reducing power (Benzie & Strain, 1996).

In bioassay-guided isolation, these crude extracts are fractionated, and each fraction is tested to track the activity back to specific compounds responsible for the antioxidant effects (Prior *et al.*, 2005). Phenolic compounds, for instance, are often isolated from these active fractions due to their high redox potential, which allows them to act as reducing agents, hydrogen donors, and singlet oxygen quenchers. Flavonoids, a large subgroup of phenolics, have also shown remarkable antioxidant properties in multiple studies (Rice-Evans *et al.*, 1997). Additionally, the synergistic effects of various phytochemicals in crude extracts often result in stronger antioxidant activities than single, isolated compounds, underscoring the importance of retaining complex interactions in the initial stages of bioassay-guided isolation (Cai *et al.*, 2004). This synergy also provides an advantage in therapeutic contexts, where the combined effects of multiple antioxidants may offer broader protection against oxidative damage. For instance, a crude extract's ability to neutralize both lipophilic and hydrophilic free radicals is attributed to the diversity of antioxidant compounds it contains (Prior *et al.*, 2005). Following fractionation and purification, techniques like LC-MS and NMR spectroscopy are employed to elucidate the structures of these bioactive antioxidants. The antioxidant potential of these compounds can then be further validated through cellular and *in vivo* models, potentially leading to the development of natural antioxidant therapies (Huang *et al.*, 2005). Thus, the antioxidant screening of crude extracts through bioassay-guided isolation serves as an effective strategy for discovering potent natural antioxidants, which hold promise for addressing oxidative stress-related health issues.

1.1.13. Brine Shrimp Lethality Assay

The Brine Shrimp Lethality Assay (BSLA) has significant value in natural product research and drug discovery due to its simplicity, affordability, and ability to offer rapid toxicity screening, especially for bioassay-guided isolation processes. This assay has proven essential for early-stage screening of potential bioactive compounds in crude extracts, helping to predict toxic, antimicrobial, and anticancer activities that may be present in these samples. Its use of brine shrimp nauplii (*Artemia salina*) offers a reliable and low-cost model to determine the cytotoxicity of crude extracts, thereby streamlining the isolation and prioritization of active compounds for further, more specialized testing. Since BSLA has shown a good correlation between the lethality against brine shrimp and known pharmacological activities of bioactive compounds, it serves as a quick filter, enabling researchers to focus on promising bioactive fractions for in-depth testing (Meyer *et al.*, 1982; Suneka & Manoranjan, 2021).

BSLA has also been recognized for its relevance in testing a wide range of natural products, from terrestrial plants to marine organisms. This broad application makes it a versatile tool that supports various fields, including pharmacology, toxicology, and ethnobotany. For instance, extracts showing high mortality rates in the BSLA are often investigated further for potential anticancer or antifungal properties, as these are commonly associated with cytotoxic agents (Suffness & Pezzuto, 1990). Moreover, the BSLA's capability to be conducted with minimal laboratory resources has made it widely accessible for preliminary screenings in many laboratories worldwide, particularly in resource-limited settings. Its adaptability to high-throughput screenings enhances its utility in large-scale studies, enabling the rapid evaluation of numerous samples concurrently (Krishnaraju *et al.*, 2005). Consequently, BSLA remains a cornerstone in natural product research, accelerating the discovery and isolation of novel bioactive compounds with potential therapeutic benefits.

1.1.14. α-Amylase Inhibition Assay for Antidiabetic Properties Study

The α-amylase inhibition assay is an essential biochemical test for evaluating the antidiabetic potential of crude plant extracts, especially in bioassay-guided isolation studies. α-amylase is a critical enzyme in the digestive system, catalyzing the hydrolysis of starch into glucose. By inhibiting α-amylase, the rate of glucose release

from dietary starch is slowed, which helps in managing postprandial blood glucose levels—a crucial factor in diabetes control (Ali *et al.*, 2006). The α-amylase inhibition assay enables researchers to screen crude extracts for compounds that may exhibit hypoglycemic effects and, therefore, potential therapeutic applications for managing diabetes. This assay is particularly beneficial in natural product research since it allows the isolation and identification of bioactive components that can inhibit α-amylase, further guiding the discovery of novel antidiabetic agents derived from natural sources.

In the α-amylase assay, extracts are typically mixed with a starch solution and the enzyme, after which the extent of starch breakdown is measured spectrophotometrically using indicators like iodine or chromogenic reagents that develop color upon reacting with the enzyme's products (McCue & Shetty, 2004). The degree of color intensity is inversely proportional to the extract's inhibitory effect on α-amylase, enabling researchers to quantify inhibition activity. Plants have been widely studied for such inhibitory activities, as many plant-derived compounds—such as polyphenols, flavonoids, and terpenoids—are known to inhibit carbohydrate-hydrolyzing enzymes. Studies have shown that several polyphenolic and flavonoid-rich extracts demonstrate strong α-amylase inhibition, which has encouraged further investigation into plants with traditional antidiabetic uses (Tundis *et al.*, 2010).

This assay is instrumental in bioassay-guided fractionation, as active fractions can be progressively isolated, purified, and tested to pinpoint individual compounds with the highest inhibitory effects. The use of α-amylase inhibition as a preliminary screen for antidiabetic properties not only accelerates the discovery of natural enzyme inhibitors but also provides a foundation for understanding the mechanisms by which these natural products act. Consequently, α-amylase inhibition assays contribute significantly to the development of plant-based antidiabetic agents, offering safer and potentially less toxic alternatives to synthetic drugs (Kazeem *et al.*, 2013). The assay's relevance in diabetes research has expanded its application across various plant species, making it a valuable tool in pharmacognosy and drug discovery.

1.1.15. *In vivo* Acute Oral Toxicity Study

The acute oral toxicity study is a fundamental step in evaluating the safety profile of crude plant extracts, especially when pursued through bioassay-guided isolation for

therapeutic potential. This study assesses the immediate toxic effects of an extract following a single oral dose, typically within 24 to 48 hours, though monitoring often extends up to 14 days to capture any delayed adverse effects (OECD, 2022). Such studies are crucial as they establish the lethal dose (LD_{50}) and identify any potential toxic effects that could affect organ systems or general health. For bioassay-guided isolation, assessing acute toxicity early on helps in determining safe dose ranges for the crude extract, subsequently guiding further fractionation and testing of individual bioactive compounds. Additionally, it provides valuable insight into potential adverse effects, ensuring that only fractions with acceptable toxicity profiles proceed through the isolation pipeline (Olson *et al.*, 2000).

Albino mice are often chosen for toxicity studies due to their well-documented physiological responses and manageable size, which make them suitable models for extrapolating data to other mammals, including humans (Parasuraman *et al.*, 2010). In a standard acute toxicity protocol, a series of doses is administered to groups of mice, and signs of toxicity—such as changes in behavior, physical appearance, weight, respiration, and mortality—are monitored. Mortality rates and clinical signs such as tremors, convulsions, and lethargy offer insight into the extract's potential hazards (Lorke, 1983). The LD_{50}, calculated from these observations, is a valuable parameter indicating the dose that is lethal to 50% of the test subjects, classifying the extract into categories of toxicity as per globally recognized standards (OECD, 2022). Additionally, sublethal doses allow researchers to observe any adverse effects on organs or tissues post-mortem, contributing to a better understanding of toxicity mechanisms.

Importantly, the acute oral toxicity study supports the broader scope of bioassay-guided isolation by establishing safe dose thresholds, thereby enabling researchers to pursue active fractions of the crude extract for *in vivo* efficacy studies without high risk of adverse reactions. Moreover, this preliminary safety assessment is indispensable in traditional medicine research, where crude extracts are used directly. Data from these studies also align with regulatory guidelines, supporting further pharmacological development and the standardization of traditional medicines (Bürger *et al.*, 2005). Thus, the acute toxicity study not only ensures the safety of bioactive fractions derived from plants but also adds credibility to their therapeutic applications in both traditional and modern medical frameworks.

1.1.16. Chromatography

Chromatography is a pivotal analytical and preparative technique extensively used for the separation, identification, and purification of complex mixtures in natural product research, pharmaceutical studies, and chemical analysis. The technique exploits differences in the physical or chemical interactions of compounds with a stationary phase and a mobile phase, allowing for precise separation of constituents in a mixture. For example, Thin Layer Chromatography (TLC) serves as a rapid and cost-effective method for preliminary compound identification and purity checks, while Column Chromatography enables the bulk isolation of bioactive compounds from plant extracts. Advanced techniques like Liquid Chromatography-Mass Spectrometry (LC-MS) combine separation and detection, offering unparalleled sensitivity and specificity for identifying and quantifying secondary metabolites such as alkaloids, flavonoids, and phenolics. Chromatographic methods have proven indispensable in natural product research, aiding in the discovery of novel bioactive compounds and ensuring their quality and reproducibility for therapeutic applications (Snyder *et al.*, 2010). Various chromatographic techniques were employed in this research that has been described below that were used to analyze and isolate compounds with precision. These methods were crucial for separating, identifying, and purifying bioactive molecules, enabling their detailed characterization and further evaluation.

1.1.16.1. Thin Layer Chromatography

Thin Layer Chromatography (TLC) is a simple, rapid, and highly effective technique used extensively in phytochemical and natural product research to separate, identify, and monitor compounds during fractionation and purification processes (Waksmundzka-Hajnos *et al.*, 2008). TLC is performed by applying a small sample of a crude extract onto a thin layer of adsorbent material, typically silica gel or alumina, coated on a glass, plastic, or aluminum plate. The plate is then placed in a solvent or solvent mixture, which moves up the plate by capillary action, carrying different compounds at varying rates based on their polarity and affinity to the stationary phase. The separated compounds form distinct spots on the TLC plate, allowing researchers to visualize individual components in a complex mixture, often under UV light or after treatment with specific reagents (Borowitz, 1966). In bioassay-guided isolation, TLC is particularly valuable for monitoring the progression of compounds from a crude

extract to fractions and eventually to isolated pure compounds. Starting from the crude extract, TLC helps determine the appropriate solvent system for column chromatography by identifying the ideal polarity to achieve adequate separation of compounds. This facilitates the systematic and efficient separation of crude mixtures into manageable fractions. Each fraction collected from column chromatography can then be monitored with TLC to confirm the separation of components and detect the presence of target compounds in specific fractions.

During repeated fractionation and purification, TLC serves as a reliable and cost-effective guide for optimizing conditions in each stage of column chromatography. By assessing Rf values (the ratio of distance traveled by the compound to that traveled by the solvent), researchers can trace compounds across various stages and modify the solvent gradient in the column to enhance separation as needed. Ultimately, TLC is instrumental in confirming the isolation of a pure compound when only one spot appears on the plate, corresponding to an individual, homogeneous substance, indicating that the compound has been effectively separated from other constituents (Harborne, 1998). Beyond its utility in guiding the isolation process, TLC can also provide insights into compound class, as different functional groups react uniquely to color-developing reagents, thereby aiding in preliminary identification. The effectiveness and simplicity of TLC make it indispensable in natural product chemistry, especially for guiding and streamlining the column chromatography process from initial crude extract stages to obtaining pure, bioactive compounds.

An extension of TLC is Preparative Thin Layer Chromatography (PTLC), used for the isolation and purification of specific compounds from complex mixtures. Unlike analytical TLC, which is typically used to monitor the presence and progress of compounds in a mixture, PTLC allows for the separation of larger quantities of a desired compound, making it highly useful for purifying fractions obtained from crude extracts in natural product isolation. In PTLC, thicker layers of adsorbent (usually silica gel) are applied to glass plates, allowing for greater compound loading and separation resolution. After development, the desired bands are scraped from the plate and the compounds are eluted with an appropriate solvent for further analysis or bioassays. PTLC is widely used as a cost-effective and efficient method in bioassay-guided isolation workflows, especially for plant extracts and other natural mixtures, as it

provides a straightforward path from crude extract to purify bioactive compounds (Harborne, 1998; Waksmundzka-Hajnos *et al.*, 2008).

1.1.16.2. Liquid Chromatography-Mass Spectrometry (LC-MS)

Liquid Chromatography-Mass Spectrometry (LC-MS) is a highly versatile analytical technique that combines the separation power of liquid chromatography with the molecular analysis capabilities of mass spectrometry, making it essential for analyzing complex samples and identifying unknown compounds (Allwood & Goodacre, 2010). LC-MS works by first separating compounds through liquid chromatography based on differences in their interactions with the mobile and stationary phases. These separated analytes are then directed into a mass spectrometer, where they are ionized and analyzed based on their mass-to-charge (m/z) ratios (Gross, 2017). Different ionization techniques enhance LC-MS applications, including Electrospray Ionization (ESI) and Atmospheric Pressure Chemical Ionization (APCI). ESI is well-suited for polar and larger molecules like proteins and peptides, offering gentle ionization to reduce fragmentation (Yamashita & Fenn, 1984). APCI, by contrast, works effectively on smaller, less polar molecules, ionizing them under a corona discharge at atmospheric pressure (Kostiainen *et al.*, 2003). Matrix-Assisted Laser Desorption/Ionization (MALDI) is particularly valuable for analyzing high molecular weight compounds and in imaging applications, where it visualizes the spatial distribution of molecules within tissues or other samples (Karas & Hillenkamp, 1988).

LC-MS configurations can also include Diode-Array Detection (DAD), resulting in LC-DAD-MS. This setup provides an additional layer of detection by measuring UV/visible absorbance spectra of compounds as they elute from the chromatography column, allowing preliminary structural insights before mass analysis. This type is widely used in plant compound analysis, pharmaceuticals, and environmental research for its sensitivity in detecting both non-UV active and UV-active compounds and its ability to provide more extensive compound profiling (Welz *et al.*, 2022). LC-DAD-MS is particularly useful in plant metabolomics, where compounds with similar mass spectra can be differentiated by their absorbance profiles.

Applications of LC-MS and its variations range across pharmacokinetics, where it monitors drugs and their metabolites, to environmental analysis for detecting pollutants at trace levels (Snyder *et al.*, 2010). This versatility makes LC-MS an essential tool for both qualitative and quantitative analysis, supporting a wide array of scientific and industrial fields by providing detailed information on the molecular composition and structure of complex mixtures.

1.1.16.3. Column Chromatography

Column Chromatography (CC) is a highly versatile and essential separation technique used extensively in chemistry and biochemistry, especially for purifying compounds in natural product isolation. In CC, a mixture of compounds is separated based on their relative affinities for a stationary phase, such as silica gel or alumina, and a mobile phase, typically a solvent mixture. Compounds with a stronger affinity for the stationary phase elute more slowly, while those with a greater affinity for the mobile phase elute faster, allowing separation. A critical factor for effective separation in CC is selecting the correct column size, which includes the column's diameter, height, and the amount of stationary phase used. A properly sized column ensures efficient compound separation, prevents overloading, and avoids tailing or broadening of compound bands, leading to higher purity and yield of isolated fractions (Harborne, 1998). The ratio of sample size to stationary phase, as well as the appropriate flow rate, are also key to achieving sharp and well-defined bands. The mobile phase composition is chosen based on the polarity and chemical properties of the target compounds, often beginning with a less polar solvent and gradually increasing polarity to optimize elution and separation. Column chromatography plays a crucial role in bioassay-guided isolation, allowing scientists to fractionate complex mixtures systematically, thereby simplifying and concentrating bioactive compounds at each step. By refining the purity of extracts across multiple stages, CC aids in progressing from a crude extract to fractions and, eventually, to a single, isolated compound with bioactivity. This systematic process of fractionation is essential for identifying active compounds in natural product research, pharmaceutical studies, and biochemistry (Waksmundzka-Hajnos *et al.*, 2008).

1.1.17. Evaluation of Anticholesterol Properties

Addressing hypercholesterolemia is vital, owing to the clear relationship between high levels of low-density lipoprotein cholesterol (LDL-C) in the plasma and a greater risk of cardiovascular disease (CVD). Cardiovascular diseases are one of the leading causes of mortality worldwide, and high LDL-C is a major contributor to the development of atherosclerosis, which leads to heart attacks, strokes, and other serious cardiovascular events. To address this, statins have become one of the most widely prescribed medications, proven to be highly effective in reducing cardiovascular risk by lowering LDL-C levels. Statins work by inhibiting the enzyme HMG-CoA reductase, which plays a key role in the biosynthesis of cholesterol in the liver. This results in a significant reduction of LDL-C levels, which in turn lowers the incidence of CVD (Catapano *et al.*, 2016).

Despite their efficacy, statins are not without drawbacks. A common issue associated with statin therapy is the development of side effects, the most notable being statin-induced myopathy, which causes muscle pain, weakness, and in some cases, rhabdomyolysis (a severe breakdown of muscle tissue). These side effects can lead to poor adherence to treatment or the need to reduce doses, which limits the effectiveness of the therapy. Additionally, a subset of patients may be statin-intolerant or unable to achieve desired LDL-C levels with statins alone, necessitating alternative or adjunctive therapies (Stroes *et al.*, 2015).

As a result, there is growing interest in exploring new approaches to manage hypercholesterolemia, particularly those that can efficiently reduce LDL-C levels while minimizing side effects. In addition to pharmacological interventions, clinical guidelines strongly emphasize lifestyle modifications, such as adopting a healthier diet, increasing physical activity, and reducing risk factors like smoking and obesity. However, in many cases, lifestyle changes alone may not be sufficient to achieve optimal cholesterol control, and the search for alternative or complementary treatments has intensified (Sahebkar *et al.*, 2016).

One promising area of research focuses on the role of nutrition and nutraceuticals in cardiovascular health. Nutritional strategies aimed at reducing LDL-C and other cardiovascular risk factors have gained significant attention. A rising trend has emerged

in the development of food supplements made with natural products known for their cholesterol-reducing properties. These supplements often contain plant-based compounds, phytochemicals, or other bioactive ingredients that have shown potential in improving lipid profiles. For example, fiber, plant sterols, and omega-3 fatty acids are well-known for their beneficial effects on cholesterol levels (Sahebkar *et al.*, 2016).

Among the natural compounds that have shown potential in managing hypercholesterolemia, berberine, an isoquinoline alkaloid, stands out as one of the most studied. Berberine is a compound found in several plants, including *Berberis* species, and has been used in traditional medicine for centuries. Modern research has demonstrated that berberine possesses a range of pharmacological activities, including antimicrobial, anti-inflammatory, and immunomodulatory effects. However, its role in cardiovascular health has garnered particular interest due to its ability to modulate lipid metabolism (Pirillo & Catapano, 2015).

Studies have shown that berberine has beneficial metabolic actions, such as reducing insulin resistance, promoting weight control, and, importantly, improving atherogenic dyslipidemia—a lipid disorder characterized by elevated LDL-C and triglycerides, and low high-density lipoprotein cholesterol (HDL-C) (Sahebkar *et al.*, 2016). One of the key mechanisms by which berberine lowers LDL-C is through its effect on hepatic LDL receptors. Berberine increases the expression of LDL receptors on liver cells by stabilizing the mRNA responsible for encoding these receptors. This leads to enhanced clearance of LDL-C from the bloodstream, thereby reducing overall cholesterol levels (Kong *et al.*, 2004).

Moreover, berberine has been shown to influence an alternative lipid-lowering pathway. Research has demonstrated that berberine can significantly reduce the expression of Proprotein Convertase Subtilisin/Kexin Type 9 (PCSK9) mRNA, as well as decrease the secretion of PCSK9 by HepG2 liver cells (Cameron *et al.*, 2008). This reduction in PCSK9 is crucial because PCSK9 plays a key role in cholesterol regulation by promoting the degradation of LDL receptors, which are responsible for clearing LDL cholesterol from the bloodstream. Berberine's ability to suppress PCSK9 production is linked to its effects on specific transcription factors, namely HNF1a (hepatocyte nuclear factor 1 alpha) and SREBP2 (sterol regulatory element-binding protein 2). These gene expression enhancers are involved in regulating PCSK9 gene expression, and

berberine's influence on them leads to the repression of PCSK9 transcription, thereby enhancing LDL receptor availability and contributing to cholesterol reduction (Li *et al.*, 2009). This mechanism adds to the potential of berberine as a promising alternative or complementary treatment for hypercholesterolemia, especially for patients who may not tolerate statins or need additional cholesterol-lowering interventions.

Despite its promise, research into berberine and related isoquinoline alkaloids as lipid-lowering agents is still in its early stages. While some studies have demonstrated berberine's clinical efficacy in reducing cholesterol levels and improving metabolic parameters, there is limited information on other structurally related alkaloids and their potential as hypolipidemic agents. Given the structural similarities between these alkaloids, it is possible that they may share similar pharmacological properties, including the ability to modulate lipid metabolism. As such, there is a growing interest in investigating these compounds as potential new therapeutic agents for the treatment of hypercholesterolemia.

The exploration of structure-activity relationships (SAR) among isoquinoline alkaloids could provide valuable insights into the development of novel drugs for hyperlipidemia. Understanding how different structural features of these molecules influence their biological activity could lead to the identification of more potent and selective compounds with fewer side effects than current therapies. This approach has the potential to yield new classes of lipid-lowering agents that could be used either as standalone treatments or in combination with existing drugs like statins.

In conclusion, the management of hypercholesterolemia remains a major challenge in the prevention of cardiovascular disease. While statins have been highly effective, their associated side effects and the need for additional lipid-lowering options have fueled the search for alternative therapies. Natural compounds like berberine, with its unique mechanisms of action, offer promising avenues for future research. Further investigation into berberine-related alkaloids and the development of new pharmacological agents based on these compounds could pave the way for innovative treatments that address both cholesterol management and cardiovascular risk reduction.

1.2. Rationale

Nature serves as a primary source for novel chemical compounds, particularly due to the intricate chemical defense systems plants develop. These systems lead to the formation of a broad spectrum of compounds with diverse structures. Natural products offer access to complex molecular structures that are often difficult or impossible to synthesize through other means. Nonetheless, only around 5-15% of higher plant species have been comprehensively studied, leaving a substantial number of terrestrial and marine species yet to be explored. Additionally, only a small fraction, under 1% of bacterial species and about 5% of all known fungi, has been identified. Microscopic organisms, in particular, hold significant potential for yielding novel bioactive compounds, as they thrive in extreme and competitive environments.

In the course of our research aimed at identifying new bioactivities for isoquinoline alkaloids, we focused on the exploration of the biodiversity within Nepal's plant kingdom, particularly the species *C. chaerophylla*, *C. govaniana*, and *C. casimiriana*. These species, despite their prevalence in the Nepalese region, have received limited scientific attention to date.

Numerous bioactivities, including anti-hepatitis, anti-amoebic, anti-tumor, and anti-liver cancer properties, have been observed in extracts, pure compounds, and alkaloids from diverse *Corydalis* species, in addition to analgesic, sedative, immune-enhancing, and liver-protecting actions (Sun *et al.*, 2006). Moreover, alkaloids of the tetrahydroprotoberberine type from *Corydalis* species have shown potential as a new group of ligands for dopamine receptors and as effective antimalarial compounds (Mo *et al.*, 2007; Wang & Mantsch, 2012; Wangchuk *et al.*, 2012). Despite the presence of certain tetrahydroprotoberberine-type alkaloids documented in *C. govaniana* (Mukhopadhyay *et al.*, 1987), the bioactivity of its pure compounds has yet to be explored. Furthermore, as of now, *C. casimiriana* Duthie and Prain remains unexplored in terms of phytochemical research. Similar is the case of *C. chaerophylla*.

This gap in research highlights the importance of further investigation into the new chemical and bioactive properties of these Nepalese species, which could lead to the discovery of novel therapeutic compounds.

1.3. Objectives

1.3.1. General Objective:

The primary objective of this research is to investigate the medicinal properties and potential therapeutic applications of *C. chaerophylla*, *C. govaniana*, and *C. casimiriana*.

1.3.2. Specific Objectives:

This research seeks to accomplish the following specific goals:

a) To extract phytochemicals from *C. chaerophylla*, *C. govaniana*, and *C. casimiriana* using sequential extraction with hexane, methanol, and chloroform.

b) To perform phytochemical screening, TPC and TFC on the extracts and analyze phytochemicals using LC-MS.

c) To conduct antimicrobial, antioxidant, antidiabetic, cytotoxic and acute oral toxicity activities of extracts.

d) To isolate pure/new compounds from these plant species.

e) To characterize the chemical composition of the purified compounds using a range of analytical spectroscopic approaches, including Mass Spectrometry, UV-VIS, FTIR, ^{1}H-NMR, ^{13}C-NMR, DEPT, as well as 2D-NMR techniques such as COSY, HMBC, HSQC, NOESY, etc.

f) To screen the isolated compound for their hypocholesterolemic property.

CHAPTER 2

2. LITERATURE REVIEW

2.1. Genus *Corydalis*

The *Corydalis* genus is widely recognized for synthesizing biologically active compounds, particularly sanguinarine, along with a group of anti-inflammatory benzylisoquinoline alkaloids (BIAs) known as cavidines. Some examples of these cavidines include apocavidine, dehydrocavidine, and dehydroapocavidine (Bhakuni & Chaturvedi, 1983). These alkaloids contribute to the medicinal value of *Corydalis* species, which are used in traditional medicine for various therapeutic purposes.

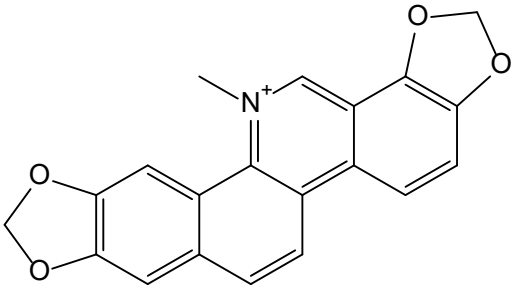

Sanguinarine

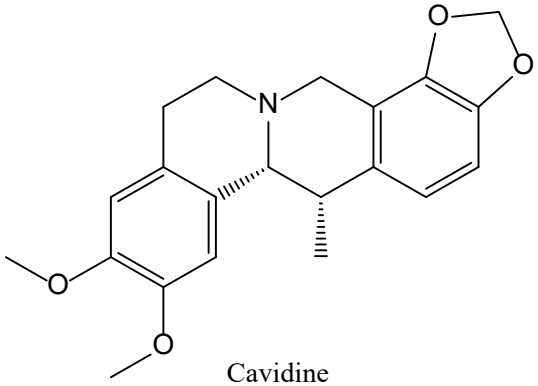

Cavidine

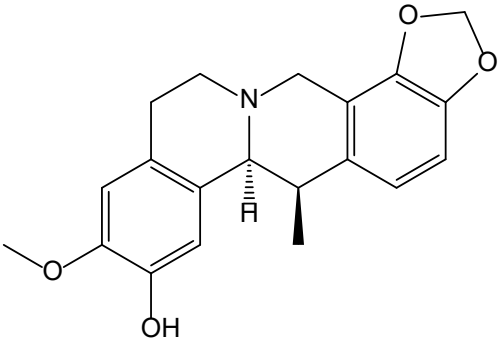

Apocavidine

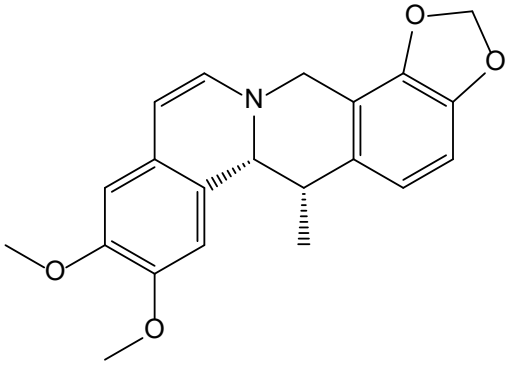

Dehydrocavidine

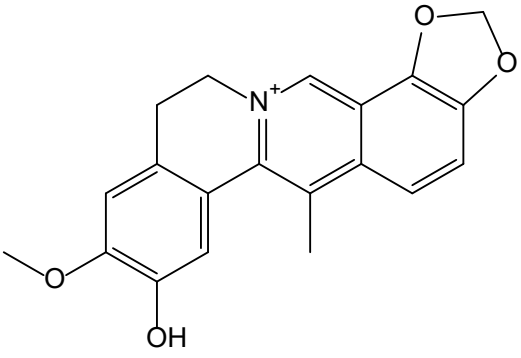

Dehydroapocavidine

In particular, an extract from *Corydalis edulis* (CE) has been discovered to stimulate insulin secretion by engaging a protein kinase C (PKC)-dependent signaling mechanism. Results from the study demonstrated that in HIT-T15 cells, CE exclusively activates novel (nPKCs) and atypical (aPKCs) isoforms, without influencing conventional PKCs (cPKCs). These findings are significant because they suggest that *C. edulis* extract could be a promising pharmaceutical substance for the treatment of type 2 diabetes mellitus (T2DM) in humans (Zheng *et al.*, 2017). This study highlights the potential of *Corydalis* species in managing metabolic disorders, particularly through novel signaling pathways that differ from those targeted by conventional treatments.

A chemical investigation of the aqueous extract of *Corydalis yanhusuo* tubers led to the isolation and structural elucidation of three pairs of trace enantiomeric hetero-dimeric alkaloids, (+)/(−)-yanhusamides A−C, featuring an unprecedented 3,8-diazatricyclo[5.2.2.02,6]undecane-8,10-diene bridged system. These structures were meticulously characterized using X-ray diffraction, comprehensive spectroscopic data analysis, and computational methods. Guided by a hypothetical biosynthetic pathway for these compounds, a gram-scale biomimetic synthesis of (±)-yanhusamides A was successfully achieved in three steps using photoenolization/Diels−Alder (PEDA) [4+2] cycloaddition. Bioactivity studies of these compounds revealed that they exhibited potent inhibition of nitric oxide (NO) production induced by lipopolysaccharides (LPS) in RAW264.7 macrophages. Further *in vivo* assays showed that oral administration of 30 mg/kg of (±)-yanhusamides A attenuated the severity of adjuvant-induced arthritis (AIA) in rats. Additionally, (±)-yanhusamides A induced a dose-dependent antinociceptive effect in the acetic acid-induced writhing assay in mice (Wang *et al.*, 2023). This study suggests that these newly discovered alkaloids from *Corydalis yanhusuo* possess significant anti-inflammatory and analgesic properties, making them potential candidates for the treatment of arthritis and related inflammatory conditions.

Further bioactivity-guided fractionation of *Corydalis yanhusuo* has resulted in the isolation of eight known isoquinoline alkaloids, including tetrahydropalmatine, isocorypalmine, stylopine, corydaline, columbamine, coptisin, 13-methylpalmatine, and dehydrocorybulbine. These compounds were further analyzed for their binding affinities to the dopamine D1 receptor. Among them, isocorypalmine exhibited the highest affinity with a Ki value of 83 nM. The study also explored the structure-affinity

relationships of these alkaloids, providing valuable insights into their potential neurological and pharmacological applications (Ma *et al.*, 2008). This research underscores the relevance of *Corydalis* alkaloids in neuropharmacology, particularly in modulating dopamine receptors, which are crucial in the treatment of conditions like Parkinson's disease and schizophrenia.

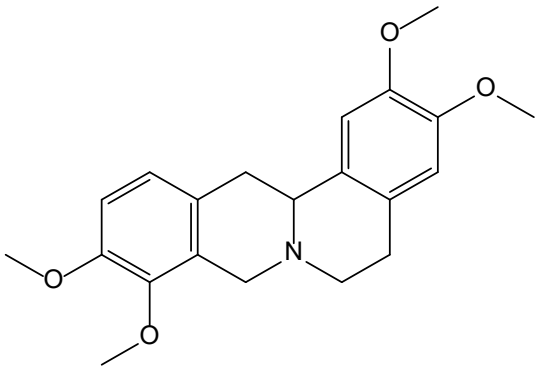

Tetrahydropalmatine

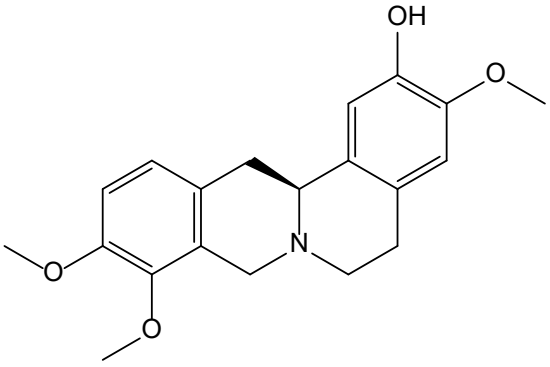

Isocorypalmine

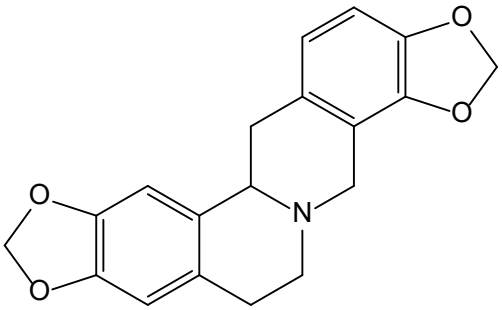

Stylopine

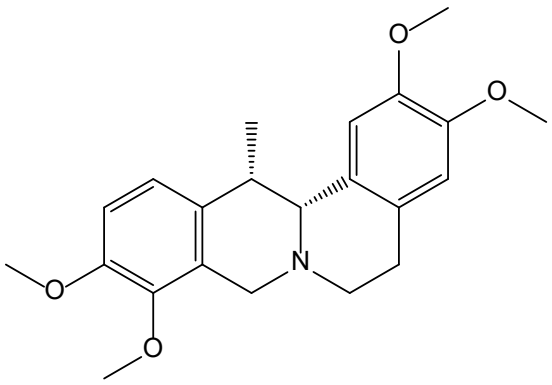

Corydaline

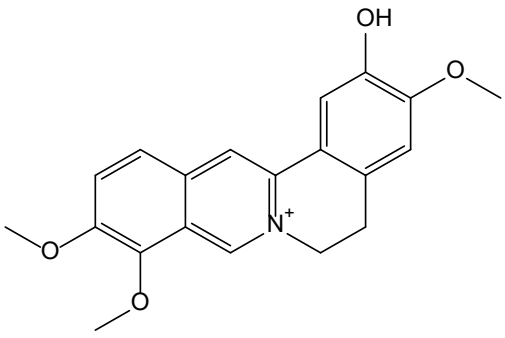

Columbamine

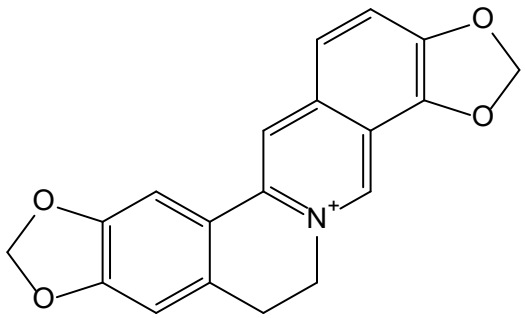

Coptisine

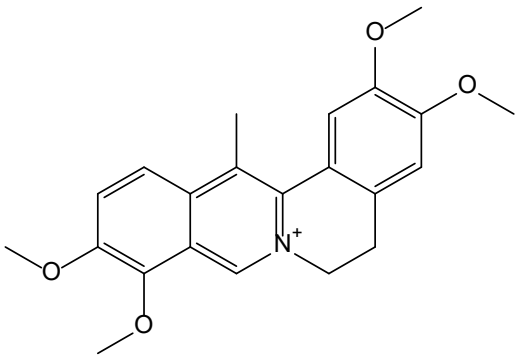

13-Methylpalmatine

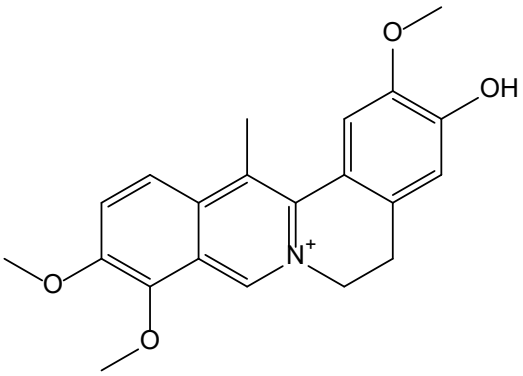

Dehydrocorybulbine

Research conducted on the species *Corydalis solida* subsp. *brachyloba*, found in Turkey, also demonstrated the isolation of several isoquinoline alkaloids. Among the compounds isolated were (+)-fumarophycine, (-)-corpaine, (-)-ophiocarpine, 13-methylcolumbamine, (±)-corydalidzine, (+)-fumaritine, (-)-africanine, and (-)-corybrachylobine. The compound (-)-corybrachylobine was particularly noteworthy as it was characterized as a new isoquinoline alkaloid. In addition to these, other minor alkaloids, including (-)-norjusiphine and corydaldine, were also isolated (Sener & Temizer, 1991). This study adds to the growing body of knowledge regarding the diversity of isoquinoline alkaloids found in *Corydalis* species, many of which have not been extensively studied for their bioactivities.

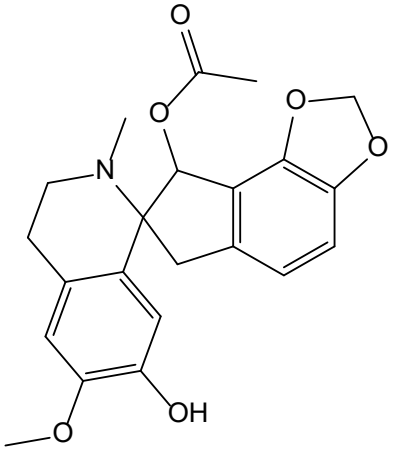

Fumarophycine

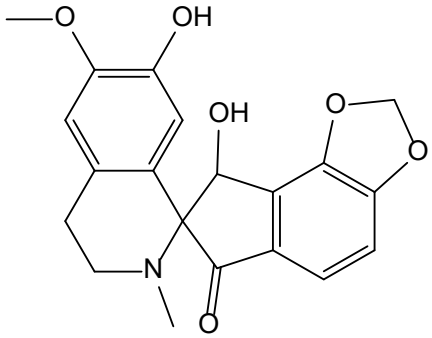

Corpaine

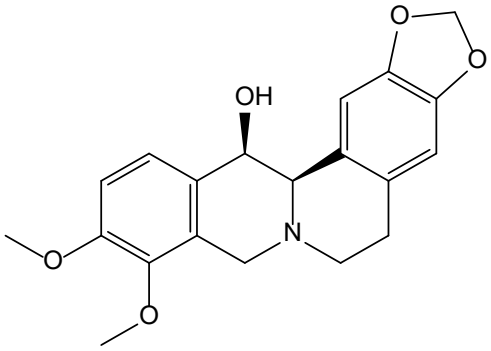

Ophiocarpine

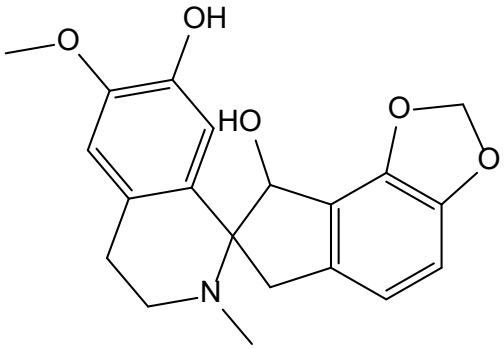

Fumaritine

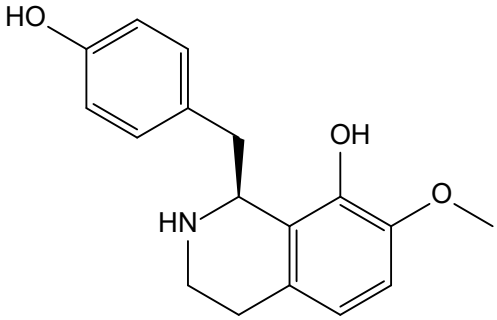

Norjusiphine

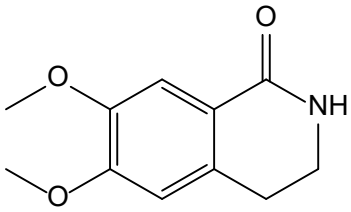

Corydaldine

Corydalis bracteata, a species found in Russia and widespread in Western and Eastern Siberia, has been the subject of recent phytochemical analysis. Despite its widespread distribution, its chemical composition had not been thoroughly studied until recently. The phytochemical analysis of its aerial parts led to the purification and structural analysis of several secondary metabolites, including an isoquinoline alkaloid—coptisine—and three flavonoids: rutin, quercetin-3-O-β-D-glucopyranoside, and kaempferol-3-O-β-D-glucopyranoside. These compounds were isolated using modern chromatographic methods and analyzed through NMR spectroscopy (Toporkova *et al.*, 2022). The identification of both alkaloid and flavonoid compounds in *Corydalis bracteata* underscores its potential as a source of bioactive substances, particularly given the medicinal properties associated with flavonoids and isoquinoline alkaloids.

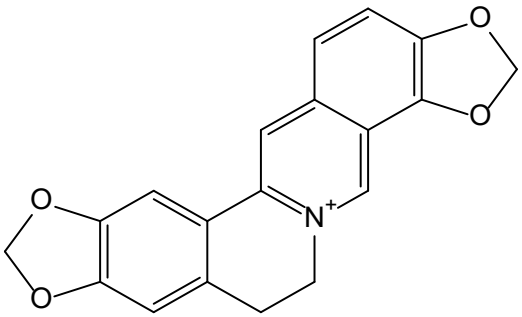

Coptisine

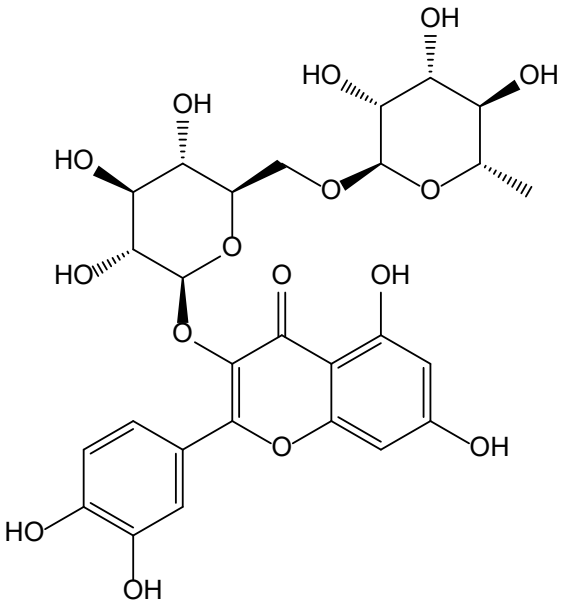

Rutin

In another study, *Corydalis adiantifolia*, a lesser-known species, was evaluated for various biological activities, including antifungal, antibacterial, insecticidal, cytotoxic, anticancer, and phytotoxic properties. The methanol extract and dichloromethane fraction of *Corydalis adiantifolia* showed moderate inhibition against the fungus *Aspergillus flavus* and some activity against HeLa cell lines, although the antibacterial activity was found to be non-significant. Phytochemical screening of the plant revealed the presence of several bioactive compounds, including alkaloids, flavonoids, saponins, diterpenes, and triterpenoids. Further chemical isolation led to the identification of three compounds: 8-acetonyldihydrosanguinarine, β-sitosterol, and β-sitosterol-β-D-glucoside, which were characterized using spectroscopic methods (Ali *et al.*, 2019). This study, being the first of its kind on *Corydalis adiantifolia*, provides foundational knowledge about its phytochemistry and biological activities, opening avenues for further exploration.

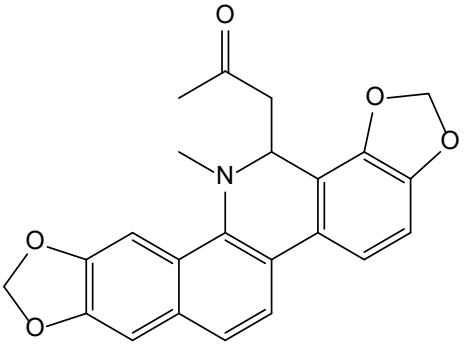

8-acetonyldihydrosanguinarine

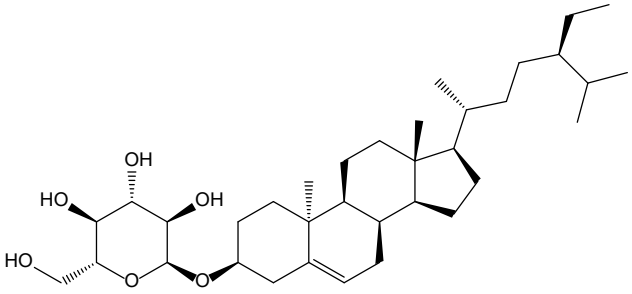

β-sitosterol-β-D-glucoside

The isoquinoline alkaloids found in *Corydalis hendersonii*, a species commonly used in Tibetan medicine, have been explored for their potential anti-gastric cancer properties. This research identified 14 alkaloid compounds, including two previously unknown natural products, that exhibited significant anti-cancer activity. One of the new compounds was found to effectively inhibit gastric cancer cell proliferation, induce G2/M phase cell cycle arrest, and promote apoptosis by modulating the Bax/Bcl-2 ratio, cytochrome c release, and caspase-9/3 activation. Additionally, this compound was shown to inhibit the PI3K/Akt/mTOR signaling pathway, which is crucial in the progression of many cancers. *In vivo* studies in MGC-803 xenograft mice confirmed the compound's anti-cancer efficacy (Luo *et al.*, 2022). This study highlights the therapeutic potential of *Corydalis hendersonii* alkaloids in the development of new anti-cancer agents, particularly for gastric cancer.

A chemical investigation of *Corydalis balansae* resulted in the isolation of three previously undescribed compounds and 17 known compounds. Among the newly discovered compounds were two lignanamide dimers and a spiro [benzofuranone-benzazepine] skeleton, which was identified in *Corydalis* for the first time. The new compounds were characterized using 1D/2D NMR, UV, and IR spectroscopy, with absolute configurations determined by X-ray diffraction and electronic circular dichroism (ECD) calculations. Bioactivity assays revealed that compound 2 exhibited significant antitumor activity against MGC-803 gastric cancer cells, inducing S-phase cell-cycle arrest and apoptosis by up-regulating PARP1, caspase-3, and Bax while down-regulating Bcl-2 (Luo *et al.*, 2022). This study demonstrates the potential of *Corydalis balansae* as a source of novel antitumor compounds, providing a basis for future drug development.

In conclusion, the *Corydalis* genus offers a rich reservoir of isoquinoline alkaloids with diverse biological activities, including anti-inflammatory, antidiabetic, neuropharmacological, and anticancer properties. The ongoing research into various *Corydalis* species continues to uncover new bioactive compounds, many of which hold significant potential for therapeutic applications across a range of diseases. The unique chemical structures and diverse pharmacological effects of *Corydalis* alkaloids make them promising candidates for drug discovery and development in modern medicine.

2.2. *Corydalis chaerophylla* D.C.

Previous research has shown that the crude extract of *C. chaerophylla* underwent isolation processes that led to the discovery of a new alkaloid, named chaerophylline. In addition to this novel compound, several known alkaloids were also identified, including (-)-corypalmine, berberine chloride, (-)-isocorypalmine, (-)-corydalmine, and (+)-bicuculline (Jha *et al.*, 2009). These alkaloids are known for their wide range of biological activities, making *C. chaerophylla* an important species for further pharmacological studies.

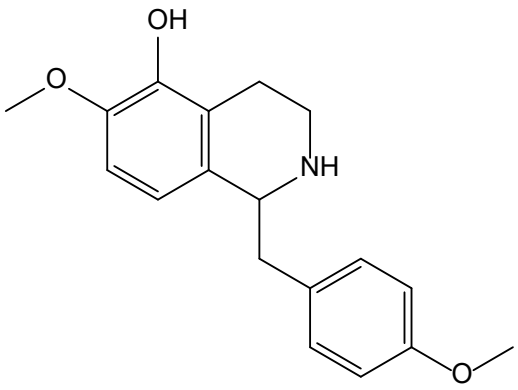

Chaerophylline

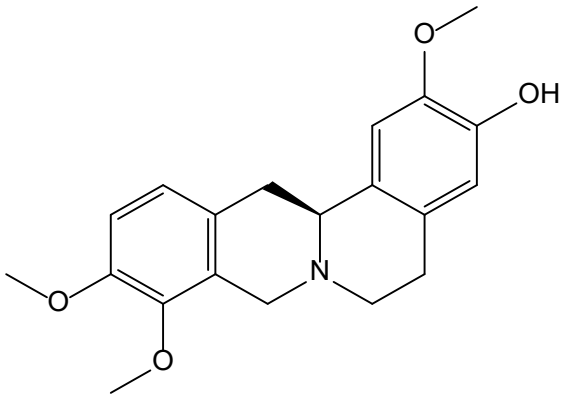

Corypalmine

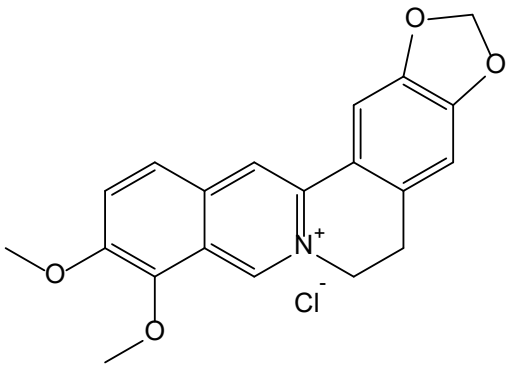

Berberine Chloride

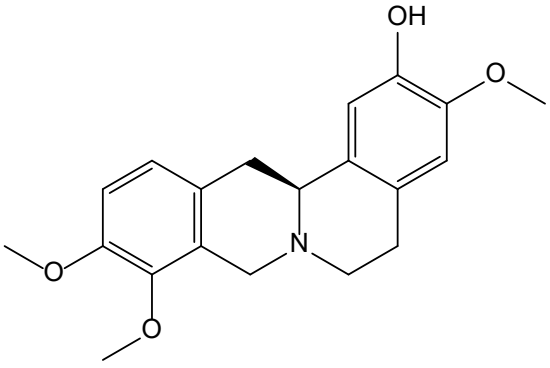

Isocorypalmine

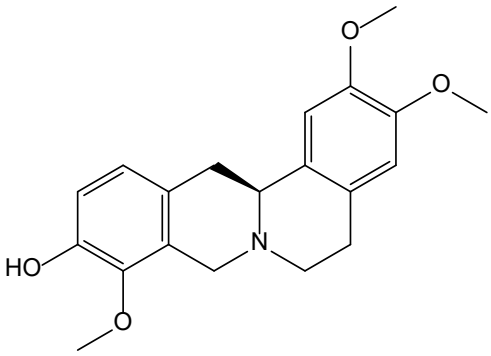

Corydalmine

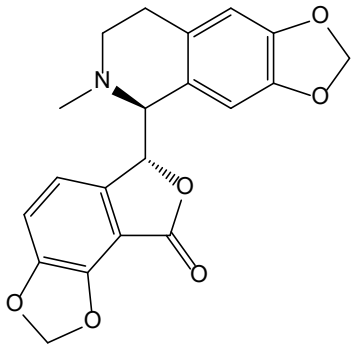

Bicuculline

In a subsequent study, the antifungal properties of chaerophylline, (-)-corydalmine, and (-)-isocorypalmine were evaluated. These compounds were tested against the spore germination of various fungi, including *Alternaria brassicae*, *Alternaria brassicicola*, *Alternaria solani*, *Helminthosporium penniseti*, *Helminthosporium* species, *Heterosporium* species, *Curvularia maculans*, *Curvularia penniseti*, and *Curvularia pallescens*. Among the tested compounds, chaerophylline exhibited strong inhibitory effects on spore germination in most of the fungal species tested. Its antifungal efficacy was assessed at concentrations of 50, 100, 200, 500, and 1000 ppm, with complete suppression of spore germination observed at the highest concentration (1000 ppm) in several fungal species. Interestingly, some fungi were sensitive to chaerophylline even at lower concentrations, demonstrating the broad-spectrum antifungal potential of this alkaloid (Tuli *et al.*, 2001).

Similarly, (-)-corydalmine showed significant antifungal activity, effectively inhibiting spore germination across all tested fungal species at concentrations ranging from 100 to 1500 ppm. At the highest concentration (1500 ppm), it demonstrated inhibition against all fungi, with remarkable sensitivity towards *Curvularia lunata* even at a low concentration of 250 ppm (Basha *et al.*, 2007). This highlights the potency of (-)-corydalmine as an antifungal agent, particularly against species of the *Curvularia* genus.

Additionally, (-)-isocorypalmine was evaluated for its antifungal activity and demonstrated statistically significant inhibition of spore germination at a concentration of 100 µg/ml. It was particularly effective against *Curvularia penniseti*, *Curvularia* species, and *Colletotrichum gloeosporioides* (Sahni *et al.*, 2004). This suggests that (-)-isocorypalmine, like chaerophylline and (-)-corydalmine, has promising antifungal

properties, making it a potential candidate for the development of natural antifungal treatments.

Overall, these studies highlight the significant antifungal potential of *C. chaerophylla* alkaloids, particularly in inhibiting spore germination across a variety of fungal species. These findings suggest that chaerophylline, (-)-corydalmine, and (-)-isocorypalmine could be further explored as natural antifungal agents, offering potential applications in agriculture and medicine for controlling fungal infections.

2.3. *Corydalis govaniana* Wall.

In a series of studies on *C. govaniana*, several alkaloids were isolated, including a newly discovered compound, govaniadine, along with three known tetrahydroprotoberberine-type alkaloids: caseadine, caseamine, and protopine. These alkaloids were subjected to enzyme inhibition assays, revealing significant urease inhibition. The IC_{50} values for govaniadine, caseadine, caseamine, and protopine were 20.2 ± 3.6 μM, 38.9 ± 2.8 μM, 66.7 ± 1.2 μM, and 54.1 ± 1.2 μM, respectively, demonstrating urease inhibitory activity comparable to the standard inhibitor acetohydroxamic acid (IC_{50} = 42.0 μM). However, none of these compounds exhibited inhibitory effects against α-chymotrypsin. This was the first study to report urease inhibition by tetrahydroprotoberberine-type alkaloids, highlighting their potential for treating urease-related conditions (Shrestha *et al.*, 2013).

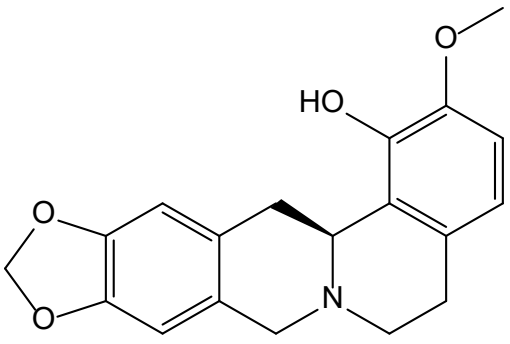

Govaniadine

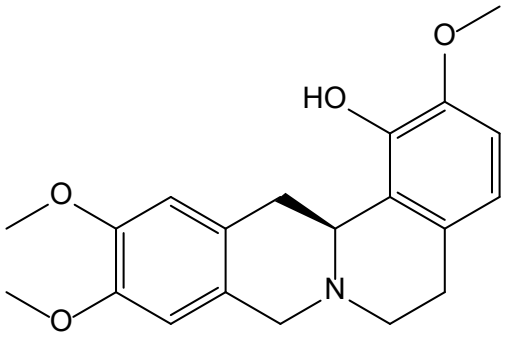

Caseadine

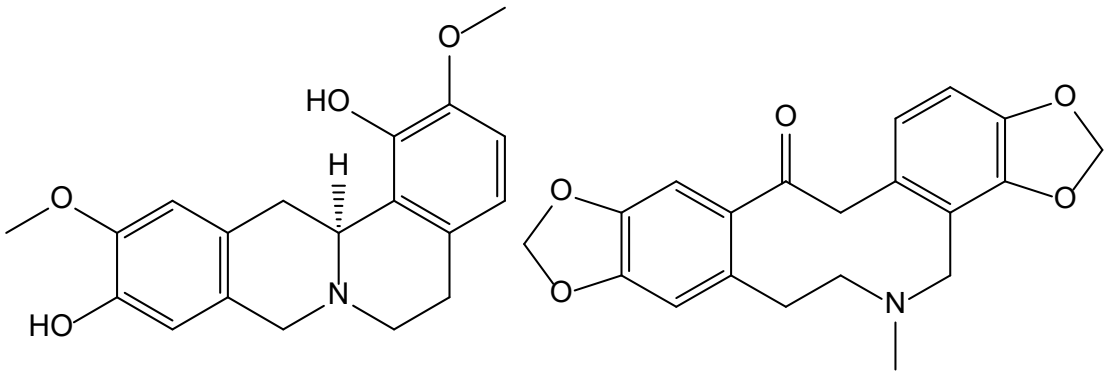

Caseamine Protopine

Another study focused on evaluating the leishmanicidal activity of govaniadine and caseadine from *C. govaniana* These alkaloids were tested against *Leishmania amazonensis* promastigotes, and their cytotoxicity was assessed on J774 macrophage cells. Govaniadine exhibited potent leishmanicidal activity, with an IC_{50} of 0.18 µg/mL, comparable to the standard drug amphotericin B (IC_{50} = 0.20 µg/mL) (Callejon *et al.*, 2014). Govaniadine also displayed significant antileishmanial effectiveness, with an IC_{50} of 27.0 ± 0.2 µg/mL against *Leishmania major*, suggesting its potential as a therapeutic agent for treating leishmaniasis (Shrestha & Adhikari, 2017a).

Further investigation into govaniadine revealed its analgesic properties. In analgesic tests using writhing and hot-plate assays, govaniadine demonstrated a significant reduction in acetic acid-induced writhing in mice in a dose-dependent manner (1.25–5.0 mg/kg, intraperitoneally). It also showed an analgesic effect in the hot-plate test at doses of 2.5 and 5 mg/kg, at all-time points (30, 60, 90, and 120 minutes). Molecular docking studies indicated that govaniadine binds to the COX-2 enzyme, and its analgesic effect was significantly antagonized by naloxone, suggesting that its mechanism of action may involve both COX-2 inhibition and interaction with the opioid system. No toxic effects were observed in mice up to a dose of 20 mg/kg over a 24-hour period (Muhammad *et al.*, 2015).

In addition to its analgesic and leishmanicidal properties, govaniadine was evaluated for its pharmacokinetic properties. *In vitro* metabolism studies using rat and human liver microsomes identified several metabolites, including O-demethylated, di-hydroxylated, and mono-hydroxylated derivatives of govaniadine. A pharmacokinetic study conducted in rats after intravenous administration showed that govaniadine follows a two-compartment model, with a high distribution rate constant and an

elimination half-life of approximately 55 minutes. The compound exhibited 96.1% plasma protein binding. These results provide important insights into the metabolic behavior and pharmacokinetic profile of govaniadine, laying the groundwork for its potential development as a drug candidate (Marques *et al.*, 2016).

In the context of cancer treatment, govaniadine has shown promising cytotoxic effects against human breast cancer (MCF-7) cells. In an SRB assay, govaniadine exhibited dose- and time-dependent cytotoxicity against MCF-7 cells, while showing lower toxicity toward normal human breast cells (MCF-10A). The compound induced apoptosis in MCF-7 cells by upregulating Bax, p53, and survivin mRNA expression. Flow cytometric analysis confirmed apoptosis via Annexin V and PI staining. Additionally, govaniadine-treated MCF-7 cells exhibited increased levels of reactive oxygen species (ROS) and glutathione S-transferase (GST), along with decreased levels of glutathione (GSH), indicating oxidative stress as a potential mechanism for apoptosis. Caspase-7 activation was also observed in govaniadine-treated cells, further supporting its role as a potent inducer of apoptosis (Sivakumaran *et al.*, 2018).

Given its broad range of biological activities, including antinociceptive, anti-urease, leishmanicidal, and cytotoxic effects, govaniadine has become a subject of further pharmacological interest. Studies evaluating its effects on human hepatoma carcinoma (HepG2) and human embryonic kidney (HEK-293T) cell lines revealed a reduction in cellular viability at concentrations ranging from 30 to 100 µM and 70 to 100 µM, respectively. However, the cytotoxic effects of govaniadine were less pronounced compared to positive controls such as T-2 toxin and camptothecin. Additionally, permeability studies using the human colon carcinoma cell line (Caco-2) indicated that govaniadine crosses the cell monolayer through passive diffusion, making it a potential candidate for further investigation in drug delivery (Marques *et al.*, 2020).

Liver diseases, including hepatic carcinoma, are a major global health issue, and natural products like govaniadine offer promising therapeutic potential. In a study investigating the hepatoprotective effects of govaniadine, along with other alkaloids from *C. govaniana* (caseadine, caseamine, and protopine), significant antioxidant activity was observed. Govaniadine demonstrated 92.2% inhibition of free radicals, comparable to propyl gallate (90.3%). In a CCl_4-induced liver injury model in rats, govaniadine significantly reduced serum enzyme levels (alanine aminotransferase, aspartate

transaminase, and alkaline phosphatase) and restored the liver's antioxidant defenses. Histopathological examination revealed a marked reduction in liver damage, and immunohistochemistry showed that govaniadine inhibited the activation of hepatic macrophages, further reducing inflammation. Additionally, govaniadine exhibited anti-inflammatory activity in a carrageenan-induced paw edema assay, demonstrating its potential as a hepatoprotective and anti-inflammatory agent (Jahan *et al.*, 2021).

Overall, govaniadine, a tetrahydroprotoberberine-type alkaloid isolated from *C. govaniana*, has demonstrated a wide array of biological activities, including anti-urease, leishmanicidal, cytotoxic, antioxidant, hepatoprotective, and anti-inflammatory effects. Its promising pharmacological profile makes it a strong candidate for further research in the development of new therapeutic agents.

2.4. *Corydalis casimiriana* Duthie and Prain ex Prain

Not much studies have been conducted on *C. casimiriana*. However, it has long been used in traditional medicine for treating syphilis, scrofula, skin infections, diarrhea, and dysentery. A study of *C. casimiriana* along with *C. govaniana*, govaniadine and six other alkaloids—caseadine, caseamine, protopine, stylopine, apocavidine, and fagarine I—were isolated. Among these, caseamine showed the strongest antioxidant activity, with an IC_{50} value of 40.8 ± 0.9 µM, while govaniadine and caseadine displayed moderate antioxidant activity, with IC_{50} values of 83.7 ± 1.7 µM and 75.7 ± 0.9 µM, respectively (Shrestha & Adhikari, 2017b). The β-glucuronidase inhibitory potential of govaniadine was also evaluated, with an IC_{50} of 41.9 ± 3.1 µM, surpassing the standard inhibitor D-saccharic acid 1,4-lactone (IC_{50} = 45.8 µM). Caseadine also exhibited significant inhibition of β-glucuronidase, with an IC_{50} of 71.6 ± 4.3 µM. This suggests that govaniadine and caseadine could be further explored for their potential in preventing intestinal tumors, which are linked to β-glucuronidase activity (Shrestha & Adhikari, 2017c).

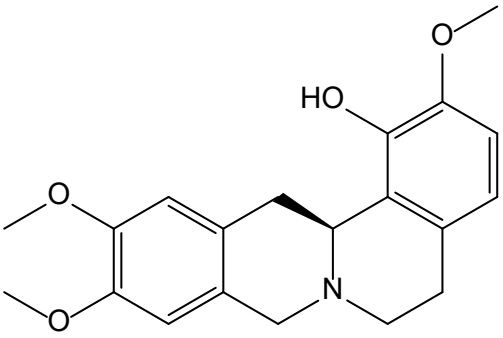

Caseadine

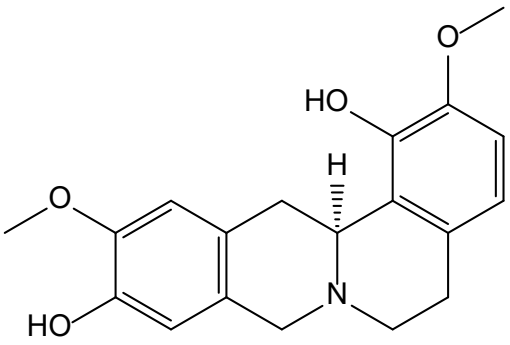

Caseamine

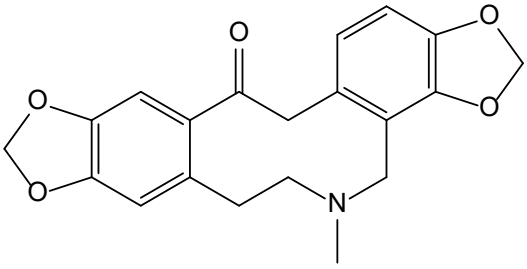

Protopine

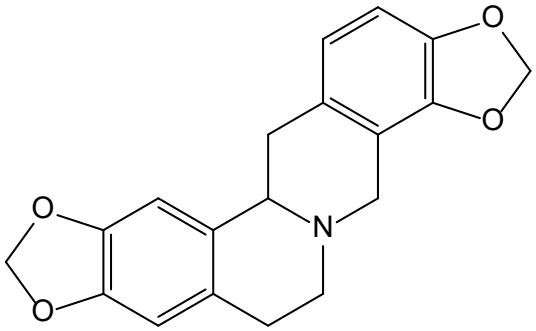

Stylopine

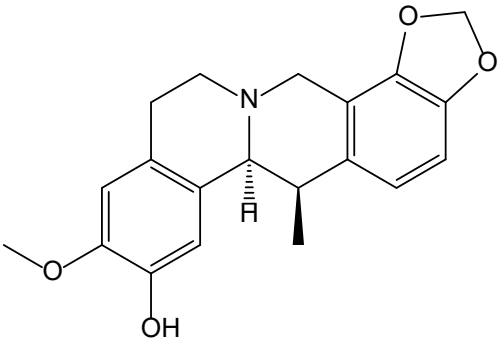

Apocavidine

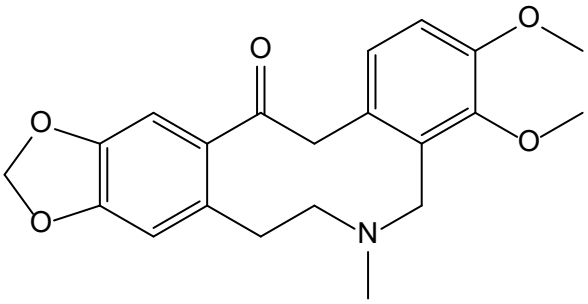

Fagarine I

CHAPTER 3

3. MATERIALS AND METHODS

3.1. Plant Materials

The entire *C. chaerophylla* plant was sourced from Phulchowki, Lalitpur, Nepal, (latitude/longitude: 27°34'47.1"N 85°23'34.5"E) at an elevation of 2400 to 2700 meters, while *C. govaniana* and *C. casimiriana* were sourced from higher elevations in Langtang, Rasuwa, Nepal, (latitude/longitude: 28°12'34.8"N 85°37'12.0"E) between 3400 and 3800 meters on the month of September 2019. The identification of these plant species was carried out by Mr. Ganga Datt Bhatt, a research officer, National Herbarium and Plant Laboratories in Godawari, Lalitpur, Nepal and voucher specimens (901, 902, and 903) were prepared and deposited.

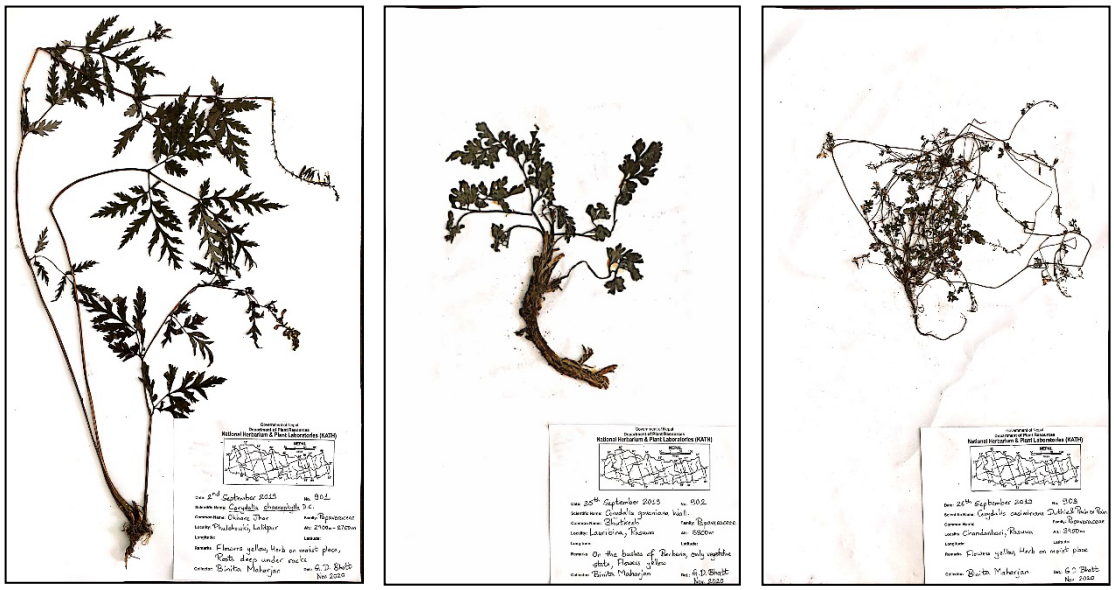

(a) (b) (c)

Figure 7: Herberium specimen of (a) *C. chaerophylla*, (b) *C. govaniana* and (c) *C. casimiriana*

3.2. Extraction and Isolation

The entire air-dried plant of *C. chaerophylla* (10 kg) was powdered and subjected to cold percolation using hexane (20 L). The hexane portion was first separated, and then the remaining plant residue was extracted using 15 liters of methanol. This methanol extract was concentrated under reduced pressure using a rotary evaporator, yielding 900 g of concentrated extract. This extract was then stirred with a 7% citric acid solution

and subsequently filtered. Following neutralization with ammonia (NH_3) solution, the filtrate was further subjected to extraction with chloroform, resulting in 140 g of chloroform extract. Each of these extracts (hexane, methanol, and chloroform) underwent preliminary phytochemical screenings and bioactivity tests. For further compound isolation, the 120 g chloroform extract was applied to a silica gel column for chromatography on a silica gel column (dimensions: 70 cm × 10 cm). The solvent system employed was a mixture of ethyl acetate and hexane (0.5/95.5), gradually increasing the ratio of ethyl acetate to hexane (5/95 and 10/90). Fractions were monitored using Thin Layer Chromatography (TLC), and based on the observed spots, the fractions were pooled into three main groups: Fraction A (16 g), Fraction B (22 g), and Fraction C (24 g). The solvent system was later modified to chloroform/methanol (90/10), resulting in two additional fractions: Fraction D (9 g) and Fraction E (32 g). Further purification of Fraction B was carried out by eluting with a 30% ethyl acetate/hexane solvent system. The resulting eluents were pooled and again passed through a column using 20% ethyl acetate/hexane, yielding white crystals of bicuculline (910 mg). Similarly, Fraction C was further processed using 40% ethyl acetate/hexane, which produced orange crystals of 8-hydroxydihydrosanguinarine (5 mg), dihydrosanguinarine (5 mg), and additional compounds like Corydalmine (10 mg) and Scoulerine (33 mg), both pale yellow crystals, using a 50% ethyl acetate/hexane solvent system. Fraction E showed significant spots under TLC analysis and was subjected to column chromatography using a smaller silica gel column (20 cm × 5 cm). The solvent system employed was dichloromethane (DCM)/methanol (95/5) with a few drops of NH_3 solution, gradually increasing the polarity. This process yielded 11 sets of fractions (E1-E11). Further analysis yielded four new compounds: Compound 1 (60 mg) from Fraction E9 and Compound 2 (30 mg) from Fraction E6 using a DCM/methanol solvent ratio of 8:2. Additionally, Compound 3 (600 mg) and Compound 4 (500 mg) were isolated from E3 and E4 fractions, respectively, using a DCM/methanol ratio of 9:1.

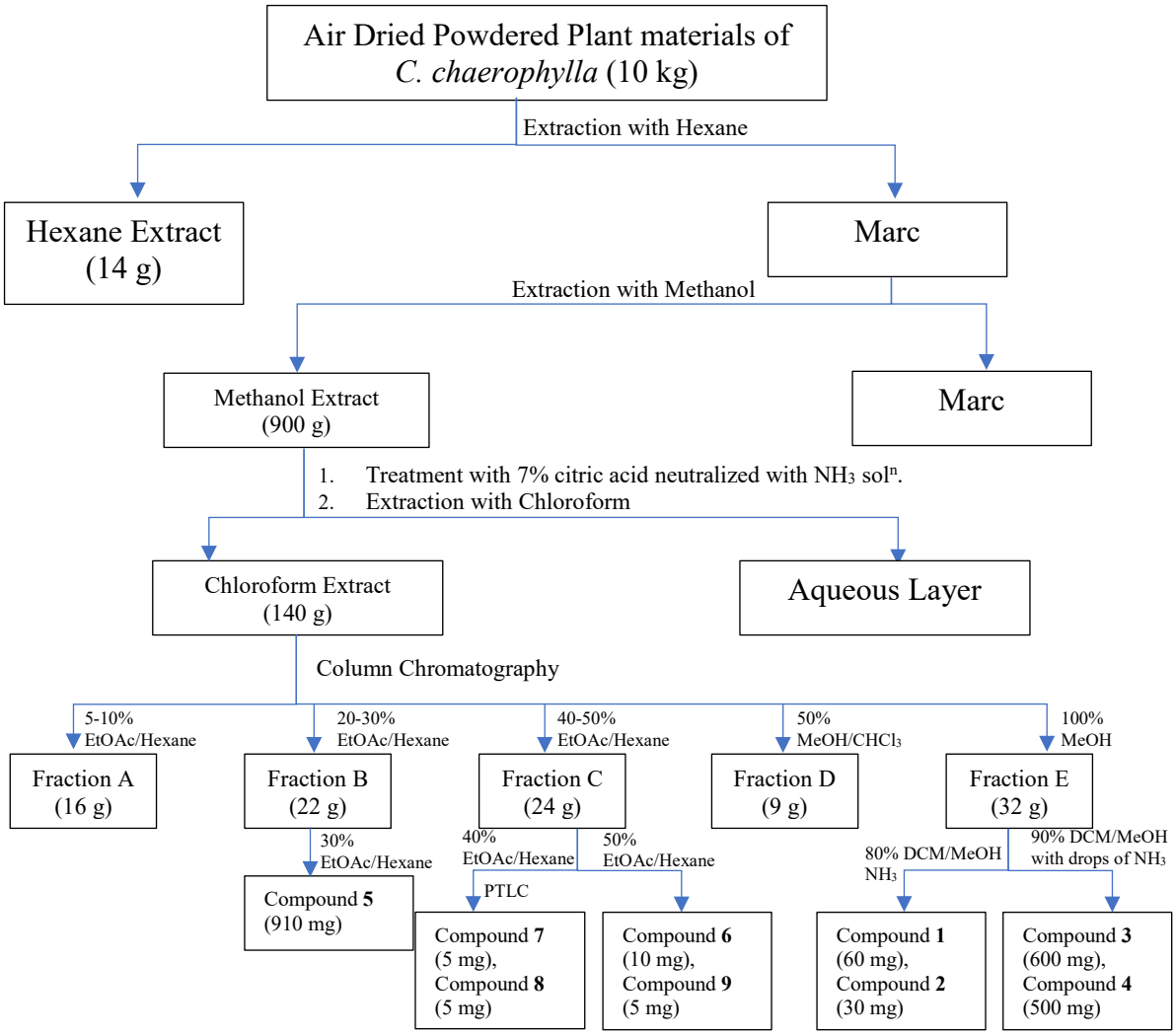

Scheme 1: Research process for the extraction, isolation and bioactivities of *C. chaerophylla*

Similarly, the entire plant of *C. govaniana* (3 kg) was processed using the same extraction method. This yielded 190 g of methanol extract, which underwent treatment with 7% citric acid, was neutralized with NH_4OH before being subsequently extracted with chloroform, yielding a 33 g chloroform fraction. This fraction was further purified through column chromatography on a silica gel column, employing an acetone/hexane solvent system with a gradual increase in polarity and a few drops of diethylamine. The pooled fractions from 10% acetone/hexane were passed again through silica gel chromatography with a 5% acetone/hexane and diethylamine solution, resulting in 838 mg of govaniadine in the form of white needle-like crystals.

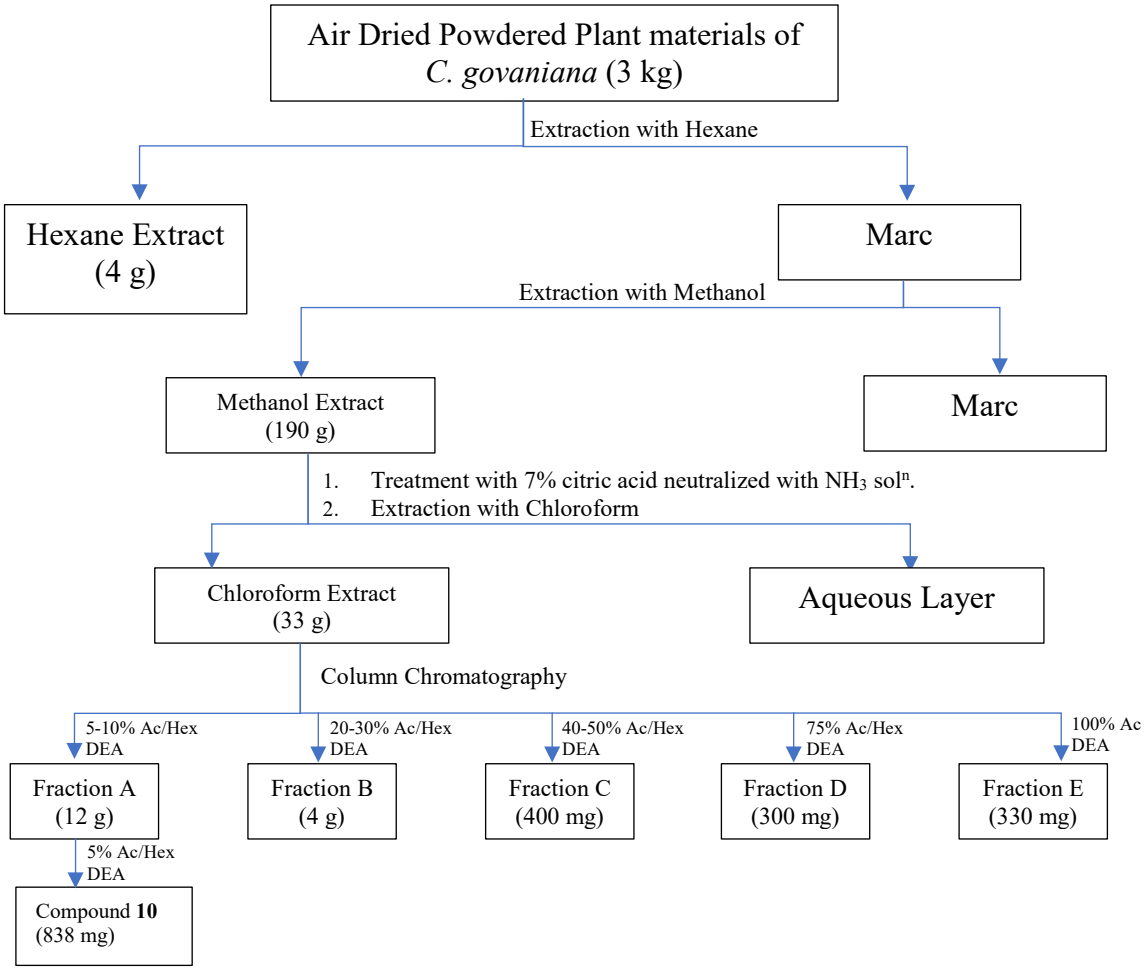

Scheme 2: Research process for the extraction, isolation and bioactivities of *C. govaniana*

The same extraction process was repeated for *C. casimiriana* (2.5 kg), producing 180 g of methanol extract and 28 g of chloroform extract. The chloroform extract was then purified using column chromatography with acetone/hexane and a few drops of diethylamine. Eluents obtained from a 10% acetone/hexane system were pooled and subjected to further purification using a 4% acetone/hexane solvent system. The isolation of 37 mg of pale-yellow crystals of stylopine was achieved through this approach. Furthermore, pooled fractions from the 15% acetone/hexane phase were processed further to obtain 76 mg of adlumidine using 3% acetone/hexane and 355 mg of adlumine with 6% acetone/hexane, both in the form of pale-yellow crystals.

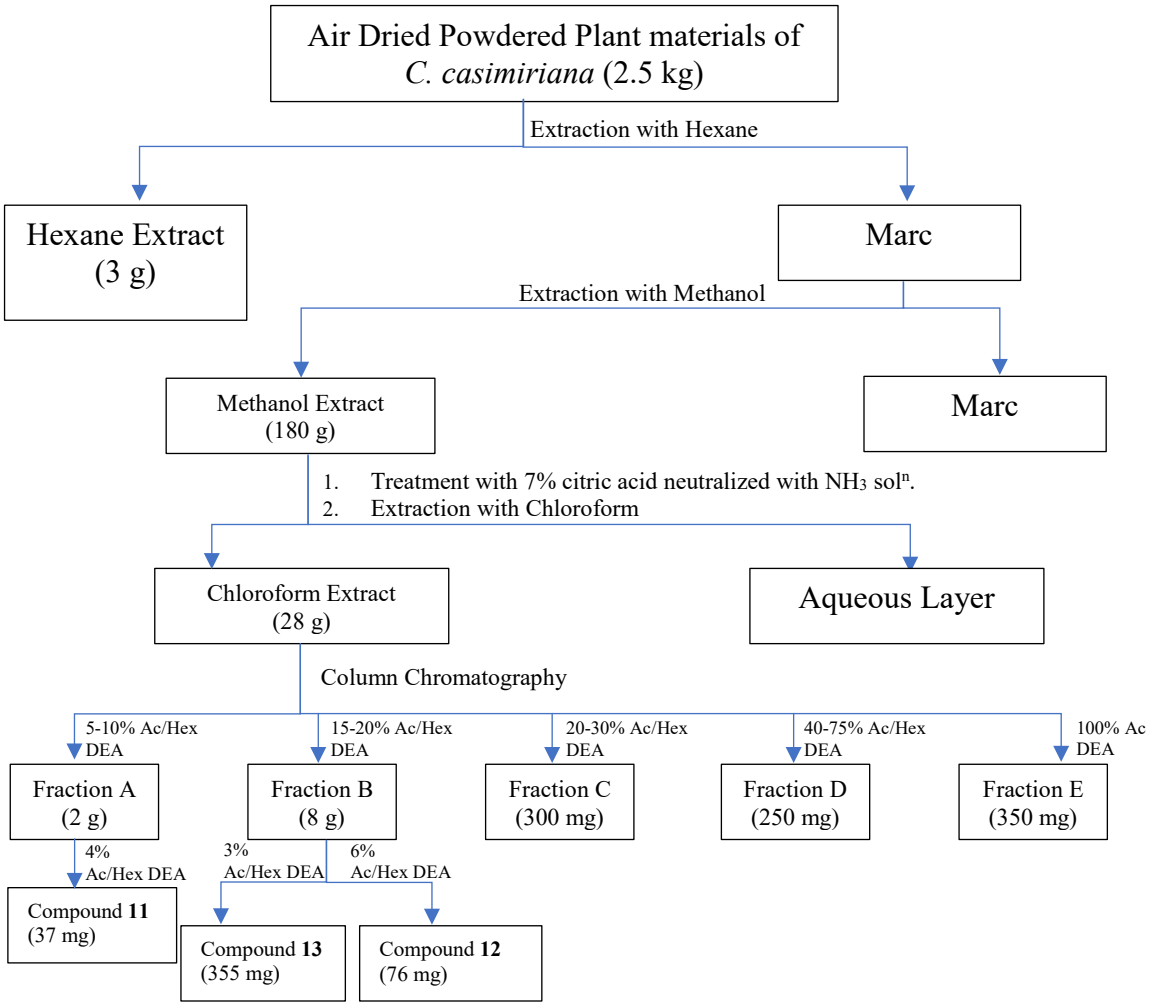

Scheme 3: Research process for the extraction, isolation and bioactivities of *C. casimiriana*

The structural elucidation of the isolated compounds was accomplished using a combination of advanced spectroscopic techniques. These included 1D and 2D Nuclear Magnetic Resonance (NMR) spectroscopy for detailed structural and connectivity analysis, Infrared (IR) and Ultraviolet (UV) spectroscopy for functional group identification and electronic transitions, respectively. Additional methods such as polarimetry and mass spectrometry were employed to determine stereochemistry and molecular mass, ensuring a comprehensive understanding of the compounds' structures.

3.3. Spectroscopic Characterization and Structural Elucidation

All NMR (Nuclear Magnetic Resonance) spectra were acquired using a Bruker 400 MHz spectrometer. This device was set to operate at 400.11 MHz for ^{1}H and 100 MHz for ^{13}C, enabling detailed analysis of the molecular structures. To obtain comprehensive data, multiple NMR techniques were employed, including ^{1}H-NMR, ^{13}C-NMR, COSY

(Correlation Spectroscopy), HMBC (Heteronuclear Multiple Bond Correlation), HSQC (Heteronuclear Single Quantum Coherence), and NOESY (Nuclear Overhauser Effect Spectroscopy). These experiments were conducted using standard Bruker pulse sequences, with optimal adjustments made to pulse width (p1), relaxation delay (d1), and mixing times to achieve the best results in terms of data resolution and reliability.

Mass spectrometry data, including fragmentation patterns of the compounds, were obtained using a Varian 500MS Ion Trap. For high-resolution electrospray ionization mass spectrometry (HR-ESI-MS), the spectra were acquired using a Waters Xevo G2 QTof mass spectrometer, providing precise mass measurements critical for molecular formula confirmation. Infrared (IR) spectra were recorded with a PerkinElmer FTIR spectrometer, which helped to identify functional groups present in the compounds.

Optical rotation measurements, which provide information about the chiral nature of the compounds, were performed using a Jasco Digital 2000 polarimeter. Additionally, circular dichroism (CD) spectra were captured with a Jasco J-2000 CD spectropolarimeter.

For the separation and purification of compounds, column chromatography was carried out using silica-gel 60 F254. Thin-layer chromatography (TLC) was conducted on pre-coated silica-gel plates (0.25 mm thick) to check the purity of the isolated compounds. The final purity was assessed by high-performance liquid chromatography (HPLC), utilizing an Agilent 1260 system furnished with a diode array detector. The separation was performed on an Agilent C18 XDB column (3 x 150 mm, 3.5 µm particle size), and the compounds were eluted under isocratic conditions using a solvent mixture of acetonitrile and water in a 70:30 ratio.

The molecular geometry free from steric hindrance was optimized using DFT calculations, aligning with spectroscopic data for structural confirmation. Initial structures were generated via Avogadro v1.2.0 (Hanwell *et al.*, 2012) and optimized using a conjugate gradient algorithm and UFF force field, energy threshold, 1.0 × 10-8 kJ/mol and number of structures, limited to 5000, continuing until energy change stabilized. These optimized structures were then refined in NWChem (Aprà *et al.*, 2020) with the B3LYP functional and 6-31G* basis set, a fine grid, and an initial trust radius of 0.1. Convergence thresholds were set for energy (1.0×10^{-6}), density (1.0×10^{-5}),

and gradient (5.0×10^{-4}). van der Waals corrections were applied without a solvent model (Langreth *et al.*, 2005), and final structures were saved in xyz format for further analysis.

3.3.1. Chaeronepaline-A:3,12-Dimethoxy-5,6-dihydroisoquinolino[2,1-b]isoquinolin-7-ium-2,9-diol (1)

Molecular formula: $C_{19}H_{18}NO_4$

Molecular weight: 324

Physical description: dark red powder

$[\alpha]^D$ +15.2(c 0.050, MeOH);

UV λ_{max} 228 274 350 444 nm;

IR (KBr) ν_{max} 3372 2922 1609 1513 1454 1277 1236 1214 cm^{-1};

^1H NMR (400 MHz, MeOD) and

^{13}C NMR (100 MHz, $CDCl_3$) data, see Table 13;

HR-ESI-MS *m/z*324.1238 $[M]^+$, calcd for $C_{19}H_{18}NO_4^+$,324.1236.

% yield : 0.0006% pertaining to dehydrated *C. chaerophylla* specimen

3.3.2. Chaeronepaline-B:7-Methyl-2,3:11,12-bis(methylenedioxy)-7,13a-secoberbin-13-14-epoxide (2)

Molecular formula: $C_{20}H_{19}NO_5$

Molecular weight: 354

Physical description: white amorphous powder

$[\alpha]^D$ -5.1 (c 0.050, MeOH);

UV λ_{max} 240 288 nm;

IR (KBr) ν_{max} 3416 2907 1612 1472 1362 1236 1037 cm^{-1} ;

^1H NMR (400 MHz, MeOD) and

^{13}C NMR (100 MHz, $CDCl_3$) data, see Table 14;

HR-ESI-MS *m/z* 354.0980 $[M+H-2H]^+$, calcd for $C_{20}H_{20}NO_5^+$, 354.0977.

% yield : 0.0003% pertaining to dehydrated *C. chaerophylla* specimen

3.3.3. Chaeronepaline-C: 7-methyl-5, 6, 7, 8- tetrahydro- 8H-spiro-9,14-dihydroxy-11,12-methylenedioxy-indane-isoquinoline (3)

Molecular formula: $C_{20}H_{19}NO_6$

Molecular weight: 370

Physical description: yellow powder

$[\alpha]^D$ +38.17 (c 0.050, MeOH);

UV λ_{max} 228 242 288 nm;

IR (KBr) ν_{max} 3416 2892 1620 1476 1391 1236 1037 cm^{-1};

^1H NMR (400 MHz, MeOD) and

^{13}C NMR (100 MHz, $CDCl_3$) data, see Table 15;

HR-ESI-MS *m/z* 370.1289 $[M + H]^+$, calcd for $C_{20}H_{20}NO_6^+$, 370.1290.

% yield : 0.006% pertaining to dehydrated *C. chaerophylla* specimen

3.3.4. Chaeronepaline-D: 7-methyl-5, 6, 7, 8- tetrahydro- 8H-spiro-9,14-dihydroxy-11,12-methylenedioxy-indane-isoquinoline-N-oxide (4)

Molecular formula: $C_{20}H_{19}NO_7$

Molecular weight: 386

Physical description: yellow powder

$[\alpha]^D$ +58.7 (c 0.050, MeOH);

UV λ_{max} 224 242 290 nm;

IR (KBr) ν_{max} 3409 2922 2649 1620 1480 1380 1236 1037 cm^{-1};

^1H NMR (400 MHz, MeOD) and

^{13}C NMR (100 MHz, $CDCl_3$) data, see Table 16;

HR-ESI-MS *m/z* 386.1240 $[M + H]^+$, calcd for $C_{20}H_{20}NO_7^+$, 386.1239.

% yield : 0.005% pertaining to dehydrated *C. chaerophylla* specimen

3.3.5. Bicuculline (5)

Molecular formula: $C_{20}H_{17}NO_6$

Molecular weight: 367

Physical description: white crystals

^1H NMR (400 MHz, MeOD) and

^{13}C NMR (100 MHz, $CDCl_3$) data, see Table 18;

% yield: 0.0091% pertaining to dehydrated *C. chaerophylla* specimen

3.3.6. Corydalmine (6)

Molecular formula: $C_{20}H_{23}NO_4$

Molecular weight: 341

Physical description: pale yellow crystals

^{1}H NMR (400 MHz, MeOD) and

^{13}C NMR (100 MHz, $CDCl_3$) data, see Table 19;

% yield: 0.00033% pertaining to dehydrated *C. chaerophylla* specimen

3.3.7. 8-Hydroxydihydrosanguinarine (7)

Molecular formula: $C_{20}H_{15}NO_5$

Molecular weight: 349

Physical description: orange crystals

^{1}H NMR (400 MHz, MeOD) and

^{13}C NMR (100 MHz, $CDCl_3$) data, see Table 20;

% yield: 0.00005% pertaining to dehydrated *C. chaerophylla* specimen

3.3.8. Dihydrosanguinarine (8)

Molecular formula: $C_{20}H_{15}NO_4$

Molecular weight: 333

Physical description: orange crystals

^{1}H NMR (400 MHz, MeOD) and

^{13}C NMR (100 MHz, $CDCl_3$) data, see Table 21;

% yield: 0.00008% pertaining to dehydrated *C. chaerophylla* specimen

3.3.9. Scoulerine (9)

Molecular formula: $C_{19}H_{21}NO_4$

Molecular weight: 327

Physical description: pale yellow crystals

^{1}H NMR (400 MHz, MeOD) and

^{13}C NMR (100 MHz, $CDCl_3$) data, see Table 22;

% yield: 0.0003% pertaining to dehydrated *C. chaerophylla* specimen

3.3.10. Govaniadine (10)

Molecular formula: $C_{19}H_{19}NO_4$

Molecular weight: 325

Physical description: white crystals

^{1}H NMR (400 MHz, MeOD) and

^{13}C NMR (100 MHz, $CDCl_3$) data, see Table 23;

% yield: 0.028% pertaining to dehydrated *C. govaniana* specimen

3.3.11. Stylopine (11)

Molecular formula: $C_{19}H_{17}NO_4$

Molecular weight: 333

Physical description: pale yellow crystals

^{1}H NMR (400 MHz, MeOD) and

^{13}C NMR (100 MHz, $CDCl_3$) data, see Tables 24;

% yield: 0.00148% pertaining to dehydrated *C. casimiriana* specimen

3.3.12. Adlumine (12)

Molecular formula: $C_{21}H_{22}NO_6$

Molecular weight: 383

Physical description: pale yellow crystals

^{1}H NMR (400 MHz, MeOD) and

^{13}C NMR (100 MHz, $CDCl_3$) data, see Table 25;

% yield: 0.00304% pertaining to dehydrated *C. casimiriana* specimen

3.3.13. Adlumidine (13)

Molecular formula: $C_{20}H_{17}NO_6$

Molecular weight: 367

Physical description: pale yellow crystals

^{1}H NMR (400 MHz, MeOD) and

^{13}C NMR (100 MHz, $CDCl_3$) data, see Table 26;

% yield: 0.0142% pertaining to dehydrated *C. casimiriana* specimen

3.4. Phytochemical Screening

Chemical analysis was conducted on the hexane, methanol, and chloroform extracts of *C. chaerophylla* to identify a variety of constituents, including alkaloids, flavonoids, phenolic compounds, tannins, saponins, carbohydrates, proteins, glycosides, steroids, terpenoids, and anthraquinones. This phytochemical screening was carried out in accordance with standard methodologies outlined in previous research (Banu & Cathrine, 2015; Iqbal *et al.*, 2015). The results of this qualitative analysis are represented using symbols: (+) indicating the presence and (-) indicating the absence of specific phytochemicals, as shown in Table 4.

By analyzing these different solvent extracts, the researchers were able to determine which bioactive compounds were present in each extract, providing valuable insights into the pharmacological potential of the plant. The use of hexane, methanol, and chloroform allows for the extraction of compounds of varying polarities, with hexane targeting non-polar compounds like lipids and terpenoids, methanol extracting more polar compounds such as phenolics and flavonoids, and chloroform acting as an intermediate, isolating compounds like alkaloids and glycosides. This method ensures a comprehensive survey of the plant's chemical profile, which can help in understanding its medicinal and therapeutic uses.

3.4.1. Phytochemical Screening Protocol

1. Tests for Alkaloids

Three specific tests were used to detect alkaloids in the extracts:

a) **Mayer's Test**: Filtrates (1 mL) were treated with Mayer's reagent (potassium mercuric iodide), and the formation of a yellow precipitate indicated the presence of alkaloids.

b) **Wagner's Test**: 1 mL of the extract was mixed with 3 drops of Wagner's reagent, and a reddish-brown precipitate was indicative of alkaloids.

c) **Dragendorff's Test**: 2 mL of the extract was combined with 0.2 mL dilute HCl and 1 mL of Dragendorff's reagent; the formation of an orange-brown precipitate confirmed alkaloids.

2. **Test for Terpenoids**

   a) **Chloroform Test**: The plant extract was treated with chloroform and concentrated sulfuric acid to observe a reddish-brown color, indicating terpenoids.

   b) **Liebermann-Burchard Test**: Extracts were treated with chloroform and acetic anhydride, followed by sulfuric acid. A dark green color confirmed the presence of terpenoids.

3. **Test for Flavonoids**

   a) **Alkaline Reagent Test**: Adding sodium hydroxide to the extract resulted in an intense yellow color, which turned colorless with dilute acid, suggesting flavonoids.

   b) **Lead Acetate Test**: Lead acetate added to the extract caused a yellow precipitate, confirming flavonoids.

   c) **Pew's Test**: Zinc powder and concentrated HCl were added to the extract; a purple-red color indicated flavonoids.

4. **Test for Steroids Compounds**

   a) **Salkowaski's Test**: Extracts in chloroform were layered with sulfuric acid, and the upper layer turned red, while the sulfuric acid layer showed yellow-green fluorescence, indicating steroids.

5. **Test for Quinones**

   The addition of concentrated sulfuric acid to the extract produced a color change, confirming quinones.

6. **Tests for Saponins**

   a) **Froth Test**: Diluting the extract with water and shaking for 15 minutes resulted in persistent foam, confirming saponins.

b) **Foam Test**: Shaking 0.5 g of the extract with 2 mL of water produced foam, indicative of saponins.

7. Test for Tannins

a) **$FeCl_3$ Test**: A greenish-black color upon adding ferric chloride indicated tannins.

b) **Potassium Dichromate Test**: The extract formed a yellow-brown precipitate with potassium dichromate, suggesting tannins.

c) **Lead Acetate Test**: Lead acetate added to the extract produced a yellow precipitate, confirming tannins.

8. Test for Phenols

a) **Ferric Chloride Test**: Mixing the extract with a ferric chloride and potassium ferrocyanide solution resulted in a bluish-green or dark-green color, indicating phenols.

b) **Liebermann's Test**: Heating extracts with sodium nitrite and sulfuric acid, followed by dilute NaOH, produced red, green, or blue color, confirming phenols.

9. Detection of Carbohydrates

a) **Molisch's Test**: Adding α-naphthol solution to the extract resulted in a violet ring, confirming carbohydrates.

b) **Benedict's Test**: Heating the filtrate with Benedict's reagent produced an orange-red precipitate, indicating reducing sugars.

c) **Fehling's Test**: After hydrolyzing with HCl and heating with Fehling's A & B, a red precipitate confirmed reducing sugars.

10. Tests for Cardiac Glycosides

a) **Modified Borntrager's Test**: Ferric chloride-treated extract boiled and treated with ammonia turned rose-pink, suggesting anthranol glycosides.

b) **Killer-Killani Test**: Adding glacial acetic acid, ferric chloride, and sulfuric acid to the extract formed a reddish-brown ring, indicating glycosides.

c) **Legal's Test**: Sodium nitroprusside and NaOH turned pink to blood-red, suggesting cardiac glycosides.

11. Test for Proteins

a) **Millon's Test**: Millon's reagent added to the extract turned reddish-brown, confirming proteins.

b) **Xanthoproteic Test**: Concentrated nitric acid treatment caused a yellow color, indicating proteins.

12. Test for Amino Acids

a) **Millon's Test**: Adding Millon's reagent to the solution resulted in a white precipitate, suggesting amino acids.

b) **Ninhydrin Test**: Ninhydrin produced a violet color, confirming amino acids.

13. Detection of Resins

Shaking the extract with $CuSO_4$ solution produced a green precipitate, indicating resins.

14. Test for Triterpenoids

Similar to the steroid test, a red or violet color at the junction confirmed triterpenoids.

3.5. Total Phenolic Content Assay

The concentration of phenolic compounds in the extracts was determined using the Folin-Ciocalteu method, a widely used technique for quantifying phenolic content. In this assay, 1 mL of Folin-Ciocalteu reagent, diluted ten times with distilled water, was combined with 1 mL of the sample (prepared at 1 mg/mL concentration in methanol). Additionally, 0.8 mL of a 1 M sodium carbonate (Na_2CO_3) solution was added to the mixture. The reaction mixture was left in the dark for 15 minutes to allow for color

development. Measurements of absorbance were taken at 765 nm using a spectrophotometer, with methanol serving as the control. Gallic acid was used as a standard reference compound, and the total phenolic content (TPC) was calculated in terms of milligrams of gallic acid equivalents (GAE) per gram of dried extract (Agbo *et al.*, 2015; Banothu *et al.*, 2017; Lallianrawna *et al.*, 2013).

The formula used for this calculation is:

$$\text{TPC} = \frac{(C \times V)}{m}$$

Where, C= concentration of gallic acid derived from the calibration curve (mg/mL)

V= volume of extract used (mL)

m= weight of plant extract (g)

This method provides a reliable estimate of the total phenolic content in the plant extracts, which is significant due to the antioxidant properties associated with phenolic compounds.

3.6. Total Flavonoid Content Assay

The total flavonoid concentration in the *C. chaerophylla* extracts was determined using the aluminium chloride ($AlCl_3$) colorimetric method. In this assay, 1 mL of the plant extract (at a concentration of 0.1 mg/mL in methanol) was mixed with 1 mL of a 2% $AlCl_3$ solution. After an incubation period of 1 hour, absorbance was measured at 415 nm using methanol as the control. Quercetin served as the standard reference compound, and the total flavonoid content (TFC) was expressed in terms of milligrams of quercetin equivalents (QE) per gram of dried material (Banothu *et al.*, 2017; Oksana *et al.*, 2012).

The formula used for calculating TFC is:

$$\text{TFC} = \frac{C \times V}{m}$$

Where, C= concentration of quercetin derived from the calibration curve (mg/mL)

V= volume of extract used (mL)

m = weight of plant extract (g)

This method quantifies the flavonoid content, which is important for evaluating the plant's potential therapeutic properties, as flavonoids are known for their antioxidant, anti-inflammatory, and anti-carcinogenic effects.

3.7. LC-DAD-MS^n

After removing the solvents from the hexane, chloroform, and methanol extracts, the dried residues were accurately weighed to 20 mg and dissolved in methanol using sonication to ensure complete dissolution. The samples were then subjected to analysis via Liquid Chromatography coupled with Diode Array Detection and Mass Spectrometry (LC-DAD-MS^n). An Agilent 1260 chromatograph with an autosampler and diode array detector (DAD) facilitated the separation process, and a Varian MS500 Ion Trap mass spectrometer (MS) was utilized in positive ion mode, using an electrospray ionization (ESI) source.

For chromatographic partition, an Agilent SBC18 column (4.6 x 50 mm, 1.8 µm) was utilized. A gradient elution was applied using mixtures of three different solvents, as detailed in Table 1.

Table 1: Ternary gradient

Min	Water 1% formic acid	Acetonitrile	MeOH
0	95	5	0
2.5	85	15	0
12	80	18	2
15.5	50	40	10
19	20	70	10
21	0	85	15
23	0	85	15
24	0	100	0
26	0	100	0
27	95	5	0

The flow rate was set at 750 µL/min, ensuring optimal separation. The diode array spectra were recorded in the range of 200-600 nm, which allowed for the detection of various compounds based on their UV absorption profiles. After passing through the column, the flow was divided using a passive T-junction, allowing concurrent detection by both the DAD and MS detectors.

The mass spectrometer's Time-Dependent Data System (TDDS) was used to capture spectra and fragment the detected ions. Alkaloids were detected predominantly in positive ion mode, in contrast to phenolic compounds, which were observed in negative ion mode. For quantification and identification purposes, known reference compounds were used: berberine, protopine, and bicuculline for alkaloids, and quercetin, catechin, epicatechin, rutin, gallic acid and chlorogenic acid for phenolics. These baseline standards allowed for the generation of calibration curves, facilitating both qualitative identification and quantitative analysis (Cheng *et al.*, 2010; Sun *et al.*, 2014; Tian *et al.*, 2019; Tian *et al.*, 2017; Wei *et al.*, 2016).

This comprehensive analytical approach enabled accurate characterization of the phytochemicals present in the plant extracts, ensuring precise identification of both alkaloid and phenolic constituents.

3.8. Antimicrobial Activity

3.8.1. Preparation of Microbial Culture Media

A Luria-Bertani (LB) broth for bacterial growth was created by dissolving 13 g of LB powder (obtained from Himedia Research Laboratories Pvt. Ltd., India) in 1 liter of distilled water. The concoction was sterilized by autoclaving at a pressure of 15 psi and a temperature of 121°C for 25 minutes to ensure the elimination of any contaminants. Once sterilized, the media was cooled to a temperature range of 40-50°C before being dispensed into sterile 15 mL Falcon tubes, with 5 mL of media per tube. These tubes were then inoculated with bacterial seed cultures and incubated for 24 hours, allowing the bacterial cultures to grow for further testing.

3.8.2. Preparation of MH Media Plates and Antimicrobial Assay

Mueller-Hinton Agar (MHA) Nutrient Agar (NA) plates, widely used for assessing antimicrobial activity, were prepared by mixing 39 g of MH agar powder (from Himedia Research Laboratories Pvt. Ltd., India) with 1 liter of water. The solution was autoclaved under the same conditions as the LB media (15 psi, 121°C, 25 minutes) to ensure sterility. After autoclaving, the media was cooled to approximately 40-50°C and poured into Petri dishes, with 25 mL of media per dish. These plates were labeled and stored in the refrigerator until use.

For the antimicrobial assay, 150 µL of a liquid bacterial suspension equivalent to 0.5 McFarland solution, was evenly spread on the surface of the prepared MHA plates using a sterile cotton swab and left for a few minutes for drying. Wells were drilled in the agar layer, and the samples—consisting of 100 µL of test solutions at 200 mg/mL concentration—were introduced into the wells. As a positive control, kanamycin, a standard antibiotic, was used at a concentration of 5 mg/mL (10 µL). The plates were then incubated at 37°C for 24 hours, after which the antimicrobial activity was evaluated by observing bacterial growth inhibition zones. The clear zones around the wells indicated the efficacy of the antimicrobial agent in inhibiting bacterial growth (Das, 2018; Klančnik *et al.*, 2010; Manandhar *et al.*, 2019).

This method provides an effective and widely accepted approach to assessing the antimicrobial properties of plant extracts, ensuring reliable results in evaluating their potential as antibacterial agents.

3.9. Antioxidant Activity

An antioxidant assay was conducted using the DPPH (2,2-diphenyl-1-picrylhydrazyl) radical scavenging method to evaluate the antioxidant potential of the sample. To begin, 4 mg of hexane extract, 1 mg of methanol extract and chloroform extracts each were dissolved in 1 mL of solvent, creating a stock solution with a concentration of 4 mg/mL of hexane extract and 1 mg/mL of methanol and chloroform extract. From this stock, several dilutions were prepared at concentrations of 4000, 2000, 1000, 500 and 250 µg/mL of hexane extract and 1000, 500, 250, 125 and 62.5 µg/mL for methanol and chloroform extracts using a two-fold dilution technique. Each of these diluted solutions (1 mL) was then mixed with 1 mL of a 0.1 mM DPPH solution (prepared by dissolving 4 mg of DPPH in 100 mL methanol).

The mixtures were vigorously shaken for two minutes to ensure proper mixing and then covered with aluminum foil to prevent any light-induced reactions. These were left to stand at room temperature in the dark for 30 minutes, allowing the DPPH to interact with the antioxidant compounds in the sample. After this period, the absorbance of the mixtures was measured at 517 nm using a spectrophotometer, with methanol serving as the reference. Ascorbic acid was used as standard. A control solution consisting of 1 mL of DPPH solution and 1 mL of methanol was used to measure the baseline

absorbance at 517 nm (Khan *et al.*, 2017; Sharma *et al.*, 2013; Shrestha & Adhikari, 2017b).

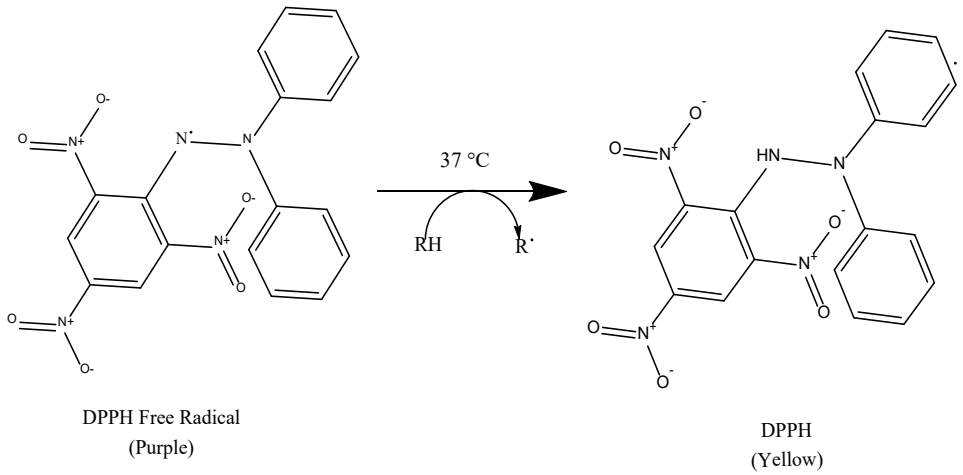

Figure 8: Mechanism of DPPH radical scavenging

The percentage of radical scavenging activity was calculated using the following formula:

$$\text{Percentage scavenging} = \frac{(A_0 - A_T)}{A_0} \times 100\%$$

Where, A_0 = Absorbance of the DPPH solution without the sample (control)

A_T = Absorbance of the DPPH free radical solution containing the sample extract.

The IC_{50} value, which represents the concentration of the sample required to inhibit 50% of the DPPH radicals, was determined by plotting the concentration of the extract against the percentage of radical scavenging activity. A dose-response curve was created in the logarithmic range, and the IC_{50} value was extracted from this plot, indicating the antioxidant efficiency of the sample.

This method is widely used to assess antioxidant activity because DPPH is a stable free radical, and its reduction (indicated by a change in color from purple to yellow) is easy to monitor through changes in absorbance, making it a reliable and quantitative approach for evaluating antioxidant compounds.

3.10. Brine Shrimp Lethality Assay

Lethality tests using brine shrimp (*Artemia salina*), also known as fairy shrimp or sea monkeys, were conducted to evaluate the toxic effects of various extracts from *C. chaerophylla*. In this assay, the nauplii (larvae) of brine shrimp were exposed to solutions containing different concentrations of the extracts for a duration of 24 hours. After the exposure period, the number of motile (living and moving) nauplii was recorded to assess the toxicity of each extract.

The efficacy of the extracts was determined based on the LC_{50} value, which is the concentration required to kill 50% of the nauplii. This LC_{50} value serves as a comparative measurement for determining the toxic potential of plant extracts, with lower LC_{50} values indicating higher toxicity.

This method is widely used as a preliminary screen for toxicity in more complex biological systems (Antonio *et al.*, 2016; Asaduzzaman *et al.*, 2015; Gadir, 2012; Islam *et al.*, 2018; Sarah *et al.*, 2017).

3.11. *In vitro* Inhibition of α-Amylase

During this investigation, the α-amylase inhibitory activity of *C. chaerophylla* extracts was evaluated using the 3,5-dinitrosalicylic acid (DNSA) method at pH 6.9. The extracts were initially diluted to a concentration where they contained at least 10% DMSO (dimethyl sulfoxide). A 200 µL aliquot of this mixture was added to the α-amylase enzyme solution and incubated at 30°C for 10 minutes, allowing the enzyme to act on the starch substrate.

After incubation, a 200 µL volume of 1% starch solution was introduced into each reaction tube, followed by another 3-minute incubation. To halt the enzyme activity, 200 µL of DNSA reagent was added. The reaction mixture was then heated in a water bath at 85-90°C for 10 minutes. Once the sample cooled down reaching room temperature, dilution was performed with 5 mL of distilled water. The absorbance of the resulting solution was measured at 540 nm using a UV spectrophotometer, and the results were compared against a control solution that contained no plant extract. A blank solution, representing 100% enzyme activity, was prepared by replacing the extract with phosphate buffer at pH 7.4.

The percentage of α-amylase inhibition was derived through the following calculation:

$$\% \text{ α-amylase inhibition} = \frac{\text{Abs}_{\text{control}} - \text{Abs}_{\text{Sample}}}{\text{Abs}_{\text{control}}} \times 100$$

where:

$\text{Abs}_{\text{Control}}$ = the absorbance of the control sample with 100% enzyme activity,

$\text{Abs}_{\text{Sample}}$ = the absorbance of the sample containing the plant extract.

A dose-response curve was generated by plotting extract concentration versus the percentage of α-amylase inhibition, allowing for the calculation of the IC_{50} value, defined as the concentration required to achieve 50% enzyme inhibition. This IC_{50} value helps determine the potency of the extract as an α-amylase inhibitor, which is important for understanding its potential in managing conditions like diabetes by slowing the breakdown of starch into glucose.

3.12. *In vivo* Acute Oral Toxicity Study

The OECD (Organization for Economic Co-operation and Development) Acute Toxic Class Method 425 was used to assess the acute oral toxicity of plant extracts, based on established chemical testing guidelines. This experiment was carried out in the pharmacology lab of the Natural Product Research Laboratory (NPRL) in Thapathali, Nepal, using mice as test subjects. Prior to the experiment, the mice were fasted for 12 hours to ensure consistency in the results. The body weight of each mouse was recorded immediately before administering the extracts.

The mice were divided into two groups: a control group and an experimental group. The control group was administered physiological saline, whereas the experimental group received the plant extract at a dose of 2000 mg/kg of body weight through an orogastric tube. After administration, clinical observations were made four times daily, with a focus on the animals' behavior and overall health. Specific attention was given to signs such as changes in skin and fur, nasal mucosa, respiratory rate, and somatomotor activity. Any symptoms such as tremors, convulsions, diarrhea, lethargy, salivation, low stimulus response, sleep disturbances, light sensitivity, or coma were noted. Abdominal palpation was also performed to check for internal reactions.

After 48 hours of clinical monitoring, during which no harmful effects were observed, the experimental group was administered the extract at the same dose. The results of the study were statistically analyzed using the "t-Test for Independent Groups" with STATISTIC V. 7.0 for Windows software. A P-value of ≤0.005 was considered statistically significant, indicating whether the effects of the extract were relevant. At the end of the study, the mice were humanely euthanized (Kumar *et al.*, 2018; OECD, 2022; Ranjitkar *et al.*, 2019).

This method is widely used to determine the safety profile of natural extracts, and the observations made during the study help in understanding the acute toxicity potential of plant-based compounds. The following table shows the system of classification and labeling of chemicals according to the guidelines of Globally Harmonized System (Ranjitkar *et al.*, 2019).

Table 2: Classification of chemicals in accordance with the Globally Harmonized System (GHS) of chemical classification and labeling, as outlined in its third edition

Ranges (mg/kg)	Category	Classification	Hazard statement
> 2000 mg/kg	Category 5	Not classified	May be harmful if swallowed
> 300 ≤ 2000 mg/kg	Category 4	Dangerous	Harmful if swallowed
> 50 ≤ 300 mg/kg	Category 3	Toxic	Toxic if swallowed
> 5 ≤ 50 mg/kg	Category 2	Very toxic	Fatal if swallowed
< 5 mg/kg	Category 1	Highly toxic	Fatal if swallowed

3.13. Hypocholesterolemic assay

The isolated and characterized compounds were subjected to the hypocholesterolemic assay by using the following protocols.

3.13.1. Chemicals

The chemicals used in the experiment included methanol, acetonitrile, and formic acid, all obtained from Sigma Aldrich. Ultrapure water was produced using a MilliQ system. The reference compounds used in the experiment—berberine, californidine, sanguinarine and protopine—were sourced from Phytolab Gmb. To ensure the accuracy

of the tests, the structures of all compounds were confirmed using proton nuclear magnetic resonance (^{1}H-NMR) and mass spectrometry (MS) prior to the experiment.

3.13.2. Reagents

Several essential reagents were used, including Eagle's Minimum Essential Medium (MEM), trypsin-EDTA, penicillin, streptomycin, sodium pyruvate, L-glutamine, and non-essential amino acid solution and fetal bovine serum (FBS), all purchased from EuroClone (Milan, Italy), along with all glass and plastic supplies used during the assay. The assay was done in two groups. In the initial set (Set 1), Govaniadine, Bicuculline, Stylopine, Adlumidine, Adlumine, as well as Berberine, Californidine, Protopine, and Sanguinarine, were prepared in dimethyl sulfoxide (DMSO, Sigma-Aldrich) at a stock concentration of 0.02 M. And in the second set (Set 2) the new isolated compounds **1 – 4** were diluted in DMSO to create a stock solution at a final concentration of 0.08 μM. Simvastatin, a reference drug, was prepared at 50 mM in 0.1 M NaOH (pH adjusted to 7.2) accordimg to the manufacturer's instruction and sterilized via filtration. Additionally, berberine chloride (cod. B3251, Sigma-Aldrich) was dissolved in DMSO at 80 mM for further use.

3.13.3. Cell Cultures

This study utilized Huh7 and HepG2 human hepatic cancer cell lines, which were maintained in MEM containing 10% FBS, along with supplements: 1% L-glutamine (200 mM), 1% sodium pyruvate (100×), 1% non-essential amino acids (100×), and 1% penicillin-streptomycin (10,000 U/mL and 10 mg/mL). The cells were maintained in a controlled environment at 37°C, with 5% CO_2 and 95% air maintaining the humidified atmosphere. During the experiments, the solvent (DMSO) concentration was kept below 0.5% v/v to avoid any interference with cell viability.

3.13.4. Cell Viability Assay on Huh7

Huh7 cells were seeded in MEM/10% FBS in a 96-well plates at a cellular density of 8,000 cells per well, and treated the following day with different concentrations of test compounds (50 μM, 25 μM, 12.5 μM, and 6.25 μM). After a 72-hour incubation period, cell viability was assessed using the sulforhodamine B (SRB) assay, which stains

cellular proteins and provides a quantitative measure of cell density (Skehan *et al.*, 1990; Vichai & Kirtikara, 2006).

3.13.5. Western Blot Analysis

Huh7 cells were initially seeded in 6-well plates containing MEM supplemented with 10% FBS at a concentration of 300,000 cells per well. The medium was substituted with DMEM containing 10% FBS and the test compounds at specified concentrations, the following day. Cells were incubated with the compounds for 72 hours, allowing for the treatment effects to manifest. After this incubation period, intracellular proteins were extracted by using a lysis buffer that contained 50 mM Tris (pH 7.5), 150 mM NaCl, 1% Nonidet-P40, and 1% v/v protease and phosphatase inhibitor cocktails to prevent degradation of proteins during the extraction process. Protein concentration was determined, and 25 µg of each protein sample was subjected to SDS-PAGE electrophoresis using a 4-20% gel under denaturing and reducing conditions. A molecular mass marker (Thermoscientific for nine compounds and Bio-Rad for four new compounds) was included to determine the size of the separated proteins. Following electrophoresis, proteins were transported to a nitrocellulose membrane employing the Trans-Blot® Turbo™ Transfer System (Bio-Rad). In order to reduce non-selective binding, a 5% non-fat dried milk solution in TBS-T20 (buffer with Tween 20) was applied to the membrane. Gentle mixing was applied for 60 minutes at room temperature, and the blotted membranes were then incubated overnight at 4°C in a diluted antibody solution prepared with 5% non-fat dried milk including anti-LDLR (rabbit polyclonal antibody, GeneTex GTX132860; dilution 1:1000), anti-PCSK9 (rabbit polyclonal antibody, GeneTex GTX129859; dilution 1:1000), anti-GAPDH (rabbit polyclonal antibody, GeneTex GTX100118; dilution 1:3000 in nine compounds analysis and 1:10000 in new compounds analysis). After the primary antibody incubation, the membranes were washed and incubated with secondary antibodies (peroxidase-conjugate goat anti-rabbit and antimouse (for nine compounds), Jackson ImmunoResearch, dilution 1:5000, cod. 111-036-045 and 115-036-062, respectively) to detect the primary antibodies. This step was carried out for 90 minutes at room temperature. To visualize the immunoreactive protein bands, the membranes were treated with Clarity™ Western Enhanced Chemi Luminescence (ECL) reagent for 5 minutes. Images of the chemiluminescent signals were captured using the Azure c400

Imaging System (Aurogene)(for nine compounds) and Uvitec Alliance Q9 imaging system (Uvitec, Cambridge, UK)(for new compounds). Lastly, the intensity of the protein bands was quantified using Image Lab™ software to assess protein expression levels. This methodology ensures precise detection and quantification of LDLR, PCSK9, and GAPDH proteins, providing insights into the biological effects of the tested compounds on cholesterol regulation pathways.

3.13.6. Total Cholesterol Content by LC-APCI-MS Analysis

After conducting the Western blot analysis, the nine compounds were evaluated for their effects on Total Cholesterol Content in cells. The assessment of total cholesterol in cells treated with the various compounds was performed using Liquid Chromatography linked with Atmospheric Pressure Chemical Ionization Mass Spectrometry (LC-APCI-MS). An Agilent 1260 Liquid Chromatograph, integrated with a Varian MS 500 Mass Spectrometer featuring an ion trap analyzer, constituted the analytical setup. The APCI ion source was operated in positive ion mode, allowing for the detection of cholesterol as a $[M\text{-}H_2O]^+$ species with a mass-to-charge ratio (m/z) of 369.5. The spectra were recorded within the m/z range of 350-550, ensuring accurate detection of cholesterol and related compounds. To ensure precise quantification, a calibration curve was created using cholesterol solutions ranging from 0.5 µg/mL to 120 µg/mL, with four levels of concentration, ensuring accurate measurement across a broad concentration range. Sample preparation involved treating the cells with 0.1 M NaOH for 1 hour at 60°C previous to injection into the chromatographic system. Following this, the samples were diluted with an equal volume of DMSO to ensure proper consistency for analysis, and were then injected for chromatography. This method allowed for the precise quantification of cholesterol levels in the treated cells, providing insight into the potential cholesterol-modulating effects of the nine tested compounds. This analysis is vital for understanding the ability of these compounds to affect cholesterol metabolism, which could contribute to their potential hypocholesterolemic properties.

3.13.7. Cholesterol Biosynthesis Assay

The newly isolated four compounds were subjected to a Cholesterol Biosynthesis Assay to evaluate their potential effects on cholesterol production. HepG2 cells were seeded

in MEM (Minimum Essential Medium) supplemented with 10% Fetal Bovine Serum (FBS) in 12-well trays at a density of 1×10^6 cells per well. After allowing the cells to adhere and grow for 24 hours, they were treated with the four new compounds at predetermined concentrations. These compounds were dissolved in DMEM (Dulbecco's Modified Eagle Medium) supplemented with 0.2% (w/v) Bovine Serum Albumin (BSA: Merck, Darmstadt, Germany) for a 48-hour incubation period. To track cholesterol biosynthesis, the cells were further incubated for an additional 24 hours in MEM medium supplemented with 2 μCi/mL $^{[2\text{-}14C]}$acetate (a radioactive acetate compound used to trace metabolic pathways; Perkin-Elmer, MA, USA). The medium also contained 0.4% (v/v) FBS and a 0.5% (v/v) solution of sodium acetate (8 mg/mL), allowing for a total incubation period of 72 hours. After incubation, the cell monolayers were lysed with 0.1 M NaOH and stored overnight at 4°C. To each cell lysate, $^{[1,2\text{-}3H]}$cholesterol (a radiolabeled form of cholesterol; Perkin-Elmer, MA, USA) was added as an internal standard reference. The process of saponification was performed at 60°C for one hour using alcoholic KOH, which helps break down fats into fatty acids and alcohol. Following saponification, lipid extraction was done using low-boiling point petroleum ether. Cholesterol and other cellular sterols were separated from the lysates through thin-layer chromatography (TLC). The mobile phase used in TLC consisted of petroleum ether (40°-60°C), diethyl ether, and acetic acid in a ratio of 70:30:1. The separated cholesterol was quantified by measuring the radioactivity of the $^{[2-14C]}$ acetate incorporation through liquid scintillation counting. Finally, the cholesterol biosynthesis in each cell lysate was expressed as counts per minute (cpm) per milligram of protein, with the protein content measured using the BCA assay (Bicinchoninic Acid assay; Thermofisher, MA, USA), according to the manufacturer's instructions (PMID: 36293049). This comprehensive assay provides detailed insights into the impact of the isolated compounds on cholesterol synthesis, which is a critical marker for assessing their potential hypocholesterolemic effects.

3.13.8. Neutral Lipid Staining with Oil Red-O

To visualize lipid accumulation through the Oil Red-O (a dye that selectively stains neutral lipids) staining, Huh7 cells were initially seeded at a density of 50,000 cells per well in 24-well plates, with each well containing sterile microscope cover glasses of 10 mm in diameter (∅) (VWR international). The cells were cultured in MEM (Minimum

Essential Medium) supplemented with 10% Fetal Bovine Serum (FBS). After 24 hours of incubation, the existing medium was replaced with fresh MEM containing the appropriate treatments with the four new compounds (as indicated in the experimental setup).

After 72 hours, the cells were gently rinsed with Phosphate Buffered Saline (PBS) and then fixed with 2% formaldehyde for 10 minutes. Following fixation, the cells were washed again with PBS (without calcium and magnesium). To prepare the cells for staining, a short rinse with 20% isopropanol was performed. Next, Oil Red-O solution (from Sigma-Aldrich, catalog number O0625) was applied. The Oil Red-O stock solution (a 0.5% weight/volume solution in isopropanol) was diluted in distilled water at a 6:4 ratio and filtered twice using 0.220 µm polyvinylidene fluoride (PVDF) and polyethersulfone (PES) filters. The staining was allowed to proceed for 20 minutes, after which the cells were rinsed first with 20% isopropanol and then with tap water for 1-2 minutes to remove excess dye. For nuclear staining, DAPI (4',6-diamidino-2-phenylindole) solution in PBS (from Sigma-Aldrich, catalog number D9542) was applied. The cells were then rinsed thoroughly with tap water, followed by two washes with distilled water.

To preserve the stained cells for imaging, the slides or cover slips were mounted using Fluoromount™ Aqueous Mounting Medium (Sigma-Aldrich, catalog number F4680). Images were captured using a Leica DMRE microscope equipped with a Leica 541 517 HC zoom camera and analyzed with Leica Application Suite X Software. Quantification of the Oil Red O-stained areas, which indicate lipid accumulation, was performed using ImageJ software (version 1.52h, NIH). The stained areas were normalized against the cell nuclei count to ensure accurate comparison of lipid content across samples. This technique is essential for studying lipid accumulation and metabolism in cells, especially in the context of conditions such as non-alcoholic fatty liver disease or other metabolic disorders.

3.13.9. Statistical Analysis

The data from the experiments are presented as the mean ± standard deviation, calculated from at least three independent trials, ensuring reliability and consistency in the results. Statistical significance between the experimental and control groups was

assessed using the Student's t-test, a common method for determining whether there is a significant difference between two means. This analysis was carried out using GraphPad software (from San Diego, CA, USA), which is widely recognized for statistical calculations. Results were considered statistically significant if the p-value was less than 0.05, meaning that there is less than a 5% probability that the observed differences occurred by chance. This threshold of significance helps in validating the effect of the treatments or compounds under study.

By adhering to these statistical parameters, the conclusions drawn from the data are both statistically sound and scientifically reliable. This approach ensures that the experimental findings are robust and credible. This comprehensive methodology provides detailed insights into the effects of various compounds on cholesterol metabolism and cell viability, employing advanced techniques such as LC-MS, Western blotting, and cell viability assays to assess potential hypocholesterolemic effects.

CHAPTER 4

4. RESULTS AND DISCUSSION

4.1. Yields of Extracts

The calculated extraction yields from the plant material of *C. chaerophylla, C. govaniana* and *C. casimiriana* are given as in the Table 3.

Table 3: Yield % of extracts of *C. chaerophylla*, *C. govaniana* and *C. casimiriana*

Extracts/Plants	*C. chaerophylla*	*C. govaniana*	*C. casimiriana*
Hexane Extract	0.14%	0.13%	0.12%
Methanol Extract	9.00%	6.33%	7.20%
Chloroform Extract	1.40%	1.10%	1.12%

4.2. Phytochemical Screening of *C. chaerophylla* Extracts

The phytochemical screening of *C. chaerophylla* extracts using hexane, methanol, and chloroform revealed a diverse range of bioactive compounds, including alkaloids, flavonoids, glycosides, steroids, terpenoids, phenolic compounds, tannins, and saponins. The findings highlight the influence of solvent polarity on the extraction efficiency of various phytochemicals. The detailed breakdown of these phytochemicals is shown in Table 4, providing further insights into the plant's chemical profile.

The hexane extract primarily contained alkaloids, flavonoids, glycosides, steroids, and terpenoids, while phenolic compounds, tannins, carbohydrates, and saponins were not detected. Hexane, a nonpolar solvent, selectively extracted lipophilic compounds such as steroids and terpenoids. This is consistent with reports that hexane efficiently dissolves nonpolar bioactive molecules, including lipids and hydrophobic alkaloids (Harborne, 1998). The detection of alkaloids, which are typically polar, suggests the presence of alkaloid derivatives with nonpolar substituents, allowing limited solubility in hexane.

Table 4: Screening of phytochemical constituents in *C. chaerophylla* extracts

Phytochemicals	Tests	Result in Extracts		
		H	M	C
Alkaloids	Dragendorff"s Test	+	+	+
	Mayer's Test	+	+	+
	Wagner's Test	+	+	+
Flavonoids	Lead Acetate Test	+	+	+
	Shinoda Test	+	+	+
Phenolic Compounds	Ferric Chloride Test	-	+	+
	Lead Acetate Test	-	+	+
	Alkaline Reagent Test	-	+	+
Carbohydrates	Molisch's Test	-	+	+
	Fehling's Test	-	+	+
	Benedict's Test	-	+	+
Proteins	Millon's Test	-	-	-
	Biuret Test	-	-	-
Glycosides	Keller-Killiani Test	+	+	+
	Legal's Test	+	+	+
Steroids	Salkowski's Test	+	+	+
Tannins	Ferric Chloride Test	-	+	+
	Lead Acetate Test	-	+	+
	Alkaline Reagent Test	-	+	+
Anthraquinones	Anthraquinones Test	-	-	-
Terpenoids	Chloroform test	+	+	+
Saponins	Foam test	-	+	-

H: hexane, M: methanol, C: chloroform

Methanol exhibited the broadest extraction range, yielding alkaloids, flavonoids, glycosides, steroids, terpenoids, phenolic compounds, carbohydrates, tannins, and saponins. Methanol's high polarity enables it to dissolve both polar and moderately polar compounds, making it the most effective solvent in this study. The presence of phenolic compounds and tannins reflects methanol's ability to solubilize hydrophilic and hydrogen-bonding compounds (Wagner & Bladt, 1996). Methanol extracts are

known for their antioxidant properties due to the presence of phenolic compounds and flavonoids (Dai & Mumper, 2010).

The chloroform extract contained alkaloids, flavonoids, glycosides, steroids, terpenoids, phenolic compounds, carbohydrates and tannins. However, it did not contain saponins, or anthraquinones. Chloroform, a semi-polar solvent, is effective in extracting compounds with intermediate polarity, including some phenolic and nitrogen-containing alkaloids (Harborne, 1998). Its moderate polarity makes it less efficient than methanol for polar compounds but more effective than hexane for semi-polar constituents.

The results emphasize that solvent polarity significantly influences the range of phytochemicals extracted. Methanol, being the most polar solvent, extracted the widest spectrum of compounds, including highly polar constituents like saponins and tannins. Chloroform, with its intermediate polarity, was effective for compounds like flavonoids and glycosides. Hexane, the least polar solvent, was selective for lipophilic compounds like terpenoids and steroids.

The consistent presence of alkaloids, flavonoids, and steroids across all extracts underscores their abundance and potential significance in *C. chaerophylla*. Phenolic compounds and tannins, predominantly extracted by methanol, are well-known for their antioxidant properties and therapeutic applications (Dai & Mumper, 2010). Steroids and terpenoids, found in all extracts, are associated with anti-inflammatory and antimicrobial activities (Richard et al., 2011).

The phytochemical screening of *C. chaerophylla* extracts demonstrates that solvent polarity is a critical factor in determining the diversity of extracted compounds. Methanol proved to be the most versatile solvent, capturing a wide range of bioactive constituents, while chloroform and hexane were more selective for semi-polar and nonpolar compounds, respectively. These findings provide a foundation for further research into the pharmacological potential of *C. chaerophylla* and the targeted isolation of its bioactive compounds.

4.3. Total Phenolic and Flavonoid Content Analysis

The total phenolic content (TPC) and total flavonoid content (TFC) were measured to assess the antioxidant potential of various extracts from *C. chaerophylla*. TPC was determined using gallic acid as the reference standard, with the results expressed in milligrams of gallic acid equivalent (GAE) per gram of dried material using the gallic acid calibration curve. TFC was calculated in milligrams of quercetin equivalent (QE) per gram of dried material, following a similar approach using a quercetin calibration curve (Lallianrawna *et al.*, 2013; Miean & Mohamed, 2001). The result revealed significant differences in the composition of bioactive compounds depending on the solvent used. This variation underscores the importance of solvent polarity in the selective extraction of phytochemicals and its influence on antioxidant potential.

Phenolic compounds, known for their ability to neutralize free radicals by donating hydrogen atoms, play a critical role in reducing oxidative stress and mitigating cellular damage (Phuyal *et al.*, 2020). Similarly, flavonoids act as potent free radical scavengers and metal ion chelators, enhancing the overall antioxidant activity of plant extracts (Wojdyło *et al.*, 2007). The high levels of TPC and TFC in the methanol and chloroform extracts of *C. chaerophylla* indicate that these solvents are particularly effective in extracting antioxidant-rich compounds.

The methanol extract demonstrated a TPC of 113.38 mg GAE/g and a TFC of 25.25 mg QE/g, while the chloroform extract exhibited similar values, with a TPC of 113.90 mg GAE/g and a TFC of 24.95 mg QE/g. This nearly identical composition suggests that both methanol and chloroform efficiently extract polar and moderately polar bioactive compounds. These findings align with prior studies indicating that polar solvents are highly effective for isolating phenolic and flavonoid compounds (Jing *et al.*, 2015; Lallianrawna *et al.*, 2013).

In contrast, the hexane extract presented a distinct phytochemical profile. Its TPC was significantly lower at 18.43 mg GAE/g, reflecting a reduced capacity to extract phenolic compounds, which are largely polar. However, the TFC in the hexane extract was notably higher at 46.45 mg QE/g, suggesting that hexane favoured the extraction of non-polar flavonoid derivatives. This polarity-dependent extraction efficiency

illustrates how solvent characteristics dictate the chemical composition of plant extracts.

Table 5: Concentration vs absorbance data of gallic acid

Concentration (µg/mL)	Average Absorbance (nm)
25	0.12
50	0.299
100	0.414
150	0.611
250	1.094
500	1.976

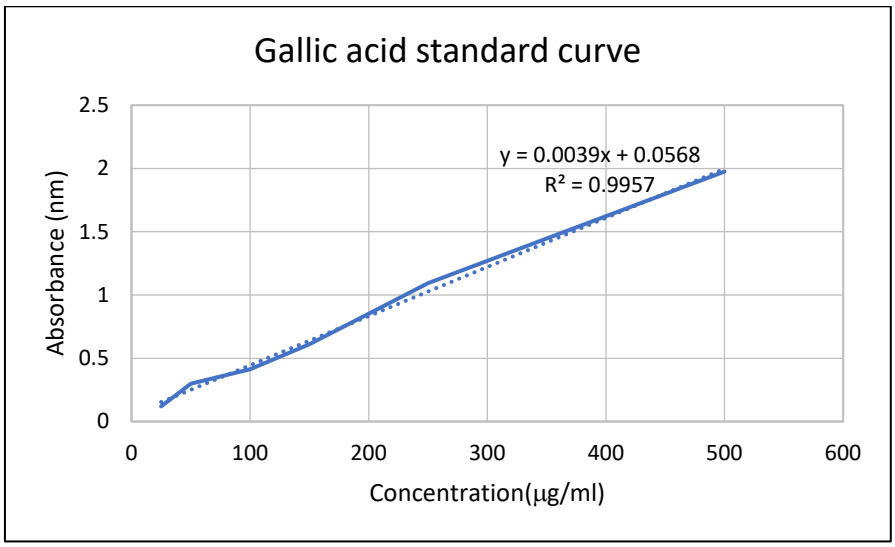

Figure 9: Calibration curve for gallic acid

Table 6: Concentration vs absorbance data of quercetin

Concentration (µg/mL)	Average Absorbance (nm)
25	0.23
50	0.42
100	0.76
150	1.10
250	1.77

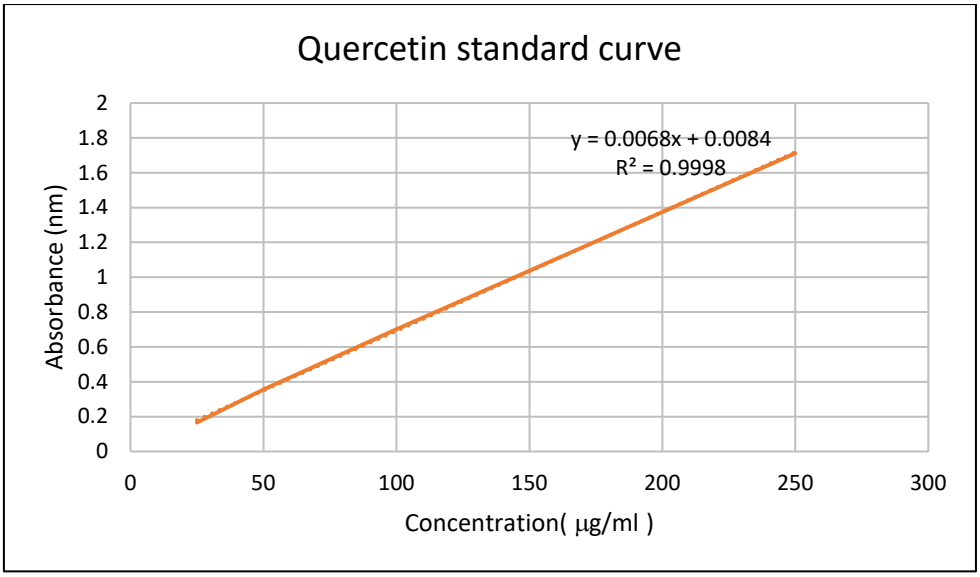

Figure 10: Calibration curve of quercetin

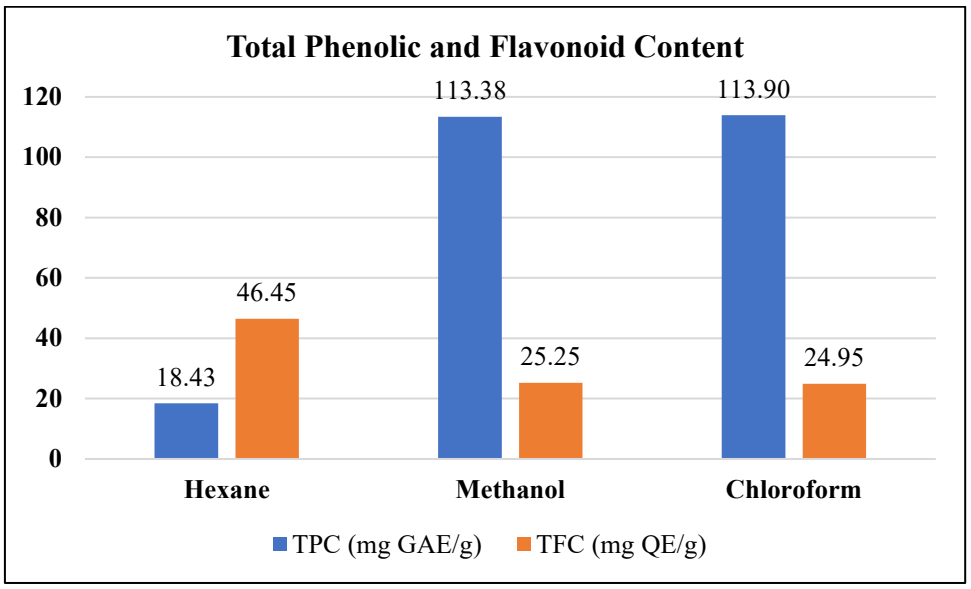

Figure 11: Total phenolic (TPC) and total flavonoid (TFC) content of the extracts of *C. chaerophylla*

The results highlight the critical role of solvent polarity in determining the type and quantity of phytochemicals extracted. Methanol, a polar solvent, interacts strongly with hydroxyl and carbonyl groups in phenolic compounds, making it ideal for extracting hydrophilic antioxidants. Chloroform, being semi-polar, also demonstrated a comparable efficiency in extracting phenolics and flavonoids due to its ability to dissolve compounds with intermediate polarity. On the other hand, hexane, a non-polar solvent, was less effective in extracting phenolics but excelled in isolating lipophilic flavonoids, which are typically embedded in plant lipids (Miean & Mohamed, 2001).

The high phenolic and flavonoid content in the methanol and chloroform extracts suggests substantial antioxidant potential, which could be harnessed for therapeutic applications. Phenolic compounds are associated with anti-inflammatory, antimicrobial, and cardioprotective effects, while flavonoids have shown promising roles in cancer prevention and neuroprotection (Dai & Mumper, 2010). These attributes may explain the traditional use of *C. chaerophylla* in herbal medicine for treating various ailments.

The significant flavonoid content in the hexane extract, despite its low phenolic levels, indicates that non-polar solvents can also yield bioactive profiles with distinct properties. This suggests that the hexane extract may have unique pharmacological applications, potentially complementing the antioxidant effects of phenolic-rich extracts.

The findings from the TPC and TFC analysis of *C. chaerophylla* extracts emphasize the importance of solvent choice in phytochemical research. Methanol and chloroform emerged as the most effective solvents for extracting phenolics and flavonoids, reflecting their strong antioxidant potential. The hexane extract, with its notable flavonoid concentration, also holds promise for specific therapeutic uses. Future studies should explore the bioactivity and pharmacological applications of these extracts to unlock the full potential of *C. chaerophylla* as a source of natural antioxidants.

4.4. Alkaloid Composition Analyzed through Liquid Chromatography Diode-Array Detection and Multistage Mass Spectrometry (LC-DAD-MS^n)

In this study, the alkaloid composition of *C. chaerophylla* extracts was investigated using a combination of Liquid Chromatography with Diode-Array Detection (LC-DAD) and Multiple Stage Mass Spectrometry (MS^n). This method was utilized to obtain comprehensive structural insights into the compounds found within the hexane, methanol, and chloroform extracts. The resulting chromatograms displayed multiple peaks, each corresponding to notable ultraviolet (UV) absorptions, facilitating the initial classification of various alkaloid groups according to their UV spectral characteristics (Sangster & Stuart, 1965).

Peaks with a maximum UV absorption at 296 nm were indicative of benzyltetrahydroisoquinoline derivatives. Peaks at 425 nm and 345 nm corresponded

to protoberberinic alkaloids, while phthalide isoquinolinic alkaloids exhibited absorption maxima at 320 nm and 290 nm. In the final portion of the chromatogram, peaks at 325 nm and 283 nm were indicative of benzophenanthridine alkaloids. These findings are summarized in Figures 12–14, where the UV spectra clearly indicate the presence of different alkaloid types across the three extracts.

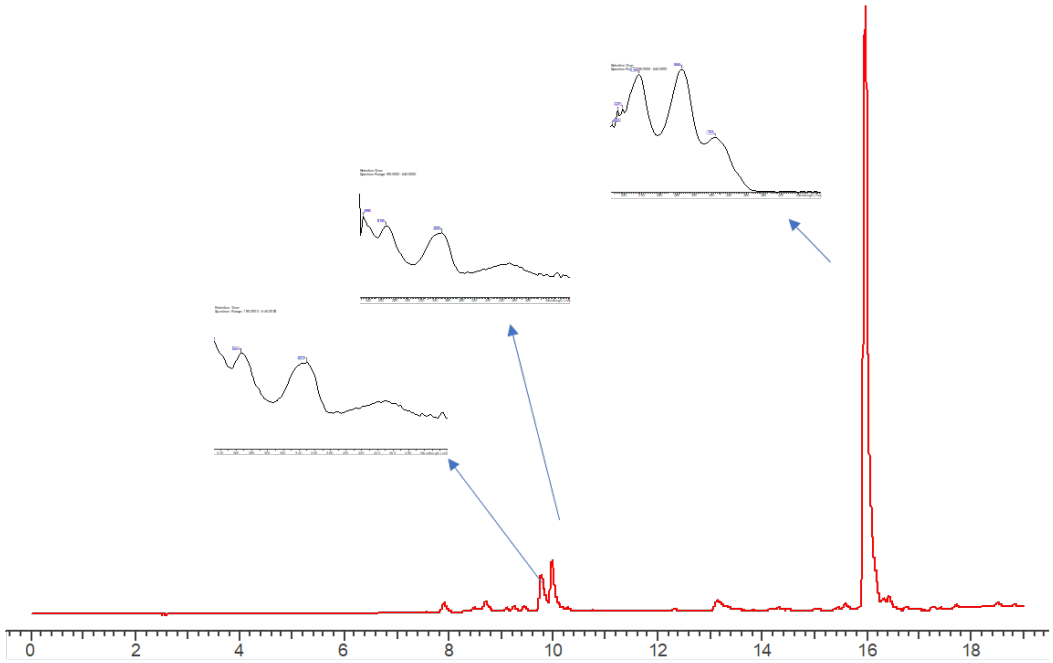

Figure 12: LC-DAD chromatogram at 280 nm for the hexane fraction, the UV spectra attributed to primary classes of isoquinoline alkaloids

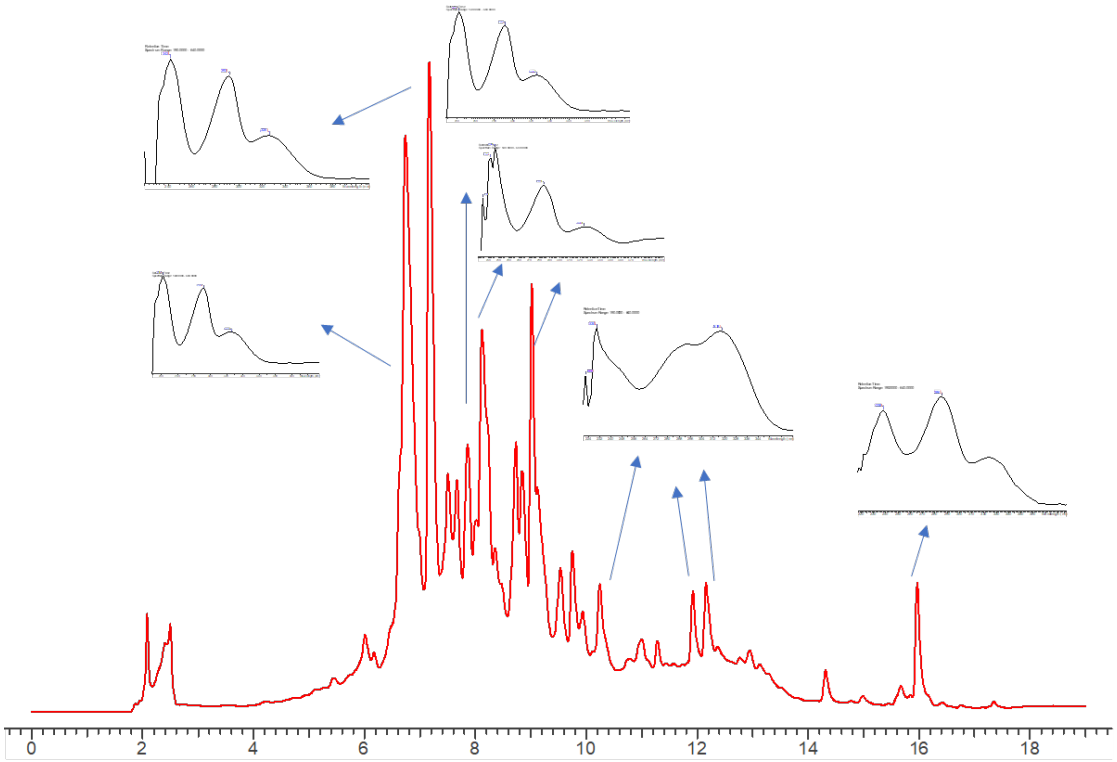

Figure 13: LC-DAD chromatogram at 280 nm for the methanol fraction, the UV spectra attributed to primary classes of isoquinoline alkaloids

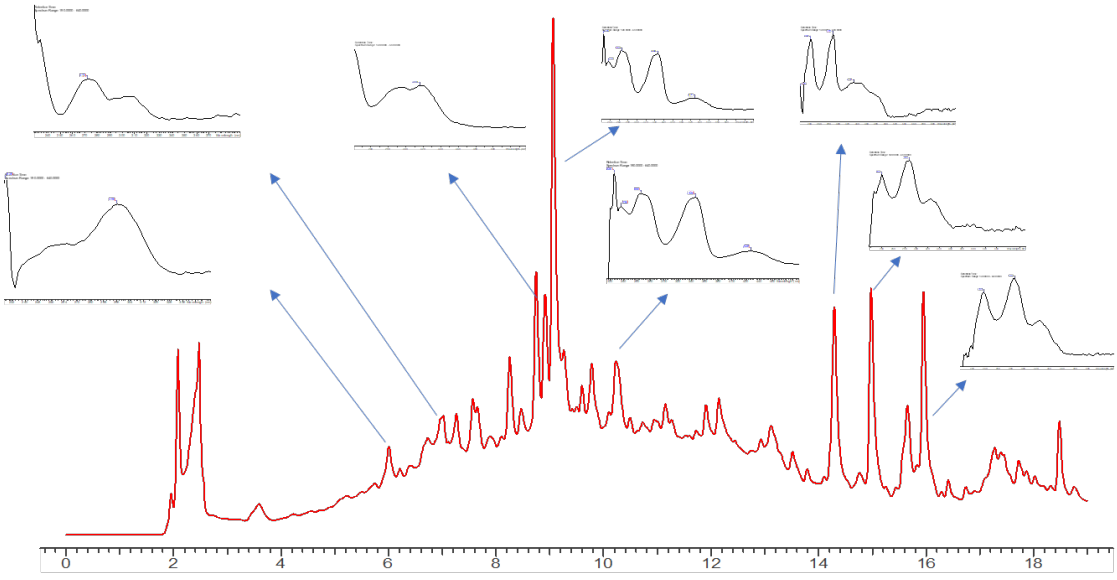

Figure 14: LC-DAD chromatogram at 280 nm for the chloroform fraction, the UV spectra attributed to primary classes of isoquinoline alkaloids

The analysis of MSn spectra, alongside comparisons with published data and reference standards, facilitated the identification of 15 distinct alkaloids (**LC-1** to **LC-15**), each

subsequently quantified through LC-DAD. Table 7 provides a summary of these compounds and their quantities. The detailed MS^n fragmentation allowed for the profiling of alkaloids across the different extracts.

Table 7: Compounds observed in LC-DAD-MS of extracts of *C. chaerophylla*

S. N.	Rt	m/z	Fragments	Compound	Extracts (mg/g)			Reference
					H	M	C	
1.	6.2	314	298.0, 269.0, 237.0, 175.0, 137.0, 107.0	Magnocurarine	-	0.12	0.08	(Y. Tian *et al.*, 2017)
2.	6.8	370	352.0, 334.0, 320.0, 290.0, 190.0, 175.0, 149.0, 131.0	N-Methyltetrahydropalmatine	0.77	23.31	218.01	
3.	8.53	340	178.0, 163.0	Tetrahydrocolumbamine	2.31	4.10	1.37	(M. Sun *et al.*, 2014; Wei *et al.*, 2016)
4.	8.58	356	192.0, 177.0, 148.0	N-Methyltetrahydrocolumbamine	0.28	1.10	1.15	
5.	8.65	324	309	Demethylene berberine	4.26	12.48	45.38	
6.	8.84	368	307.0, 190.0	Bicuculline*	17.94	93.24	115.30	
7.	9.04	400	382.0, 355.0, 337.0, 319.0, 279.0	Protoberberine derivative	0.05	4.14	8.28	
8.	9.31	354	338.0, 190.0, 188.0, 149.0, 130	Protopine*	5.08	58.69	99.04	(M. Tian *et al.*, 2019; Y. Tian *et al.*, 2017)
9.	9.34	356	338.0, 190.0	Hunnemanine	0.58	64.29	64.49	
10.	9.4	338	323.0, 294.0, 307.0, 279.0	Jatrorrhizine*	22.04	116.04	63.16	(M. Sun *et al.*, 2014; Y. Tian *et al.*, 2017)
11.	9.5	368	338.0, 353.0, 321.0,	Berberastine	3.22	6.38	2.16	(Y. Tian *et al.*, 2017)

			320.0, 307.0, 278.0					
12.	9.76	352	336.0, 321.0, 308.0, 292.0, 278.0, 292.0, 275.0	Palmatine	3.30	8.30	2.09	(M. Sun *et al.*, 2014; Wei *et al.*, 2016)
13.	11.5	366	348.0, 323.0, 307.0, 190.0	Dehydrocorydaline	0.22	0.21	-	(M. Sun *et al.*, 2014)
14.	15.8	332	317.0, 304.0, 274.0, 246.0	Sanguinarine*	1.88	2.52	0.36	(M. Tian *et al.*, 2019; Y. Tian *et al.*, 2017)
15.	16.3	334	319.0, 304.0, 275.0, 246.0, 261.0	Dihydrosanguinarine	54.32	1.19	2.06	(Y. Tian *et al.*, 2017)

H: hexane, M: methanol, C: chloroform; compounds indicated with "*" were also confirmed by standard injection

The methanol extract exhibited the highest diversity of compounds, with prominent alkaloids such as hunnemanine (64.29 mg/g), protopine (58.69 mg/g), bicuculline (93.24 mg/g) and jatrorrhizine (116.04 mg/g). This corresponds with its high TPC (113.38 mg GAE/g) and TFC (25.25 mg QE/g), highlighting the effectiveness of methanol in extracting polar and moderately polar bioactives. Methanol's polar nature facilitates the solubilization of phenolic acids and flavonoids, which are responsible for the plant's antioxidant properties (Phuyal *et al.*, 2020). Similarly, the chloroform extract demonstrated comparable phenolic and flavonoid contents, with significant amounts of jatrorrhizine (63.16 mg/g) and bicuculline (115.30 mg/g). This reflects chloroform's semi-polar characteristics, making it effective for extracting compounds with intermediate polarity (Lallianrawna et al., 2013). This also aligns with the phytochemical screening results, which revealed the presence of alkaloids, flavonoids, and phenolic compounds, particularly in the methanol and chloroform extracts.

The unexpectedly high content of dihydrosanguinarine (54.32 mg/g) in the hexane extract, despite its moderate polarity, could result from several factors. Dihydrosanguinarine may possess hydrophobic moieties or interact with nonpolar components in the plant matrix, such as lipids or terpenoids, which are efficiently

extracted by hexane. Additionally, environmental conditions during extraction, such as pH or temperature, may facilitate its partitioning into hexane by stabilizing less polar derivatives or complexes. Matrix effects, such as co-extraction or stabilization of dihydrosanguinarine with nonpolar compounds, and potential localization in hydrophobic plant compartments, could also contribute. Experimental artifacts, including carryover effects or co-elution in the LC-DAD-MS analysis, may further amplify its apparent concentration. These factors highlight the complex interplay of compound chemistry, solvent polarity, and plant-specific biochemistry in extraction processes.

The mass fragmentation shown by LC-DAD-MS of fifteen compounds identified are presented here.

4.4.1. Magnocurarine (LC-1)

The molecular ion $[M+H]^+$ at m/z 314 indicated the presence of magnocurarine. This was followed by the loss of a dimethylamino group, producing a fragment at m/z 269. Further fragmentation resulted in the formation of an ion at m/z 175, indicating the removal of a hydroxybenzylic moiety. This clear fragmentation pattern confirmed the presence of magnocurarine.

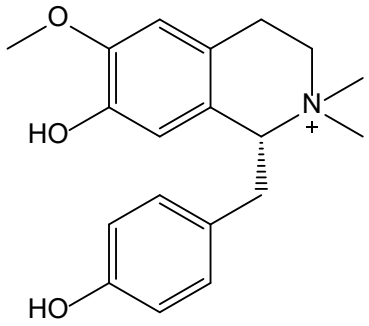

Figure 15: Structure of magnocurarine (**LC-1**)

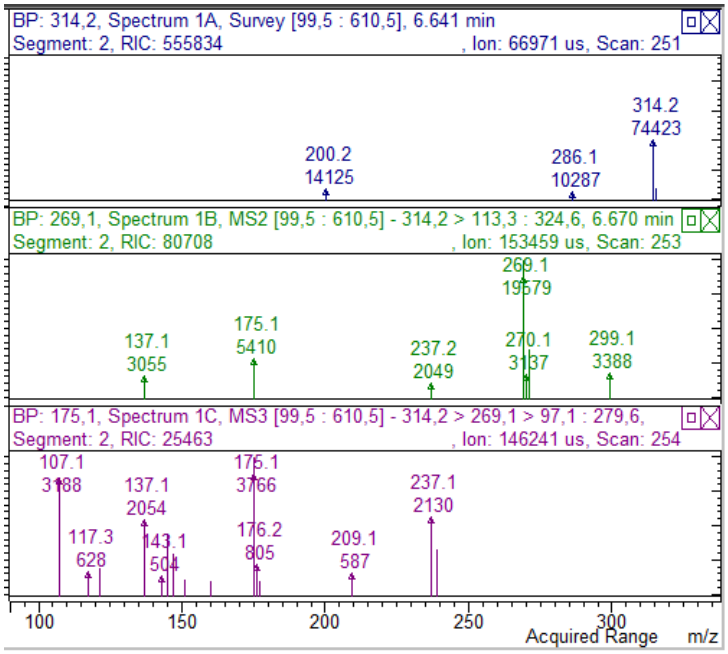

Figure 16: Mass spectrum of fragmentation of magnocurarine

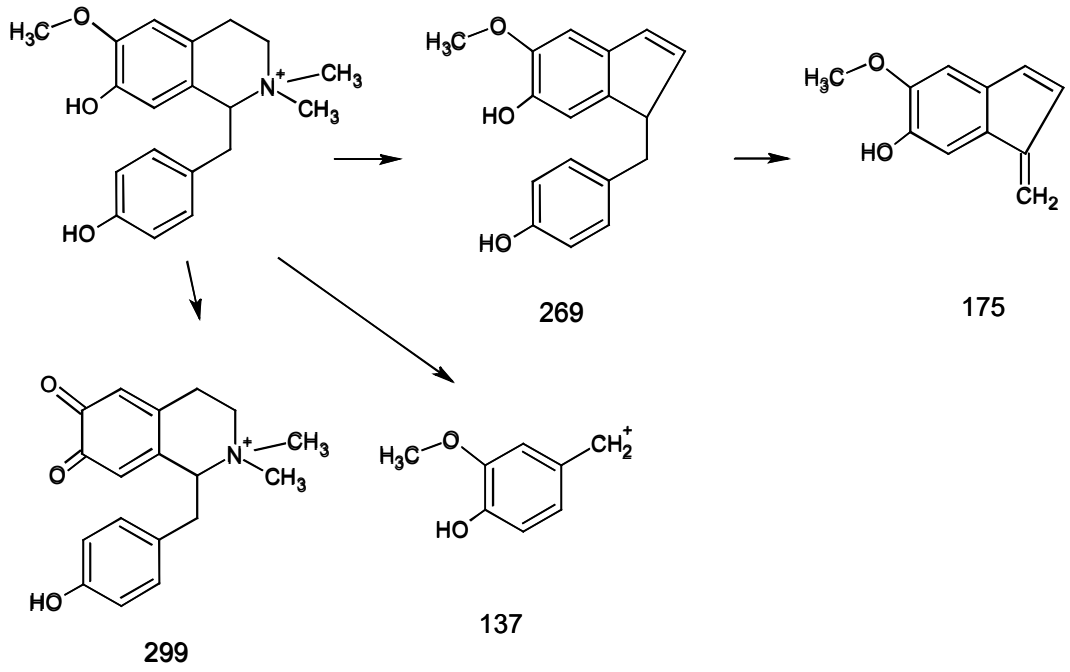

Figure 17: Mass fragmentation pattern of magnocurarine

4.4.2. N-Methyltetrahydropalmatine (LC-2)

For N-Methyltetrahydropalmatine, the protonated molecular ion peak $[M+H]^+$ was detected at m/z 370, and subsequent loss of a methyl group yielded a fragment at m/z 352. Additionally, the detection of a peak at m/z 190 suggested an N-methyl-isoquinolinium segment, further confirming the identification.

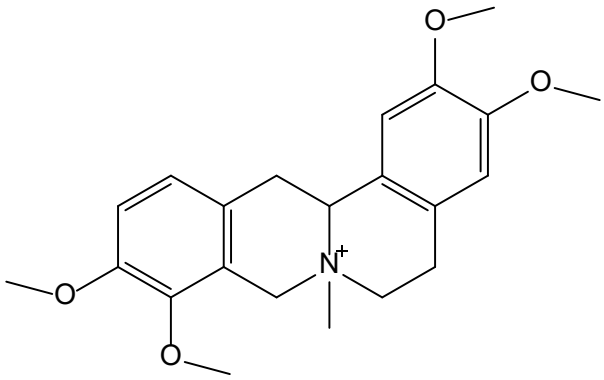

Figure 18: Structure of N-methyltetrahydropalmatine (**LC-2**)

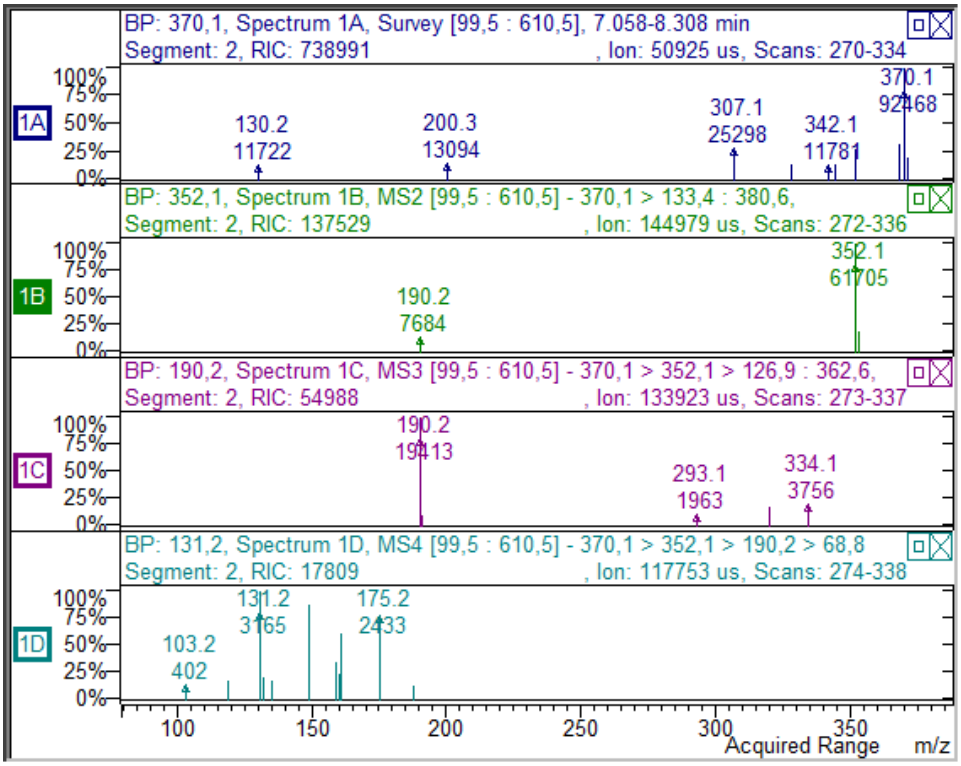

Figure 19: Mass spectrum of fragmentation of N-methyltetrahydropalmatine

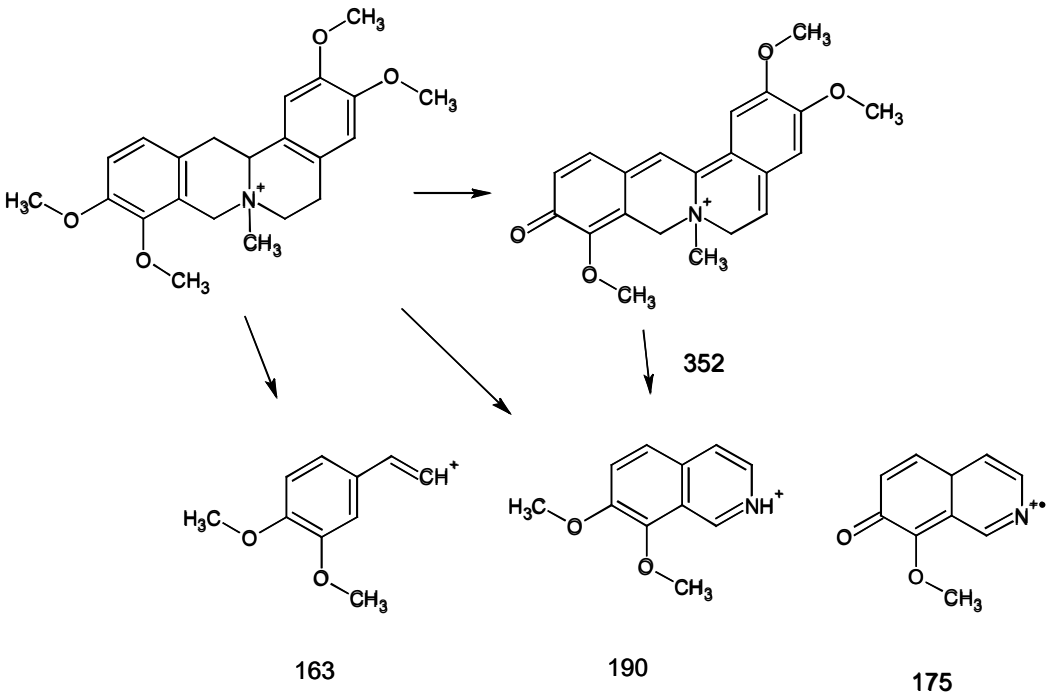

Figure 20: Mass fragmentation pattern of N-methyltetrahydropalmatine

4.4.3. Tetrahydrocolumbamine (LC-3)

A similar fragmentation pattern was observed for tetrahydrocolumbamine, identified by its protonated molecular ion peak $[M+H]^+$ at m/z 342. The MS^2 spectrum showed an ion at m/z 178, attributed to a methoxy-hydroxy-isoquinolinium species.

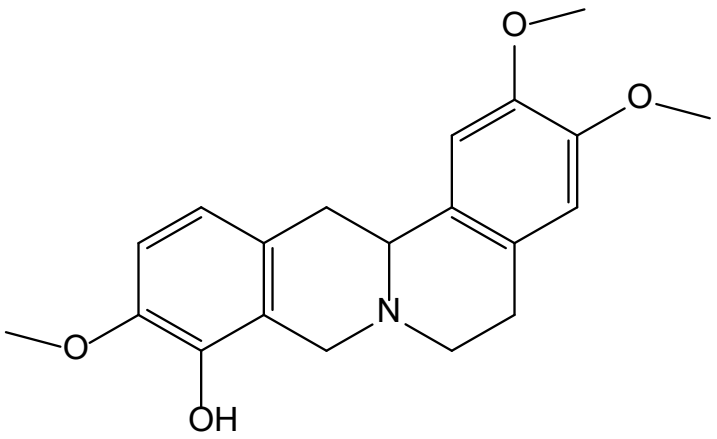

Figure 21: Structure of tetrahydrocolumbamine (**LC-3**)

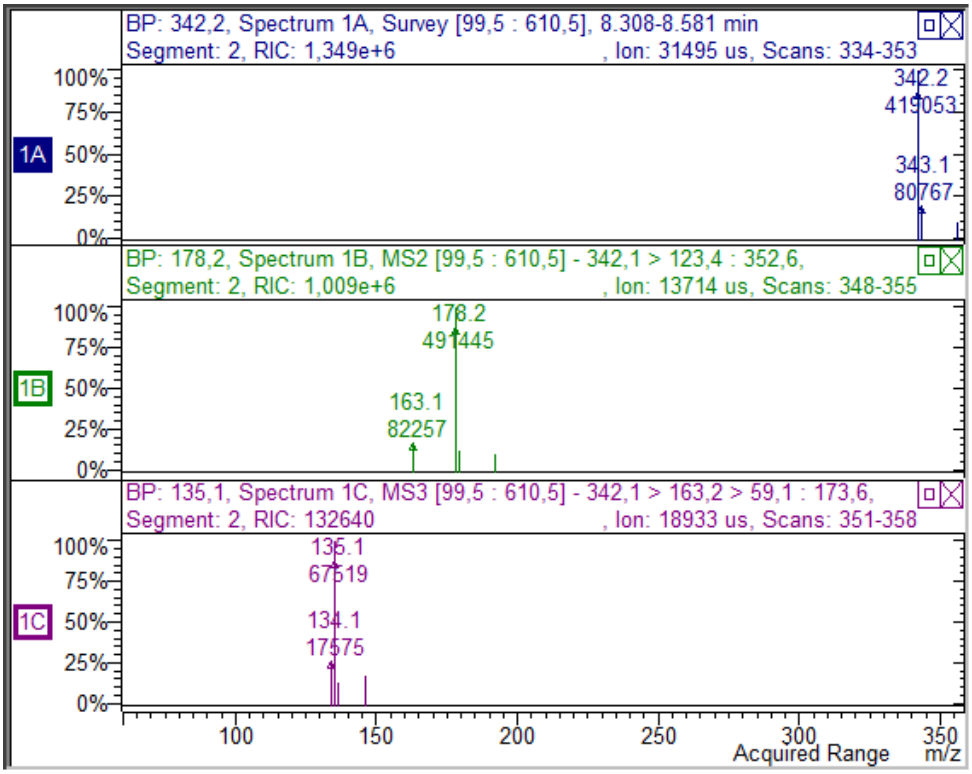

Figure 22: Mass spectrum of fragmentation of tetrahydrocolumbamine

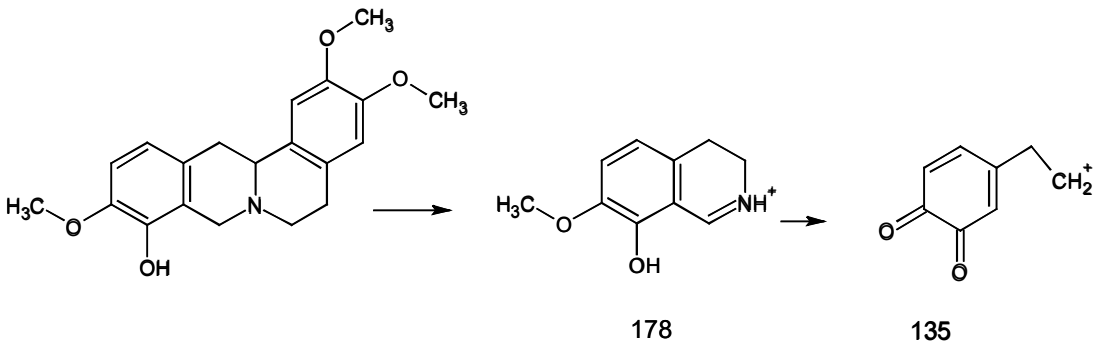

Figure 23: Mass fragmentation pattern of tetrahydrocolumbamine

4.4.4. N-Methyltetrahydrocolumbamine (LC-4)

A structurally related compound, N-Methyltetrahydrocolumbamine, was characterized by its molecular ion at m/z 356. Its MS^2 fragmentation yielded ions at m/z 192, 177, and 148, consistent with the loss of a methyl group and carbon monoxide (CO), forming the N-methyl-methoxy-hydroxy-dihydroisoquinolinium species.

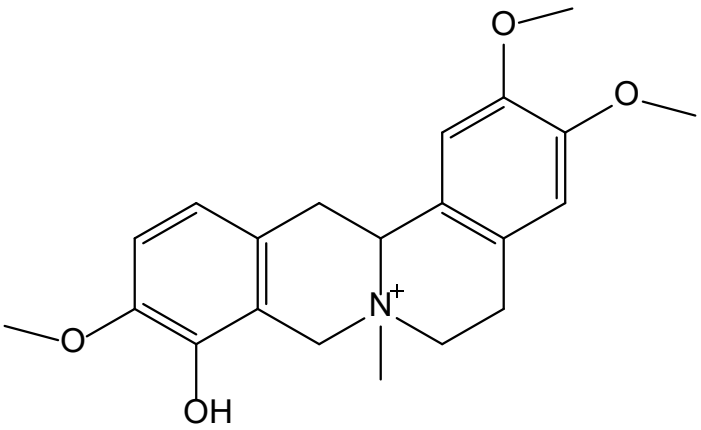

Figure 24: Structure of N-methyltetrahydrocolumbamine (**LC-4**)

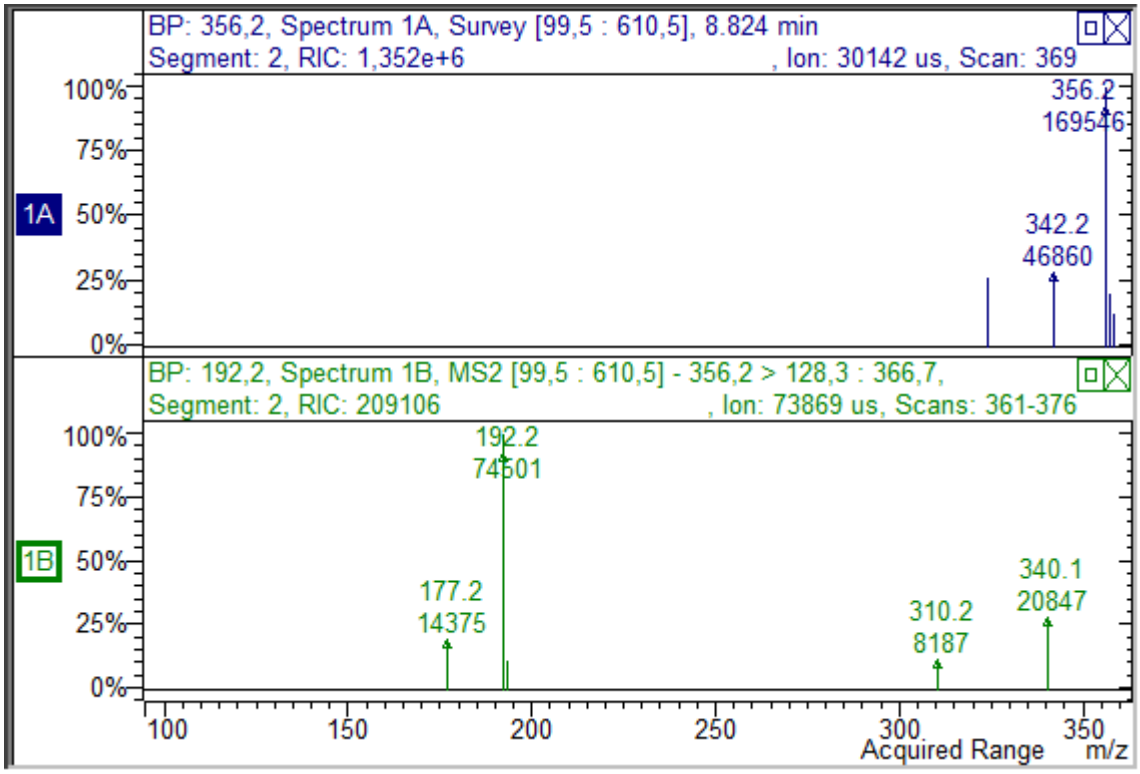

Figure 25: Mass spectrum of fragmentation of N-methyltetrahydrocolumbamine

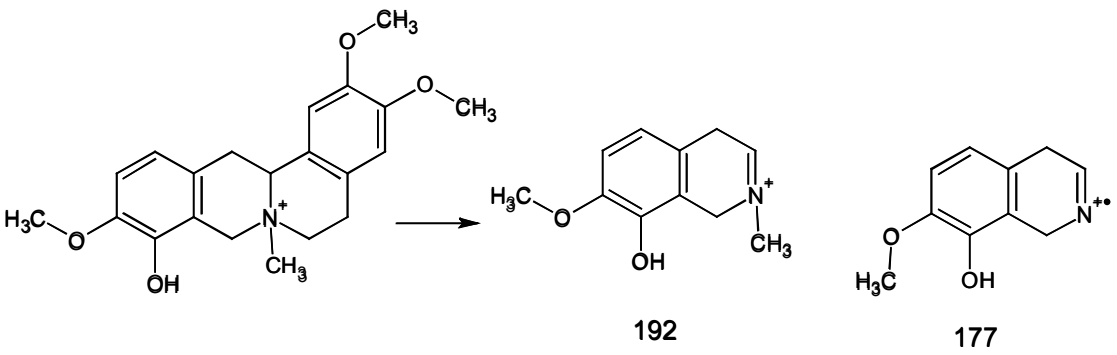

Figure 26: Mass fragmentation pattern of N-methyltetrahydrocolumbamine

4.4.5. Demethylene Berberine (LC-5)

The molecular ion $[M+H]^+$ at m/z 324 underwent stepwise losses of 15 and 17 Da, resulting in fragments at m/z 309 and 307. The MS^3 spectrum revealed further losses of 15 Da, resulting in ions at m/z 294 and 279. Continued fragmentation at m/z 294 led to ions at m/z 269, 266, and 237. This pattern allowed the assignment of the compound as demethylene berberine or its isomer.

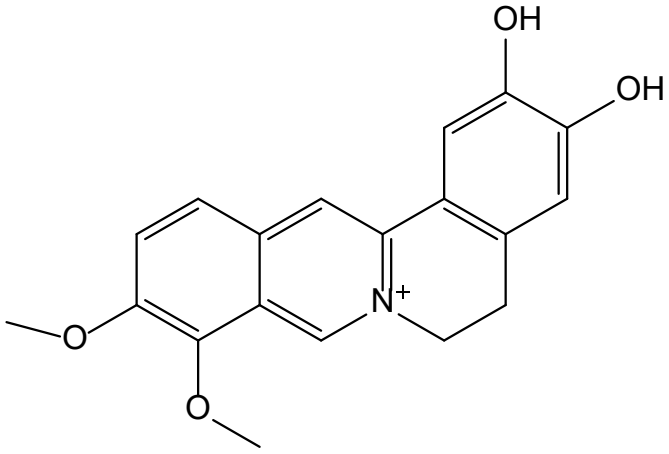

Figure 27: Structure of demethylene berberine (**LC-5**)

4.4.6. Bicuculline (LC-6)

The molecular ion at m/z 368, observed as $[M+H]^+$, was consistent with the structure of bicuculline, a derivative of phthalide isoquinoline. Ion fragmentation led to the generation of an m/z 190 ion attributed to the N-methyl-isoquinolinium moiety, with a subsequent m/z 175 fragment emerging from methyl removal. The compound was verified by co-injection alongside a reference standard.

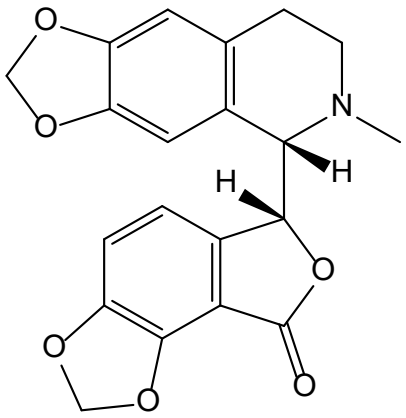

Figure 28: Structure of bicuculline (**LC-6**)

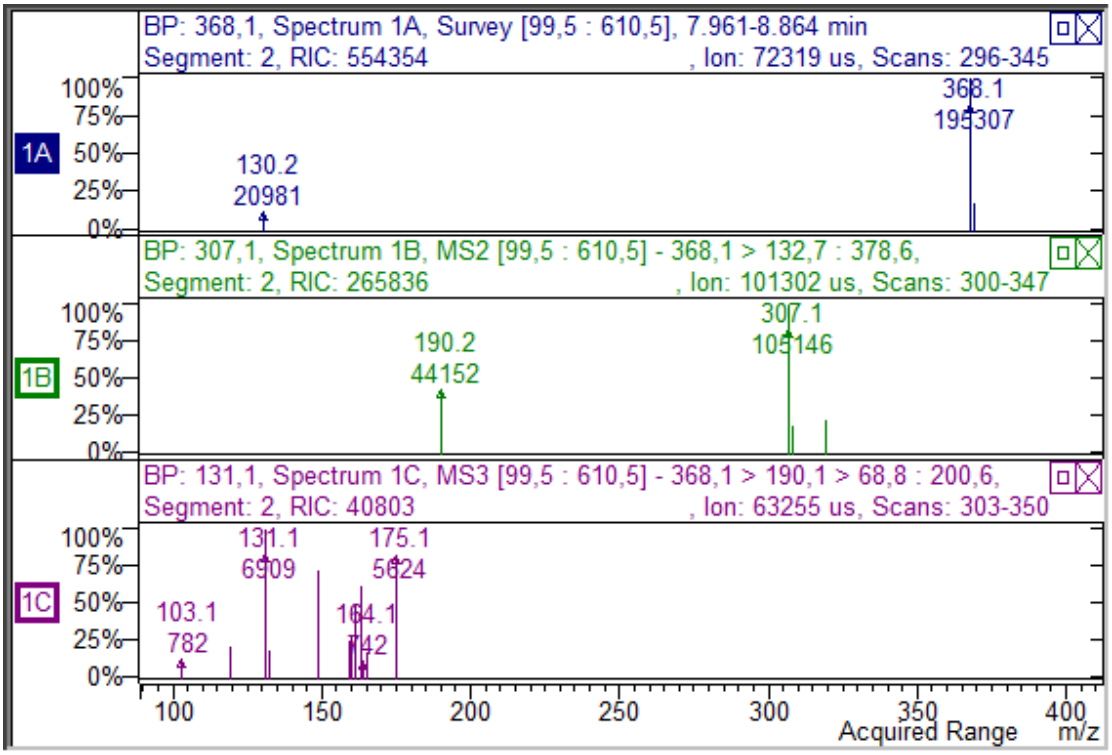

Figure 29: Mass spectrum of fragmentation of bicuculline

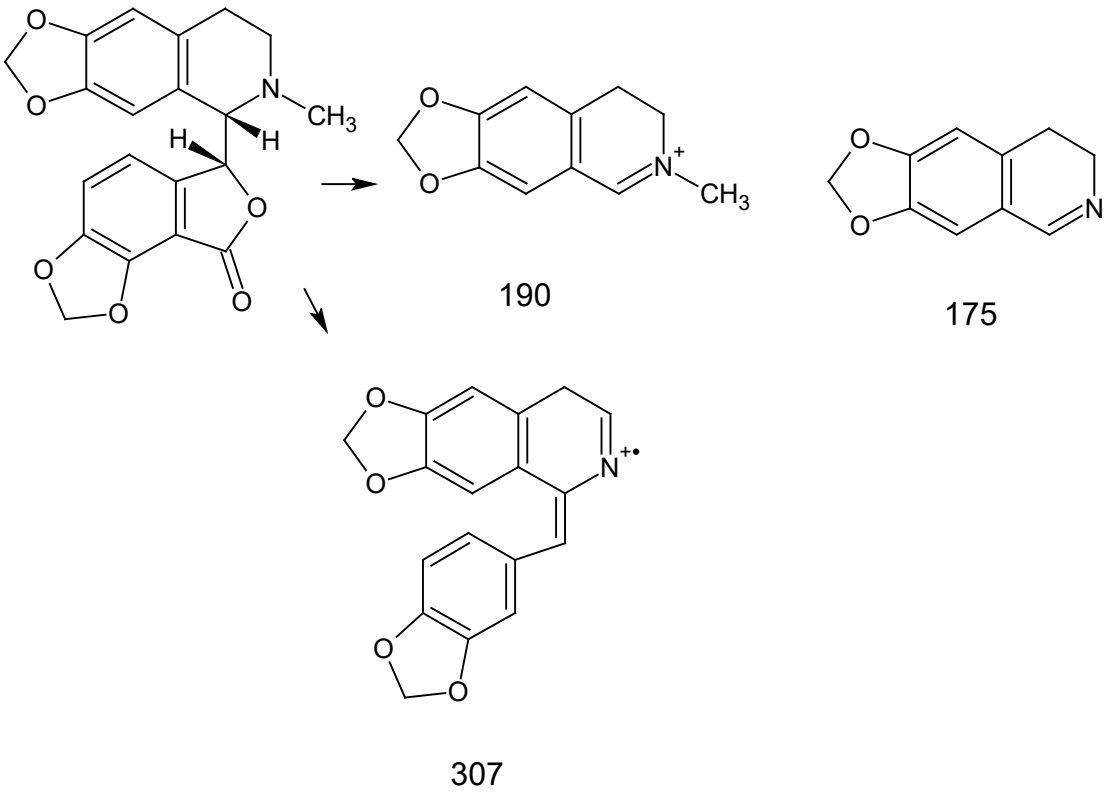

Figure 30: Mass fragmentation pattern of bicuculline

4.4.7. Protoberberine Derivative (LC-7)

For the compound with a molecular ion $[M+H]^+$ at m/z 400, the compound lost a water molecule leading to the formation of a fragment at m/z 382, with further fragmentation revealing ions at m/z 337, 319, and 289. This indicated the presence of a protoberberine derivative with attached hydroxyl and methoxyl groups. A structural hypothesis for this compound was suggested based on these fragmentations.

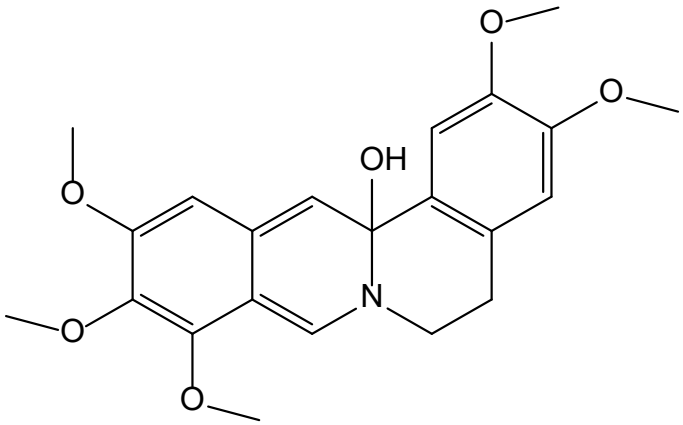

Figure 31: Structure of protoberberine derivative (**LC-7**)

4.4.8. Protopine (LC-8)

Protopine was identified by its molecular ion $[M+H]^+$ at m/z 354. The loss of water generated a fragment at m/z 336, while further fragmentation produced ions at m/z 188 and 204, associated with structural fragmentation and secondary dehydration of the isoquinoline unit.

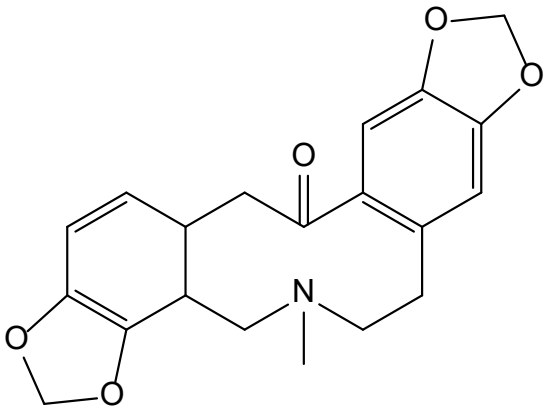

Figure 32: Structure of protopine (**LC-8**)

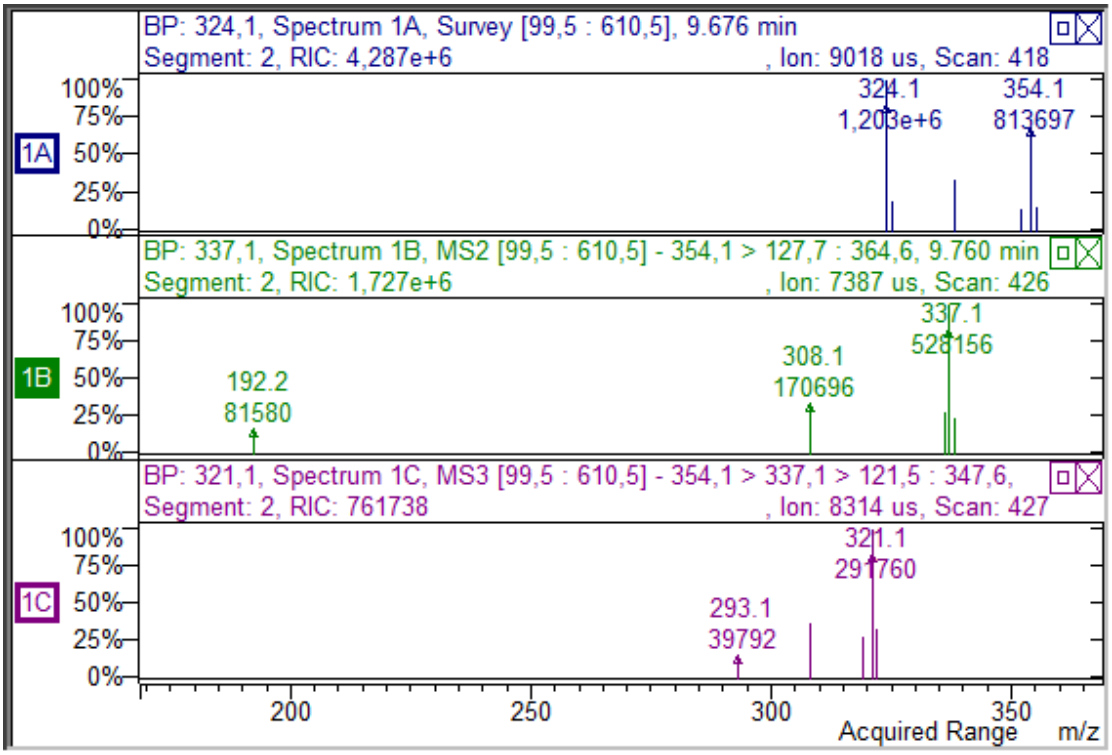

Figure 33: Mass spectrum of fragmentation of protopine

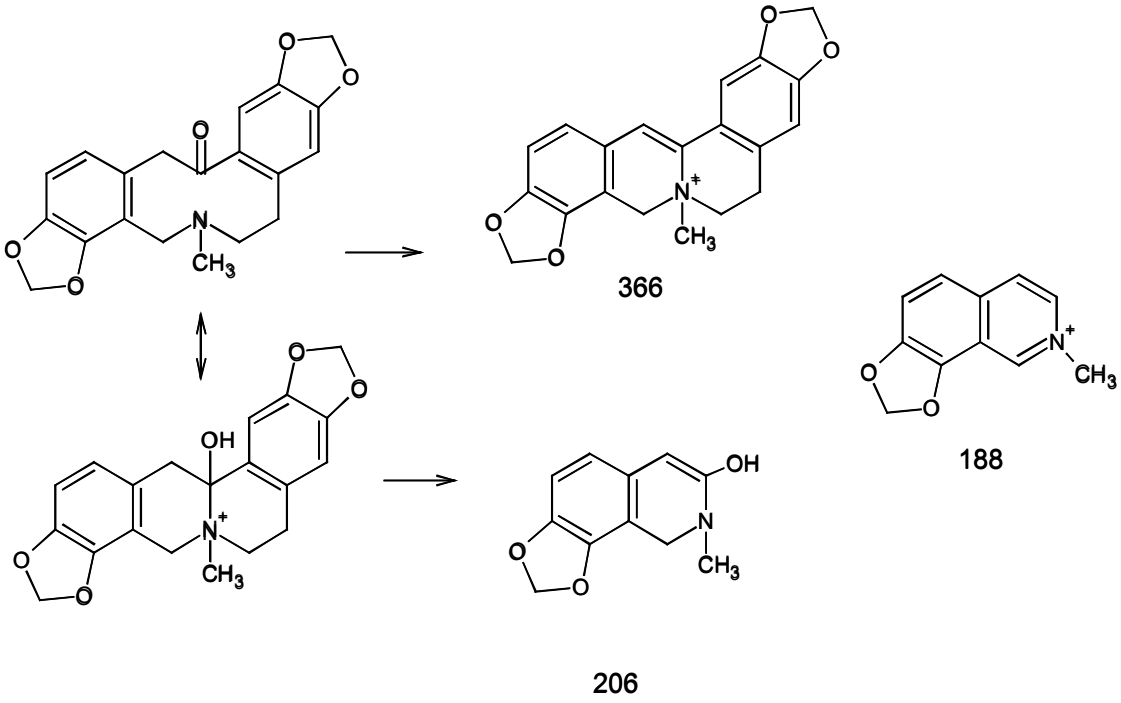

Figure 34: Mass fragmentation pattern of protopine

4.4.9. Hunnemanine (LC-9)

A compound presenting a similar fragmentation pattern, with molecular ion $[M+H]^+$ at m/z 356, was identified as hunnemanine, belonging to a benzophenanthridine class. The intense fragment at m/z 190 was a key feature.

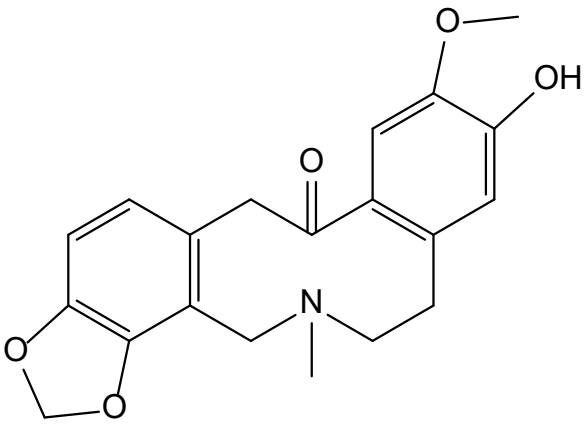

Figure 35: Structure of hunnemanine (**LC-9**)

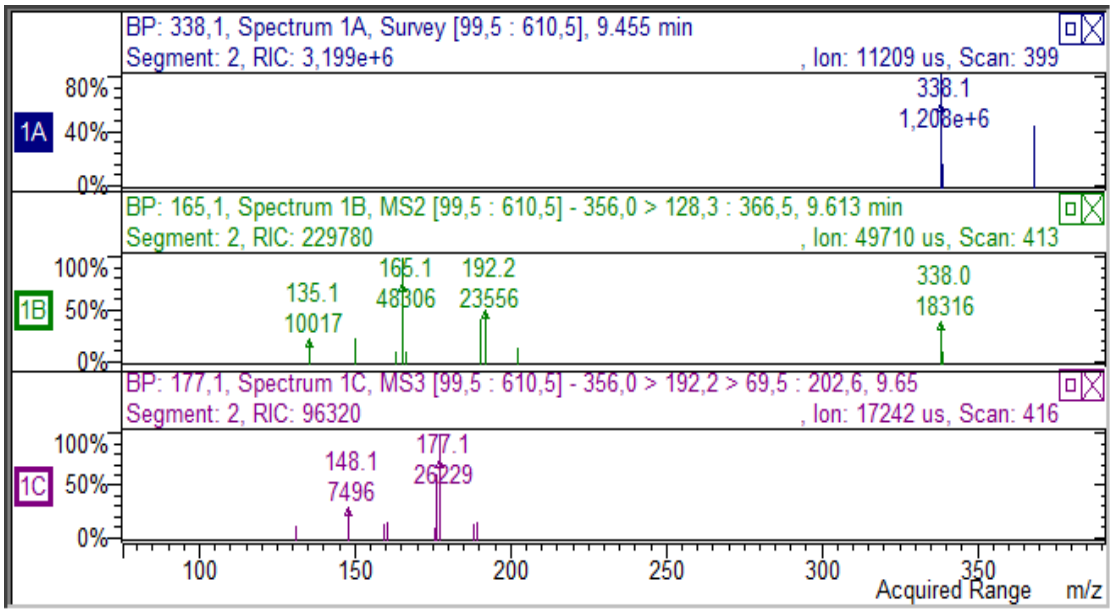

Figure 36: Mass spectrum of fragmentation of hunnemanine

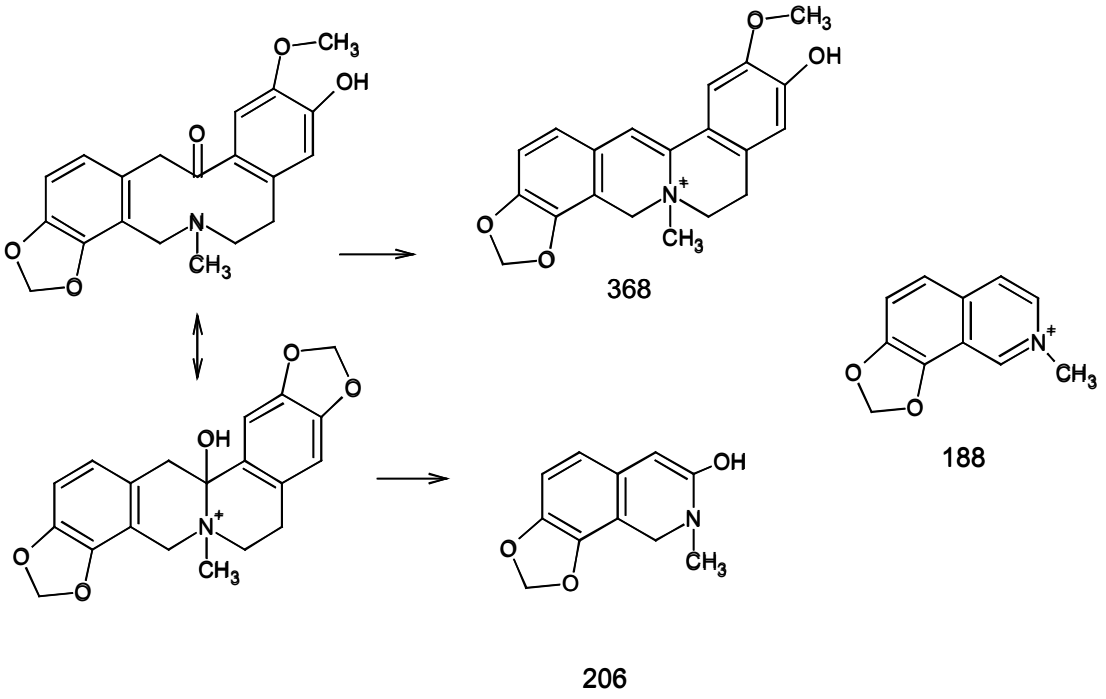

Figure 37: Mass fragmentation pattern of hunnemanine

4.4.10. Jatrorrhizine (LC-10)

Jatrorrhizine, a protoberberine alkaloid, was identified by its molecular ion $[M+H]^+$ at m/z 338. Fragmentation resulted in ions at m/z 323/324 and 307, caused by the loss of methyl groups. The fragmentation pattern, along with the separation of isoquinoline and benzyl moieties (ion at m/z 190), matched the data of an authentic standard.

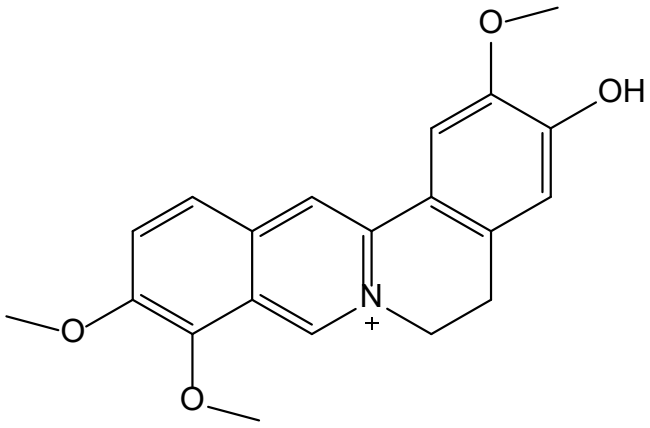

Figure 38: Structure of jatrorrhizine (**LC-10**)

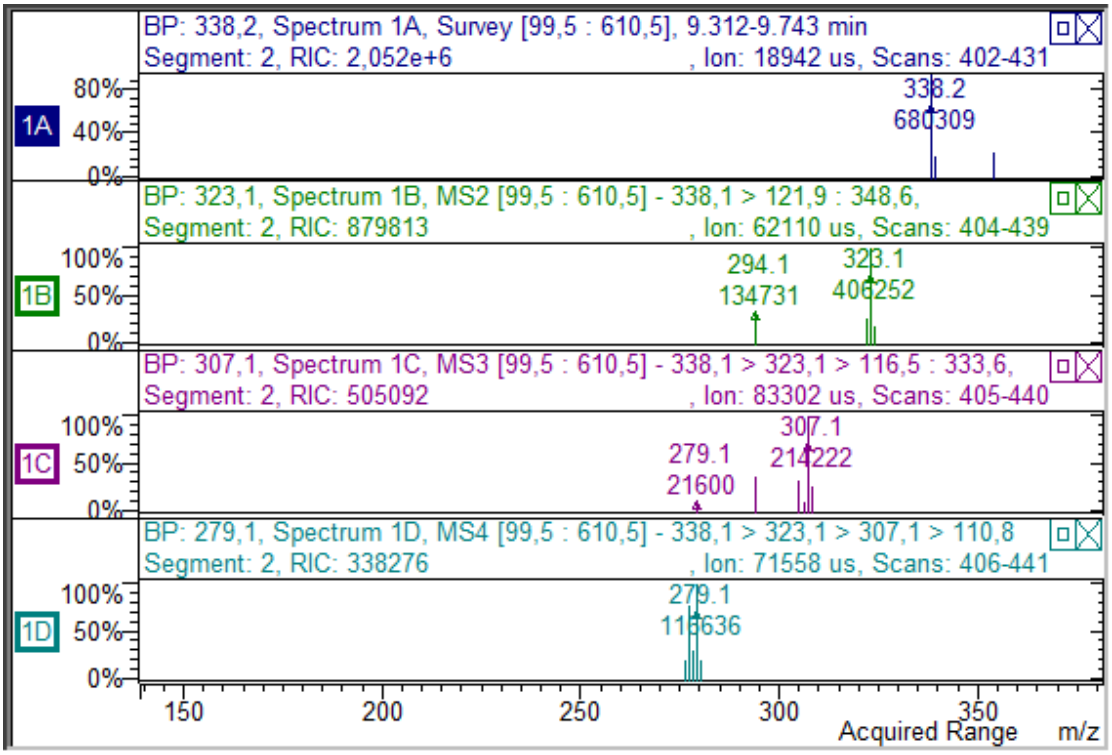

Figure 39: Mass spectrum of fragmentation of jatrorrhizine

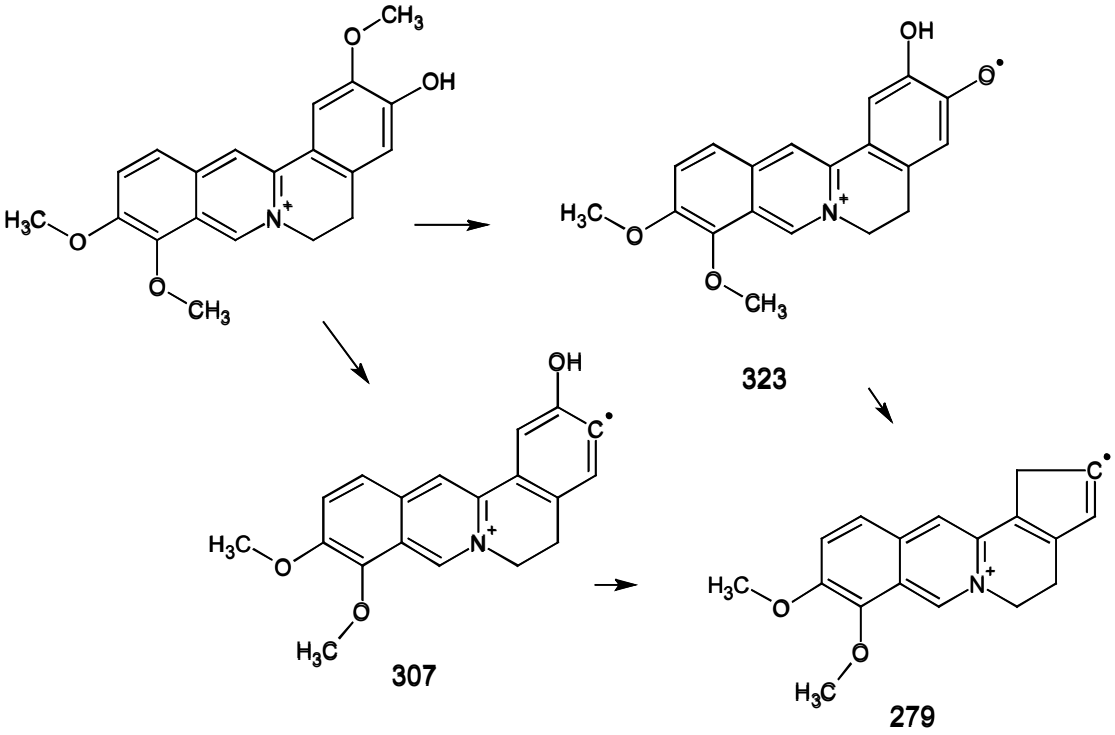

Figure 40: Mass fragmentation pattern of jatrorrhizine

4.4.11. Berberastine (LC-11)

A compound showing m/z 368 in the molecular ion $[M+H]^+$ underwent water and methyl group losses, leading to its assignment as berberastine.

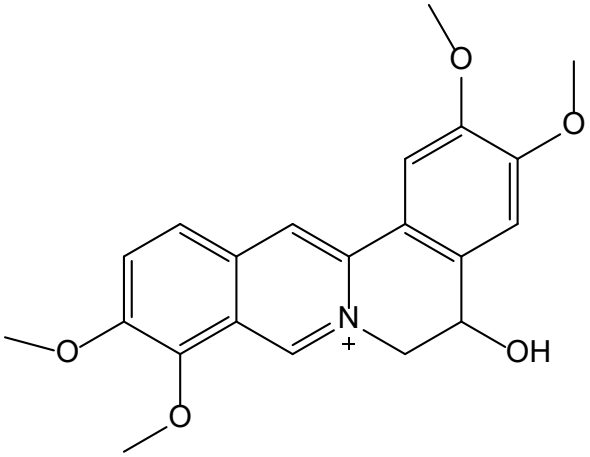

Figure 41: Structure of berberastine (**LC-11**)

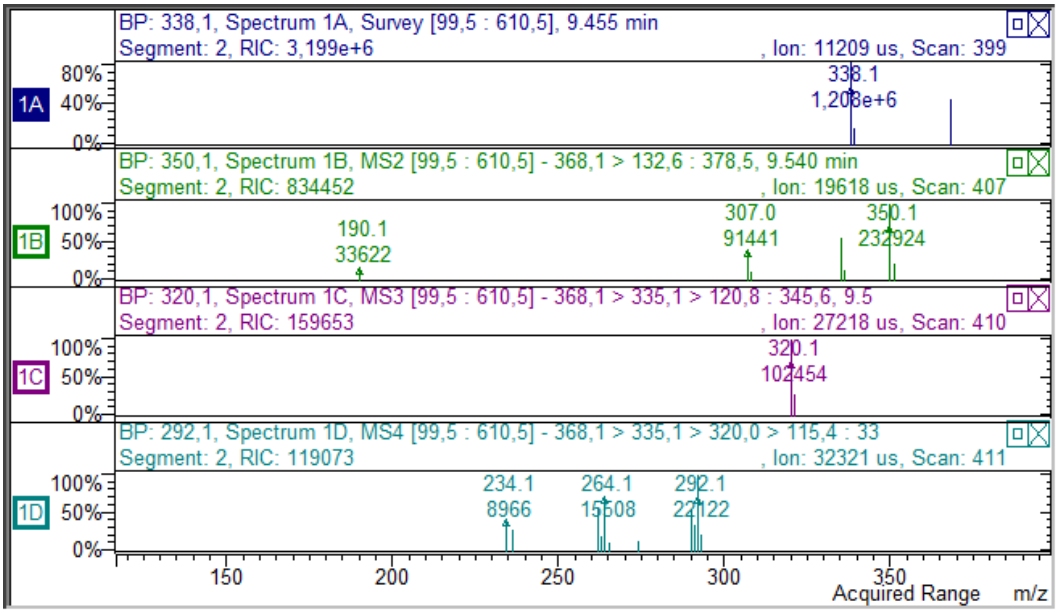

Figure 42: Mass spectrum of fragmentation of berberastine

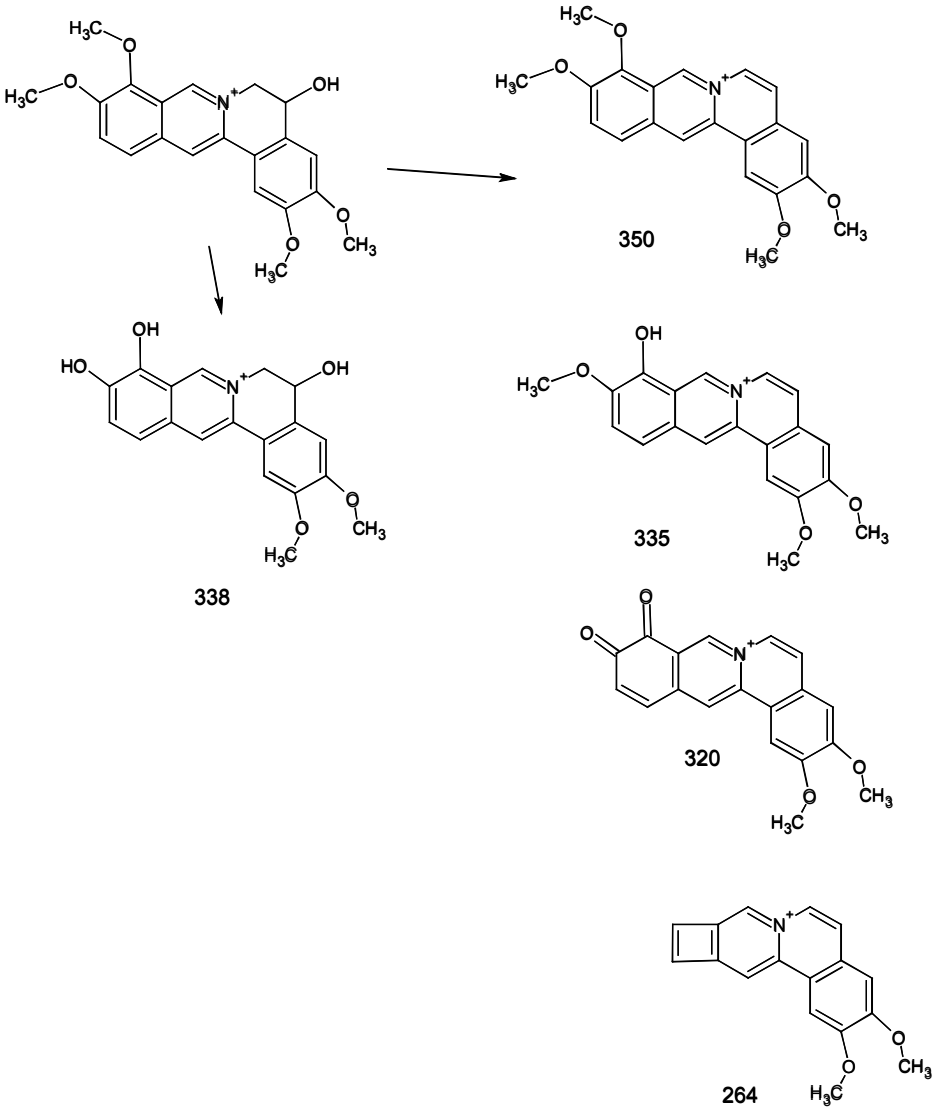

Figure 43: Mass fragmentation pattern of berberastine

4.4.12. Palmatine (LC-12)

Palmatine was identified with a molecular ion $[M+H]^+$ at m/z 352, and the MS^2 fragment at m/z 336 was indicative of the loss of a methyl group. Additional strong signals at m/z 348 and 307 were also detected.

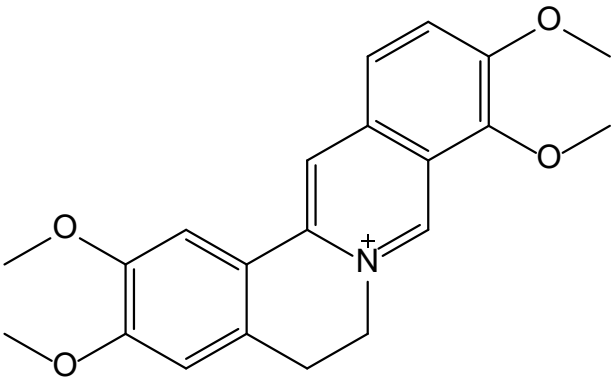

Figure 44: Structure of palmatine (**LC-12**)

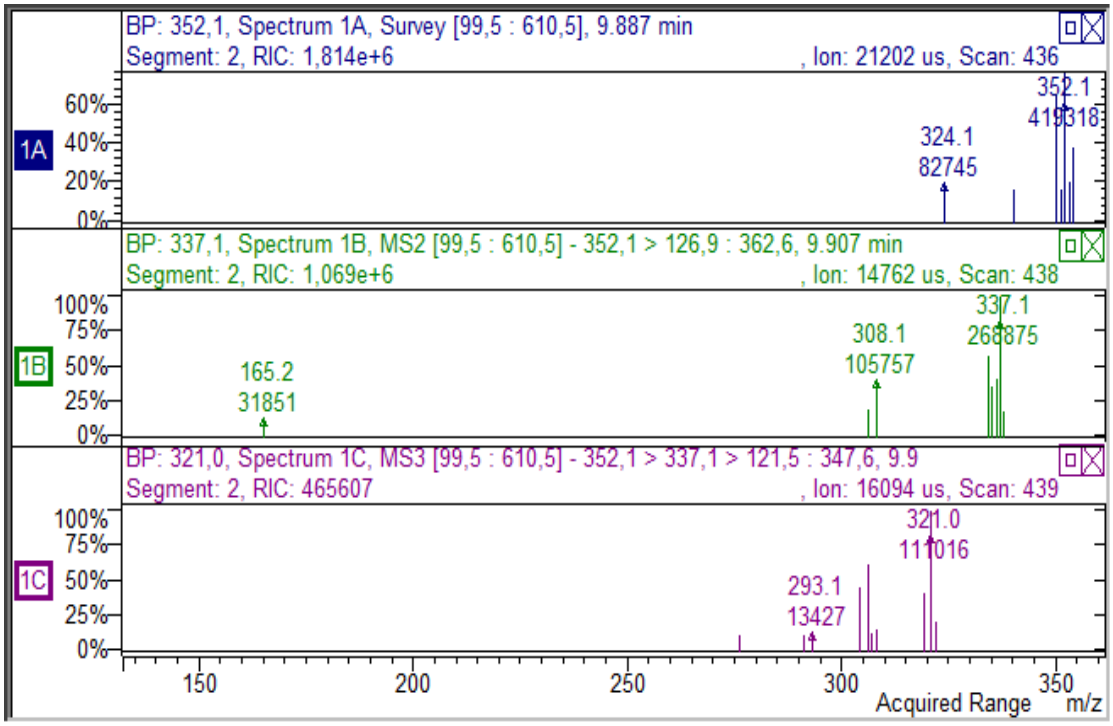

Figure 45: Mass spectrum of fragmentation of palmatine

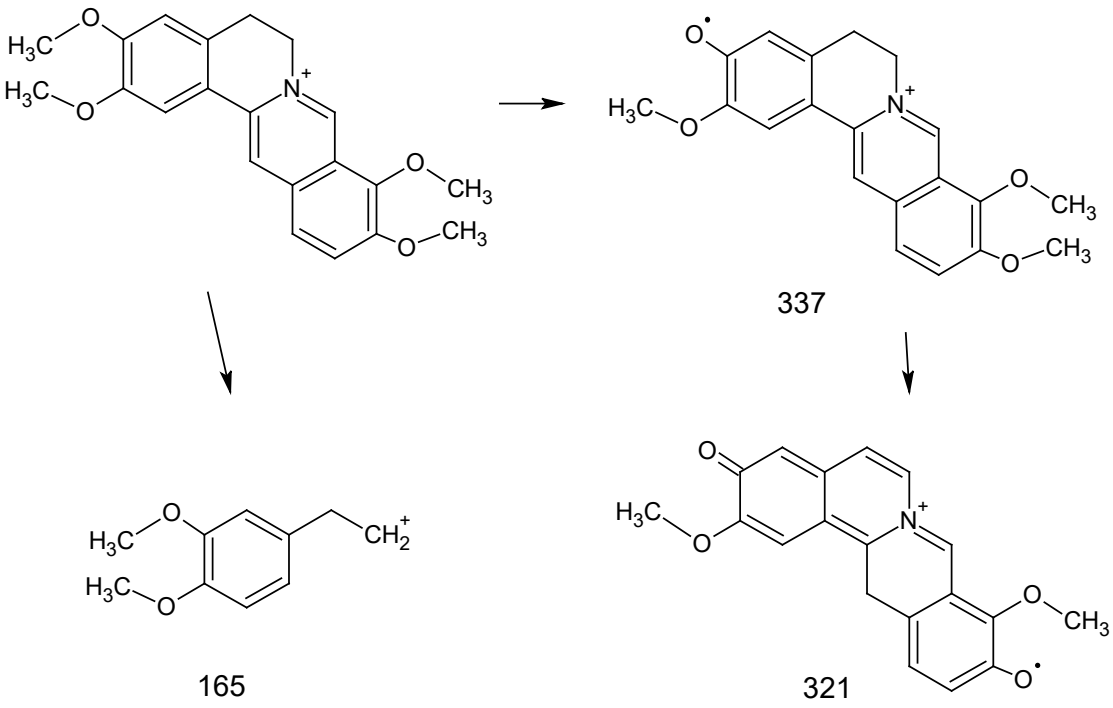

Figure 46: Mass fragmentation pattern of palmatine

4.4.13. Dehydrocorydaline (LC-13)

The molecular ion peak $[M+H]^+$ at m/z 366, supporting fragments at m/z 348, 318, 307, and 190, led to a tentative designation of the compound as dehydrocorydaline.

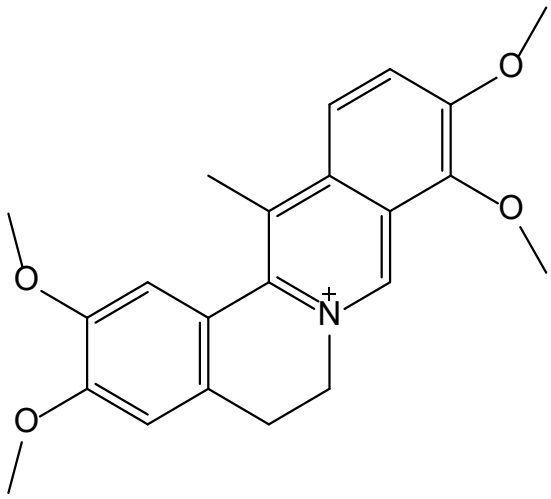

Figure 47: Structure of dehydrocorydaline (**LC-13**)

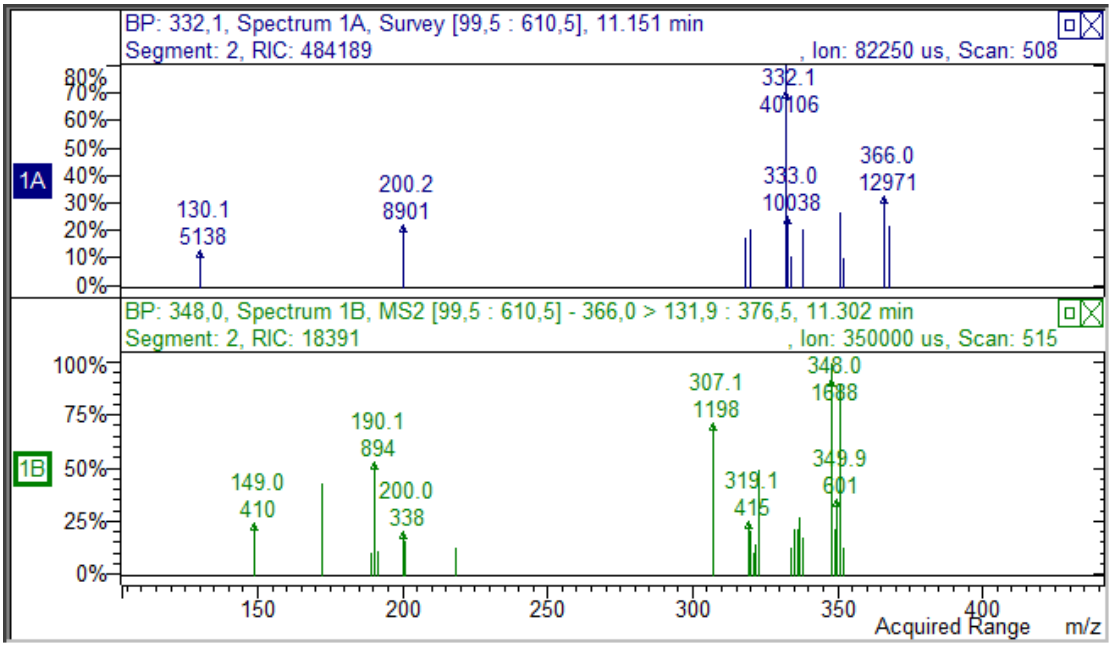

Figure 48: Mass spectrum of fragmentation of dehydrocorydaline

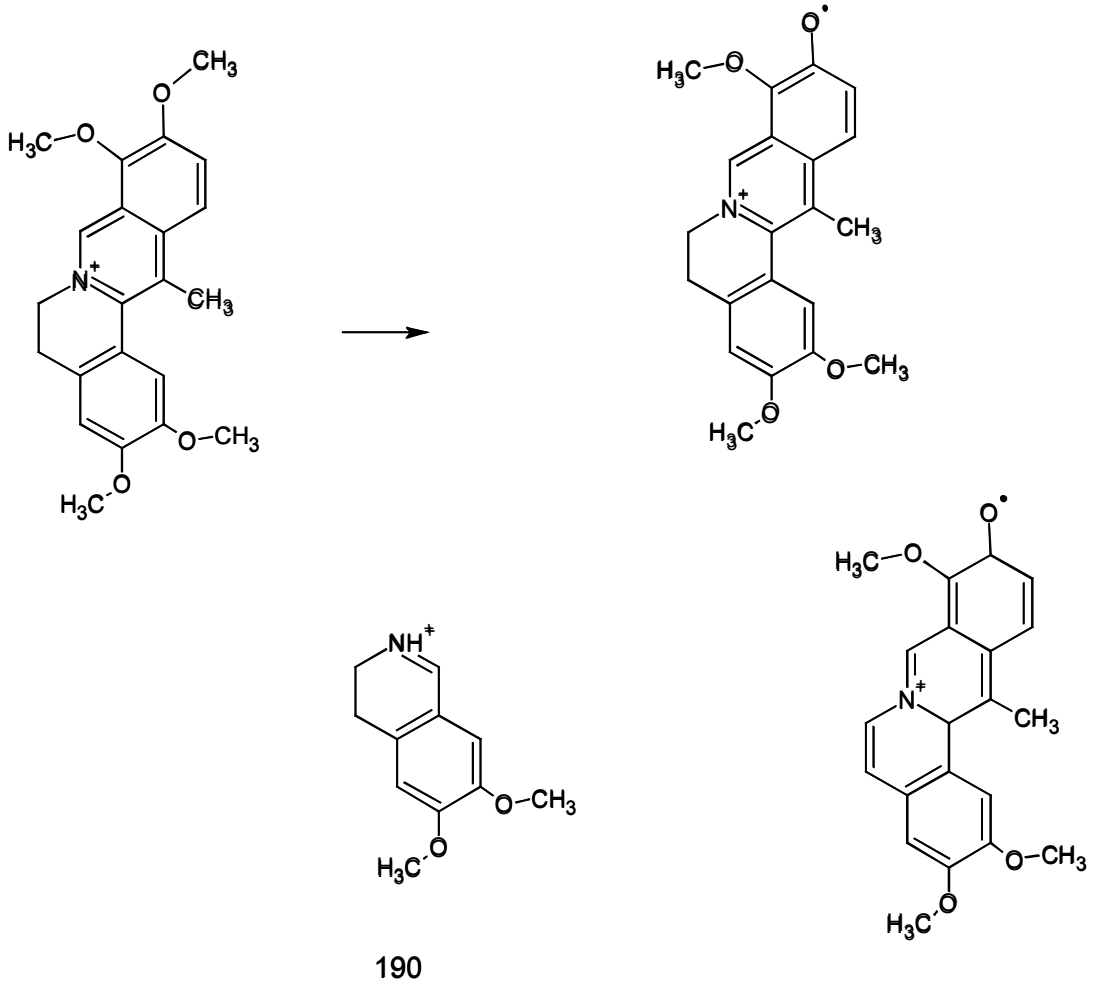

Figure 49: Mass fragmentation pattern of dehydrocorydaline

4.4.14. Sanguinarine (LC-14)

The intense peak at m/z 332 was identified as sanguinarine, a benzophenanthridine alkaloid. This identification was supported by fragments at m/z 317 and an intense signal at m/z 304, which matched data from reference literature and compounds.

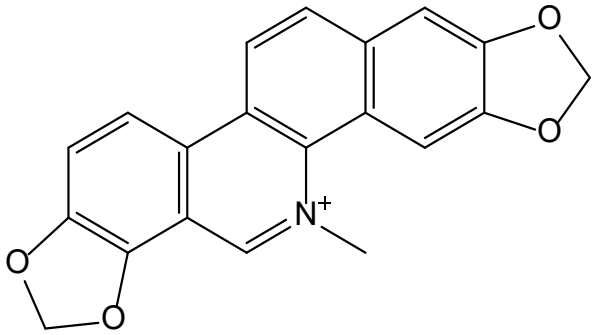

Figure 50: Structure of sanguinarine (**LC-14**)

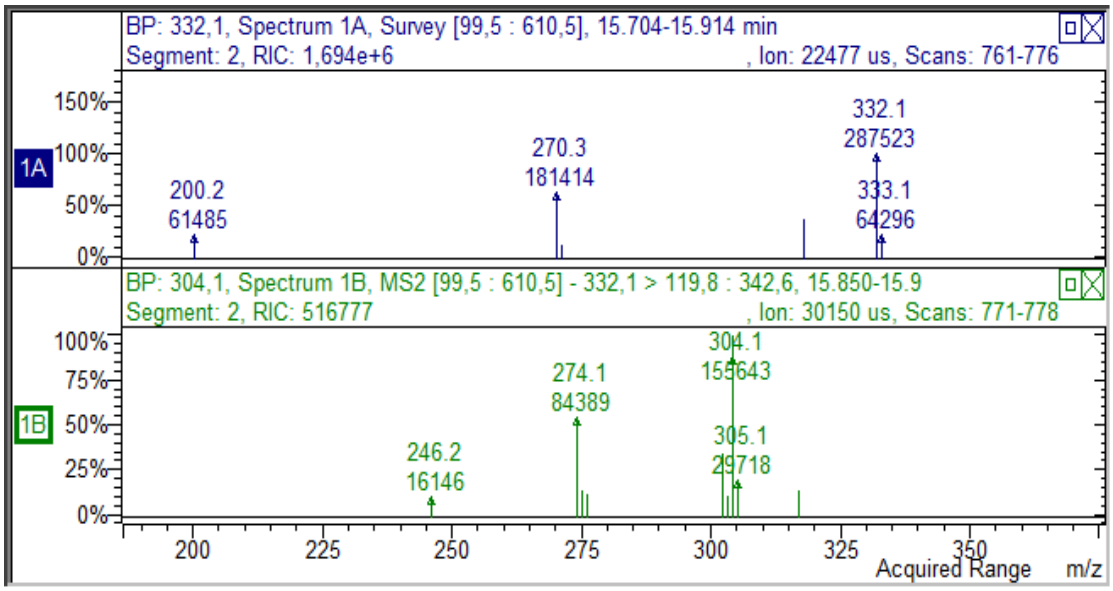

Figure 51: Mass spectrum of fragmentation of sanguinarine

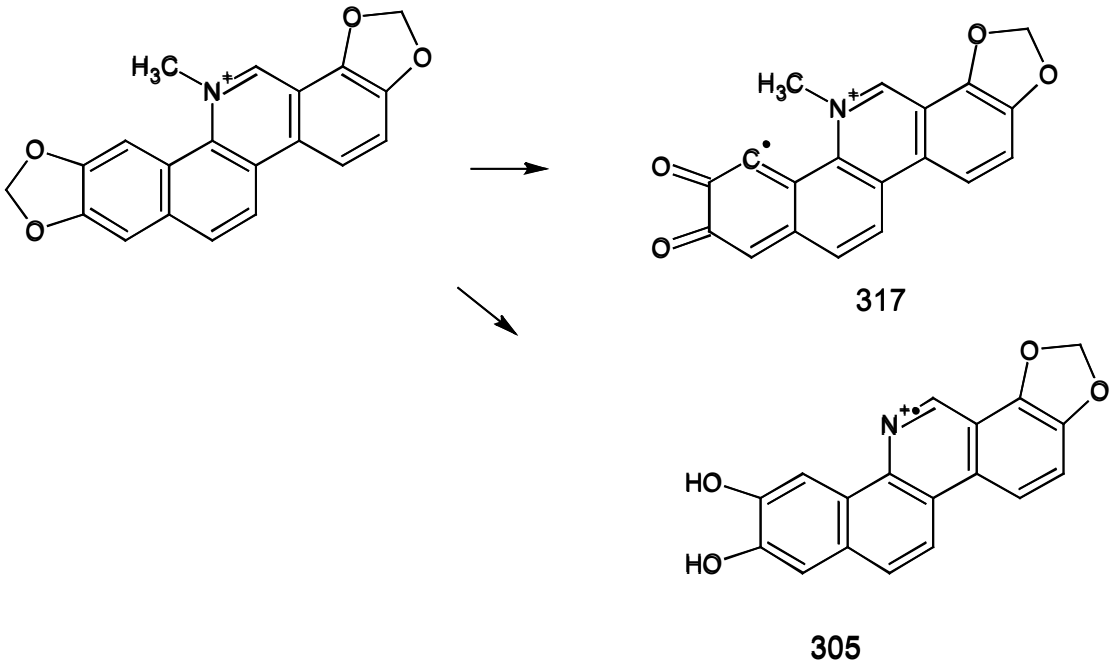

Figure 52: Mass fragmentation pattern of sanguinarine

4.4.15. Dihydrosanguinarine (LC-15)

The second intense peak at m/z 334 with a similar fragmentation pattern and an intense MS^2 signal at m/z 319 and 304 was designated as dihydrosanguinarine.

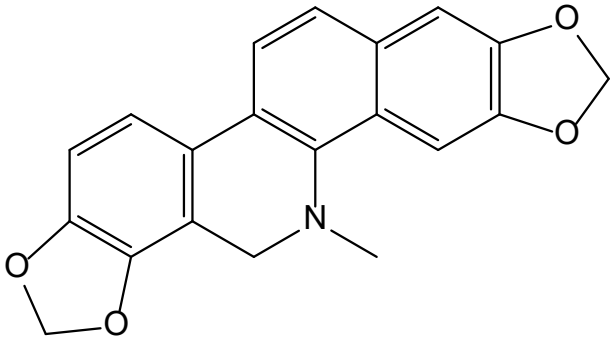

Figure 53: Structure of dihydrosanguinarine (**LC-15**)

The *C. chaerophylla* extract demonstrated a rich diversity of alkaloids, each identified and characterized through LC-DAD-MS^n analysis. The study confirmed the presence of various classes of alkaloids, including protoberberine, benzophenanthridine, and phthalide isoquinoline derivatives. The analysis also highlighted how solvent polarity affects the extraction of specific alkaloid classes, with methanol and chloroform showing higher efficiency in extracting a broader range of alkaloids compared to

hexane. This makes *C. chaerophylla* a promising botanical source for the extraction of bioactive alkaloids.

4.5. Antimicrobial Screening Analysis

The zone of inhibition (ZOI), represents a transparent area surrounding an antimicrobial disk where microorganisms fail to grow, indicating the effectiveness of the tested substance in inhibiting microbial activity (Nisar *et al.*, 2013). The antimicrobial potential of plant extracts was assessed by measuring the inhibition zone diameter for a variety of bacterial and fungal cultures. Specifically, the antimicrobial activity of *C. chaerophylla* extracts was determined by measuring the ZOI at a fixed concentration of 200 mg/mL. The ability of hexane, methanol, and chloroform extracts to inhibit the growth of specific microbes was quantified by the size of the inhibition zone, expressed in centimeters.

The extracts were tested against two Gram-positive bacteria— *Staphylococcus aureus* (ATCC 6538P) and *Bacillus subtilis* (ATCC 6051) —two Gram-negative bacteria— *Klebsiella pneumoniae* (ATCC 700603) and *Escherichia coli* (ATCC 8739)—as well *Candida albicans* (ATCC 2091), a fungal strain. The results are displayed in Table 8, showcasing the antimicrobial efficacy of the plant extracts.

Table 8: Antimicrobial activity of extracts of *C. chaerophylla*

Bacterial/Fungal strain	Reference culture	Type	Positive control (c+) cm	Negative control (c-) cm	Hexane Extract ZOI (cm)	Methanol Extract ZOI (cm)	Chloroform Extract ZOI (cm)
Escherichia coli	ATCC 8739	Gram-ve	2.6	0	0	2.5	1.8
Klebseilla pneumoniae	ATCC 700603	Gram-ve	1.8	0	0	1.2	1.7
Bacillus subtilis	ATCC 6051	Gram+ve	2.6	0	0	1.2	1.7
Staphylococcus aureus	ATCC 6538P	Gram+ve	2.6	0	1.3	2.0	2.3
Candida albicans	ATCC 2091	Fungi	2.4	0	1.5	2.0	2.3

Kanamycin, at a concentration of 5 mg/mL, served as the positive control.

Among the tested extracts, the methanol extract exhibited the highest antimicrobial activity, producing ZOIs of 2.5 cm for *Escherichia coli*, 2.0 cm for *Candida albicans*, and 1.2 cm for *Bacillus subtilis*. Similarly, the chloroform extract showed strong activity, particularly against *Staphylococcus aureus* (2.3 cm) and *C. albicans* (2.3 cm). These findings suggest that methanol and chloroform are effective solvents for extracting phenolics, flavonoids, and alkaloids, which are known for their antimicrobial properties (Phuyal et al., 2020; Wojdyło et al., 2007). The broad-spectrum activity of these extracts can be attributed to their ability to disrupt microbial cell walls, inhibit nucleic acid synthesis, or interfere with microbial enzymatic functions.

In contrast, the hexane extract showed limited activity, with ZOIs of 1.3 cm and 1.5 cm against *S. aureus* and *C. albicans*, respectively. This reduced efficacy is likely due to the selective extraction of nonpolar compounds, such as terpenoids and lipophilic flavonoid derivatives, which may have weaker antimicrobial effects compared to polar phenolics and alkaloids. The hexane extract's activity against specific strains suggests it contains nonpolar bioactive compounds with targeted antimicrobial effects, though these compounds may not act as broad-spectrum agents.

The variation in antimicrobial activity across extracts underscores the importance of solvent polarity in the extraction process. Polar solvents like methanol effectively dissolve phenolic acids, flavonoids, and alkaloids, which are potent antimicrobial agents. Chloroform, with its intermediate polarity, also extracts significant amounts of these bioactives, resulting in comparable activity to methanol. Hexane, being nonpolar, extracts lipophilic compounds that exhibit limited but targeted antimicrobial effects.

The strong activity of methanol and chloroform extracts against both Gram-positive (*S. aureus* and *B. subtilis*) and Gram-negative (*E. coli* and *K. pneumoniae*) bacteria suggests the presence of compounds capable of overcoming structural and functional differences between these microbial types. Notably, Gram-negative bacteria, with their outer membrane barriers, are typically more resistant to antimicrobial agents, yet the extracts were effective, particularly against *E. coli*. Furthermore, the notable activity against *C. albicans* highlights the potential of these extracts in antifungal applications.

These findings align with previous studies demonstrating the antimicrobial potential of plant-derived phenolics and alkaloids. Compounds such as flavonoids and tannins are

known to destabilize microbial cell membranes and inhibit critical enzymes, while alkaloids interfere with nucleic acid and protein synthesis (Nisar *et al.*, 2013; Wojdyło *et al.*, 2007). The identification of these compounds in *C. chaerophylla* through phytochemical screening and their presence in the polar extracts further validates their contribution to the observed antimicrobial activity.

The promising results from this study highlight the potential of *C. chaerophylla* extracts as natural antimicrobial agents. The broad-spectrum activity of methanol and chloroform extracts and the targeted activity of hexane extracts provide a basis for further research to isolate and identify the specific bioactive compounds responsible. These compounds could serve as leads for the development of novel antimicrobial therapies, addressing the growing concern of antibiotic resistance and the need for alternative treatments.

4.6. Antioxidant Screening Analysis

The outcomes from the DPPH assay, displaying the proportion of of free radicals scavenged by each extract based on their absorbance at 517 nm, are summarized in Table 9.

Table 9: IC_{50} values for DPPH assay of different extracts at of *C. chaerophylla*

Extracts	Concentration (µg/mL)	Percentage Scavenged	IC_{50} (µg/mL)
Hexane Extract	4000	69.80	1586 ± 3
	2000	59.24	
	1000	37.35	
	500	21.29	
	250	14.36	
Methanol Extract	1000	64.72	758.3 ± 3
	500	54.02	
	250	25.19	
	125	8.73	
	62.5	3.87	
Chloroform Extract	1000	64.26	261.5 ± 3
	500	57.13	
	250	39.23	
	125	26.33	
	62.5	15.25	

Ascorbic acid, with an IC_{50} of 12 µg/mL, was employed as the reference standard in the assay.

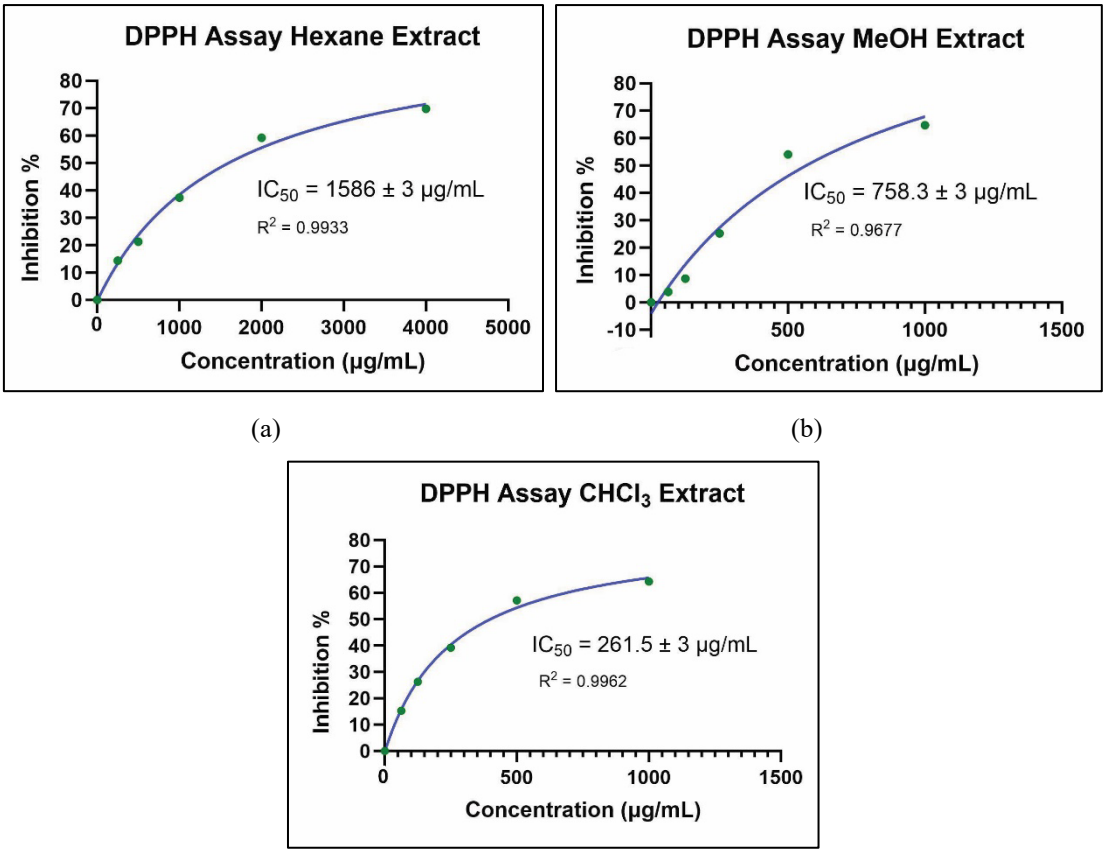

Figure 54: DPPH free radical scavenging assay of (a) hexane, (b) methanol and (c) chloroform extract of *C. chaerophylla*

The IC_{50} values, representing the concentration required to scavenge 50% of DPPH radicals, were calculated for the extracts of *C. chaerophylla* in hexane, methanol, and chloroform. The IC_{50} values were observed as 1586 ± 3 µg/mL for hexane, 758.3 ± 3 µg/mL for methanol, and 261.5 ± 3 µg/mL for chloroform.

These results indicate that the hexane extract was the least effective in scavenging DPPH radicals, whereas the methanol extract demonstrated moderate scavenging activity. The chloroform extract, however, showed the most potent antioxidant activity among the three, with the lowest IC_{50} value, indicating its superior ability to neutralize free radicals. The variation in antioxidant effectiveness is likely due to the higher concentration of phenolic constituents present in the methanol and chloroform extracts as opposed to the hexane extract.

Phenolic compounds are well-known for their antioxidant properties, primarily due to their ability to donate hydrogen atoms from their hydroxyl groups, thereby neutralizing free radicals and mitigating oxidative stress (Aberoumand & Deokule, 2008; Mensor *et*

al., 2001). This capacity to reduce oxidative damage makes these compounds valuable in protecting biological systems from the harmful effects of oxidative stress, which is associated with aging, cancer, cardiovascular diseases, and neurodegenerative disorders. The higher antioxidant activity of the chloroform and methanol extracts aligns with their phenolic content, which supports their potential use in natural antioxidant therapies.

However, the higher antioxidant activity (lower IC_{50} value) of the chloroform extract compared to the methanol extract, despite their similar TPC and TFC, can be attributed to differences in the composition and reactivity of the compounds extracted by each solvent. Chloroform, being semi-polar, likely extracted phenolic compounds with higher antioxidant potency due to their specific structural features, such as more hydroxyl groups or conjugated systems, which enhance free radical scavenging. Additionally, synergistic interactions between phenolic and non-phenolic compounds in the chloroform extract may amplify its antioxidant activity. In contrast, methanol, a highly polar solvent, extracted a broader range of phenolics, potentially including less reactive or complex compounds, such as glycosylated flavonoids, which exhibit reduced hydrogen-donating ability. Furthermore, the chloroform extract might contain non-phenolic antioxidants, such as alkaloids or terpenoids, contributing to its superior performance. These variations highlight the influence of solvent selectivity and compound-specific reactivity on antioxidant activity.

In summary, the DPPH assay highlights the significant role of solvent selection in the extraction of antioxidant compounds from *C. chaerophylla*. The high phenolic content in the chloroform and methanol extracts is directly linked to their greater antioxidant activity, positioning these extracts as promising candidates for further research in oxidative stress-related therapies.

4.7. *In vivo* Brine Shrimp Lethality Assay

The increase in brine shrimp nauplii mortality with higher concentrations of *C. chaerophylla* extracts indicates that the hexane, methanol, and chloroform extract likely contain toxic compounds exhibiting dose-dependent activity. This suggests that higher extract concentrations result in increased toxicity to the brine shrimp, revealing bioactive compounds with potential toxic effects.

Table 10: LC_{50} values for brine shrimp lethality assay of different extracts of *C. chaerophylla*

Extracts	Concentration (µg/mL)	Percentage Mortality	LC_{50} (µg/mL)
Hexane Extract	1000	100	112.3 ± 3
	500	100	
	250	80	
	125	56.67	
	62.5	43.33	
Methanol Extract	1000	100	196.0 ± 3
	500	96.67	
	250	56.67	
	125	46.67	
	62.5	43.33	
Chloroform Extract	1000	100	153.9 ± 3
	500	100	
	250	100	
	125	43.33	
	62.5	23.33	

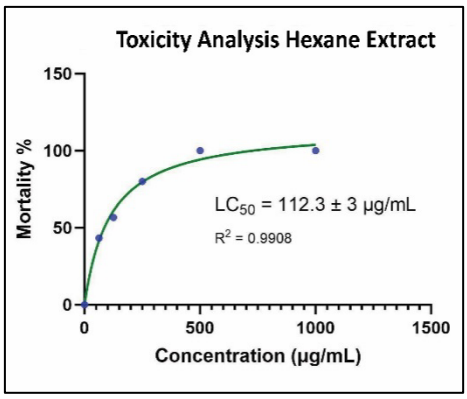

(a)

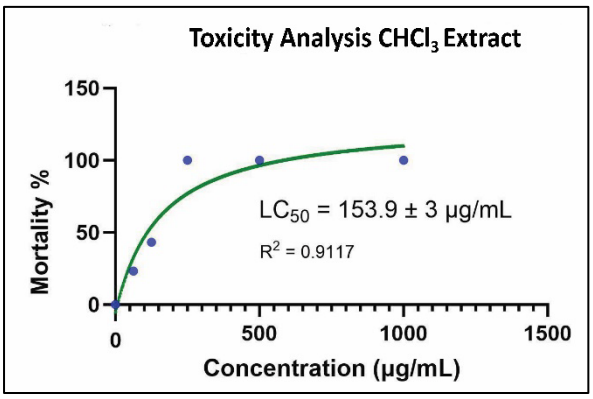

(b)

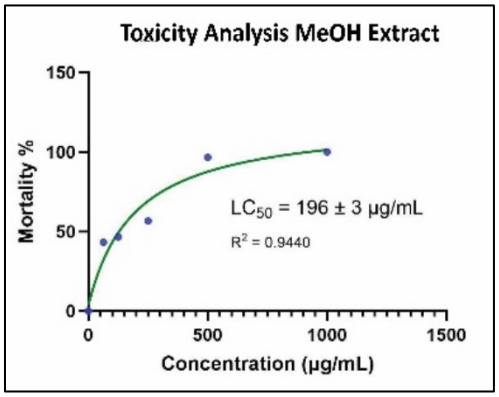

(c)

Figure 55: Brine shrimp lethality assay of (a) hexane, (b) methanol and (c) chloroform extract of *C. chaerophylla*

The lethality concentration (LC_{50}), which represents the concentration required to kill 50% of the brine shrimp population, was calculated for each extract. The hexane extract had the lowest LC_{50} value at 112.3 ± 3 µg/mL, followed by the chloroform extract at 153.9 ± 3 µg/mL, and the methanol extract at 196.0 ± 3 µg/mL (Table 10). These values suggest that all three extracts exhibit significant toxic activity, as LC_{50} values below 1000 µg/mL are generally considered indicative of toxicity (Olowa & Nuñeza, 2013). Among the extracts, the hexane extract displayed the highest toxicity, with the lowest LC_{50} value, indicating that it is the most potent in killing brine shrimp.

This toxicity, observed in the brine shrimp lethality test, provides evidence of strong bioactive compounds within the plant, possibly with anticancer properties. The dose-dependent lethality suggests that *C. chaerophylla* could contain compounds that disrupt cellular processes, which may be relevant in cancer research. As all the extracts demonstrated cytotoxicity at concentrations below 1000 µg/mL, they show potential for further investigation in pharmacological studies, particularly in the development of anticancer agents.

The brine shrimp assay is widely used as a preliminary screening tool for cytotoxicity and potential anticancer properties, and these results suggest that *C. chaerophylla* warrants further study for its bioactive constituents that may have therapeutic applications in treating cancer and other diseases associated with cell proliferation.

4.8. α-Amylase Inhibition Assay

This study utilized an *in vitro* α-amylase inhibition assay to explore the potential antidiabetic properties of *C. chaerophylla* extracts. This assay helps evaluate the ability of plant extracts to inhibit α-amylase, an enzyme responsible for breaking down complex carbohydrates into simpler sugars, which subsequently elevates blood glucose levels.

Table 11: IC_{50} values for α-amylase inhibition of different extracts of *C. chaerophylla*

Extracts	Concentration (µg/mL)	Percentage Mortality	IC_{50} (µg/mL)
Hexane Extract	5000	70.31	1156 ± 3
	2500	51.17	
	1250	41.83	
	625	31.48	
	312.5	22.19	
Methanol Extract	500	65.17	51.52 ± 2
	250	60.19	
	125	51.30	
	62.5	39.34	
Chloroform Extract	500	70.93	93.13 ± 2
	250	62.04	
	125	41.65	
	62.5	38.61	

Acarbose was used as the standard.

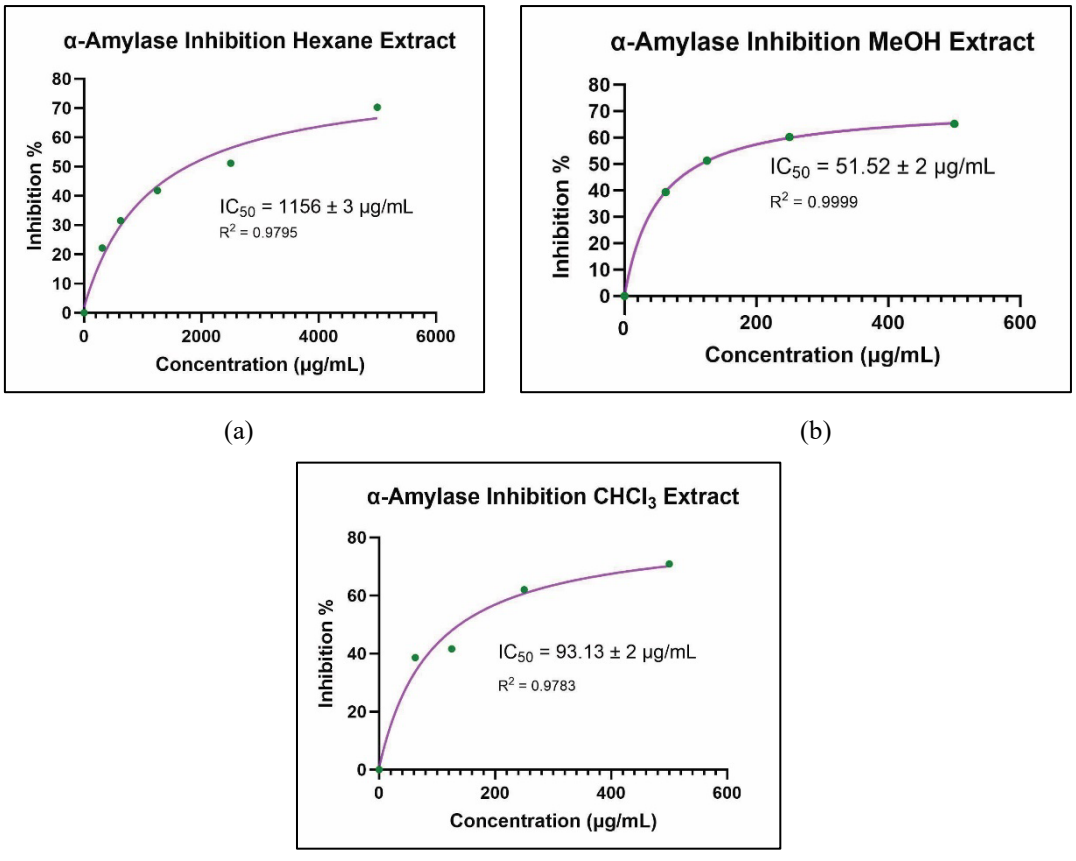

(a) (b)

(c)

Figure 56: α-Amylase inhibition assay of (a) hexane, (b) methanol and (c) chloroform extract of *C. chaerophylla*

The results showed that the methanol extract exhibited the most significant inhibitory activity, with an IC_{50} value of 51.52 ± 2 µg/mL. The chloroform extract followed, with an IC_{50} of 93.13 ± 2 µg/mL, while the hexane extract demonstrated the least activity, with an IC_{50} of 1156 ± 3 µg/mL. The lower the IC_{50} value, the more potent the extract is at inhibiting α-amylase, indicating that the methanol extract was the most effective at reducing enzyme activity.

The α-amylase enzyme plays a crucial role in the hydrolysis of the 1,4-glucosidic bonds in starch, glycogen, and other carbohydrates. By inhibiting this enzyme, glucose release into the bloodstream is delayed, leading to a reduction in postprandial (after-meal) blood sugar spikes. This is a key mechanism for managing diabetes, particularly type 2 diabetes, where controlling postprandial hyperglycemia is essential to prevent long-term complications (Sun *et al.*, 2020).

The study on the antioxidant and α-amylase inhibitory activities of *C. chaerophylla* extracts highlights the complex interplay between solvent-specific extraction efficiencies and the functional bioactivities of phytochemicals. While the chloroform extract exhibited superior antioxidant activity in the DPPH assay (IC_{50} = 261.5 ± 3 µg/mL), the methanol extract demonstrated greater efficiency in inhibiting α-amylase (IC_{50} = 51.52 ± 2 µg/mL). This apparent discrepancy arises from the distinct chemical compositions and mechanisms of action underlying these bioactivities.

The chloroform extract's potent antioxidant activity can be attributed to its selective extraction of phenolic compounds with high free radical scavenging efficiency, such as those with multiple hydroxyl groups or conjugated systems. These compounds are particularly effective in neutralizing DPPH radicals due to their electron-donating properties (Mensor et al., 2001). In contrast, the methanol extract, while rich in phenolics and flavonoids, may have included a broader spectrum of phenolic compounds, including those with lower antioxidant reactivity. Additionally, synergistic interactions between phenolic and non-phenolic compounds in the chloroform extract might enhance its antioxidant potential.

However, the methanol extract outperformed the chloroform extract in α-amylase inhibition. This can be attributed to methanol’s ability to extract a wider variety of bioactive compounds, including specific phenolics and flavonoids known to interfere

with carbohydrate-hydrolyzing enzymes (Sun *et al.*, 2020). Flavonoids, for example, can bind to the active site of α-amylase, inhibiting its enzymatic activity. Furthermore, methanol's polar nature may facilitate the extraction of glycosylated flavonoids or tannins, which are particularly effective in inhibiting enzymes like α-amylase.

The differences in activity also highlight the distinct functional roles of phenolics and flavonoids. While their antioxidant properties depend on their ability to neutralize free radicals, their enzyme-inhibitory effects rely on their capacity to interact with specific enzyme active sites. The composition and structural diversity of the bioactive compounds extracted by each solvent likely influence their performance in these assays.

These findings suggest that while the chloroform extract is better suited for antioxidant applications, the methanol extract holds promise for managing diabetes through α-amylase inhibition. The results underscore the importance of understanding the functional specificity of phytochemicals and the role of solvent polarity in targeting different therapeutic mechanisms. Further research is needed to isolate and characterize the specific compounds responsible for these activities and to evaluate their potential synergistic effects.

4.9. *In vivo* Acute Oral Toxicity Study

Table 12: Median lethal dose (LD_{50}) of different extracts of *C. chaerophylla*

Extracts	LD_{50} (mg/kg BW)	Hazard Statement	Remarks
Hexane	> 2000 mg/kg BW	May be harmful if swallowed	No death at 2000 mg/kg
Methanol	1000.36 mg/kg BW	Harmful if swallowed	Death with convulsion
Chloroform	515 mg/kg BW	Harmful if swallowed	Death with convulsion

The median lethal dose (LD_{50}) values of different *C. chaerophylla* extracts were evaluated to assess their toxicity in mice. The LD_{50} represents the dose at which 50% of the test population would be expected to die from exposure. In this study, the hexane extract had an LD_{50} of greater than 2000 mg/kg body weight (BW), indicating that it may be considered relatively non-toxic, as no deaths were observed even at the highest tested dose. The methanol extract, with an LD_{50} of 1000.36 mg/kg BW, was found to be harmful, as it caused death accompanied by convulsions in the test animals. The

chloroform extract was the most toxic, with an LD_{50} of 515 mg/kg BW, also causing death with convulsions (Table 12).

The results suggest that the hexane extract is the least hazardous, as no deaths were observed even at 2000 mg/kg BW, implying that it poses minimal acute toxicity when ingested. This indicates that the bioactive compounds present in the hexane extract may have lower toxicity or are present in concentrations that do not pose immediate risks.

The methanol extract, with an LD_{50} of 1000.36 mg/kg BW, demonstrates moderate toxicity. Its harmful effects, including convulsions leading to death, suggest that some bioactive compounds in the methanol fraction could interfere with the central nervous system or other critical biological pathways. Despite its potential therapeutic value, the safety of methanol extract needs to be carefully evaluated, especially at higher doses.

The chloroform extract, having the lowest LD_{50} at 515 mg/kg BW, is the most toxic of the three extracts tested. The presence of cytotoxic or neurotoxic compounds in the chloroform extract likely contributes to its lethality. The convulsions observed before death further indicate that this extract may contain compounds that affect neurological function.

The varying toxicity levels among the extracts can be attributed to their different chemical compositions, as each solvent extract different classes of compounds. Hexane, being a non-polar solvent, primarily extracts lipophilic compounds, which may account for its lower toxicity. In contrast, methanol and chloroform, more polar solvents, extract a wider range of bioactive compounds, including those that might be harmful at higher doses.

Despite its safety, the hexane extract showed limited pharmacological activity in antioxidant, antimicrobial, and α-amylase inhibition assays, likely due to its composition of nonpolar lipophilic compounds, such as terpenoids and sterols, which are less bioactive in the tested pathways. In contrast, the methanol and chloroform extracts, rich in reactive phenolics, flavonoids, and alkaloids, demonstrated strong bioactivity but higher toxicity, suggesting their bioactive compounds may interfere with critical biological pathways. The safety of the hexane extract makes it suitable for applications prioritizing low toxicity, while the methanol and chloroform extracts require careful dose optimization to harness their therapeutic potential safely. These

findings highlight the need to balance safety and efficacy in developing *C. chaerophylla*-based formulations. Further studies should focus on isolating bioactive compounds to enhance therapeutic value while minimizing toxicity.

4.10. Structural Elucidation of New Isolated Compounds

4.10.1. Chaeronepaline-A (1)

The compound **1** was thoroughly analyzed through mass spectrometry, showing a molecular ion at $[M+H]^+$ with an *m/z* value of 324. This indicated the molecular mass of the compound. The fragmentation pattern was key in identifying structural features, particularly with the loss of a methyl group, which produced a fragment ion at *m/z* 309. Based on the high-resolution mass spectrometry (HR-MS) data, the molecular formula of the compound was calculated as $C_{19}H_{18}NO_4$. This formula gave insights into the presence of specific functional groups and atom counts.

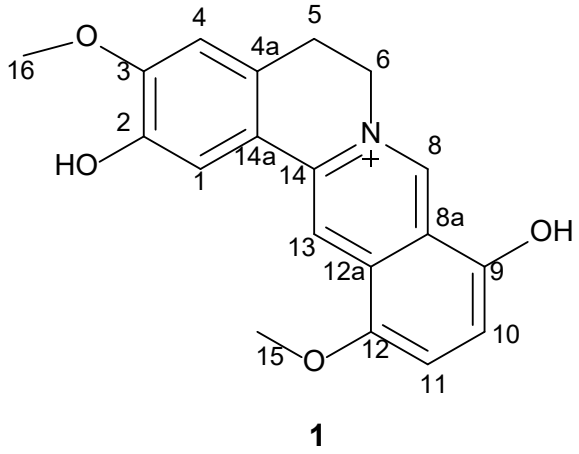

1

Figure 57: Structure of chaeronepaline-A (**1**)

The proton NMR (^{1}H-NMR) spectrum provided further structural details. Four singlets appeared at δ 9.30 (H-8), 8.03 (H-13), 7.39 (H-1), and 6.93 (H-4), each integrating for a single proton. These singlets likely indicated distinct hydrogen environments in the compound, possibly aromatic groups. Additionally, the occurrence of two distinct singlets at δ 3.94 (H-16) and 3.90 (H-15), integrating for three protons each, confirmed the existence of two methoxy groups (-OCH_3) attached to the compound's aromatic system. This detail was important for understanding the positioning of substituents on the aromatic ring.

Other notable findings from the NMR spectrum included two ortho-coupling doublets (*J = 8.0*) were observed at δ 7.58 (H-11) and 6.94 (H-10), which supported the presence of an aromatic ring system with adjacent hydrogens, and two aliphatic triplets (*J=6.2*) at δ 4.64 (H-6) and 3.16 (H-5), each integrating for two protons, showing clear evidence of aliphatic chains or linkages within the compound. The chemical shifts and coupling constants provided further evidence for the structure's complexity, particularly the involvement of an aromatic system.

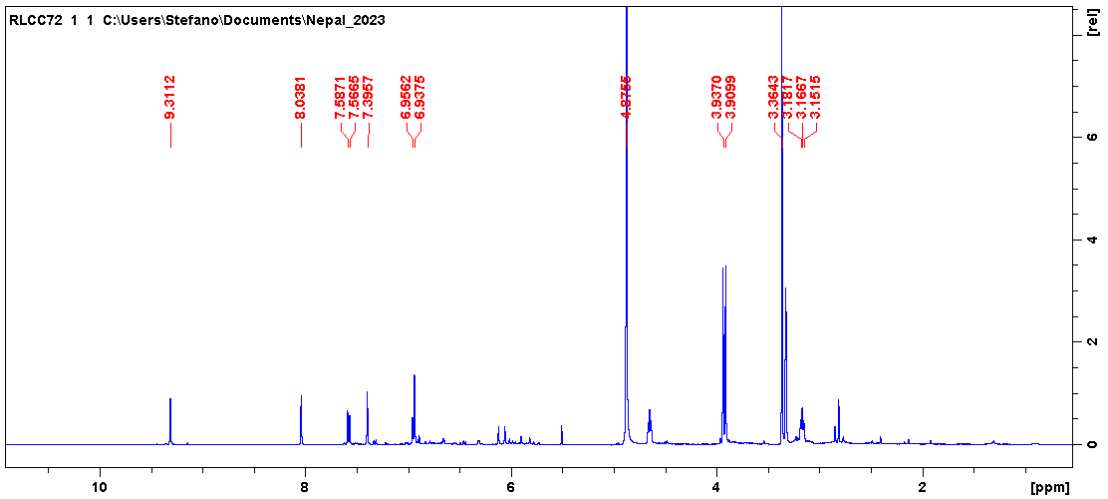

Figure 58: [1]HNMR spectra of compound **1**

Table 13: [13]C NMR and [1]H NMR data for compound **1** (δ in ppm, 100 MHz and 400 MHz respectively, in $MeOD_4$).

Position	δ_C	δ_H
1	111.1 CH	7.39, s, 1H
2	146.6 C	-
3	149.3 C	-
4	110.0 CH	6.93, s, 1H
4a	126.2 C	-
5	27.3 CH_2	3.16, t, 2H, *J=6.2*
6	54.2 CH_2	4.64, t, 2H, *J=6.2*
7	-	-
8	145.9 CH	9.30, s, 1H
8a	120.1 C	-
9	162.0 C	-
9a	-	-
10	107.9 CH	6.94, d, 1H, *J=8.0*
11	123.3 CH	7.58, d, 1H, *J=8.0*

12	149.7 C	-
12a	132.4 C	-
13	117.9 CH	8.03, s, 1H
14	134.6 C	-
14a	120.2 C	-
15	55.6 CH_3	3.90, s, 3H, OCH_3
16	55.2 CH_3	3.94, s, 3H, OCH_3
17	-	-
18	-	-

The HSQC-DEPT spectrum helped to identify all non-quaternary positions, revealing that the compound contained six aromatic CH groups, two aliphatic CH_2 groups, and one benzylic and N-linked carbons. These structural features were essential for mapping out the compound's framework. For instance, the benzylic group at δ_H 3.16 – δ_C 27.3, linked to C-5, and the N-linked group at δ_H 4.64 – δ_C 54.2 at C-6 suggested a connection between these positions in the molecule's skeleton. Also, the two methoxyl positions were confirmed.

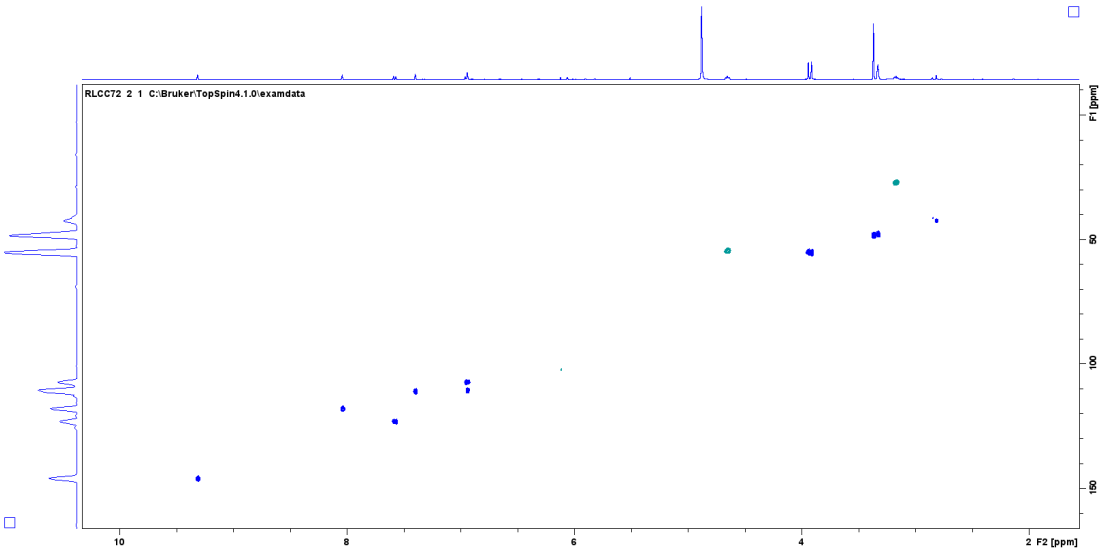

Figure 59: HSQC spectra of compound **1**

The complete structure of the compound was pieced together by using HMBC (Heteronuclear Multiple Bond Correlation), COSY (Correlation Spectroscopy), and NOESY (Nuclear Overhauser Effect Spectroscopy) data. HMBC correlations provided crucial long-range interactions, such as those from the singlet at δH 7.39 (H-1), which correlated with C-4a (δ_C 126.2), C-3 (δ_C 149.3) and C-14 (δ_C 134.6), and those from δ_H

6.93 (H-4), correlating with C-2 (δ_C 146.6), C-14a (δ_C 120.2) and C-5 (δ_C 27.3). These correlations strongly suggested the presence of an electron-attracting group at C-2 and methoxyl substitution at C-3. The methoxyl group attached at δ_H 3.94 had clear HMBC correlations with C-3, confirming a 3-methoxyl substitution. Other diagnostic correlations, such as those from H-5 (δ_H 3.16) to C-4 (δ_C 110.0), C-14a and C-4a, supported the direct linkages between critical positions 4a and 5 in the molecular structure.

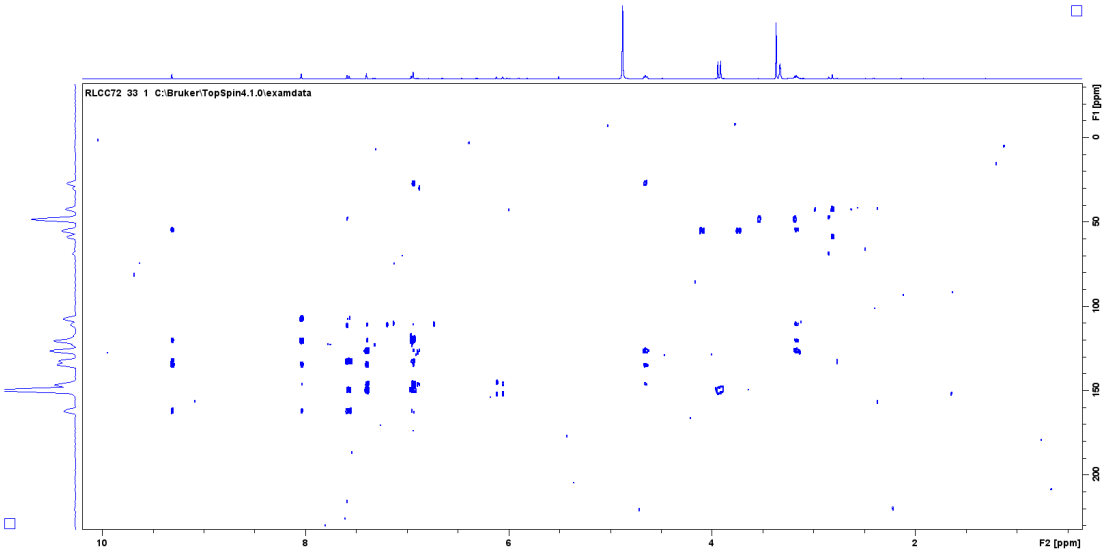

Figure 60: HMBC spectra of compound **1**

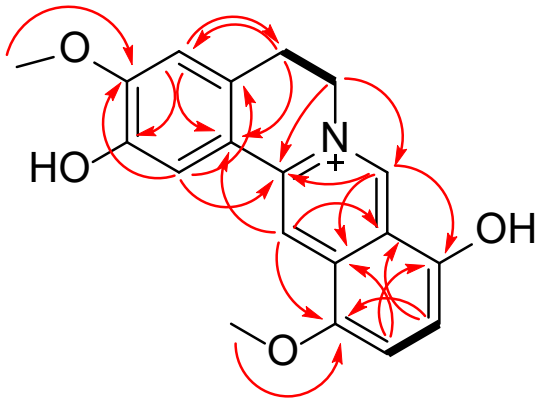

1

Figure 61: Key HMBC (red arrows), ^{1}H-^{1}H COSY (bold) correlation of compound **1**

The COSY spectrum supported this by showing coupling between H-5 and H-6, while the HMBC correlation from H-6 to C-4a and C-14 further solidified the existence of a

3,4-dihydroquinoline moiety. Further diagnostic HMBC from H-6 is observed with C-8 (δ_C 145.9). Additional HMBC correlations from H-8 (δH 9.30) to C-14 confirming the six-membered ring structure of 3,4-dihydroisoquinoline derivatives. and C-12a (δ_C 132.4) and C-9 (δ_C 162.0) pointed toward the presence of a hydroxyl group at C-9, further clarifying the nature of the functional groups. The proton H-13 exhibited significant long-range HMBC interactions with two carbons: C-8a (δ_C 120.1) and C-12 (δ_C 149.7). The correlation with C-12 is especially noteworthy because it aligns with the methoxy group observed at δ_H 3.90, confirming the existence of a methoxy group attached at the 12th position of the compound's structure. This kind of long-range correlation helps in identifying the placement of functional groups, particularly for the 12-linked methoxy substitution. Furthermore, the two ortho-coupling doublets, assigned to protons at positions H-10 and H-11, also showed long-range HMBC correlations. These protons exhibited interactions with several critical carbons: C-8a, C-12, C-9, and C-12a. These correlations reinforce the connectivity and orientation of these positions within the aromatic system. The strong interactions between H-10 and H-11 with these carbons help in confirming the structure's geometry and the positions of key functional groups around the aromatic ring system.

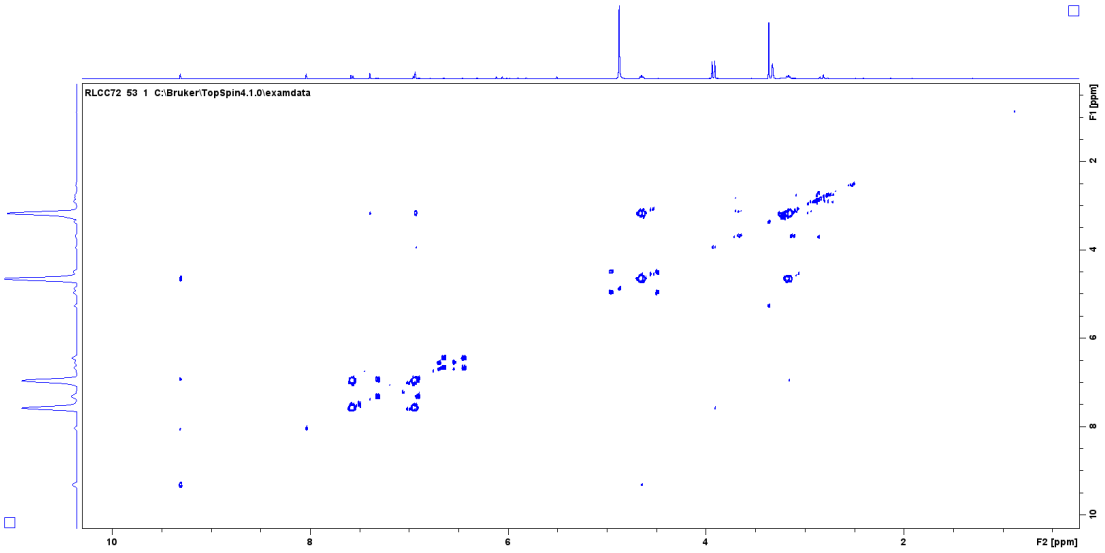

Figure 62: COSY spectra of compound **1**

Finally, NOESY spectra confirmed spatial interactions, the cross peak between H-16 and H-4, and, H-15 with H-13, and H-11, which verified the positions of the methoxy groups and established the overall connectivity of the structure. These detailed spectral

analyses culminated in the identification of the compound **1** as 3,12-Dimethoxy-5,6-dihydroisoquinolino[2,1-b]isoquinolin-7-ium-2,9-diol, and named Chaeronepaline-A.

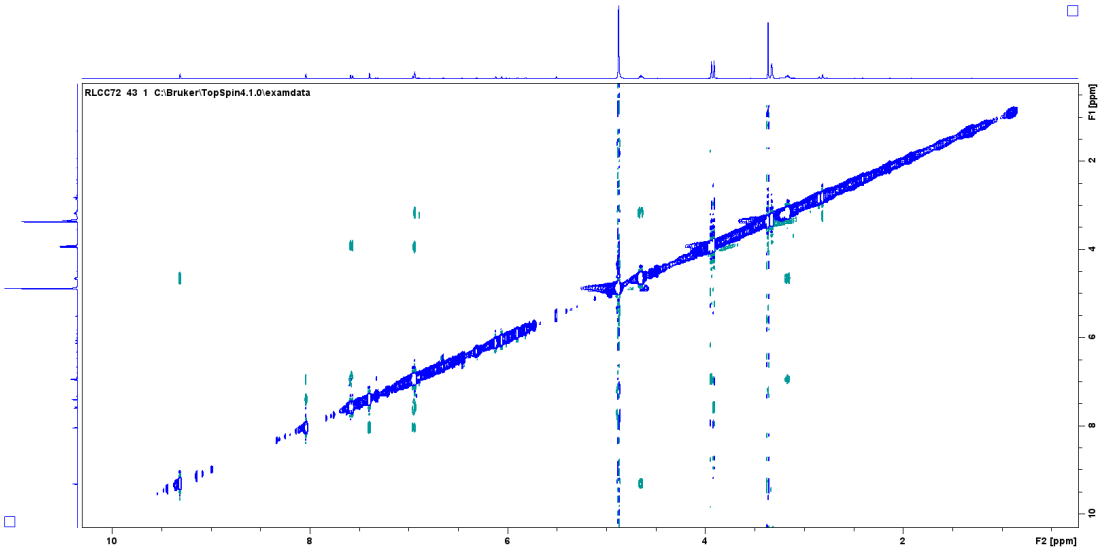

Figure 63: NOESY spectra of compound **1**

As per our knowledge, this compound is being reported for the first time from natural sources, indicating its novelty and potential importance in the field of natural product chemistry. Its unique structure and the methodological rigor used in its identification highlight its significance in the broader context of alkaloid research and potential bioactivity studies.

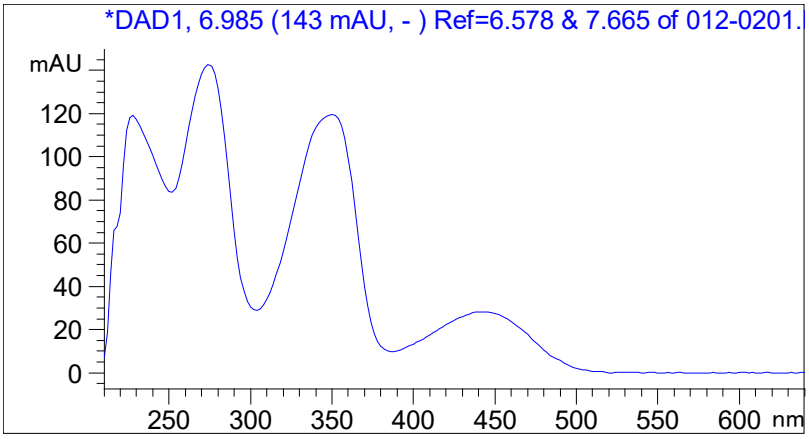

Figure 64: UV spectra of compound **1**

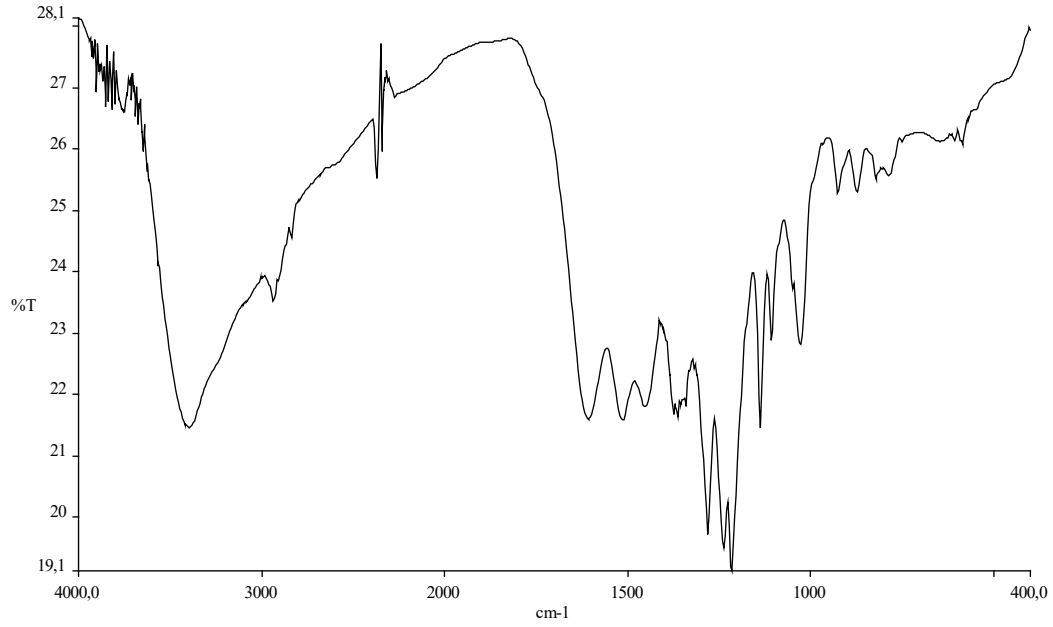

Figure 65: IR spectra of compound **1**

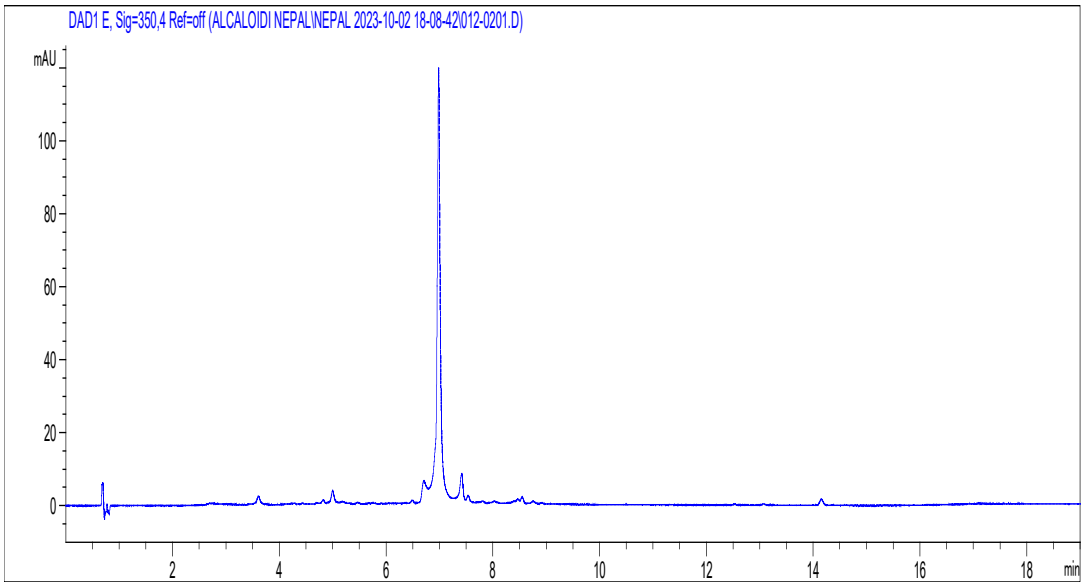

Figure 66: Chromatogram of compound **1** at 350 nm

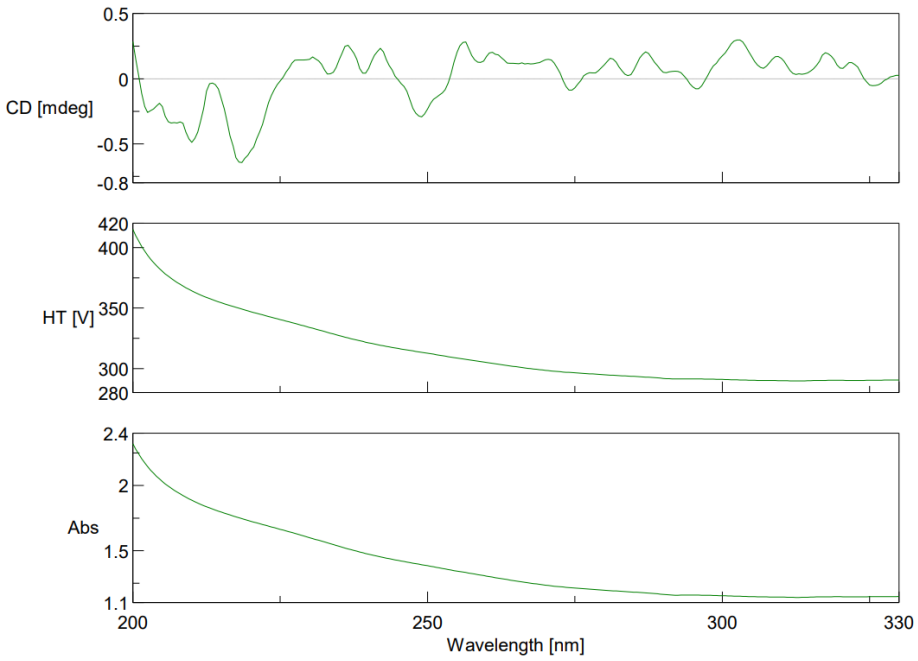

Figure 67: Circular dichroism of compound **1**

The behaviour of the new alkaloids was evaluated using liquid chromatography with multiple stage mass spectrometry (LC-MS^n) in positive ion mode, allowing the observation of relevant ion species useful for structural elucidation and for the development of further analytical methods.

Compound **1** presented a charged nitrogen in the structure; in the spectrum, it was observed as $[M]^+$ ions at *m/z* 324 in positive ion mode. When CID was performed in an ion trap, the $[M]^+$ ion produced the prominent product at *m/z* 309, due to the loss of methyl radical (Figure 68). This product ion was further subjected to MS^3 analysis leading to the ion at *m/z* 294 corresponding to the loss of a further methyl radical, confirming the presence of two methoxyl groups in the structure. Ion at *m/z* 294 was subjected to MS^4, which afforded the product ion at *m/z* 266, corresponding to a loss of 28Da.

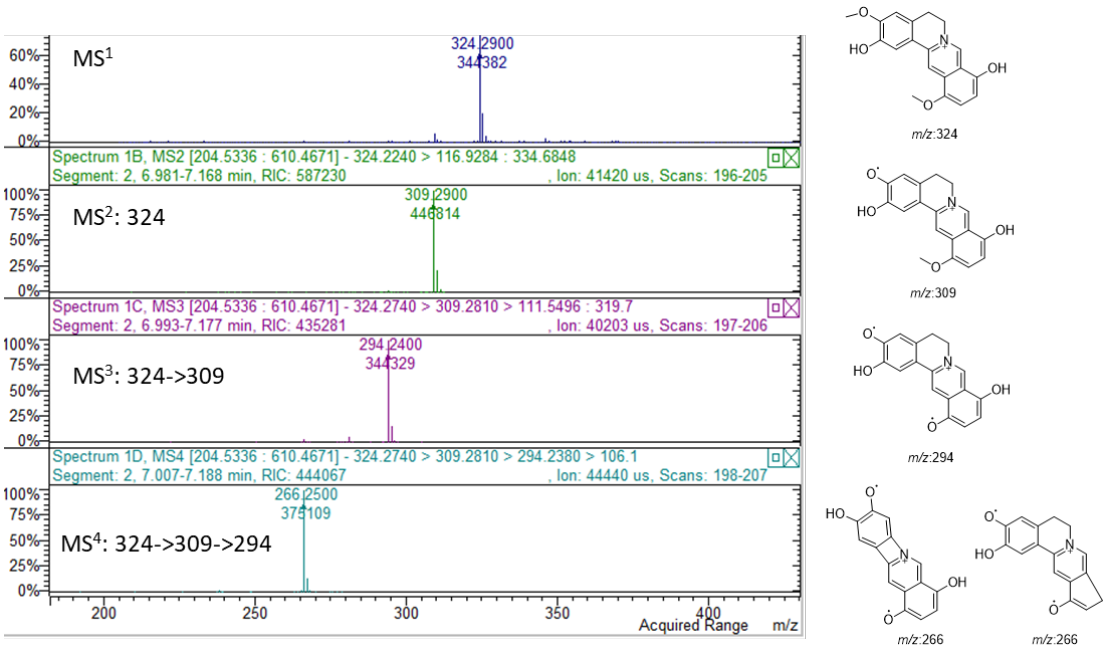

Figure 68: Mass fragmentation pattern of compound **1**

4.10.2. Chaeronepaline-B (2)

The compound (**2**) revealed a molecular ion $[M+H]^+$ at *m/z* 354. From the HR-MS data, the molecular formula was deduced as $C_{20}H_{20}NO_5$, suggesting the presence of multiple functional groups.

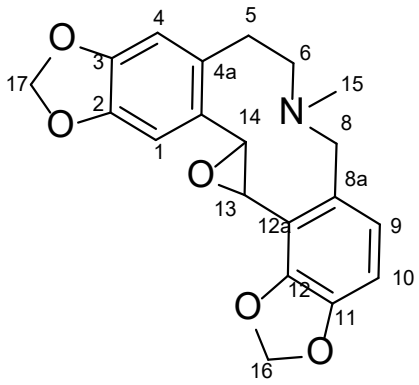

2

Figure 69: Structure of chaeronepaline-B (**2**)

The ^{1}H-NMR spectrum provided crucial details, showing two singlets in the deshielded region at δ_H 7.14 (H-1) and 6.79 (H-4), each integrating for one proton. Additionally,

two ortho-coupled doublets (*J=7.0*) appeared at δ_H 6.86 (H-9) and 6.81 (H-10), also integrating one proton each. These signals supported the presence of two distinct aromatic rings, indicating a structure consistent with previous studies on protopine-type alkaloids (Simoes-Pires *et al.*, 2014). Singlets at δ_H 6.00 (H-16) and 6.00 (H-17), integrating two protons each, pointed to the presence of two methylenedioxy groups, which are common in such alkaloid structures.

In the aliphatic region, several broad signals were observed: δ_H 4.48 (H-6, 2H), 3.86 (H-14, 1H), 3.85 (H-13, 1H), 3.77 (H-8, 1H), 3.51 (H-8, 1H), and 3.22 (H-5, 2H). These signals suggested the presence of aliphatic N-linked methylene and methyne groups, likely connected to an electron-withdrawing functional group. The broad signals, particularly those attributed to methylene, closely aligned with those previously reported for protopine. This suggested that compound (**2**) could belong to the same family of alkaloids (Anet & Brown, 1967; Simoes-Pires *et al.*, 2014).

One notable feature was a singlet at δ_H 2.91 (H-15), integrating for three protons, which indicated the presence of an N-linked methyl group. Due to the compound's instability, further purification altered the ^{1}H-NMR signals, leading to the decision to perform structure elucidation on the partially purified compound.

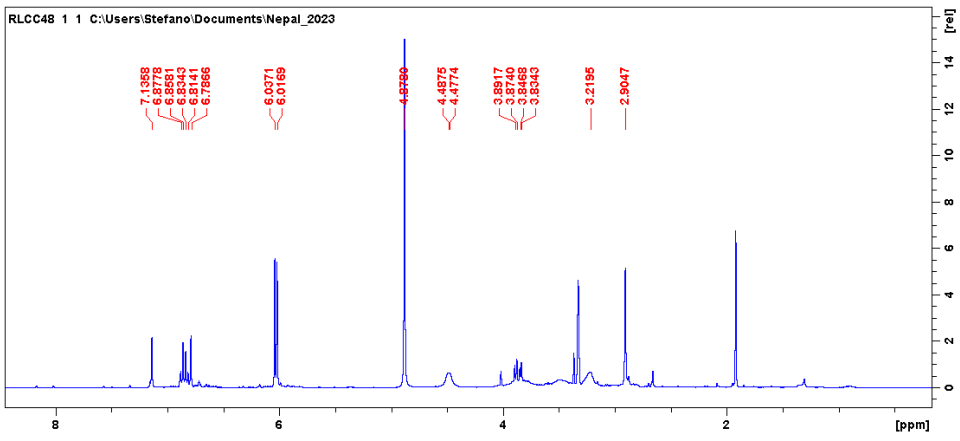

Figure 70: ^{1}HNMR spectra of compound **2**

Table 14: ^{13}C NMR and ^{1}H NMR data for compound **2** (δ in ppm, 100 MHz and 400 MHz respectively, in $MeOD_4$).

Position	δ_C	δ_H
1	115.9 CH	7.14, s, 1H
2	148.7 C	-
3	148.8 C	-
4	108.8 CH	6.79, s, 1H
4a	124.5 C	-
5	24.6 CH_2	3.25, m, 2H
6	53.7 CH_2	4.48, m, 2H
7	-	-
8	55.0 CH_2	3.77-3.51, m, 2H
8a	127.8 C	-
9	122.9 CH	6.86, d, 1H, *J=7.0*
9a	-	-
10	108.6 CH	6.81, d, 1H, *J=7.0*
11	148.2 C	-
12	148.1 C	-
12a	124.0 C	-
13	56.5 CH*	3.85, m*, 1H
14	56.5 CH*	3.86, m*, 1H
14a	127.8 C	-
15	41.3 CH_3	2.91, s, 3H
16	102.0 CH_2	6.00, s, 2H
17	102.0 CH_2	6.00, s, 2H
18	-	-

The HSQC-DEPT analysis identified four aromatic CH groups, located at δ_H 7.14-δ_C 115.9 (C-1), δ_H 6.79-δ_C 108.9 (C-4), δ_H 6.86-δ_C 122.9 (C-10), and δ_H 6.81-δ_C 108.6 (C-9). Additionally, the two methylenedioxy groups were assigned to δ_H 6.00-δ_C 102.0 (C-16 and C-17). In the aliphatic region, two partially overlapping* CH groups were observed at δ_H 3.85-δ_C 56.5 (C-13 and C-14), which were identified as benzylic groups connected to an epoxide. A benzylic CH_2 was found at δ_H 3.25-δ_C 24.6 (C-5), along with two N-linked CH_2 groups at δ_H 4.48-δ_C 53.7 (C-6) and broad signals at δ_H 3.77-3.51 (δ_C 55.0, C-8). The N-linked methyl group was observed at δ_H 2.91-δ_C 41.3 (C-15).

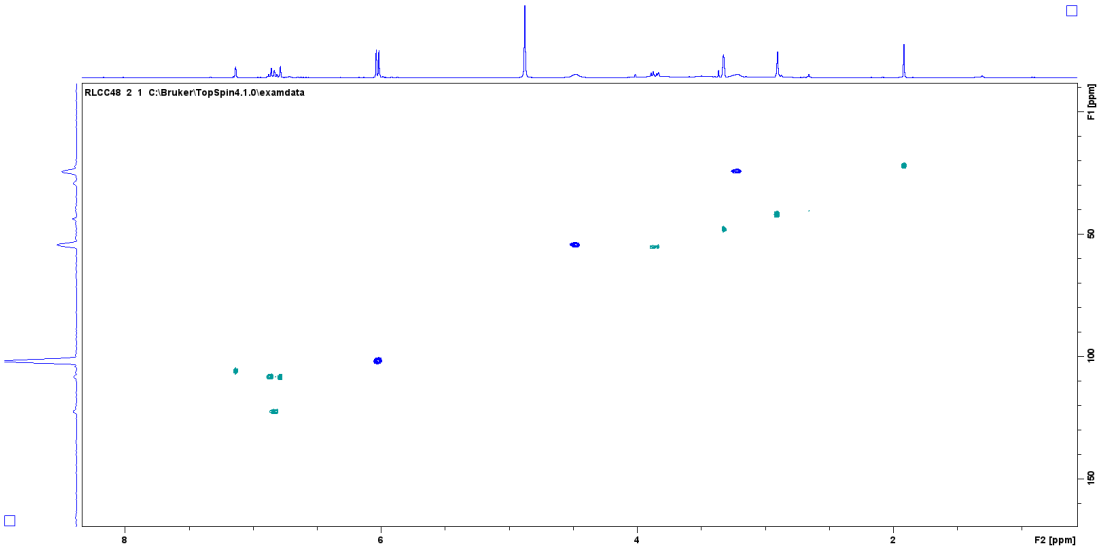

Figure 71: HSQC spectra of compound **2**

The structure was elucidated using obtained data from HSQC-DEPT, HMBC, COSY, and NOESY spectra. HMBC correlations from H-1 (δ_H 7.14) with carbon resonances at C-3 (δ_C 148.8), C-4a (δ_C 124.5), and C-14 (δ_C 56.5) provided key structural insights, while the diagonostic long range correlations from H-4 (δ_H 6.79) with C-2 (δ_C 148.7) and C-14a (δ_C 127.8) further supported the proposed structure. NOESY correlations between H-4 (δ_H 6.79) and H-5 (δ_H 3.25), as well as H-1 (δ_H 7.14)and H-13/H-14 (δ_H 3.85/3.86), reinforced the connectivity between key functional groups.

Furthermore, HMBC long-range correlations extending from H-5 (δ_H 3.25) to C-4 (δ_C 108.8) and C-14a (δ_C 127.8), along with correlations from H-14 with C-4a, confirmed the presence of a protopine-type moiety in the compound. Additional NOESY correlations were noted between H-6 (δ_H 4.48) and both H-5 (δ_H 3.25) and the N-methyl group, as well as between H-8 and the N-methyl group, further supporting the structural arrangement. A diagnostic HMBC correlation from H-13 (δ_H 3.85) with C-12 (δ_C 148.1) established the position of the epoxide at the 13-14 position. Furthermore, the long-range HMBC correlations from H-9 (δ_H 6.86) with C-8 (δ_C 55.0), C-11 (δ_H 148.2), and C-12a (δ_H 124.0) clarified the location of the second methylenedioxy group in the structure. Complete structure assignments are reported in Tables 14.

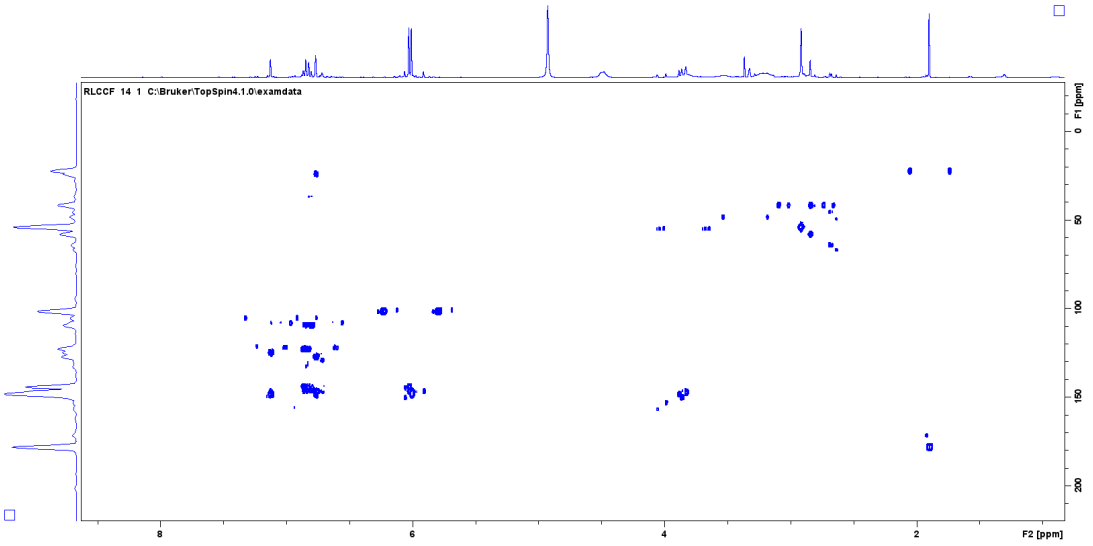

Figure 72: HMBC spectra of compound **2**

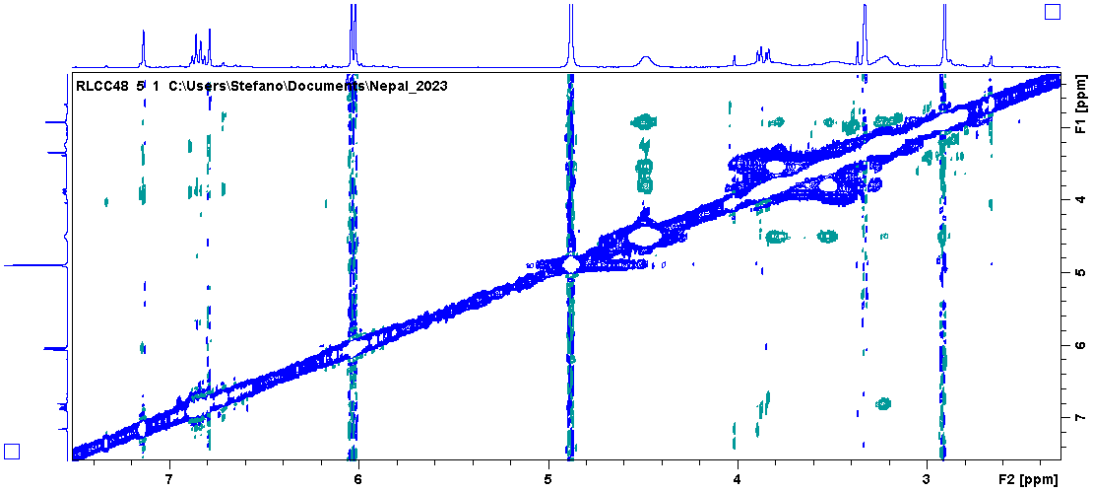

Figure 73: NOESY spectra of compound **2**

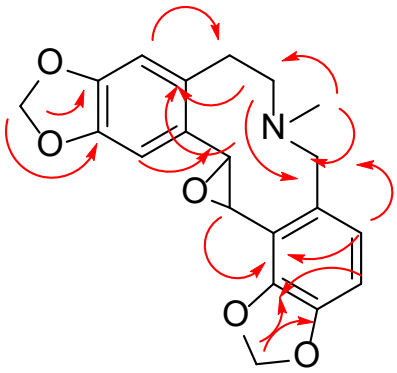

2

Figure 74: Key HMBC (red arrows), ^{1}H-^{1}H COSY (bold) correlation of compound **2**

The compound was ultimately identified as a derivative of protopine, distinguished by the presence of a 13-14-epoxide group instead of the usual keto function at position 14. The structure was assigned as 7-Methyl-2,3:11,12-bis(methylenedioxy)-7,13a-secoberbin-13-14-epoxide, and the proposed name for the compound is Chaeronepaline-B. The structural assignment was further validated by MS^n fragmentation data, which showed intense fragments at *m/z* 188 and 149 in the MS^2 spectrum, consistent with the proposed structure.

The compound exhibited optical activity, as evidenced by the circular dichroism (CD) spectrum, which showed a negative effect at 205 nm and 215 nm. However, due to the limited amount of isolated compound, it was not possible to assign the absolute configuration of the molecule with certainty at this stage. Further analysis will be required to conclusively determine the stereochemistry of chaeronepaline-B.

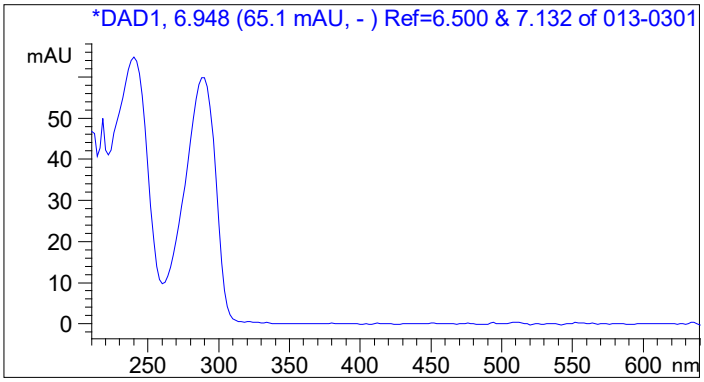

Figure 75: UV spectra of compound **2**

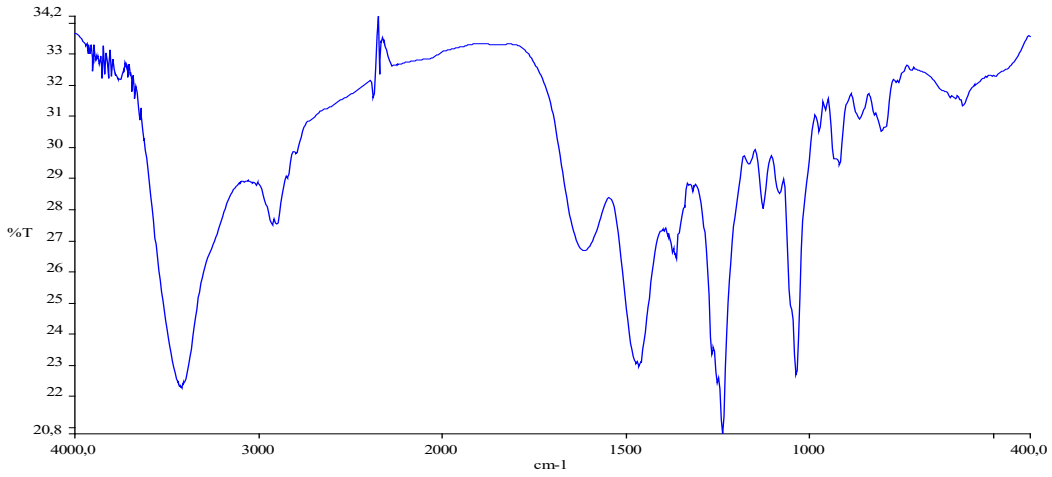

Figure 76: IR spectra of compound **2**

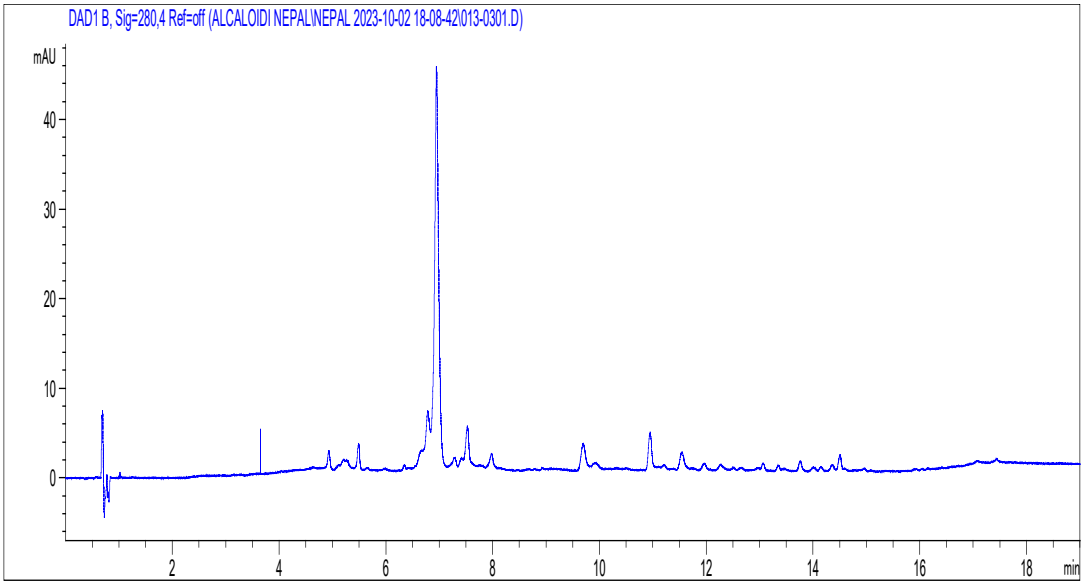

Figure 77: Chromatogram of compound **2** at 280 nm. Purity of compound **2** 94% (HPLC-DAD).

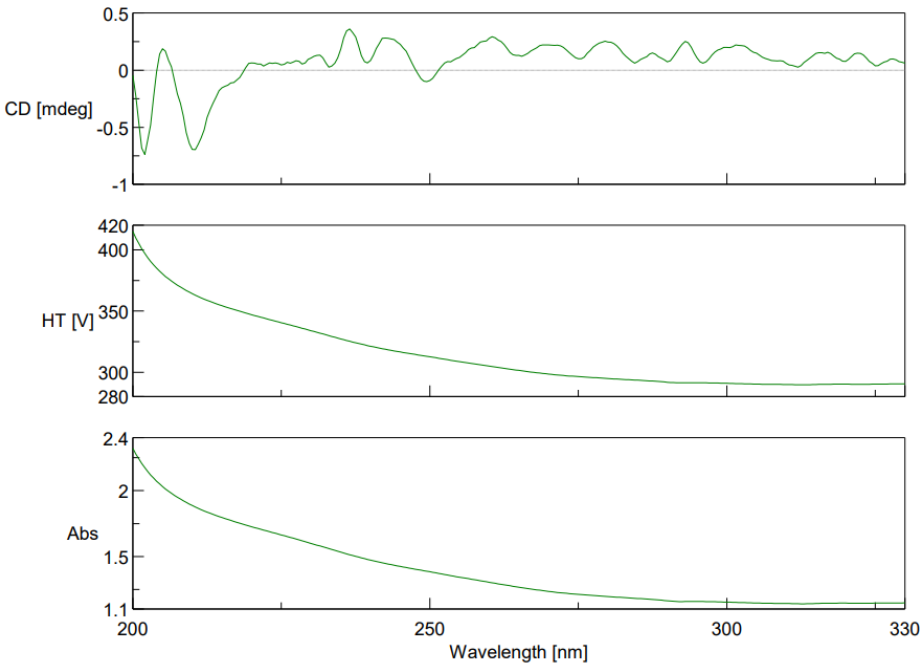

Figure 78: Circular dichroism of compound **2**

Compound **2** presented peculiar behaviour in mass spectrometry. When ionised in positive mode, it presented ion $[M+H]^+$ at *m/z* 354. When CID was performed, ion at *m/z* 354 produced ions at *m/z* 336(2a), 206 (2b), 188 (2c) and 149 (2d) *m/z* corresponding to sequential loss of 18, 148, 166, 206 Da (Figure 79). The ion *m/z* 188 and 149 are diagnostic for protopine-type alkaloids (Shim *et al.*, 2013).

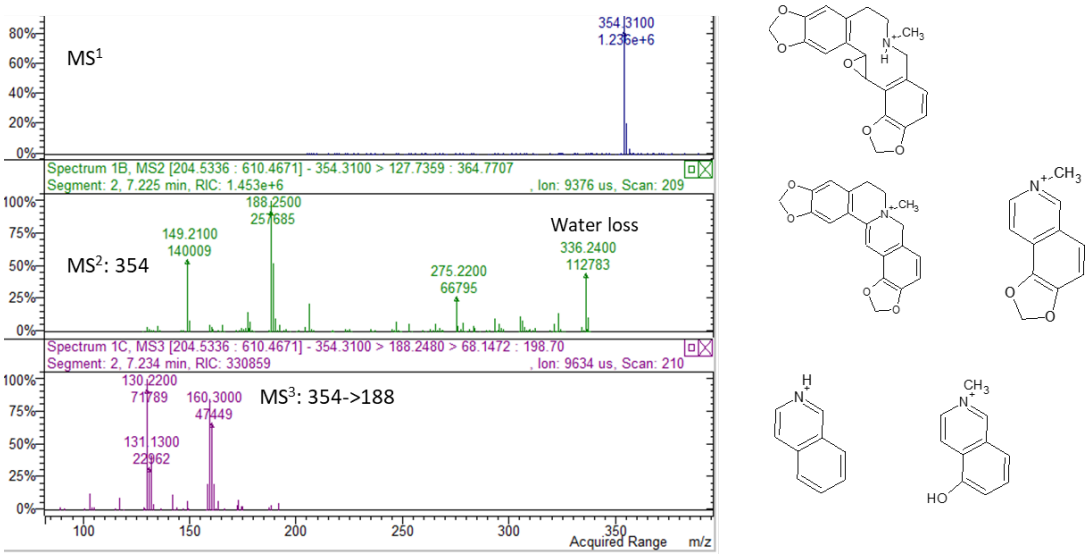

Figure 79: Mass fragmentation pattern of compound **2**

4.10.3. Chaeronepaline-C (3)

The MS of the compound (**3**) presented molecular ion at *m/z* $[M+H]^+$ 370. The molecular formula deduced from the HR-MS data was $C_{20}H_{20}NO_6$.

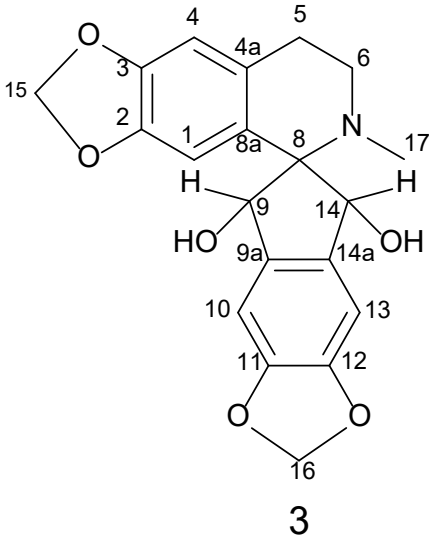

3

Figure 80: Structure of chaeronepaline-C (**3**)

The H-NMR revealed the presence of four singlets at δ_H 6.89 (H-13), 6.87 (H-10), 6.68 (H-4) and 6.30 (H-1), the first integrating for two protons and the other three integrating for one proton. Further signals are detected as singlets at δ_H 6.00 (H-16) and 5.81 (H-15), both integrating for two protons. Finally, two more singlets, integrating one proton each, are observed at δ_H 5.53 (H-14) and 5.34 (H-9). in the aliphatic region, three

multiplets were detected at δ_H 3.68 (H-6), 3.62 (H-6) and 2.97 (H-5), the first two integrating one proton each and the third integrating for two protons. One singlet suggesting the presence of one N-linked methyl group was detected at δ_H 2.84 (H-17, 3H).

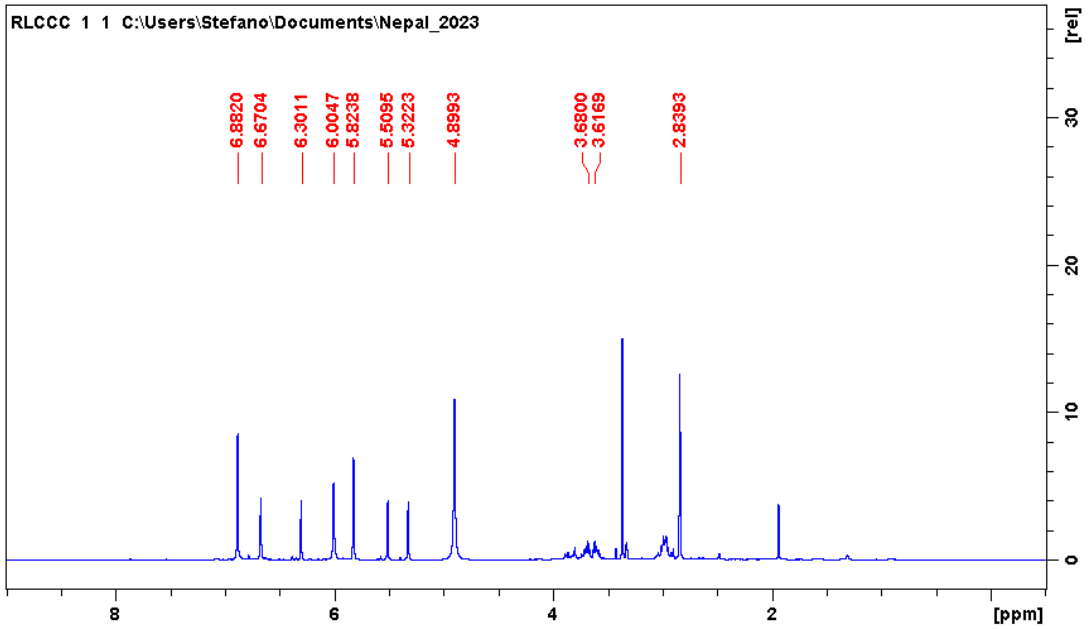

Figure 81: ^{1}HNMR spectra of compound **3**

Table 15: ^{13}C NMR and ^{1}H NMR data for compound **3** (δ in ppm, 100 MHz and 400 MHz respectively, in $MeOD_4$).

Position	δ_C	δ_H
1	109.1 CH	6.30, s, 1H
2	145.3 C	-
3	147.4 C	-
4	108.2 CH	6.68, s, 1H
4a	128.3 C	-
5	21.5 CH_2	2.97, m, 2H
6	47.2 CH_2	3.62 3.68, m, 2H
7	-	-
8	81.6 C	-
8a	120.0 C	-
9	77.8 CH	5.34, s, 1H
9a	120.3 C	-
10	108.7 CH	6.87, s, 1H
11	149.1 C	-
12	143.5 C	-
12a	-	-
13	115.8 CH	6.89, s, 1H
14	76.3 CH	5.53, s, 1H
14a	135.9 C	-
15	100.7 CH_2	5.81, s, 2H
16	101.7 CH_2	6.00, s, 2H
17	37.9 CH_3	2.84, s, 3H
18	-	-

Complete structure assignment was obtained by combining HSQC-DEPT, HMBC, COSY and NOESY data. One tetrahydro isoquinoline moiety was supported by the two CH observed at δ_H 6.30- δ_C 109.1 (C-1) and δ_H 6.68-δ_C 108.2 (C-4) and by the relevant long range HMBC correlations observed from δ_H 6.30 (H-1) with δ_C 128.3 (C-4a), δ_C 147.4 (C-3) and a quaternary carbon resonance at δ_C 81.6 (C-8) as well as by the one observed from δ_H 6.68 (H-4) with δ_C 145.3 (C-2), δ_C 120.0 (C-8a) and δ_C 21.5 (C-5). The other correlations allowing the identification of the dehydro pyperidine ring were detected from H-6 (δ_H 3.62/3.68) with C-4a (δ_C 128.3), C-8 (δ_C 81.6) and C-17 (δ_C 37.9), this latter assigned to the N-linked methyl group. The singlets at δ_H 5.53 (H-14) and 5.34 (H-9) were assigned to oxygen-bearing CH due to the shift of their carbons

that, were δ_C 76.3 (C-14) and 77.8 (C-9), respectively. From these signals assigned to positions H-14 (δ_H 5.53) and H-9 (δ_H 5.34) diagnostic HMBC were observed with C-8 (δ_C 81.6) and C-8a (δ_C 120.0), supporting the direct linkage of these CH with the tetrahydroquinoline moiety. The chemical shift of the quaternary position C-8 suggests the presence of a spiro derivatives (Popova *et al.*, 1980). The protons H-14 and H-9 present a COSY correlation, suggesting a "w" type long range coupling. From the H-9 and H-14, identical and numerous long range HMBC correlations can be observed and are depicted in the Figure 87. In particular, long range correlations were observed from the H-9 and C-14 (δ_C 76.3) and from H-14 and C-9 (δ_C 77.8), supporting the linkage of the two CH to one quaternary carbon (C-8). Furthermore, from H-14, two bond correlations are observed with C-8 and C-14a (δ_C 135.9). Three bond correlations were observed with C-8a, C-9a (δ_C 120.3) and C-13 (δ_C 115.8), but also four bond correlations were observed with C-10 (δ_C 108.7) and C-12 (δ_C 143.5), and five bond correlations were observed with C-11 (δ_C 149.1). The same correlations were also observed from H-9. These HMBC correlations suggest the presence of a planar and rigid portion of the compound. Due to the presence of the H-9 and H-14 as well as the singlets ascribed to H-10 (δ_H 6.87) and H-13 (δ_H 6.89) and the methylenedioxy H-16 (δ_H 6.00), the second portion of the molecule was assigned to an indane derivative bearing a methylene dioxy substituent and sharing one carbon of the pentacyclic hydrocarburic cycle with the isoquinoline moiety. NOESY correlations allowed to establish relative stereochemistry, and we imposed the alpha configuration to H-14. The H-14 showed NOESY with signal at δ_H 3.62 that on the basis of our hypothesis can be ascribed to H-6α, while H-9 presents NOESY correlation with proton at δ_H 3.68 that consequently canbe ascribed to H-6β. Both H-9 and H-14 show NOESY correlation with the N-methyl group.

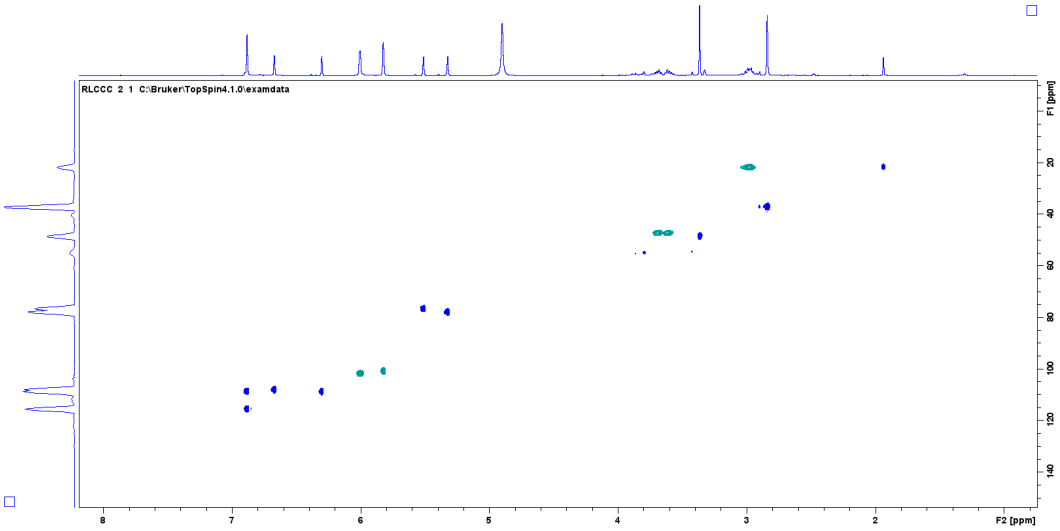

Figure 82: HSQC spectra of compound **3**

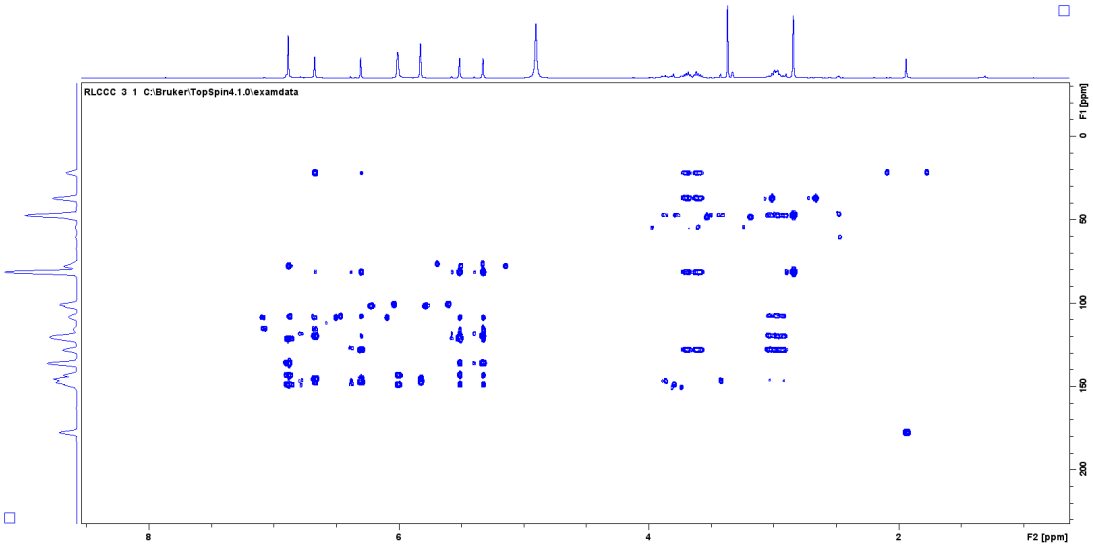

Figure 83: HMBC spectra of compound **3**

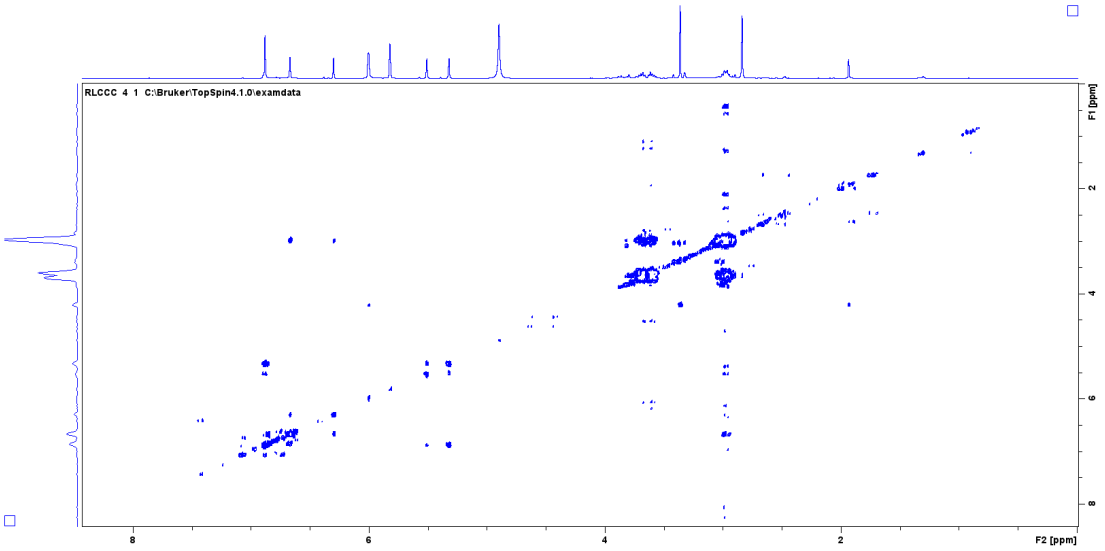

Figure 84: COSY spectra of compound **3**

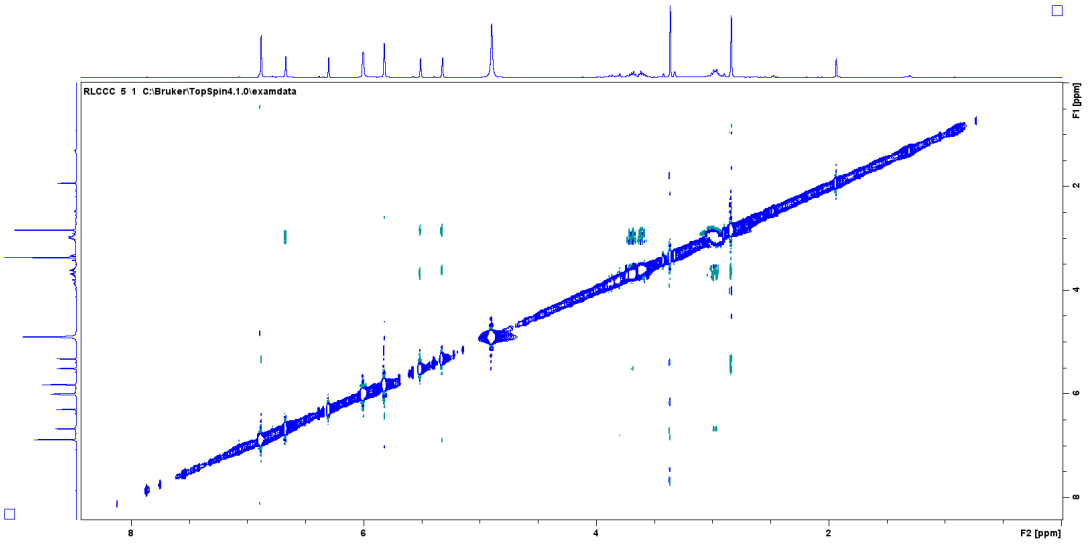

Figure 85: NOESY spectra of compound **3**

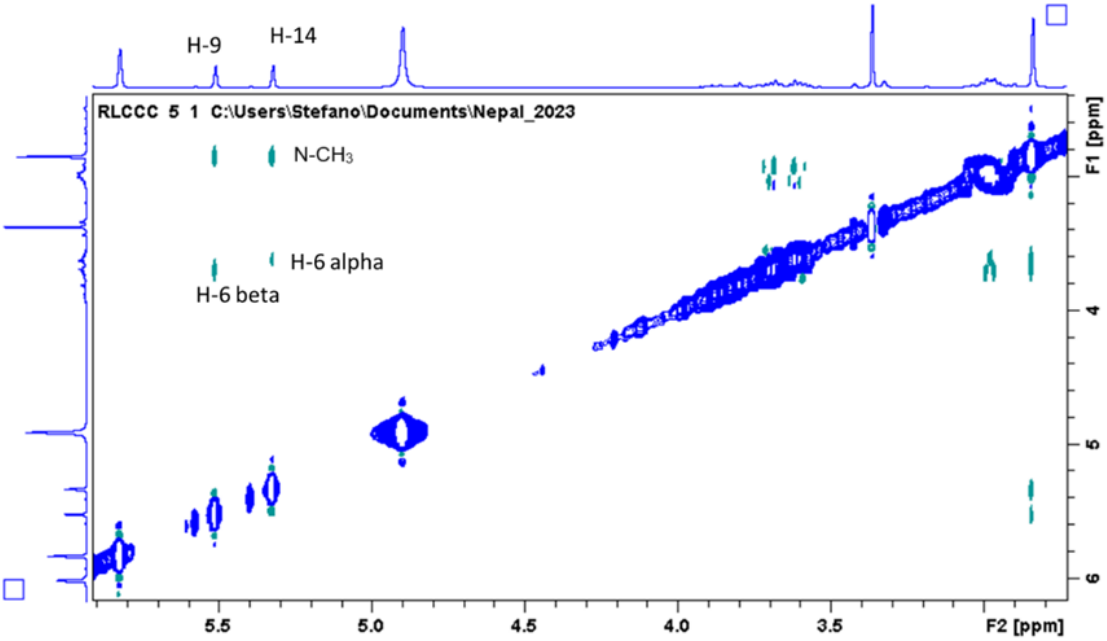

Figure 86: Detail of diagnostic NOESY spectrum for compound **3**

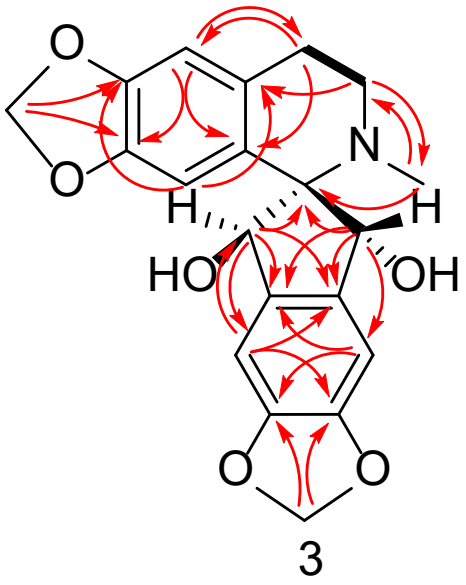

Figure 87: Key HMBC (red arrows), ^{1}H-^{1}H COSY (bold) correlation and stereochemistry of compound **3**

The structure of the compound is a spiroindane isoquinoline characterised by the presence of two methylenedioxy substituents, one for each aromatic ring. The structure is formed by a tetrahydro isoquinoline moiety fused with an oxygenated indane, and the basic carbon skeleton is like ochrobirine (Manske *et al.*, 1969; Mukhopadhyay *et al.*, 1987), but with a different position of the methylenedioxy substituent in the indane

portion. The compound (**3**) is characterized as 7- Methyl-5, 6, 7, 8- tetrahydro- 8H-spiro-9,14-dihydroxy-11,12-methylenedioxy-indane-isoquinoline and named Chaeronepaline-C.

The compound present optical activity (+38), and the CD spectrum showed two negative cotton effects, one at 215 nm and one at 295, while a positive effect was recorded at 270nm. The literature (Shamma *et al.*, 1972) assigned absolute configuration for ochrobirine since opposite cotton effects in CD spectrum recorded in methanol. On the basis of our data, we can assume that compound **3** presented opposite absolute configuration at the carbons 6, 9 and 14 of ochrobirine. Complete assignment of absolute stereochemistry could be confirmed only after asymmetric synthesis.

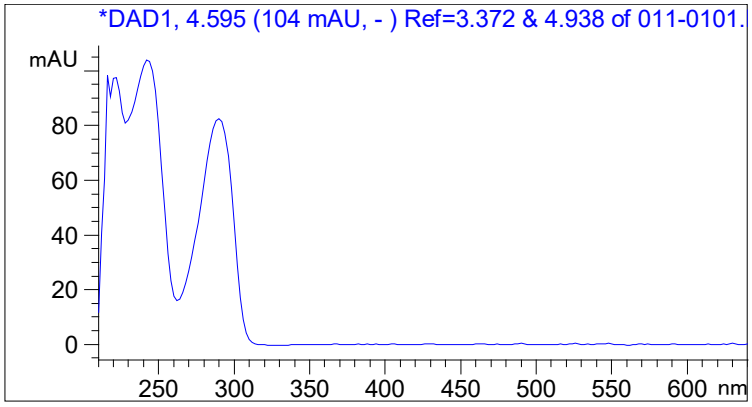

Figure 88: UV spectra of compound **3**

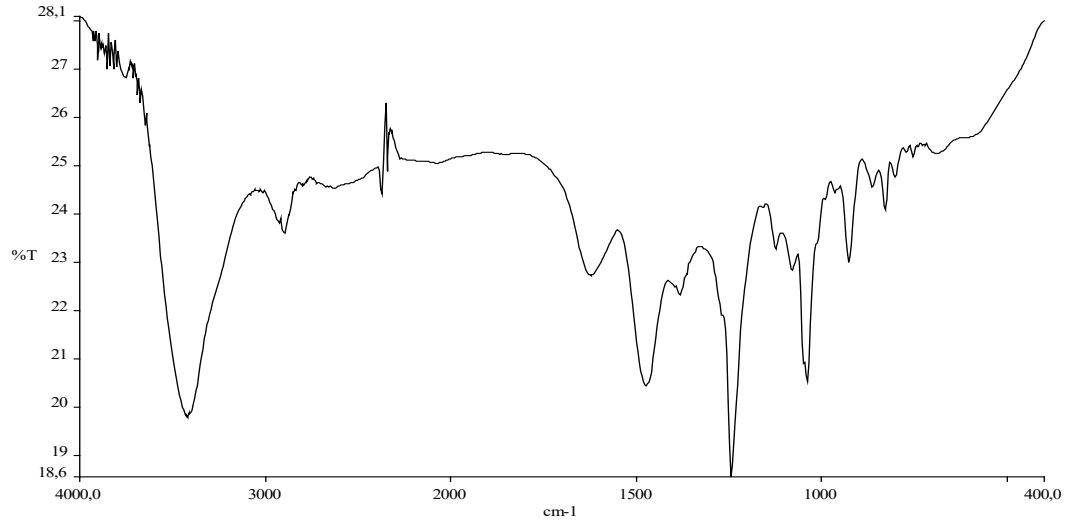

Figure 89: IR spectra of compound **3**

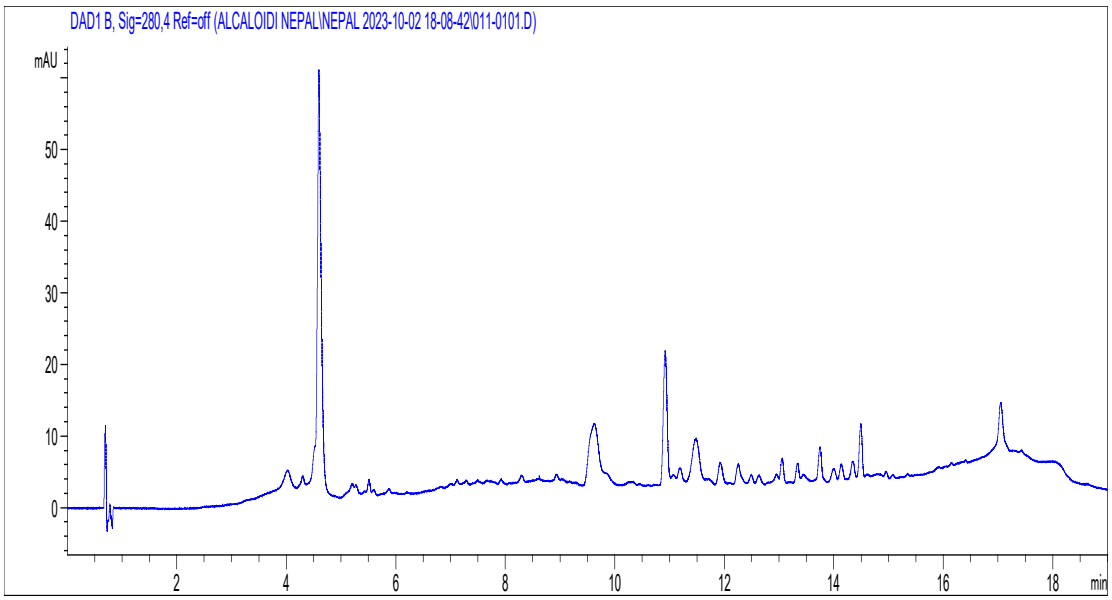

Figure 90: Chromatogram of compound **3** at 280 nm

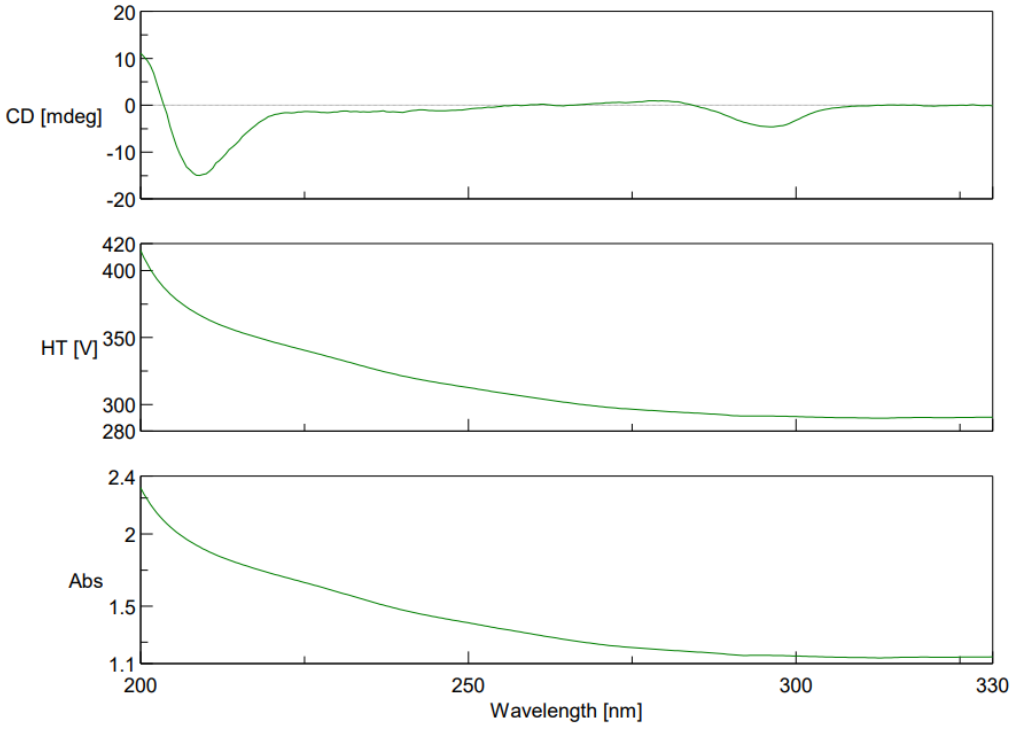

Figure 91: Circular dichroism of compound **3**

An ion [M+H]+ at m/z 370 was observed for compound **3** in positive ion mode. When CID was performed, ion at *m/z* 370 produced ions at *m/z* 352, corresponding to a loss of 18 Da (Figure 92). In MS^3, ion at *m/z* 352 afforded the product ion at *m/z* 190 corresponding to the formation of methylenedioxy 1,2-dehydro methylisoquinoline ion. This latter was subjected to CID fragmentation leading to the formation of 131, 149 and

175, corresponding to 1,2-dehydroisoquinoline, a species that originated due to nitrogen loss (uneven ion) and a methylenedioxy 1,2 dehydro isoquinoline.

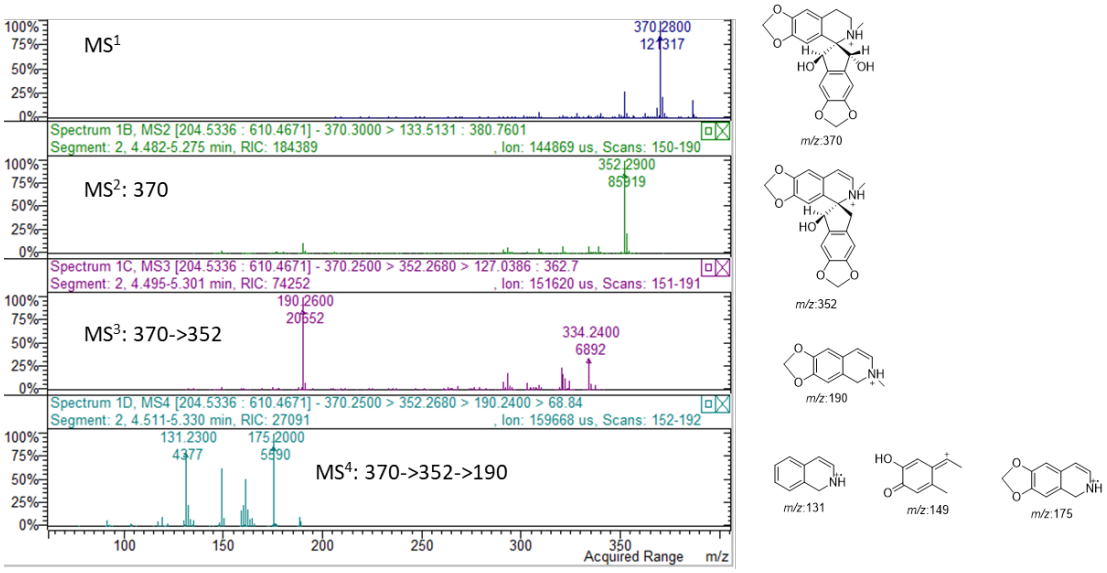

Figure 92: Mass fragmentation pattern of compound **3**

4.10.4. Chaeronepaline-D (4)

The MS of compound (**4**) presented molecular ion at $[M+H]^+$ 386, with relevant fragments at *m/z* 370, suggesting that it contained a further oxygen atom compared to the previous derivative. The molecular formula deduced from the HR-MS data was $C_{20}H_{20}NO_7$ (Mol. wt.: 386).

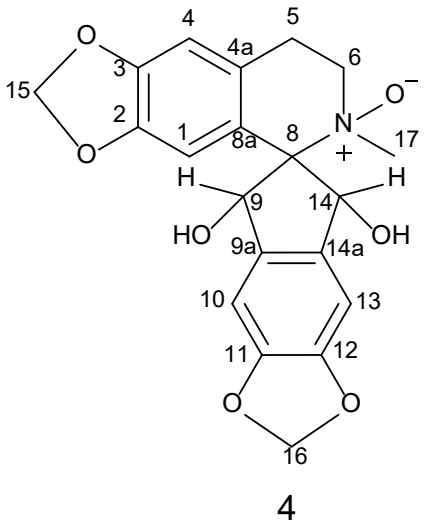

4

Figure 93: Structure of chaeronepaline-D (**4**)

H-NMR presented similarity to compound **3** with an almost superimposable spectrum related to the indane portion and small differences in the chemical shift of position 1 (δ_H 6.30) and 4 (δ_H 6.71) and 9 (δ_H 5.39) and 14 (δ_H 5.58). In contrast, significant differences were observed in the chemical shift of the N-methyl (H-17) that appeared deshielded with δ_H 2.97. The analysis of 2D spectra allowed to establish the same spiroindane isoquinoline moiety and compound was characterised as the N-Oxide derivative of **3** as 7- Methyl-5, 6, 7, 8- tetrahydro- 8H-spiro-9,14-dihydroxy-11,12-methylenedioxy-indane-isoquinoline-N-oxide and named Chaeronepaline-D. Compound **4** presented the same behaviour as 3 at circular dichroism and presented optical rotation activity, as for the compound 3 we imposed H-14 as alpha. NOESY correlations are observed from H-14 with H-6α (δ_H 3.80), while from H-9 with H-6 β (δ_H 3.74) and from H-9 and H-14 with the N-Methyl group. On the basis of the literature, we assume that compound **4** presented opposite absolute configuration at the carbons 6 (δ_C 47.0), 9 (δ_C 77.4) and 14 (δ_C 75.9) compared to ochrobirine. In any case, the complete assignment of absolute stereochemistry could be confirmed only after asymmetric synthesis.

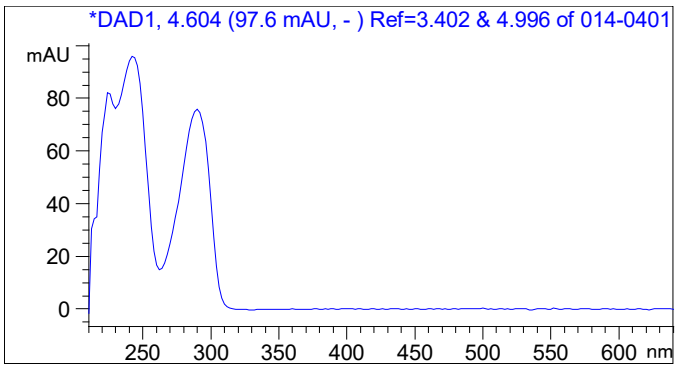

Figure 94: UV spectra of compound **4**

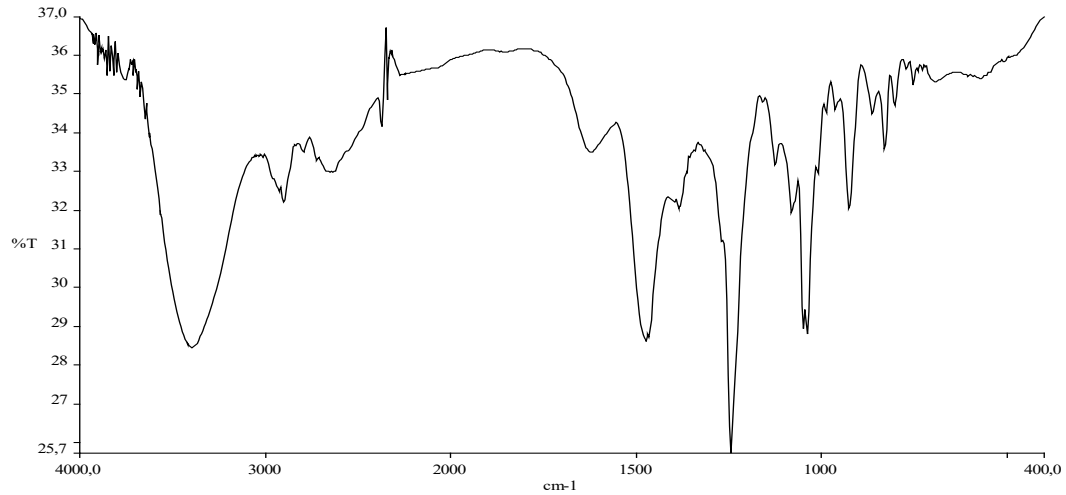

Figure 95: IR spectra of compound **4**

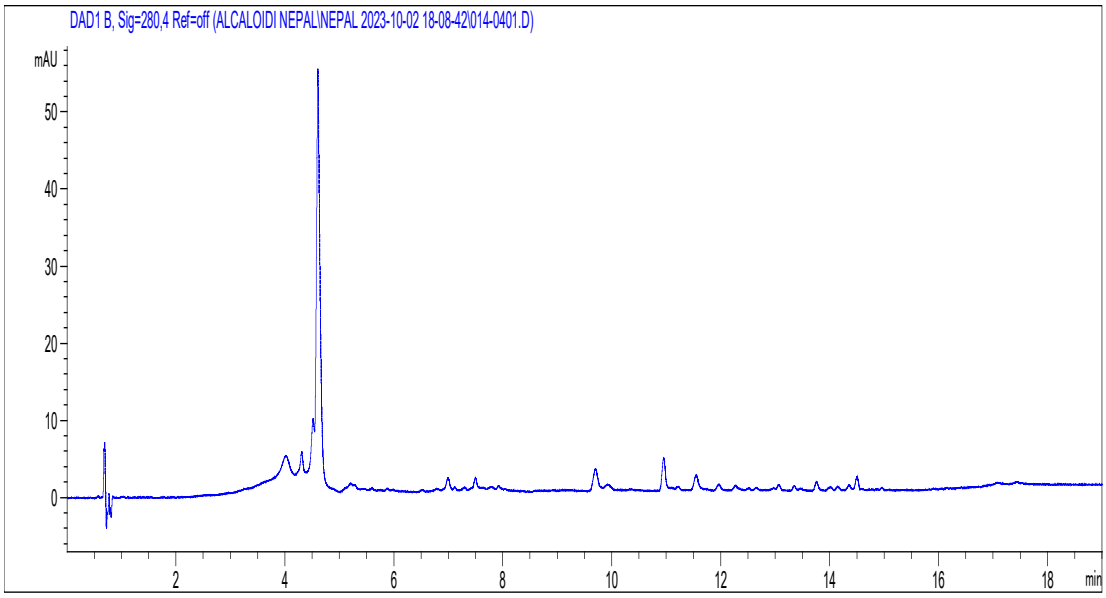

Figure 96: Chromatogram of compound **4** at 280 nm

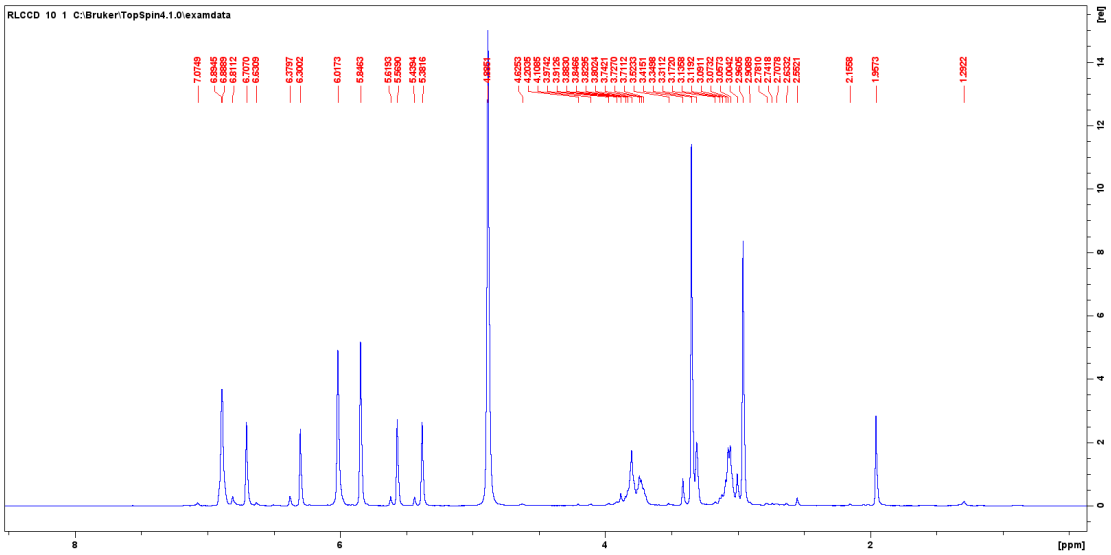

Figure 97: [1]HNMR spectra of compound **4**

Table 16: [13]C NMR and [1]H NMR data for compound **4** (δ in ppm, 100 MHz and 400 MHz respectively, in $MeOD_4$).

Position	δ_C	δ_H
1	108.8 CH	6.30, s, 1H
2	144.9 C	-
3	147.4 C	-
4	107.7 CH	6.71, s, 1H
4a	127.9 C	-
5	21.5 CH_2	3.08, m, 2H
6	47.0 CH_2	3.80 3.74, m, 2H
7	-	-
8	82.4 C	-
8a	118.1 C	-
9	77.4 CH	5.39, s, 1H
9a	120.8 C	-
10	108.8 CH	6.91, s, 1H
11	148.9 C	-
12	142.8 C	-
12a	-	-
13	115.1 CH	6.90, s, 1H
14	75.9 CH	5.58, s, 1H
14a	135.1 C	-
15	101.4 CH_2	5.85, s, 2H
16	102.4 CH_2	6.02, s, 2H
17	36.9 CH_3	2.97, s, 3H
18	-	-

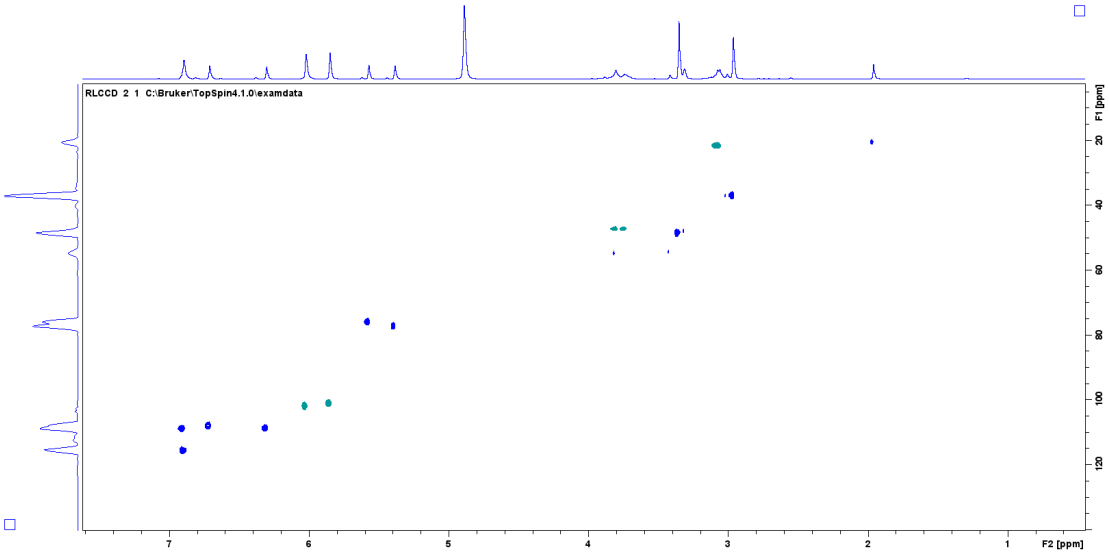

Figure 98: HSQC spectra of compound **4**

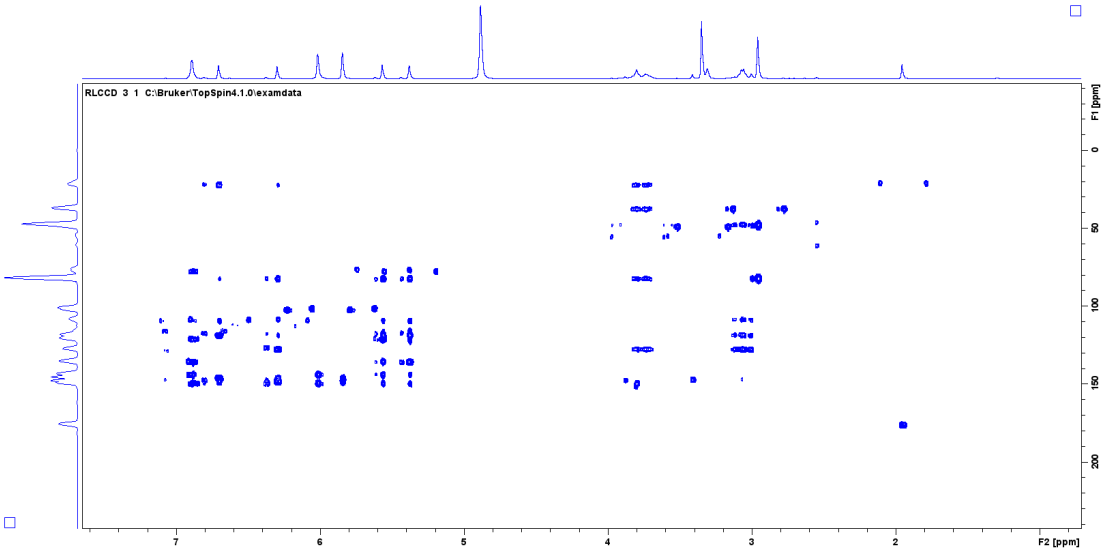

Figure 99: HMBC spectra of compound **4**

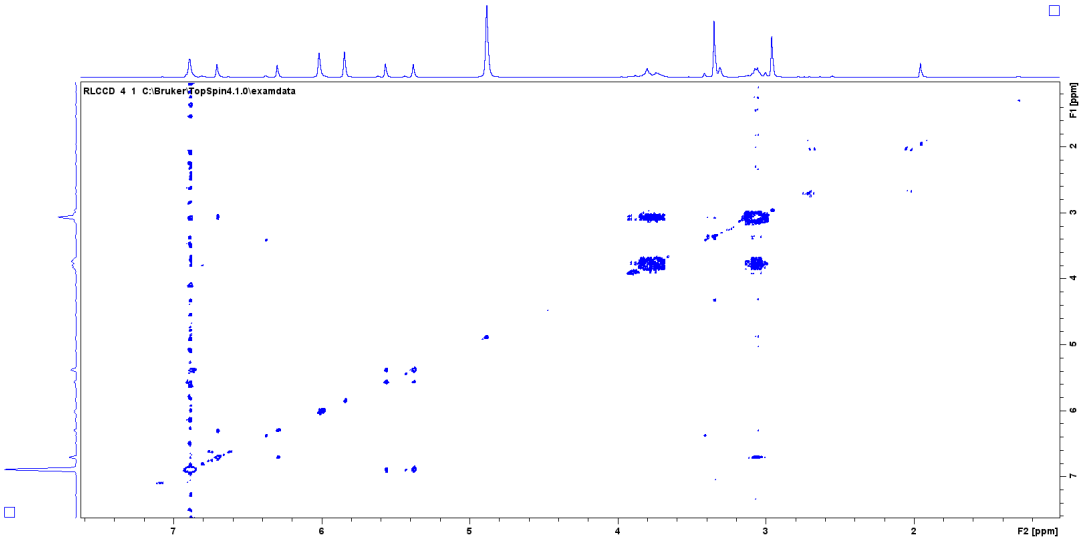

Figure 100: COSY spectra of compound **4**

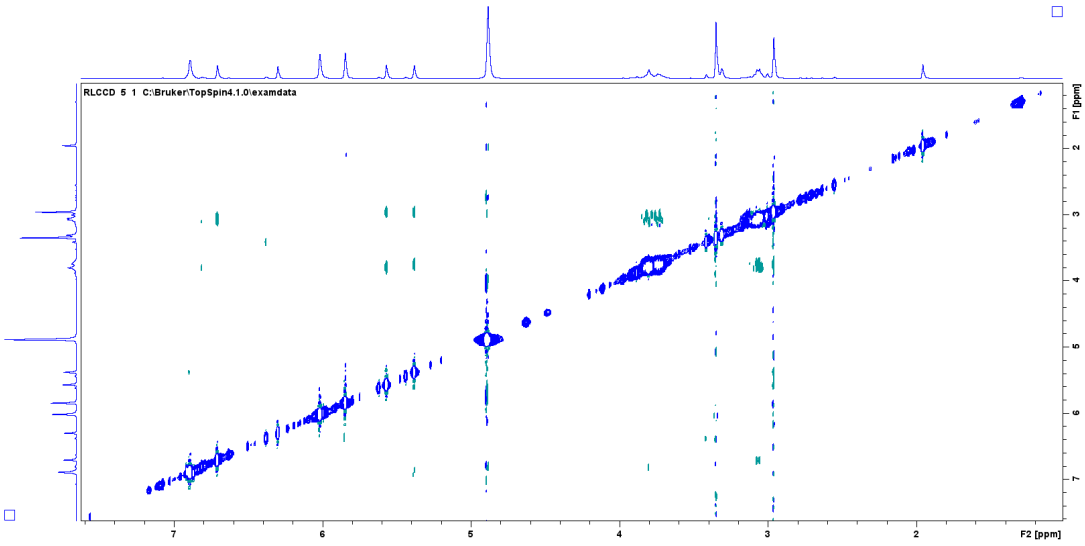

Figure 101: NOESY spectrum of compound **4**

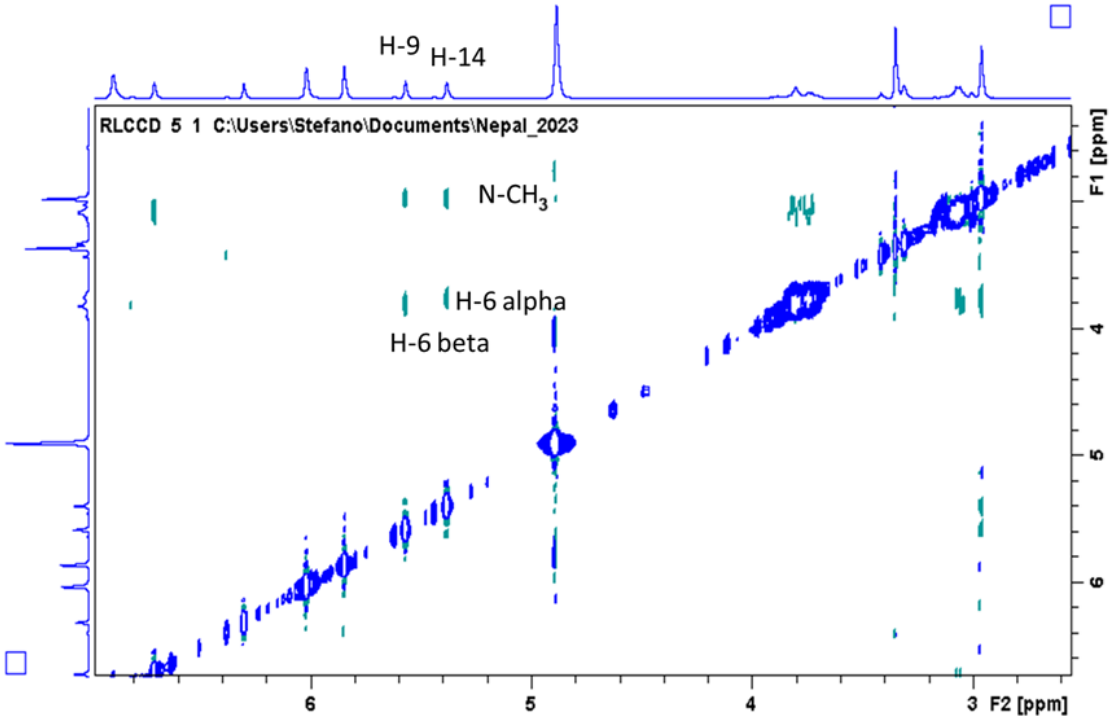

Figure 102: NOESY spectrum of compound **4**, detail

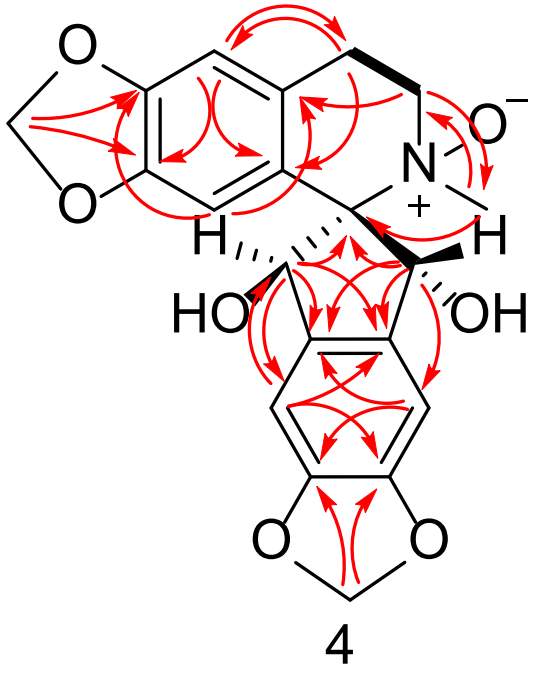

Figure 103: Key HMBC (red arrows), ^{1}H-^{1}H COSY (bold) correlation and stereochemistry of compound **4**

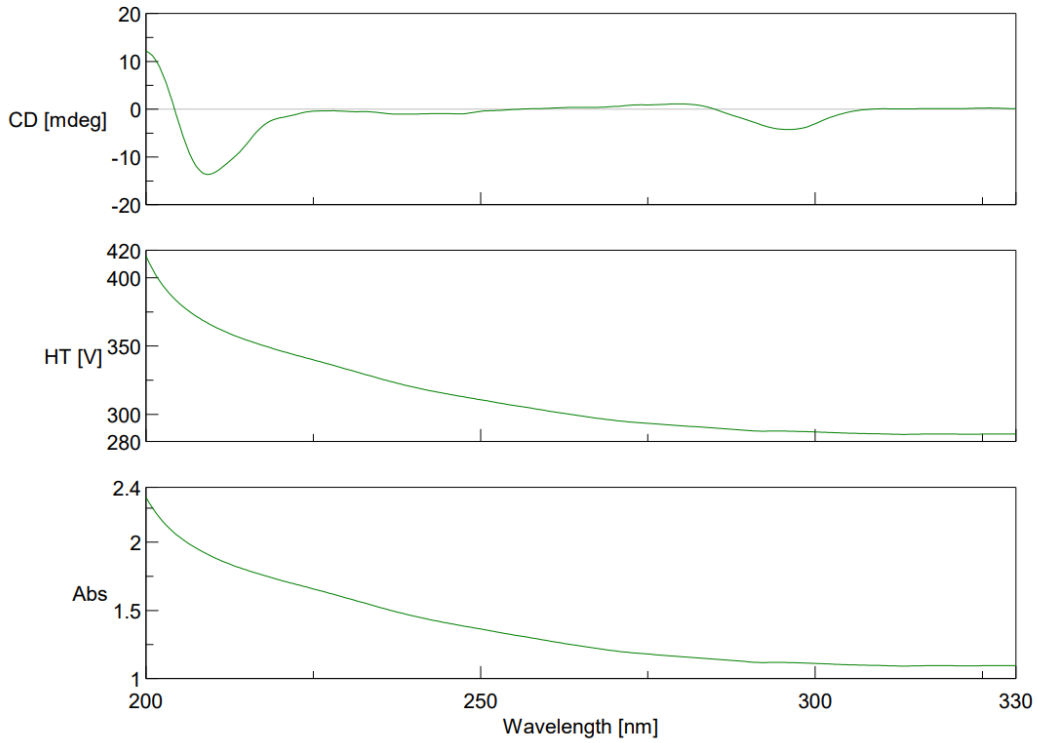

Figure 104: Circular dichroism of compound **4**

Compound **4** presented ion $[M+H]^+$ at *m/z* 386 in positive ion mode, with a difference of 16Da compared to compound **3**, corresponding to the N oxide derivative. When CID was performed, the $[M+H]^+$ ion produced the prominent product at *m/z* 368, which was formed by the loss of 18Da. In MS^3, ion at *m/z* 368 afforded the product ion at *m/z* 206, corresponding to the formation of methylenedioxy 1,2-dehydromethylisoquinoline N oxide ion. This latter undergo to CID fragmentation leading the formation of 191 corresponding to methylenedioxy 1,2 dehydro isoquinoline N oxide ion, which was formed by the loss of methyl radical (Figure 105).

The observed behaviour in mass spectrometry allowed to identify these compounds with the observation of diagnostic fragments and can be a useful strategy for the further study of the presence of such derivatives also in other *Corydalis* species.

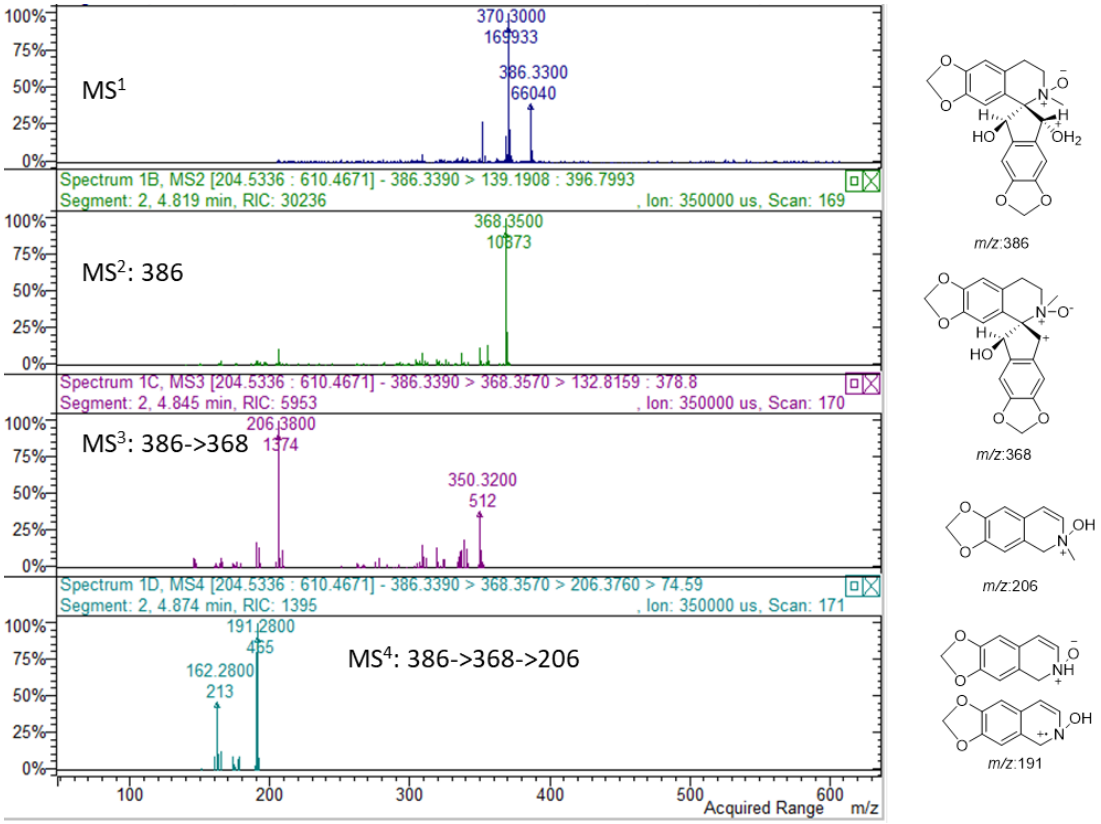

Figure 105: Mass fragmentation pattern of compound **4**

4.10.5. DFT calculations

The optimized molecular structures of all four compounds were obtained after generation of several geometries each with numerous SCF cycles. The structures with charges spanned larger energy space as the minima was tough to be located. The final total energies (Hartree) of compound01-compound04 were -1090.32554988, -1204.36416090, -1279.60114715, and -1354.77451142 respectively indicating the rise in magnitude with the increasing number of atoms. The optimized molecular structures are given in Figure 106 and saved in xyz format files.

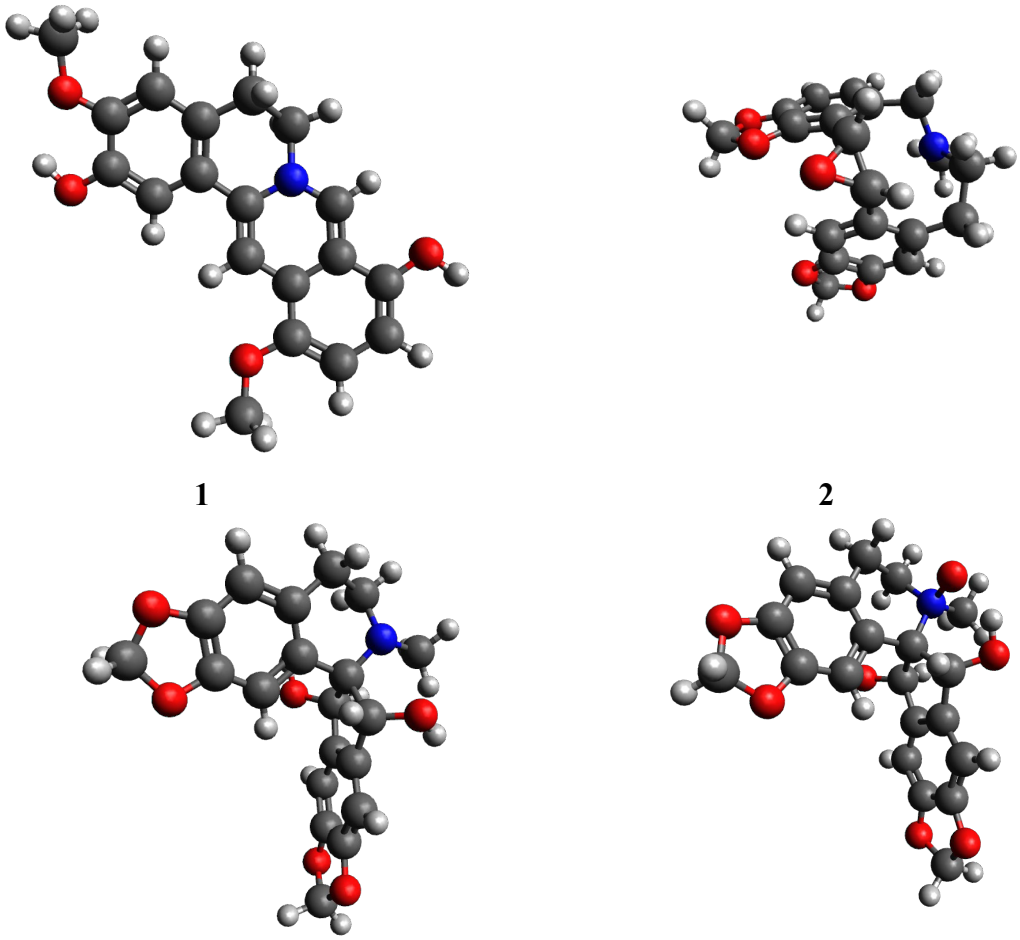

Figure 106: Ball and stick model of the DFT optimized structures of the compounds **1-4**

Table 17: Smiles strings for the compounds **1-4**

Compounds	Smiles
1	[N+]24=CC1=C(O[H])C=CC(=C1C=C2C3=CC(=C(C=C3CC4)OC)O[H])OC
2	N5(C)CCC1=CC6=C(C=C1[C@@H]2O[C@@H]2C3=C(C=CC4=C3OCO4)C5)OCO6
3	C2C1=CC6=C(C=C1C4(N(C2)C)[C@H](O[H])C3=CC5=C(C=C3[C@H]4O[H])OCO5)OCO6
4	C2C1=CC6=C(C=C1C4([N@@+](C2)([O-])C)[C@H](O[H])C3=CC5=C(C=C3[C@H]4O[H])OCO5)OCO6

4.11. Structure Elucidation of Isolated Known Compounds

4.11.1. Bicuculline (5)

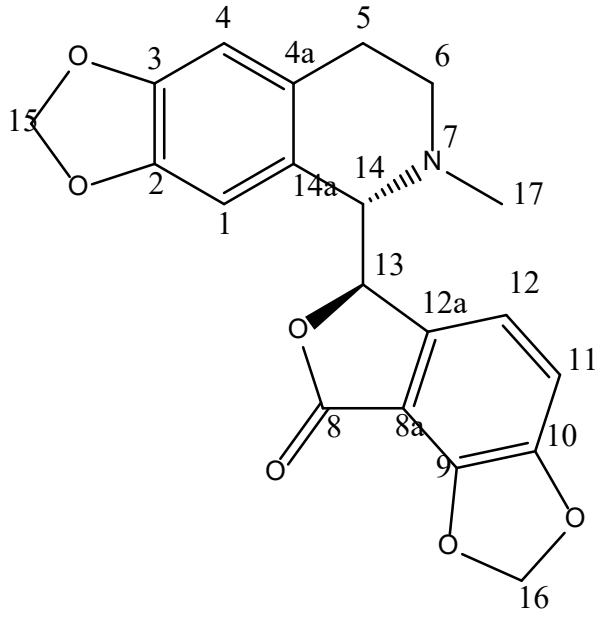

Figure 107: Structure of bicuculline (**5**)

Table 18: ^{13}C NMR and ^{1}H NMR data for bicuculline (**5**) (δ in ppm, 100 MHz and 400 MHz respectively, in $MeOD_4$).

Position	δ_C	δ_H
1	107.4	6.97, s, 1H
2	145.7	-
3	147.2	-
4	108.3	6.88, s, 1H
4a	124.1	-
5	27.3	2.77 2.73, m, 2H
6	50.0	2.74 2.64, m, 2H
7		-
8	167.2	-
8a	110.1	-
9	145.7	-
10	147.6	-
11	113.3	7.08, d, 1H
12	116.4	7.07, d, 1H
12a	140.9	-
13	83.3	6.28, d, 1H
14	74.2	4.88, d, 1H
14a	130.0	-
15	101.2	6.06, s, 2H
16	101.2	6.26, s, 2H
17	43.6	2.26, s, 3H

Compound **5**, exhibited distinct chemical shifts in both its proton (δ_H) and carbon (δ_C) NMR spectra. The proton NMR data showed characteristic peaks, including a singlet at δ_H 6.97 corresponding to position 1 with a carbon shift of δ_C 107.4, and another singlet at δ_H 6.88 for position 4, aligning with a carbon shift of δ_C 108.3. Multiplets observed for positions 5 and 6, ranging from δ_H 2.73 to δ_H 2.77 and δ_H 2.64 to δ_H 2.74, suggested methylene linkages associated with carbons at δ_H 27.3 and δ_H 50.0, respectively. Notably, the downfield shifts at positions 11 and 12, with δ_H 7.08 and δ_H 7.07, revealed aromatic protons coupled to carbons at δ_C 113.3 and δ_C 116.4.

Other significant signals included a doublet at δ_H 6.28 linked to carbon δ_C 83.3 at position 13, indicating a likely hydroxylated carbon. The δ_H 4.88 signal at position 14 correlated with carbon δ_C 74.2, further supporting a functionalized center. Methylenedioxy groups at positions 15 and 16 displayed singlets at δ_H 6.06 and δ_H 6.26, both with a carbon shift of δ_C 101.2, indicating symmetry in the structure. The methyl group at position 17 was observed at δ_H 2.26 and matched with a carbon shift of δ_C 43.6, confirming its placement.

Compound **5** showed molecular weight of 367 and the molecular formula $C_{20}H_{17}NO_6$, was established. Collectively, this data aligned closely with the previously reported spectral information for bicuculline, substantiating the structural assignment through consistent NMR shifts and confirming its identification based on literature values (Manske, 1933).

4.11.2. Corydalmine (6)

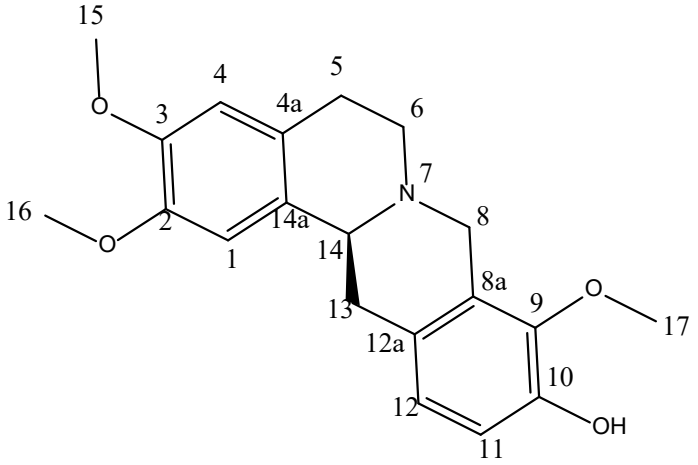

Figure 108: Structure of corydalmine (**6**)

Table 19: ^{13}C NMR and ^{1}H NMR data for corydalmine (**6**) (δ in ppm, 100 MHz and 400 MHz respectively, in $MeOD_4$).

Position	δ_C	δ_H
1	110.0	6.97, s, 1H
2	146.7	-
3	148.2	-
4	112.6	6.88, s, 1H
4a	127.4	-
5	27.6	2.77 2.73, m, 2H
6	53.6	2.74 2.64, m, 2H
7	-	-
8	56.1	3.67 3.57, d, 2H
8a	129.4	-
9	154.9	-
10	138.9	-
11	119.8	6.75, d, 1H
12	125.3	6.59, d, 1H
12a	128.8	-
13	35.8	3.06 2.81, d, 2H
14	68.0	4.29, m, 1H
14a	129.1	-
15	56.1	3.75, s, 3H
16	56.1	3.75, s, 3H
17	60.3	3.68, s, 3H

The NMR data for compound **6** reveals distinct signals across both the proton (^{1}H) and carbon (^{13}C) spectra, supporting the structure assignment. Starting with the proton NMR data, the spectrum shows key singlet signals at δ_H 6.97 and 6.88, each corresponding to a single proton (H-1 and H-4), suggesting isolated protons on an aromatic ring. Additional multiplets are observed at δ_H 2.77 and 2.73 (2H for H-5), along with another multiplet for H-6 at δ_H 2.74 and 2.64, indicating the presence of methylene groups, characteristic of a benzylic environment near a nitrogen atom or oxygen. Furthermore, a doublet at δ_H 3.67 and 3.57 (H-8) hints at an N-linked methylene group. Signals at δ_H 6.75 and 6.59 are ortho-coupled doublets (J = 8 Hz), indicating aromatic protons likely in proximity (H-11 and H-12), suggesting a substituted aromatic ring in the compound's structure. Additional signals at δ_H 4.29 for a single proton (H-14) suggest a proton on a

methine linked to an oxygenated carbon. The singlets at δ_H 3.75 and 3.68 (3H each) correspond to methoxy groups, often present in compounds like corydalmine.

In the carbon NMR data, the downfield shift of carbons at δ_C 110.0 (C-1) and 112.6 (C-4) corroborates the presence of electron-rich aromatic carbons, aligning with the observed singlet proton signals. The carbonyl or highly deshielded carbons at δ_C 146.7 (C-2) and 148.2 (C-3) provide additional structural detail, suggesting the presence of electronegative substituents on the aromatic ring. The methylene carbons are evident in shifts like δ_C 27.6 (C-5) and 53.6 (C-6), while the benzylic methylene (C-8) and the oxygenated methine (C-14) appear at δ_C 56.1 and 68.0, respectively. The characteristic methoxy carbons, seen at δ_C 56.1 and 60.3, further support the structure, with their singlet protons in the proton NMR data.

Compound **6** showed molecular weight of 341 and the molecular formula $C_{20}H_{23}NO_4$, was established. These data match previously reported spectral data for corydalmine, confirming the identity and structural consistency with literature sources (Jha *et al.*, 2009).

4.11.3. 8-Hydroxydihydrosanguinarine (7)

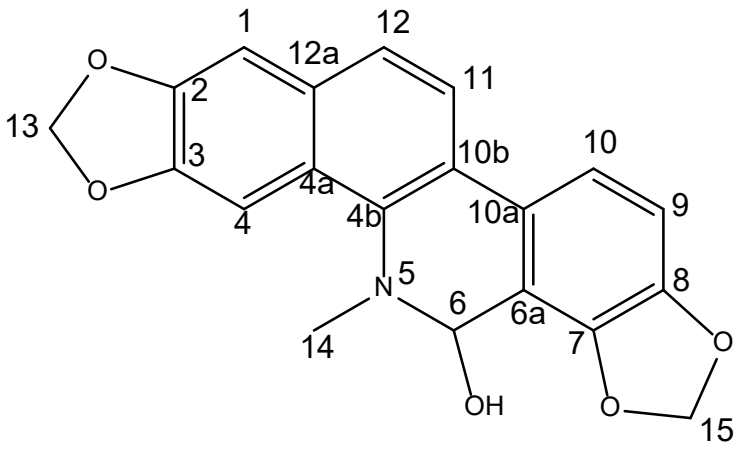

Figure 109: Structure of 8-hydroxydihydrosanguinarine (**7**)

Table 20: ^{13}C NMR and ^{1}H NMR data for 8-hydroxydihydrosanguinarine (**7**) (δ in ppm, 100 MHz and 400 MHz respectively, in $MeOD_4$).

Position	δ_C	δ_H
1	104.3	7.16, s, 1H
2	147.8	-
3	147.8	-
4	99.7	7.64, s, 1H
4a	126.0	-
4b	138.0	-
6	85.2	5.42, s, 1H
6a	112.5	-
7	145.0	-
8	148.1	-
9	108.6	6.98, d, 1H, *J=8.1*
10	116.1	7.48,d, 1H, *J=8.1*
10a	125.7	-
10b	122.8	-
11	119.6	7.79, d, 1H, *J=8.1*
12	123.5	7.51, d, 1H, *J=8.1*
12a	131.0	-
13	101.5	6.07, s, 2H
14	39.6	2.76, s, 3H
15	101.9	6.11, s, 2H

The compound **7** displays distinct proton and carbon NMR characteristics that align with the structure of a hydroxylated dihydrosanguinarine derivative. In the proton NMR spectrum, a singlet at δ_H 7.16 (1H) corresponds to position 1, indicative of an isolated proton in an aromatic environment. Another aromatic singlet is observed at δ_H 7.64 for position 4 (1H), reflecting the symmetry of the aromatic system. The doublets at δ_H 6.98 and δ_H 7.48, both with a coupling constant J = 8.1 Hz, correspond to protons at positions 9 and 10, confirming ortho coupling in an aromatic ring. Similar aromatic doublets at δ_H 7.79 and δ_H 7.51 for positions 11 and 12, respectively, also display ortho coupling, further supporting the presence of a benzene ring. The aliphatic proton at δ_H 5.42, a singlet at position 6, is characteristic of a benzylic position, typically influenced by adjacent nitrogen and oxygen atoms in such alkaloid structures. Additionally,

methylene protons appear as singlets at δ_H 6.07 and δ_H 6.11 (each integrating for two protons), suggesting the presence of methylenedioxy groups, common in similar alkaloid structures. The presence of a methyl group is confirmed by the singlet at δ_H 2.76 (3H) at position 14, indicating N-methyl substitution.

In the carbon NMR data, the aromatic carbons exhibit deshielded signals, with carbons at positions 2 and 3 both resonating at δ_C 147.8, likely due to conjugated double bonds or an electron-withdrawing effect. The methylenedioxy carbons are noted at δ_C 101.5 and δ_C 101.9, consistent with methylenedioxy functionality. The carbon at δ_C 85.2 at position 6 is particularly deshielded, aligning with a benzylic position impacted by nitrogen. Additional downfield shifts, such as δ_C 148.1 at position 8 and δ_C 145.0 at position 7, further confirm the compound's resonance structure within the aromatic framework. Finally, the methyl carbon at δ_C 39.6 at position 14 supports the N-methyl substitution in this compound.

Compound **7** showed molecular weight of 349 and the molecular formula $C_{20}H_{15}NO_5$, was established. The comprehensive analysis of these NMR data strongly supports the identification of Compound **7** as 8-hydroxydihydrosanguinarine. This data aligns well with previously reported values for dihydrosanguinarine derivatives, confirming the compound's identity based on literature comparisons (Zhang *et al.*, 1995).

4.11.4. Dihydrosanguinarine (8)

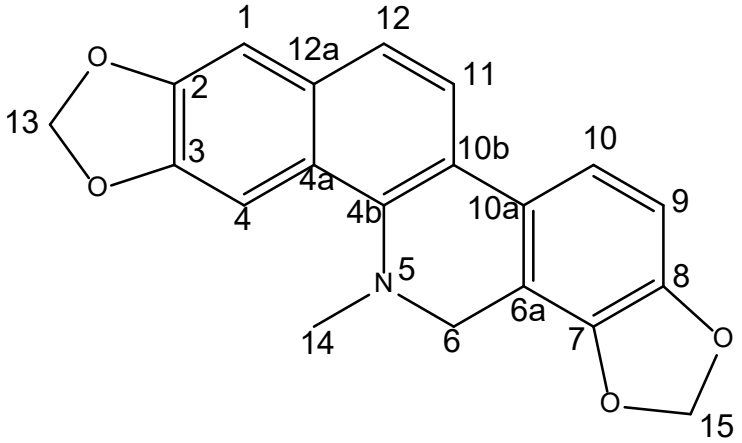

Figure 110: Structure of dihydrosanguinarine (**8**)

Table 21: ^{1}H NMR and ^{13}C NMR data for dihydrosanguinarine (**8**) (δ in ppm, 100 MHz and 400MHz respectively, in $MeOD_4$).

Position	δ_C	δ_H
1	103.9	7.14, s, 1H
2	146.0	-
3	147.1	-
4	100.0	7.61, s, 1H
4a	125.5	-
4b	142.3	-
5	-	-
6	48.5	4.18, s, 1H
6a	114.0	-
7	144.0	-
8	146.1	-
9	106.9	6.37, d, 1H, *J=8.5*
10	116.1	7.36, d, 1H, *J=8.5*
10a	127.5	-
10b	124.3	-
11	120.0	7.79, d, 1H, *J=8.0*
12	124.2	7.51, d, 1H, *J=8.0*
12a	131.0	-
13	101.8	6.05, s, 2H
14	40.4	2.58, s, 3H
15	101.8	6.05, s, 2H

Compound **8**, exhibits distinctive proton and carbon NMR characteristics that align well with its established structure. In the proton NMR data, the singlet at δ_H 7.14 corresponds to a single proton at position 1, indicating an isolated aromatic proton, supported by the carbon resonance at δ_C 103.9. Another singlet at δ_H 7.61 is assigned to position 4, aligning with the carbon resonance at δ_C 100.0, which is typical for an aromatic proton in a unique electronic environment. The doublets at δ_H 6.37 (J=8.5 Hz) and δ_H 7.36 (J=8.5 Hz) correspond to positions 9 and 10, respectively, revealing an ortho-coupling relationship in the aromatic ring, with carbons resonating at δ_C 106.9 and δ_C 116.1, respectively. Additionally, the doublets at δ_H 7.79 (J=8.0 Hz) and δ_H 7.51 (J=8.0 Hz) are assigned to positions 11 and 12, indicating another ortho-coupled set of aromatic protons and corresponding to carbons at δ_C 120.0 and δ_C 124.2.

In the aliphatic region, the singlet at δ_H 4.18 for position 6, corresponding to a carbon at δ_C 48.5, suggests a methine proton attached to a carbon in a deshielded environment. The singlet at δ_H 6.05 for two protons at positions 13 and 15, both at δ_C 101.8, represents two methylene groups, each attached to an oxygen atom in a methylenedioxy group. The methyl group at position 14 resonates as a singlet at δ_H 2.58, matching a carbon resonance at δ_C 40.4, indicating a typical N-methyl group associated with a nitrogen atom in an aromatic system.

The carbon NMR data further solidifies the structural assignment of dihydrosanguinarine, with notable deshielded carbon signals at δ_C 146.0, δ_C 147.1, and δ_C 144.0, which are characteristic of quaternary carbons in a conjugated system. Other key signals include the carbons at δ_C 125.5 (C-4a), δ_C 142.3 (C-4b), δ_C 114.0 (C-6a), and δ_C 127.5 (C-10a), which are typical of complex aromatic ring systems with electron-donating and electron-withdrawing substituents.

Compound **8** showed molecular weight of 333 and the molecular formula $C_{20}H_{15}NO_4$, was established. These NMR signals for Compound **8** show excellent agreement with previously reported data, confirming the identity and structure of this compound as dihydrosanguinarine, described in existing literature sources (Pandey *et al.*, 1979).

4.11.5. Scoulerine (9)

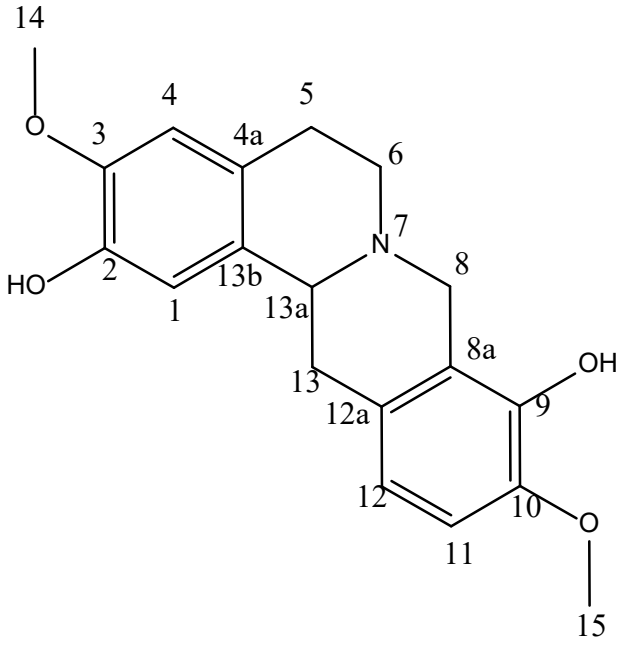

Figure 111: Structure of scoulerine (**9**)

Table 22: ^{1}H NMR and ^{13}C NMR data for scoulerine (**9**) (δ in ppm, 100 MHz and 400 MHz respectively, in $MeOD_4$).

Position	δ_C	δ_H
1	113.1	6.82, s, 1H
2	144.2	-
3	145.9	-
4	111.8	6.71, s, 1H
4a	127.7	-
5	27.6	2.77 2.73, m, 2H
6	53.6	2.74 2.64, m, 2H
7	-	-
8	55.8	3.67 3.57, d, 2H
8a	121.4	-
9	141.7	-
10	144.9	-
11	111.2	6.64, d, 1H
12	125.5	6.64, d, 1H
12a	128.9	-
13	35.8	3.06 2.81, d, 2H
13a	68.2	4.29, m, 1H
13b	129.5	-
14	56.1	3.77, s, 3H
15	57.3	3.83, s, 3H

For Compound **9**, the ^{1}H NMR and ^{13}C NMR data were carefully analyzed to confirm its structure. In the ^{1}H NMR data, the aromatic protons at positions δ_H 6.82 (s, 1H, H-1) and δ_H 6.71 (s, 1H, H-4) were consistent with characteristic isolated aromatic signals, suggesting the presence of two distinct aromatic environments. The doublet signals at δ_H 6.64 (d, 1H, J = 8.0 Hz, H-11) and δ_H 6.64 (d, 1H, J = 8.0 Hz, H-12) indicate an ortho-coupled aromatic pair, which aligns well with a typical benzylisoquinoline structure. The methylene protons, observed as multiplets at δ_H 2.77 and 2.73 (m, 2H, H-5) and δ_H 2.74 and 2.64 (m, 2H, H-6), were also noted, showing aliphatic shifts that are common in this class of compounds.

The presence of methoxy groups was confirmed by singlet signals at δ_H 3.77 (s, 3H, H-14) and δ_H 3.83 (s, 3H, H-15), which correspond to the carbons at δ_C 56.1 and δ_C 57.3, respectively, as indicated in the carbon spectrum. These methoxy groups contribute to

the electron-donating effects on the aromatic system, providing chemical stability to the scoulerine structure. Another interesting feature is the benzylic methylene group at δ_H 3.67 and δ_H 3.57 (d, 2H, H-8) with a corresponding carbon shift at δ_C 55.8, supporting the benzylisoquinoline framework.

In the ^{13}C NMR data, aromatic carbons are represented by shifts at δ_C 113.1 (C-1), δ_C 111.8 (C-4), and δ_C 111.2 (C-11), consistent with substituted aromatic carbons. The quaternary carbons, especially δ_C 144.2 (C-2), δ_C 145.9 (C-3), δ_C 127.7 (C-4a), and δ_C 141.7 (C-9), further validate the substitution pattern and confirm the integrity of the isoquinoline core. A key feature is the methine carbon at δ_C 68.2 (C-13a), associated with the proton at δ_H 4.29 (m, 1H), which is typical of a chiral center in benzylisoquinoline derivatives.

Compound **9** showed molecular weight of 327 and the molecular formula $C_{19}H_{21}NO_4$, was established. Overall, the NMR data matched closely with those of previously reported scoulerine in the literature, affirming the compound's identity through its characteristic NMR profile. The consistent proton and carbon shifts confirm scoulerine's structure, aligning with known data for this alkaloid (Sener & Temizer, 1991).

The isolation of new and known compounds from *C. chaerophylla* represents a significant advancement in understanding the phytochemical diversity and pharmacological potential of this plant. The identification of four new compounds, Chaeronepaline A, B, C, and D compounds (**1-4**), highlights the plant's chemical uniqueness and its potential as a source of new bioactive molecules. These compounds may contribute to the plant's traditional medicinal uses and open avenues for exploring their therapeutic applications through further biological and pharmacological studies.

In addition to the new compounds, the isolation of known bioactive alkaloids such as bicuculline (**5**), corydalmine (**6**), 8-hydroxydihydrosanguinarine (**7**), dihydrosanguinarine (**8**), and scoulerine (**9**) reinforces the plant's pharmacological relevance. These compounds are well-documented for their diverse biological activities, including antimicrobial, anti-inflammatory, antioxidant, and neuroprotective effects. Their presence in *C. chaerophylla* aligns with the bioactivities observed in the plant's extracts and validates its traditional use in treating various ailments.

The co-occurrence of new and known compounds suggests a synergistic chemical ecology within *C. chaerophylla*, where diverse alkaloids contribute to its overall pharmacological profile. The structural variations between the newly identified Chaeronepaline A – D, and the known alkaloids provide valuable insights into the biosynthetic pathways of this plant, underscoring its evolutionary significance. Furthermore, the new compounds add to the growing library of natural products, with potential applications in drug discovery and development.

The successful isolation and characterization of these compounds also emphasize the importance of combining advanced chromatographic and spectroscopic techniques for elucidating complex plant metabolites. These findings pave the way for further research on *Corydalis chaerophylla* to evaluate the biological activities of both new and known compounds and to assess their potential for pharmaceutical applications. Overall, the study underscores the rich chemical diversity of this species and its promising role in contributing to natural product-based therapeutics.

4.11.6. Govaniadine (10)

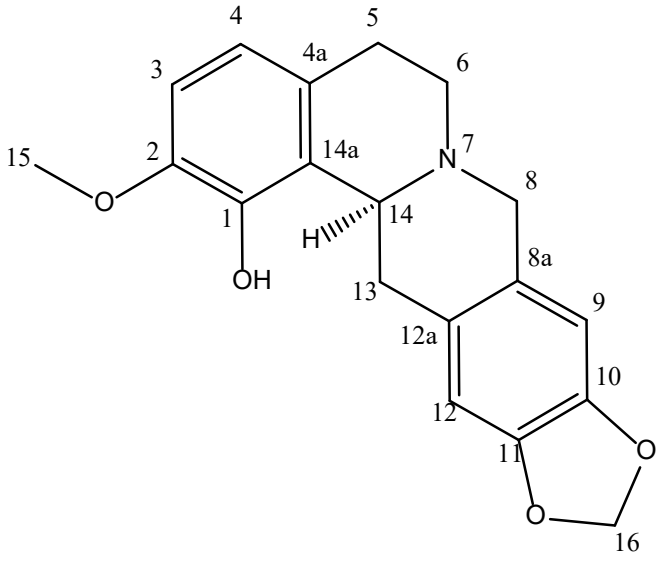

Figure 112: Structure of govaniadine (**10**)

Table 23: ^{13}C NMR and ^{1}H NMR data for govaniadine (**10**) (δ in ppm, 100 MHz and 400 MHz respectively, in $MeOD_4$).

Position	δ_C	δ_H
1	146.8	-
2	144.4	-
3	111.1	6.76, d, 1H
4	120.4	6.58, d 1H
4a	128.5	-
5	29.8	2.80 2.95, m, 2H
6	49.0	2.62 3.06 m, 2H
7	-	-
8	58.6	3.83 3.93, d, 2H
8a	127.3	-
9	107.1	6.55, s, 1H
10	146.8	-
11	147.4	-
12	109.4	6.53, s, 1H
12a	128.9	-
13	32.8	2.60 3.64, dd, 2H
14	57.2	4.00, dd, 1H
14a	125.9	-
15	56.8	3.82 s, 3H
16	102.0	5.85 5.86, d, 2H

Compound **10**, was characterized using both ^{1}H and ^{13}C NMR spectroscopy data. The proton NMR spectrum revealed a downfield doublet signal at δ_H 6.76, integrating for one proton at position 3, indicating an aromatic proton in conjugation. Another doublet was observed at δ_H 6.58, assigned to position 4, which also integrates for one proton, suggesting ortho coupling within the aromatic ring. A singlet at δ_H 6.55 was noted at position 9, indicative of a distinct aromatic environment, and another singlet at δ_H 6.53 corresponded to position 12, both signals reinforcing the presence of an isolated aromatic system. Additionally, a multiplet signal was detected for two protons at δ_H 2.80–2.95 and δ_H 2.62–3.06 at positions 5 and 6, respectively, suggesting the presence of methylene groups linked to an electron-rich system, likely in a benzylic environment.

Further, the spectrum displayed a distinctive doublet at δ_H 5.85–5.86 for two protons, attributed to position 16, likely indicative of a methylenedioxy moiety, confirmed by

its integration. Additional signals at δ_H 3.83–3.93 at position 8 for two protons and at δ_H 3.82 as a singlet for three protons at position 15 suggested the presence of O-linked methylene and methoxy groups, respectively. A double doublet at δ_H 2.60–3.64, integrating for two protons at position 13, and a distinctive double doublet at δ_H 4.00 for one proton at position 14 indicate a complex coupling pattern that may arise from an aliphatic group in close interaction with the aromatic system.

The carbon NMR spectrum corroborated these findings, with resonances noted at δ_C 146.8 for position 1 and δ_C 144.4 for position 2, which align with electron-deficient aromatic carbons. The carbons at δ_C 111.1 and δ_C 120.4 (positions 3 and 4) further confirmed the presence of an aromatic ring with characteristic chemical shifts for carbons in a benzene-type system. Additionally, the signals at δ_C 128.5 and δ_C 125.9 (positions 4a and 14a) signify quaternary carbons within the aromatic framework. Positions 5 and 6 methylene carbons resonate at δ_C 29.8 and δ_C 49.0, respectively, consistent with benzylic methylenes, while position 8 at δ_C 58.6 aligns with an O-linked methylene. The methoxy group at δ_C 56.8 at position 15 and the methylenedioxy group at δ_C 102.0 at position 16 complete the structural elucidation.

Compound **10** showed molecular weight of 325 and the molecular formula $C_{19}H_{19}NO_4$, was established. This detailed NMR data is consistent with previously reported spectral values for govaniadine, confirming the structure as matching literature data for this compound (Shrestha *et al.*, 2013).

4.11.7. Stylopine (11)

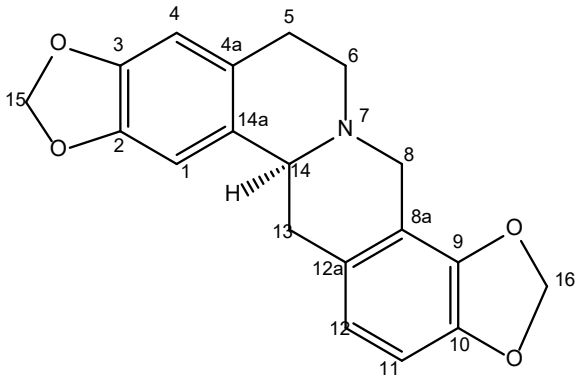

Figure 113: Structure of stylopine (**11**)

Table 24: ^{13}C NMR and ^{1}H NMR data for stylopine (**11**) (δ in ppm, 100 MHz and 400 MHz respectively, in $MeOD_4$).

Position	δ_C	δ_H
1	106.7	6.97, s, 1H
2	145.7	-
3	146.2	-
4	109.2	6.88, s, 1H
4a	127.1	-
5	27.6	2.77 2.73, m, 2H
6	53.6	2.74 2.64, m, 2H
7	-	-
8	56.1	3.67 3.57, d, 2H
8a	117.2	-
9	144.4	-
10	148.2	-
11	110.8	6.81, d, 1H
12	123.7	6.76, d, 1H
12a	128.5	-
13	35.8	3.06 2.81, d, 2H
14	68.2	4.29, m, 1H
14a	129.3	-
15	101.2	6.06, s, 2H
16	101.5	6.07, s, 2H

For the ^{1}H and ^{13}C NMR analysis of Compound **11**, the data provides insight into the structural framework and proton-carbon linkages within the compound. The ^{1}H NMR reveals a singlet at δ_H 6.97 attributed to the aromatic proton at position 1, with the corresponding carbon signal at δ_C 106.7. Another aromatic singlet appears at δ_H 6.88, assigned to position 4 with δ_C 109.2. The multiplet signals for the methylene group protons are observed at δ_H 2.77 and 2.73 (2H) corresponding to δ_C 27.6, assigned to position 5, and additional methylene group signals appear at δ_H 2.74 and 2.64 (2H) with a carbon resonance at δ_C 53.6, linked to position 6.

The data also includes doublets at δ_H 6.81 (1H, J coupling consistent with aromatic protons) assigned to position 11 with δ_C 110.8, and at δ_C 6.76 assigned to position 12 with δ_C 123.7, suggesting an aromatic ring structure involving these protons. The methylene signals at δ_H 3.67 and 3.57 (d, 2H) correspond to position 8 with δ_C 56.1,

while position 13 shows multiplets at δ_H 3.06 and 2.81 (2H), linked to δ_C 35.8, indicating proximity to functional groups or within a complex environment. Notably, the hydroxyl-linked carbon resonates at δ_C 68.2, with its corresponding proton signal at δ_H 4.29 as a multiplet at position 14. Additional singlets observed at δ_H 6.06 and 6.07, each integrating for two protons and resonating with δ_C 101.2 and δ_C 101.5 respectively, likely represent methylenedioxy groups, suggesting aromatic substituents linked via oxygen bridges, typical of stylopine structures.

Compound **11** showed molecular weight of 333 and the molecular formula $C_{19}H_{17}NO_4$, was established. The overall data interpretation aligns well with the characteristic structure of stylopine, including the methylenedioxy groups and aromatic substitutions, and this profile is consistent with previously reported data for stylopine in the literature, affirming its identity (Chrzanowska, 1995).

4.11.8. Adlumine (12)

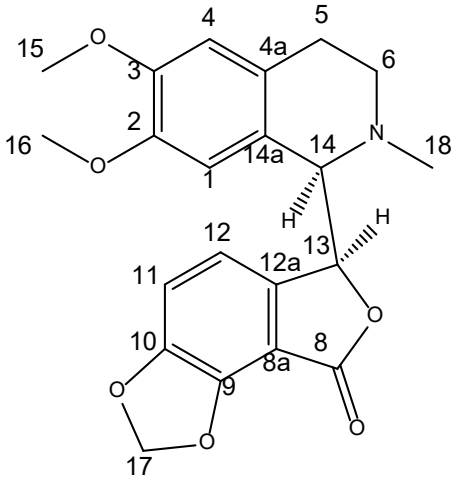

Figure 114: Structure of adlumine (**12**)

Table 25: ^{13}C NMR and ^{1}H NMR data for adlumine (**12**) (δ in ppm, 100 MHz and 400 MHz respectively, in $MeOD_4$).

Position	δ_C	δ_H
1	111.1	6.67, s, 1H
2	146.6	-
3	147.6	-
4	111.7	6.53, s, 1H
4a	128.0	-
5	28.0	2.77 2.52, m, 2H
6	51.0	3.11 2.53, m, 2H
7	-	-
8	167.5	-
8a	109.2	-
9	144.1	-
10	148.9	-
11	116.1	7.23, d, 1H, *J=8.0*
12	116.1	7.23, d, 1H, *J=8.0*
12a	141.5	-
13	82.7	5.80, d, 1H, *J=3.5*
14	65.4	4.07, d, 1H, *J=3.5*
14a	123.4	-
15	55.1	3.72, s, OCH_3
16	55.0	3.77, s, OCH_3
17	103.1	6.08, m, 2H
18	43.2	2.60, s, CH_3

Compound **12** exhibited a molecular weight of 383 and was assigned the molecular formula $C_{19}H_{17}NO_4$, was established. The ^{1}H-NMR and ^{13}C-NMR spectra (Table 25) revealed specific signals for two methylenes [δ_H/δ_C 2.77 m, 2.52 m/28.0 (CH_2-5); 2.53 m, 3.11 m /51.0 (CH_2-6)], two methines [δ_H/δ_C 5.80 d (*J* =3.5 Hz) /82.7 (CH-13); 4.07 d (*J* =3.5 Hz)/65.4 (CH-14)], two methoxy signals [δ_H/δ_C 3.72/55.1, 3.77/55.0]; four distinct aromatic methines were identified [δ_H/δ_C 6.53 s / 111.7 (CH-4), 6.67 s /111.1 (CH-1); 7.23 d (*J* = 8.0 Hz)/116.1 (CH-11); 7.23 d (*J* = 8.0 Hz)/116.1 (CH-12)] along with a dioxygenated methylene group [δ_H/δ_C 6.08 s /103.1, (9-OCH_2O-10)], And a methyl group signal at δ_H/δ_C 2.60 s/43.2 (Me-N). These spectral features align with those of the previously documented compound (+)-adlumine (Seger *et al.*, 2004).

4.11.9. Adlumidine (13)

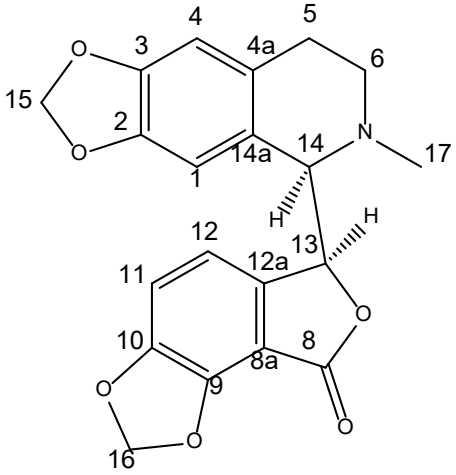

Figure 115: Structure of adlumidine (**13**)

Table 26: ^{13}C-NMR and ^{1}H- NMR chemical shift values of adlumidine (**13**) (ppm, Acetone-d_6, 100 and 400 MHz, respectively)

Position	δ_C	δ_H
1	108.2	78, s, 1H
2	147.6	-
3	149.7	-
4	108.8	6.50, s, 1H
4a	131.3	-
5	29.0	2.50 2.72, m, 2H
6	52.0	2.46 3.06, m, 2H
7	-	-
8	164.3	-
8a	108.2	-
9	144.9	-
10	151.0	-
11	113.7	7.09, d, 1H, (*J=8.0*)
12	116.8`	7.27, d, 1H, (*J=8.0*)
12a	142.3	-
13	84.1	5.73, d, 1H (*J=2.5*)
14	66.7	4.07, d, 1H (*J=2.5*)
14a	124.7	-
15	101.7	5.87 s
16	104.0	6.13 s
17	45.2	2.43 s

Compound **13** molecular weight 367 and the molecular formula $C_{20}H_{17}NO_6$, was confirmed based on its ^{1}H-NMR and ^{13}C-NMR spectra (Table 26). The spectra revealed discrete signals for two methylenes [δ_H/δ_C 2.50 m, 2.72 m/29.0 (CH_2-5); 2.46 m, 3.06m /52.0 (CH_2-6)], two methine groups [δ_H/δ_C 4.07 d (*J* =2.5 Hz) /66.7 (CH-13); 5.73 d (*J* =2.5 Hz)/84.1 (CH-14)], four discrete aromatic methine signals [δ_H/δ_C 6.50 s / 108.8 (CH-4), 6.78 s /108.2 (CH-1); 7.09 d (*J* = 8.0 Hz)/113.7 (CH-11); 7.27 d (*J* = 8.0 Hz)/116.8 (CH-12)]. Additionally, two dioxygenated methylene groups were observed [δ_H/δ_C 6.13 s /104.0, (9-OCH_2O-10); 5.87 s/101.7, (2-OCH_2O-3], along with a methyl signal at δ_H/δ_C 2.43 s/45.2 (Me-N). These data aligned well with those of the previously documented compound (+)-adlumidine (Blaskó *et al.*, 1982).

The phytochemical investigation of *C. govaniana* and *C. casimiriana*, leading to the isolation and identification of alkaloid with known pharmacological properties. From *C. govaniana*, the prominent alkaloid govaniadine (**10**) was successfully isolated, while *C. casimiriana* yielded stylopine (**11**), adlumine (**12**), and adlumidine (**13**).

The isolation of govaniadine from *C. govaniana* is consistent with earlier reports that highlight the richness of the *Corydalis* genus in isoquinoline alkaloids (Shrestha *et al.*, 2013). Govaniadine is particularly noteworthy due to its diverse pharmacological activities, including anti-inflammatory, antispasmodic, and antimicrobial effects (Muhammad *et al.*, 2015; Sivakumaran *et al.*, 2018). Its presence in *C. govaniana* reinforces the ethnopharmacological uses of the plant in traditional medicine, especially in alleviating pain and inflammation. Further studies on its biological activities and underlying mechanisms could pave the way for its potential therapeutic applications.

The isolation of stylopine, adlumine, and adlumidine from *C. casimiriana* underscores the phytochemical diversity within this species. Stylopine, a benzylisoquinoline alkaloid, has been extensively studied for its anti-inflammatory, hepatoprotective, and antimicrobial properties (Wangchuk, *et al.*, 2012) . Its presence in *C. casimiriana* highlights the plant's therapeutic potential, particularly for liver and microbial infections.

Adlumine and adlumidine, both benzylisoquinoline alkaloids, have been less studied than stylopine but are gaining attention due to their promising bioactivities. Adlumine is known for its anti-tumor and anti-inflammatory properties, while adlumidine is

emerging as a candidate for antimicrobial and potential neuroprotective studies (Seger *et al.*, 2004). Their isolation from *C. casimiriana* provides new insights into the chemical profile of the plant and warrants further investigation into their pharmacological activities.

The identification of these alkaloids from three distinct *Corydalis* species contributes to the growing understanding of the genus's phytochemical diversity. The differences in the isolation of different alkaloids may reflect species-specific biosynthetic pathways influenced by genetic and ecological factors. Such variability underscores the importance of systematic phytochemical studies in uncovering bioactive compounds with therapeutic potential (Newman & Cragg, 2020).

The findings from this study not only validate the traditional use of these plants but also provide a basis for future pharmacological and clinical investigations. Detailed studies on the bioactivities of chaeronepaline A-D, bicuculline, corydalmine, 8-hydroxydihydrosanguinarine, dihydrosanguinarine, scoulerine, govaniadine, stylopine, adlumine, and adlumidine, along with structure-activity relationship (SAR) analyses, could facilitate the development of new drugs. Furthermore, the exploration of sustainable extraction and cultivation practices will ensure the conservation of these medicinal plants while meeting the demands of pharmaceutical applications.

4.12. Compounds Obtained from Commercial Source

Berberine (**14**), Californidine (**15**), Sanguinarine (**16**) and Protopine (**17**) were obtained from were commercially sourced from PhytoLab GmbH & Co. KG, Dutendorfer Straße 5-7, 91487 Vestenbergsgreuth, Germany.

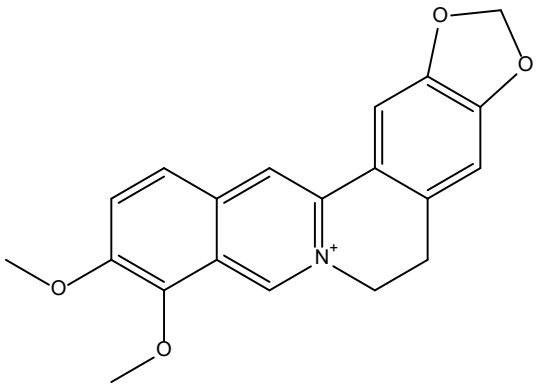

Berberine (**14**)

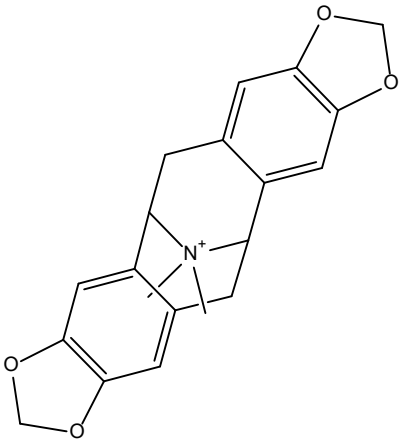

Californidine (**15**)

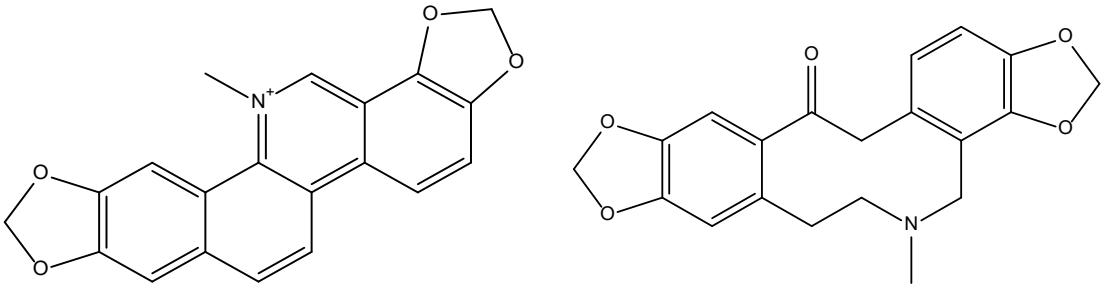

Sanguinarine (**16**) Protopine (**17**)

Figure 116: Structure of berberine (14), californidine (15), sanguinarine (16) and protopine (17)

4.13. Hypocholesterolemic Assay of the Isolated Compounds

4.13.1. Set 1: Nine Known Compounds

The physical and spectral data for govaniadine isolated from *C. govaniana*, bicuculline from *C. chaerophylla*, as well as stylopine, adlumine, and adlumidine from *C. casimiriana*, were found to be consistent with those previously reported in the literature. Additionally, berberine, sanguinarine, protopine, and californidine were acquired from commercial providers.

These derivatives of tetrahydroprotoberberine were chosen for their similarity to berberine, aiming to compare their activities and explore whether the occurrence of a nitrogen with positive charge in the isoquinoline framework and hydrogenation applied to the heterocyclic ring structure is essential for their effects on LDLR and PCSK9 expression. Among these compounds, sanguinarine and californidine were noted for possessing ionized nitrogen atoms, while tertiary nitrogen moieties are present in the remaining compounds, except for protopine, which features a secondary amine group. Both berberine and sanguinarine exhibit aromatic charged nitrogen, whereas californidine uniquely contains an aliphatic quaternary nitrogen.

In terms of structural differences, protopine lacks a C-C linkage within the heterocyclic ring. Additionally, adlumidine, adlumine, and bicuculline lack the “C” ring, classifying them as phthalideisoquinoline alkaloids. Further structural variation exists between bicuculline and adlumine, which differ as epimers at the first position. Adlumine and adlumidine belong to the threo-phthalideisoquinoline class of alkaloids, contrasting with bicuculline as having erythro configuration (Elango *et al.*, 1982).

The selection of these nine isoquinolinic derivatives as potential hypocholesterolemic agents was made based on their structural similarity to berberine. These compounds, with the exception of berberine, had not been previously tested for their bioactive properties in this context. *In vitro* assessments were conducted to determine their capacity to promote LDLR and PCSK9 induction in human hepatocyte (Huh7) cells. The data gathered from these bioactivity evaluations contributes to the preliminary investigation of structure-activity relationships among these alkaloids, enabling a deeper understanding of how structural variations influence their potential hypocholesterolemic effects.

The potential hypocholesterolemic potential of the isolated natural compounds were investigated by initially evaluating their *in vitro* cytotoxic effects on Huh7 hepatocyte cell lines. The analysis revealed that govaniadine, protopine, sanguinarine, and stylopine notably decreased cell viability at 100 μM concentration. This impact was comparable to berberine's effect, which demonstrated a significant reduction in cell viability at a concentration of 80 μM (Figure 117). With potent cytotoxic action, protopine caused a statistically significant decline in cell viability at concentrations as low as 12.5 μM, whereas sanguinarine showed the strongest impact, bringing about approximately a 90% decrease in cell viability at 3.125 μM. Based on these results, the effects of these alkaloids were subsequently evaluated at concentrations deemed non-cytotoxic, with sanguinarine being omitted from further assessments on LDLR and PCSK9 expression owing to its high cytotoxicity under the assay conditions.

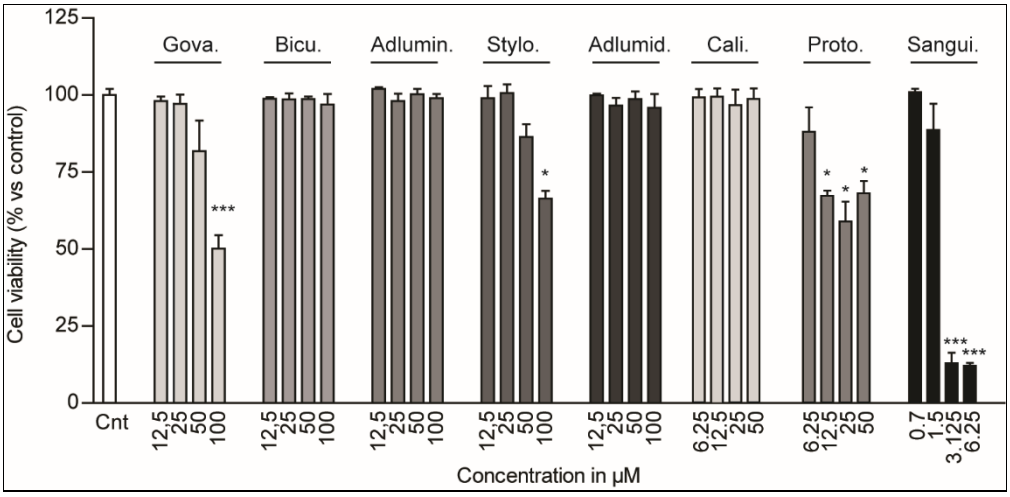

Cells were seeded in MEM supplemented with 10% FBS in a 96-well plate at a density of 8,000 cells per well. After 24 hours, treatments were applied at the specified concentrations and incubated for 72 hours. Cell viability was then assessed using the SRB assay. Statistical significance was noted as *p<0.05 and ***p<0.001 compared to the control. Abbreviations: Cnt – Control; Gova – Govaniadine; Bicu – Bicuculline; Adlumin – Adlumine; Stylo – Stylopine; Adlumid – Adlumidine; Cali – Californidine; Proto – Protopine; Sangui – Sanguinarine.

Figure 117: Determination of non-cytotoxic concentrations of tested alkaloids in Huh7 cell line.

Berberine was used as a reference compound for initial evaluation, following experimental conditions from previous research (Kong *et al.*, 2004). A 72-hour incubation with the cells at a dose of 10 µM resulted in a notable elevation of LDLR expression (1.64-fold) and a 66% decrease in PCSK9 levels (Figure 118), therefore verifying berberine's actions on these targets.

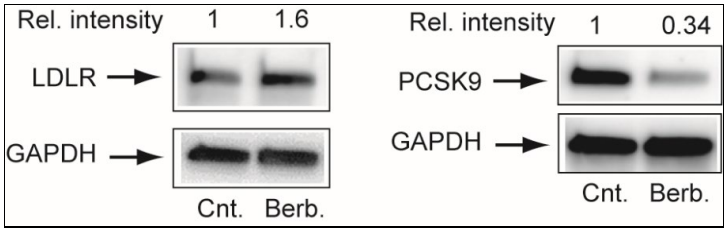

Cells were seeded in MEM supplemented with 10% FBS in 6-well plates at a density of 300,000 cells per well. The following day, cells were treated with berberine (10 µM) in fresh medium for 72 hours. Total protein extracts were then prepared, and protein expression levels of LDLR and PCSK9 were analyzed via western blot, with GAPDH serving as the loading control. Densitometric analysis of the bands was performed using ImageLab™ software, with the relative band intensities indicated above each image. Abbreviations: Cnt – Control; Berb – Berberine.

Figure 118: Effect of berberine on LDLR and PCSK9 protein levels assessed in the Huh7 cell line.

In assessing the potential of tetrahydroprotoberberine alkaloids, govaniadine, bicuculline, and adlumine, under identical experimental conditions, were tested to assess their impact on LDLR (low-density lipoprotein receptor) and PCSK9 (proprotein convertase subtilisin/kexin type 9) expression levels. For this experiment, govaniadine

was applied at concentrations of 50 µM and 25 µM, while bicuculline and adlumine were tested at 100 µM and 50 µM. Simvastatin, a widely used HMG-CoA reductase inhibitor, served as a positive control attributing to its well-documented ability to strongly induce the expression of both LDLR and PCSK9 as supported by (Ferri *et al.*, 2017).

Govaniadine significantly enhanced LDLR expression, showing a 2.8 ± 1.2 fold increase at 50 µM. This effect was accompanied by an increase in PCSK9 expression, though this rise (3.3 ± 2.0 fold) was not statistically significant (Figure 119). At 25 µM, govaniadine demonstrated a similar pattern, significantly increasing LDLR expression, thus exhibiting a behavior distinct from Berberine, which primarily reduces PCSK9 levels.

Adlumine, tested at 50 µM, also demonstrated a favorable impact on LDLR expression, with an increase of 2.2 ± 0.7 fold, while it reduced PCSK9 levels by 0.7 folds; -30 ± 6%. At a lower concentration (25 µM), this effect persisted, though it was less pronounced and not statistically significant. Structurally, adlumine resembles berberine due to the inclusion of two methoxy groups attached to a single aromatic ring, which may explain its similar behavior in reducing PCSK9.

In contrast, bicuculline, which features two methoxy groups in place of the methylenedioxy moiety on one of its aromatic rings, exhibited a lesser effect on LDLR and PCSK9 expression, indicating its comparatively weaker bioactivity. This suggests that the differences in substitution patterns in the aromatic rings significantly impact their biological effects.

Overall, govaniadine displayed a statin-like profile by inducing both LDLR and PCSK9, albeit with a weaker effect. Meanwhile, adlumine exhibited behavior similar to berberine by increasing LDLR expression while concurrently reducing PCSK9 levels, indicating a more favorable profile for potential hypocholesterolemic activity.

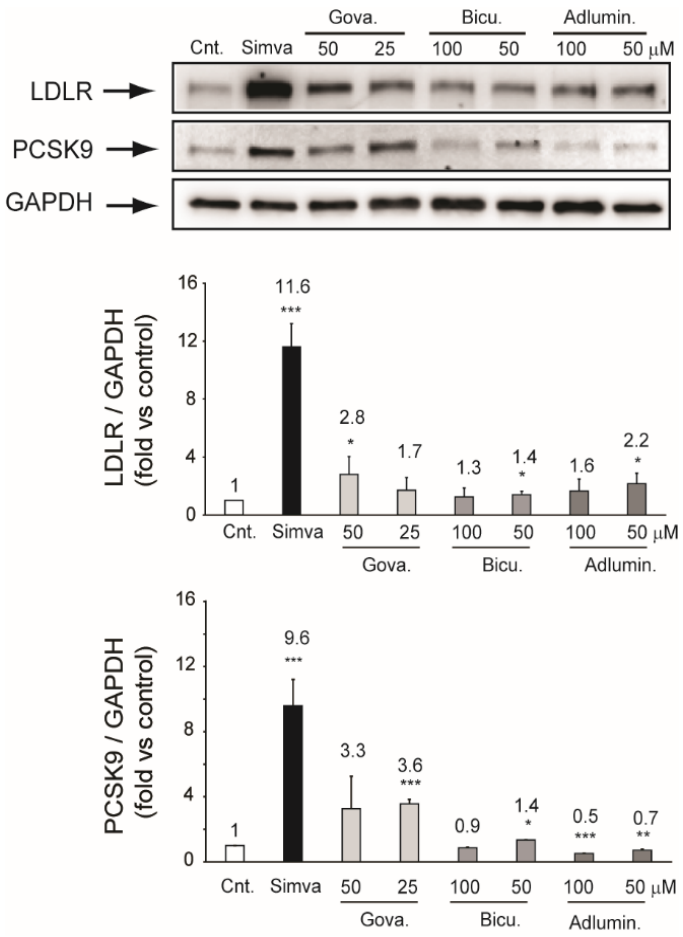

Cells were seeded at a density of 300,000 cells per well in MEM containing 10% FBS, in 6-well plates. The following day, cells were treated with medium containing specified concentrations of the alkaloids. After 72 hours, total protein extracts were prepared, and LDLR and PCSK9 expression levels were analyzed via western blot, with GAPDH as the loading control. Densitometric analysis of the bands was conducted using ImageLab™ software, with relative band intensities shown above the histograms. Significance levels are indicated as *p<0.05; **p<0.01; ***p<0.001 compared to the control. Abbreviations: Cnt – Control; Gova – Govaniadine; Bicu – Bicuculline; Adlumin – Adlumine.

Figure 119: Effect of govaniadine, bicuculline, and adlumine on LDLR and PCSK9 expression in Huh7 cell line.

In an additional series of trials, the effects of four more alkaloids, stylopine, adlumidine, protopine, and californidine, on the expression levels of LDLR and PCSK9 were investigated. The outcomes of these alkaloids were dose-dependent, exhibiting different behaviors at varying concentrations.

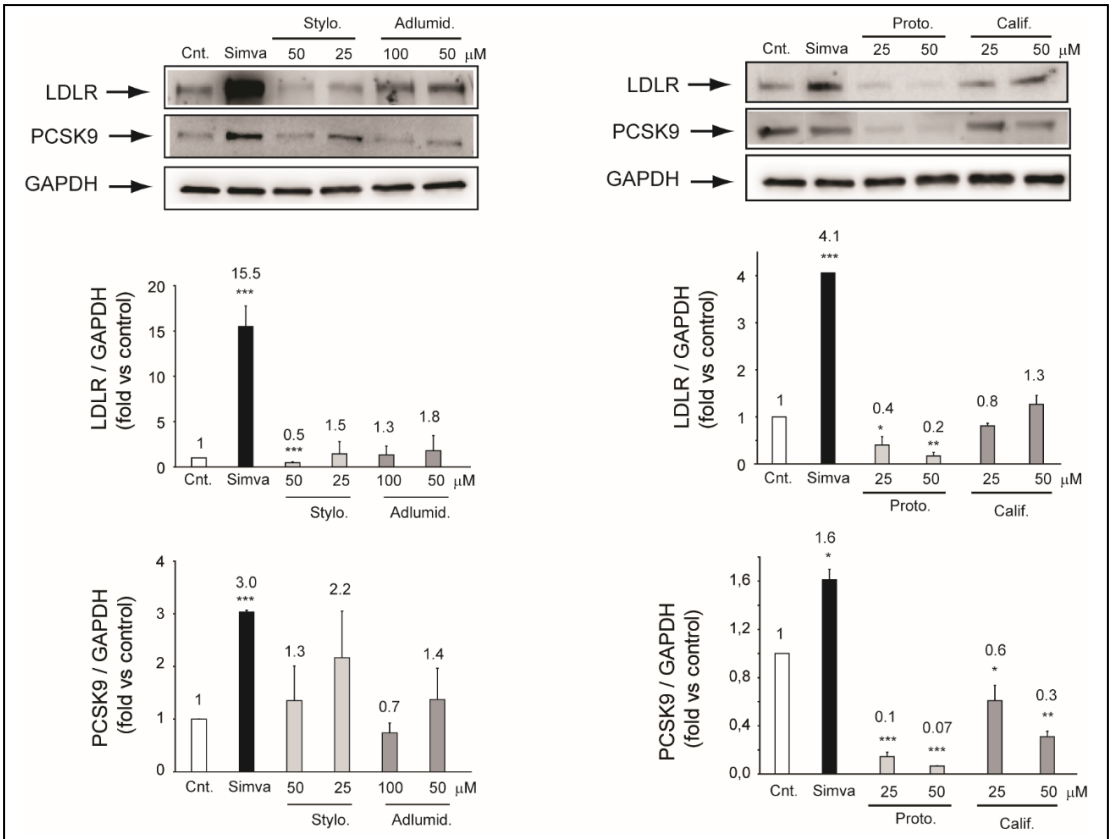

Cells were seeded at a density of 300,000 cells per well in a 6-well plate using MEM supplemented with 10% FBS. The following day, cells were treated with media containing specified concentrations of the alkaloids. After a 72-hour incubation period, total protein extracts were obtained, and LDLR and PCSK9 protein levels were assessed through western blot analysis, with GAPDH serving as the loading control. Densitometric values were analyzed using ImageLab™ software, and the relative band intensities are shown above the histograms. Statistical significance is represented as *p<0.05; **p<0.01; ***p<0.001 compared to control. Abbreviations: Cnt – Control; Stylo – Stylopine; Adlumid – Adlumidine; Calif – Californidine; Proto – Protopine.

Figure 120: Effect of stylopine, adlumidine, californidine and protopine on LDLR and PCSK9 expression in Huh7 cell line.

Stylopine showed a decrease in LDLR expression (+0.5 fold) at 50 μM, but at a lower concentration of 25 μM, it induced LDLR expression (+1.5 fold) (Figure 120). This suggests that its ability to regulate LDLR is more effective at lower concentrations. Conversely, at 50 μM, adlumidine showed a different effect by enhancing the expression of both LDLR and PCSK9 (+1.8 and +1.4 fold, respectively). However, at a higher concentration of 100 μM, PCSK9 expression was reduced to +0.7 fold, demonstrating a nuanced concentration-dependent response. Adlumidine exhibited a similar pattern of activity as seen with its 1-epimer derivative, bicuculline, as in the earlier experimental results.

Protopine exhibited a distinct behaviour by significantly downregulating both LDLR and PCSK9 at 50 μM (-83 ± 8% for LDLR and -93 ± 1% for PCSK9). This strong

suppression persisted even at 25 μM (Figure 120). A more nuanced effect was observed with californidine, where LDLR expression was elevated at 50 μM but reduced at 25 μM (Figure 120). However, Californidine consistently reduced PCSK9 levels at both concentrations, with +0.6 fold at 25 μM and +0.3 fold at 50 μM.

A comparative analysis between govaniadine and californidine with berberine was also conducted. All three compounds, govaniadine, californidine, and berberine, were shown to induce LDLR expression similarly to simvastatin at 2.5 μM (Figure 121). At the given doses, californidine and berberine reduced PCSK9 expression by 20%, presenting an inverse effect to simvastatin, which enhances PCSK9 levels. In comparison, govaniadine exhibited a similar effect to statins by raising both LDLR and PCSK9, albeit with reduced efficacy compared to simvastatin (Figure 121A and 121B).

Further investigation into the molecular mechanisms of californidine and govaniadine revealed their influence on intracellular content of total cholesterol, which was assessed using LC-MS. Simvastatin reduced intracellular content of total cholesterol by more than 70%, likely due to the activation of the SREBP pathway, which induces both LDLR and PCSK9 expression (Figure 121A-C). Interestingly, on the observation of LC-MS data obtained, all tested alkaloids reduced total cholesterol levels. In particular, berberine and californidine demonstrated a strong cholesterol-lowering effect, similar to simvastatin (Figure 121C). This result suggests that both berberine and californidine not only induce LDLR but also have a beneficial, opposing effect on PCSK9 expression, making them promising candidates for further investigation into cholesterol-lowering therapies.

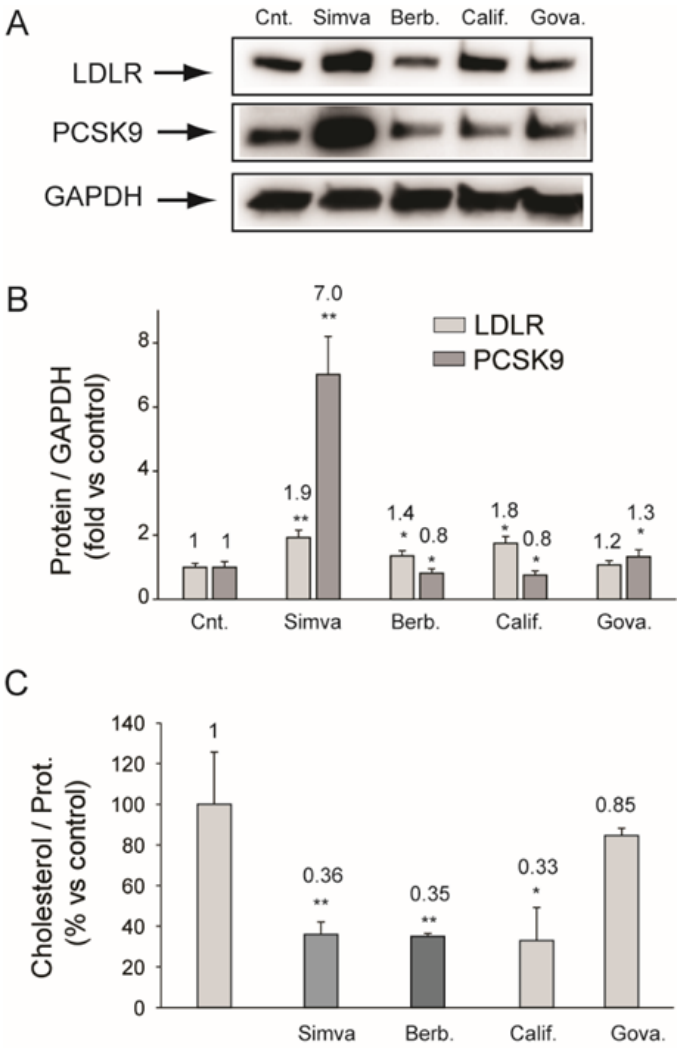

Cells were plated at a density of 300,000 cells per well in a 6-well tray with MEM supplemented with 10% FBS. The following day, cells were exposed to media containing specified concentrations of alkaloids. A) After a 72-hour incubation, total protein extracts were collected, and LDLR and PCSK9 protein levels were assessed via western blot, using GAPDH as a loading control. B) Densitometric analysis of the bands was conducted using ImageLab™ software, with relative band intensities displayed above the histograms. C) Under the same conditions, intracellular cholesterol content was measured through LC/MS following NaOH saponification. Statistical significance is indicated as *p<0.05 and **p<0.01 compared to the control. Abbreviations: Cnt – Control; Simva – Simvastatin; Berb. – Berberine; Calif – Californidine; Gova. – Govaniadine.

Figure 121: Effect of berberine, californidine and govaniadine on PCSK9 and LDLR expression in Huh7 cell line.

This investigation identified significant pharmacological features in a selection of alkaloids, pointing to their suitability for further *in vivo* studies on hypocholesterolemic effects. Initial insights into structure-activity relationships emerged, illustrating how these compounds influence LDLR and PCSK9 function.

Govaniadine demonstrated a "statin-like" mechanism of action by inducing both LDLR and PCSK9. This indicated that govaniadine might operate similarly to statins, which

are widely used for managing cholesterol levels. Stylopine, on the other hand, showed minimal effects on both proteins. This contrast between the two compounds suggested that the specific substituents attached to the aromatic ring positions 1, 2, and 3 played a critical role in their activity on the targeted pathways.

Further comparative analysis of adlumine, adlumidine, and bicuculline revealed additional structural influences on bioactivity. Adlumine, which differs from adlumidine by the presence of methoxyl substituents or a methylenedioxy group at positions 6 and 7 of the tetrahydroquinoline unit, exhibited similar activity to berberine. However, adlumidine and bicuculline, both 1-epimers of the same molecular skeleton, produced less pronounced effects. This indicates that the two methoxy groups, which were present in berberine and adlumine but absent in adlumidine and bicuculline, were essential for the observed effects. The data also indicated that the lactone group and stereochemistry had only limited influence on the compounds' activities.

Protopine demonstrated a distinct behavior compared to the other alkaloids, as it effectively reduced both LDLR and PCSK9 functions. This proposes an inhibitory action on the SREBP pathway, which is responsible for regulating cholesterol homeostasis. As a result, protopine was not expected to have hypocholesterolemic action despite its effect on these pathways.

Californidine showed promising results, with a noteworthy rise in LDLR, a drop in PCSK9 expression, and a decrease in intracellular cholesterol levels. This behavior mirrored that of berberine and positioned californidine as a potential cholesterol-lowering agent. Both californidine and berberine share common molecular features, including a quaternary nitrogen atom (aromatic in berberine and aliphatic in californidine) accompanied by at least one methylenedioxy functional group. These structural elements may be key contributors to their bioactivity. The cholesterol-lowering effects of berberine were previously shown to be mediated through the inhibition of micropinocytosis (Zimetti *et al.*, 2015), and further studies were suggested to investigate whether californidine might operate via a similar mechanism.

Overall, these findings provided essential insights into the structural requirements for inducing LDLR and PCSK9 expression and identified alkaloids with promising hypocholesterolemic potential for further investigation.

4.13.2. Set 2: Four New Compounds

A separate experimental investigation was carried out with the four newly isolated compounds (**1–4**) to assess their effects on key cholesterol-related proteins, LDL-R and PCSK9. Initially, the cytotoxicity of these compounds was examined in human hepatocyte-derived Huh7 cells by exposing them to varying concentrations for 72 hours in a medium containing 10% fetal bovine serum (FBS). Based on the results of the sulforhodamine B (SRB) assay, compounds **2** and **3** exhibited significant cytotoxic activity at concentrations of 50 μM and 100 μM, respectively (Figure 122).

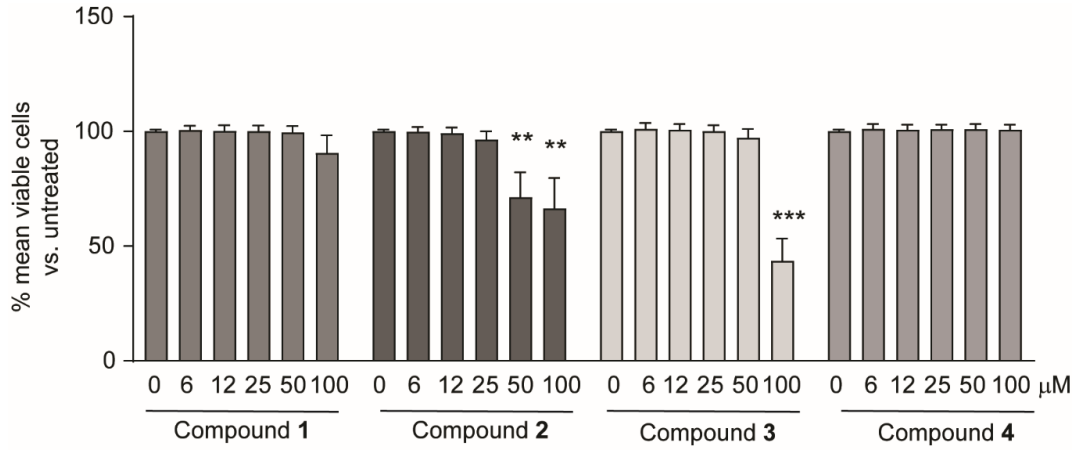

Cytotoxicity was assessed using the SRB assay following a 72-hour incubation of Huh7 cells with compound concentrations of 6.25, 12.5, 25, 50, or 100 μM. Results are presented as mean ± SD from three separate experiments. Statistical significance was evaluated using Student's t-test, with **p<0.01 and ***p<0.001 compared to the untreated control.

Figure 122: Cytotoxicity assay of compound **1 – 4**.

Subsequently, a series of experiments was conducted to evaluate the impact of the four alkaloids how they influence the intracellular LDL-R and PCSK9 expression levels by Western blot analysis. For these tests, Huh7 cells were incubated with specific concentrations of each compound for 72 hours. Specifically, the cells were treated with 100 μM of compound **4**, 50 μM of compounds **1** and **3**, and 25 μM of compound **2**. Simvastatin, a known HMG-CoA reductase inhibitor, served as a positive control owing to its ability to induce LDL-R and PCSK9 expression, while berberine, an isoquinoline alkaloid, served as a benchmark because of its well-documented inhibitory effect on PCSK9 transcription.

As anticipated, simvastatin induced significant increases in both LDL-R (8.3 ± 2.4 fold) and PCSK9 (4.9 ± 2.3 fold) expression levels. In contrast, berberine exhibited only a

modest effect on LDL-R while showing a strong inhibition of PCSK9 (-75%) (Figure 123). Among the tested alkaloids, compounds **2** and **3** demonstrated a notable increase in LDL-R expression, with compound **2** increasing LDL-R by 3.0 ± 1.2 fold and compound **3** by 2.4 ± 0.4 fold (Figure 123). However, compounds **1** and **4** did not produce any significant changes in LDL-R or PCSK9 levels. Although compound **3** appeared to slightly induce PCSK9 expression, the observed change was not statistically significant.

Taken together, compounds **2** and **3** demonstrated a positive effect on LDL-R expression, suggesting their potential as hypocholesterolemic agents.

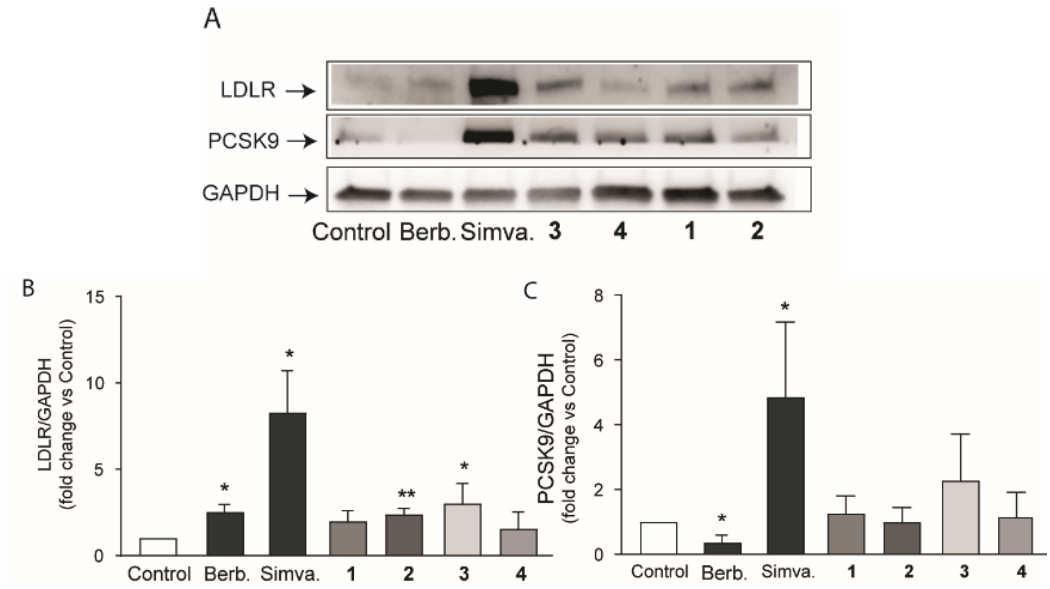

Cells were treated for 72 hours with simvastatin (5 µM), compound 4 (100 µM), compounds 1 and 3 (both at 50 µM), and compound 2 (25 µM). A) Western blot analysis illustrating LDL-R and PCSK9 expression levels following treatment, with GAPDH serving as the loading control; B) Densitometric quantification of the LDL-R/GAPDH ratio; C) Densitometric quantification of the PCSK9/GAPDH ratio. Data are expressed as mean ± SD from three independent experiments. Statistical significance was determined by Student's T-test, with *p<0.05, **p<0.01, and ***p<0.001 compared to the control. Simva: simvastatin.

Figure 123: Effect of compound **1 – 4** on LDL-R and PCSK9 expression in Huh7 cell line.

To further explore the hypocholesterolemic potential of the newly isolated alkaloids, their effects on PCSK9 secretion from the Huh7 cell line were examined. Berberine was used as a positive control, and, consistent with previous studies (Lupo *et al.*, 2019), it successfully reduced extracellular PCSK9 levels by 40.5% (Figure 124). When the four alkaloids were tested, all showed varying degrees of inhibition in PCSK9 secretion. Among them, compounds **1** and **2** exhibited the most potent and effective activity,

demonstrating the strongest reduction in PCSK9 secretion. This indicates that these compounds may hold significant potential for reducing cholesterol levels by targeting PCSK9 secretion, similar to berberine's known mechanism of action.

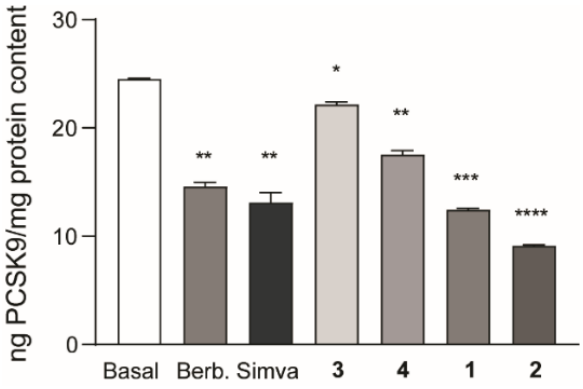

Cells were treated with berberine (10 µM), simvastatin (5 µM), compound 4 (10 µM), compounds 1 and 3 (each at 5 µM), and compound 2 (2.5 µM) for a duration of 72 hours. Following incubation, conditioned media were collected, and PCSK9 levels were measured via an ELISA assay. Results are shown as mean ± SD from three separate experiments, with statistical significance determined using Student's T-test (*p<0.05 compared to control). Berb: berberine.

Figure 124: Effect of compound **1 – 4** on PCSK9 secreted by Huh7 cell line.

The data suggested that compounds **2** and **3** have potential hypocholesterolemic effects through the upregulation of LDL-R (Figure 123). However, compound **2** appeared to differ from compound **3** by additionally inhibiting PCSK9 secretion (Figure 124). This dual activity implies that compound **2** may work through a mechanism similar to that of berberine, which has been shown to inhibit PCSK9 transcription, resulting in reduced intracellular and extracellular PCSK9 levels (Cameron *et al.*, 2008).

Following this, cholesterol biosynthesis was examined in the hepatoma HepG2 cell line. As projected, both simvastatin and berberine significantly reduced cholesterol biosynthesis (Figure 125). While the new alkaloids did not match the efficacy of simvastatin or berberine, all showed some inhibitory effects on cholesterol synthesis, with compound **2** displaying the most potent activity (Figure 125). This result further supports the potential of compound **2** as a hypocholesterolemic agent by not only reducing PCSK9 secretion but also inhibiting cholesterol biosynthesis.

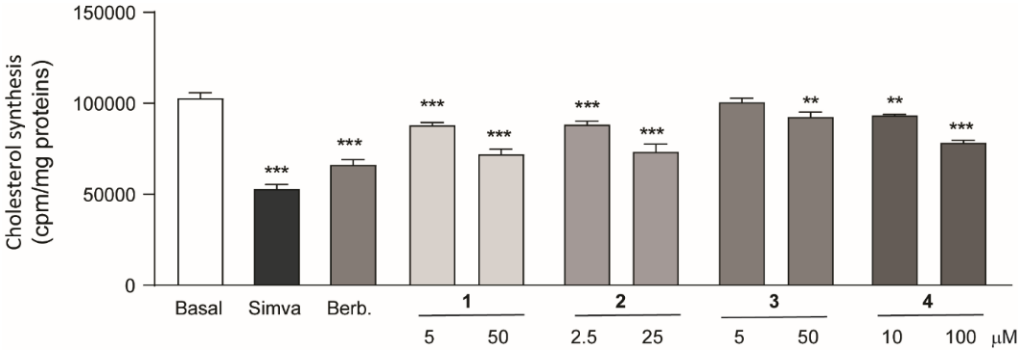

Cells were treated with simvastatin (5 μM), berberine (20 μM), or compounds at specified concentrations for 48 hours. Following this incubation period, cells were exposed to 14C-acetate in MEM supplemented with 0.4% FCS. After an additional 24 hours, the incorporation of 14C-acetate into cholesterol was measured. Results are displayed as mean ± SD from three independent assessments, with significance noted using Student's T-test (**p<0.01; ***p<0.001 compared to control). Simva: simvastatin; Berb: berberine.

Figure 125: Effect of compound **1 – 4** on cholesterol biosynthesis in HepG2 cell line.

The data indicated that these alkaloids, particularly compound **2**, exhibited a mechanism of action similar to berberine, by reducing both PCSK9 expression and cholesterol biosynthesis. These effects collectively led to a significant increase in LDL-R expression. Upon further structural analysis, it was found that compound **2** is a protopine derivative. This compound differs structurally from protopine due to the presence of an epoxy group at positions 13-14, whereas in protopine, position 14 is occupied by a keto group and position 13 by a CH_2 group.

This structural variation appears to significantly impact the bioactivity of the compound. Previous set of studies, have shown that 50 μM of protopine strongly downregulated both LDLR and PCSK9 in the same cellular model, underscoring how minor structural modifications in these compounds can lead to distinct biological effects (Maharjan *et al.*, 2022). This highlights the importance of structure-activity relationships in the design and evaluation of potential hypocholesterolemic agents.

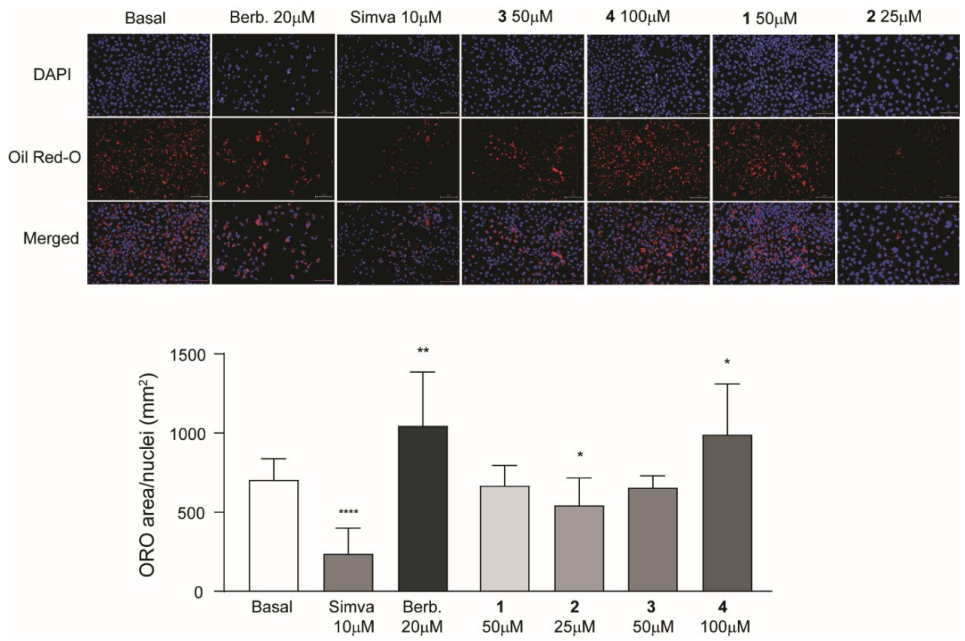

Cells were treated with positive controls and compounds at the specified concentrations for 72 hours. Following the incubation, neutral lipids were stained using Oil Red-O. Data are expressed as mean ± SD from three independent experiments. The top panel displays representative images of Oil Red-O staining (n=6). Statistical significance was assessed by Student's T-test (*p<0.05; **p<0.01; ****p<0.0001 compared to control). Simva: simvastatin; Berb: berberine.

Figure 126: Accumulation of neutral lipids after compound **1 – 4** treatments on Huh7 cell line.

Ultimately, the activity of the compounds newly derived from *C. chaerophylla* on lipid accumulation in the Huh7 cell line were tested, and the results are illustrated in Figure 126. The analysis showed that, following treatment with the compounds, there was no significant variation in the amount of neutral lipids—namely triglycerides and cholesterol esters—except when compounds **2** and **4** were applied. In these cases, compound **2** resulted in a marked reduction in lipid accumulation, resembling the effect of simvastatin rather than berberine. On the other hand, compound **4** exhibited a more berberine-like effect on lipid accumulation.

Although compound **2** had already demonstrated a berberine-like mechanism by reducing PCSK9 secretion and cholesterol biosynthesis while inducing LDL-R expression, this assay further revealed a protective effect against liver lipid accumulation. These findings suggest that compound **2** may have an additional effect on triglyceride synthesis pathways, which could open up new areas for research into its potential therapeutic benefits. This raises the possibility that compound **2** could not only target cholesterol regulation but also exert a broader impact on lipid metabolism, particularly in liver cells.

CHAPTER 5

5. CONCLUSION AND RECOMMENDATIONS

5.1. CONCLUSION

This research thoroughly investigated the phytochemicals derived from *Corydalis chaerophylla, C. govaniana* and *C. casimiriana* to elucidate their *in vitro* and *in vivo* biological properties, highlighting their potential for therapeutic applications. The study utilized hexane, methanol, and chloroform to extract compounds from these plants. *C. chaerophylla* extracts followed by phytochemical screening, revealing fifteen distinct alkaloids through LC-DAD-MS^n analysis. The hexane extract was notably rich in dihydrosanguinarine, and spectrophotometric analysis demonstrated a higher flavonoid content compared to phenolics. Conversely, the methanol and chloroform extracts contained significant amounts of jatrorrhizine and bicuculline, with the methanol extract also rich in N-methyltetrahydropalmatine. Both methanol and chloroform extracts showed a predominance of phenolic compounds over flavonoids in spectrophotometric assays, while also displaying notable antimicrobial activity across tested pathogens. The chloroform extract, in particular, exhibited robust DPPH scavenging activity, suggesting strong antioxidant potential. All three extracts demonstrated toxicity in the brine shrimp assay, with LC_{50} values above 1000 µg/mL, indicative of toxic properties. Additionally, the methanol and chloroform extracts emerged as effective α-amylase inhibitors, suggesting potential for antidiabetic applications. However, acute oral toxicity studies in mice indicated potential toxicity for methanol and chloroform extracts at higher doses.

The findings also underscore significant bioactivity of specific alkaloids isolated from aforementioned species including some from commercial source, in modulating LDLR and PCSK9, with notable structural variations among compounds influencing their interactions with these targets. For example, californidine and adlumine demonstrated a promising pharmacological profile, showing an upregulation of LDLR and downregulation of PCSK9. Similarly, govaniadine showed effects akin to simvastatin, impacting both LDLR and PCSK9 levels. Protopine, distinct in its polycyclic structure, had the opposite effect, reducing levels of both targets. Importantly, berberine and

californidine also markedly lowered intracellular cholesterol, comparable to simvastatin's efficacy.

The detailed phytochemical analysis of *C. chaerophylla* led to the identification of four new alkaloids. Structural elucidation revealed compound **1** as a protoberberine type with methoxy groups at positions 3 and 12 and hydroxyls at 2 and 9, while compound **2** comprises an N-methyl tetrahydroquinoline linked to a benzyl acid moiety. Compounds **3** and **4** were identified as a spiroindane benzoquinoline and its N-oxide derivative, respectively. Notably, compound **2** exhibited the most promising activity in modulating cholesterol-related pathways, including inhibition of cholesterol biosynthesis, lipid accumulation, and PCSK9 secretion, while significantly enhancing LDL-R expression. Further studies *in vivo* are recommended to confirm compound **2**'s hypocholesterolemic potential.

5.2. RECOMMENDATIONS

1. Further *in vivo* studies on compound **2** are necessary to validate its hypocholesterolemic effects and to understand its mechanism in more complex biological systems.
2. Additional alkaloids from *C. chaerophylla, C. govaniana* and *C. casimiriana* could be isolated and tested for different bioactivities, including LDLR and PCSK9 expressions, to expand the library of potential therapeutic agents from these plants.
3. The finding suggests to continue the work on compound 2 (Chaeronepaline-B) for the application to downregulate the cholesterol level in cancer patients.

CHAPTER 6

6. SUMMARY

This research focused on the phytochemical investigation and biological evaluation of *C. chaerophylla*, *C. govaniana*, and *C. casimiriana*, three high-altitude plants from Nepal's Himalayan region, known for their rich isoquinoline alkaloid content and potential therapeutic applications. Sequential extraction using hexane, methanol, and chloroform revealed significant bioactivities, with *C. chaerophylla* extracts containing 15 alkaloids identified through LC-DAD-MSn analysis. The chloroform extract exhibited the highest phenolic content, strong antioxidant activity (IC_{50} = 261.5 µg/mL), and potent antimicrobial properties, while the methanol extract showed effective α-amylase inhibition (IC_{50} = 51.52 µg/mL), suggesting antidiabetic potential. Acute oral toxicity studies indicated dose-dependent toxicity for methanol and chloroform extracts in mice. Chromatographic separation of the chloroform extract yielded four new alkaloids, Chaeronepaline A-D from *C. chaerophylla*, alongside known alkaloids from the three species. Structural elucidation of these compounds was achieved using advanced spectroscopic techniques and computational calculations. Among the alkaloids tested, californidine, adlumine, and govaniadine demonstrated notable hypocholesterolemic activity, influencing LDLR and PCSK9 expression and reducing intracellular cholesterol. Particularly, compound **2** (Chaeronepaline-B) showed promising cholesterol-lowering effects, warranting further *in vivo* validation. This study highlights the therapeutic potential of *Corydalis* species and their alkaloids, providing a foundation for future pharmacological research and drug development.

7. REFERENCES

Aberoumand, A., & Deokule, S. S. (2008). Comparison of Phenolic Compounds of Some Edible Plants of Iran and India. *Pakistan Journal of Nutrition*, **7**(4): 582–585. https://doi.org/10.3923/pjn.2008.582.585

Abreu, A. C., McBain, A. J., & Simões, M. (2012). Plants as Sources of New Antimicrobials and Resistance-Modifying Agents. *Natural Product Reports*, **29**(9): 1007–1021. https://doi.org/10.1039/c2np20035j

Agbo, M. O., Uzor, P. F., Akazie-Nneji, U. N., Eze-Odurukwe, C. U., Ogbatue, U. B., & Mbaoji, E. C. (2015). Antioxidant, Total Phenolic and Flavonoid Content of Selected Nigerian Medicinal Plants. *Dhaka University Journal of Pharmaceutical Sciences*, **14**(1): 35–41. https://doi.org/10.3329/dujps.v14i1.23733

Al-Khayri, J. M., Rashmi, R., Toppo, V., Chole, P. B., Banadka, A., Sudheer, W. N., Nagella, P., Shehata, W. F., Al-Mssallem, M. Q., Alessa, F. M., Almaghasla, M. I., & Rezk, A. A. S. (2023). Plant Secondary Metabolites: The Weapons for Biotic Stress Management. *Metabolites,* **13**(6): https://doi.org/10.3390/metabo13060716

Ali, H., Houghton, P. J., & Soumyanath, A. (2006). α-Amylase Inhibitory Activity of Some Malaysian Plants Used to Treat Diabetes; with Particular Reference to *Phyllanthus amarus*. *Journal of Ethnopharmacology*, **107**(3): 449–455. https://doi.org/10.1016/j.jep.2006.04.004

Ali, I., Ali, Z., Alishba, Zamarrud, Hussain, H., & Ahmad, V. U. (2019). Phytochemical Isolation and Biological Activities of *Corydalis adiantifolia* from Baltistan. *Journal of the Chemical Society of Pakistan*, **41**(3): 535–543. https://doi.org/10.52568/000758/jcsp/41.03.2019

Allwood, J. W., & Goodacre, R. (2010). An Introduction to Liquid Chromatography-Mass Spectrometry Instrumentation Applied in Plant Metabolomic Analyses. *Phytochemical Analysis*, **21**(1): 33–47. https://doi.org/10.1002/pca.1187

Anet, F. A. L., & Brown, M. A. (1967). The Nuclear Magnetic Resonance Spectrum of

Protopine: Rate of Racemization and Ring Inversion. *Tetrahedron Letters*, **48**: 4881–4884. https://doi.org/https://doi.org/10.1016/S0040-4039(01)89624-6

Antonio, C. N. S., Elnatan, B. de S., Marcos, F. aacute bio G. R., Maria, R. J. R. A., Paulo, N. B., H eacute lcio, S. dos S. R. P., Selene, M. de M., Raquel, O. dos S. F., & Carolina, S. de P. C. (2016). Cytotoxicity, Antifungal and Antioxidant Activities of the Essential Oil from *Eupatorium ballotifolium* Kunth (Asteraceae). *African Journal of Pharmacy and Pharmacology*, **10**(16): 346–355. https://doi.org/10.5897/ajpp2016.4537

Aprà, E., Bylaska, E. J., De Jong, W. A., Govind, N., Kowalski, K., Straatsma, T. P., Valiev, M., Van Dam, H. J. J., Alexeev, Y., Anchell, J., Anisimov, V., Aquino, F. W., Atta-Fynn, R., Autschbach, J., Bauman, N. P., Becca, J. C., Bernholdt, D. E., Bhaskaran-Nair, K., Bogatko, S., … Harrison, R. J. (2020). NWChem: Past, Present, and Future. *Journal of Chemical Physics*, **152**: 184102. https://doi.org/10.1063/5.0004997

Asaduzzaman, M., Rana, S., Hasan, S. M. R., Hossain, M., & Das, N. (2015). Cytotoxic (Brine Shrimp Lethality Bioassay) and Antioxidant Investigation of *Barringtonia acutangula* (L.). *International Journal of Pharma Sciences and Research*, **6**(8): 1179–1185. https://www.ijpsr.info/docs/IJPSR15-06-08-005.pdf

Azmir, J., Zaidul, I. S. M., Rahman, M. M., Sharif, K. M., Mohamed, A., Sahena, F., Jahurul, M. H. A., Ghafoor, K., Norulaini, N. A. N., & Omar, A. K. M. (2013). Techniques for Extraction of Bioactive Compounds from Plant Materials: A Review. *Journal of Food Engineering*, **117**(4): 426–436. https://doi.org/10.1016/j.jfoodeng.2013.01.014

Azwanida, N. N. (2015). A Review on the Extraction Methods Use in Medicinal Plants, Principle, Strength and Limitation. *Medicinal & Aromatic Plants*, **4**(3): 3–8. https://doi.org/10.4172/2167-0412.1000196

Ballabh, B., & Chaurasia, O. P. (2007). Traditional Medicinal Plants of Cold Desert Ladakh-Used in Treatment of Cold, Cough and Fever. *Journal of Ethnopharmacology*, **112**(2): 341–349. https://doi.org/10.1016/j.jep.

2007.03.020

Banday, A. H., Azha, N. ul, Farooq, R., Sheikh, S. A., Ganie, M. A., Parray, M. N., Mushtaq, H., Hameed, I., & Lone, M. A. (2024). Exploring the Potential of Marine Natural Products in Drug Development: A Comprehensive Review. *Phytochemistry Letters*, **59**: 124–135. https://doi.org/10.1016/j.phytol. 2024.01.001

Banothu, V., Neelagiri, C., Adepally, U., Lingam, J., & Bommareddy, K. (2017). Phytochemical Screening and Evaluation of *In Vitro* Antioxidant and Antimicrobial Activities of the Indigenous Medicinal Plant *Albizia odoratissima*. *Pharmaceutical Biology*, **55**(1): 1155–1161. https://doi.org/10.1080/13880209.2017.1291694

Banu, K. S., & Cathrine, L. (2015). General Techniques Involved in Phytochemical Analysis. *International Journal of Advanced Research in Chemical Science*, **2**(4): 25–32. www.arcjournals.org

Barthwal, R., & Mahar, R. (2024). Exploring the Significance, Extraction, and Characterization of Plant-Derived Secondary Metabolites in Complex Mixtures. *Metabolites*, **14**(2): 119. https://doi.org/10.3390/metabo14020119

Basha, S. A., Jha, R. N., Pandey, V. B., & Singh, U. P. (2007). Effect of 1-Corydalmine, an Alkaloid Isolated from *Corydalis chaerophylla* Roots on Spore Germination of Some Fungi. *Mycobiology*, **35**(2): 69. https://doi.org/10.4489/ myco.2007.35.2.069

Benzie, I. F. F., & Strain, J. J. (1996). The Ferric Reducing Ability of Plasma (FRAP) as a Measure of "Antioxidant Power": The FRAP Assay. *Analytical Biochemistry*, **239**(1): 70–76. https://doi.org/10.1006/abio.1996.0292

Bhakuni, D. S., & Chaturvedi, R. (1983). The Alkaloids of *Corydalis meifolia*. *Journal of Natural Products*, **46**(4): 466–470. https://doi.org/10.1016/S0140-6736(00)89764-0

Bhambhani, S., Kondhare, K. R., & Giri, A. P. (2021). Diversity in Chemical Structures and Biological Properties of Plant Alkaloids. *Molecules*, **26**(11): 3374.

https://doi.org/10.3390/molecules26113374

Blaskó, G., Gula, D. J., Shamma, M., & Blaskó, G. (1982). The Phthalideisoquinoline Alkaloids. *Journal of Natural Products*, **45**(2): 105–122. https://doi.org/10.1021/np50020a001

Borowitz, I. J. (1966). Thin-Layer Chromatography. A Laboratory Handbook. *Journal of Colloid and Interface Science*, **21**(1): 124–125. https://doi.org/10.1016/0095-8522(66)90095-x

Brand-Williams, W., Cuvelier, M. E., & Berset, C. (1995). Use of a Free Radical Method to Evaluate Antioxidant Activity. *LWT - Food Science and Technology*, **28**(1): 25–30. https://doi.org/10.1016/S0023-6438(95)80008-5

Bürger, C., Fischer, D. R., Cordenunzzi, D. A., de Borba Batschauer, A. P., Filho, V. C., & dos Santos Soares, A. R. (2005). Acute and Subacute Toxicity of the Hydroalcoholic Extract from *Wedelia paludosa* (*Acmela brasiliensis*) (Asteracea) in Mice. *Journal of Pharmacy and Pharmaceutical Sciences*, **8**(2): 370–373. https://www.researchgate.net/profile/Adair-Santos/publication/7635723_Acute_and_subacute_toxicity_of_the_hydroalcoholic_extract_from_Wedelia_paludosa_Acmela_brasiliensis_Asteracea_in_mice/links/00b4952407024ee1ef000000/Acute-and-subacute-toxicity-of-the-hydroalcoholic-extract-from-Wedelia-paludosa-Acmela-brasiliensis-Asteracea-in-mice.pdf

Cai, Y., Luo, Q., Sun, M., & Corke, H. (2004). Antioxidant Activity and Phenolic Compounds of 112 Traditional Chinese Medicinal Plants Associated with Anticancer. *Life Sciences*, **74**(17): 2157–2184. https://doi.org/10.1016/j.lfs.2003.09.047

Callejon, D. R., Riul, T. B., Feitosa, L. G. P., Guaratini, T., Silva, D. B., Adhikari, A., Shrestha, R. L. S., Marques, L. M. M., Baruffi, M. D., Lopes, J. L. C., & Lopes, N. P. (2014). Leishmanicidal Evaluation of Tetrahydroprotoberberine and Spirocyclic Erythrina-Alkaloids. *Molecules*, **19**(5): 5692–5703. https://doi.org/10.3390/molecules19055692

Cameron, J., Ranheim, T., Kulseth, M. A., Leren, T. P., & Berge, K. E. (2008).

Berberine Decreases PCSK9 Expression in HepG2 Cells. *Atherosclerosis*, **201**(2): 266–273. https://doi.org/10.1016/j.atherosclerosis.2008.02.004

Catapano, A. L., Graham, I., De Backer, G., Wiklund, O., John Chapman, M., Drexel, H., Hoes, A. W., Jennings, C. S., Landmesser, U., Pedersen, T. R., Reiner, Ž., Riccardi, G., Taskinen, M. R., Tokgozoglu, L., Monique Verschuren, W. M., Vlachopoulos, C., Wood, D. A., Zamorano, J. L., Badimon, L., … Wald, D. (2016). 2016 ESC/EAS Guidelines for the Management of Dyslipidaemias. *European Heart Journal*, **37**(39): 2999-3058l. https://doi.org/10.1093/eurheartj/ehw272

Chang, C.-C., Yang, M.-H., Wen, H.-M., & Chern, J.-C. (2002). Estimation of Total Flavonoid Content in Propolis by Two Complementary Colometric Methods. *Journal of Food and Drug Analysis*, **10**(3): 3. https://doi.org/https://doi.org/10.38212/2224-6614.2748

Chen, J., Li, W., Yao, H., & Xu, J. (2015). Insights into Drug Discovery from Natural Products Through Structural Modification. *Fitoterapia*, **103**: 231–241. https://doi.org/10.1016/j.fitote.2015.04.012

Cheng, X., Shi, Y., Zhen, S., Sun, H., & Jin, W. (2010). HPLC–MS Analysis of Ethanol Extract of *Corydalis yanhusuo* and Simultaneous Determination of Eight Protoberberine Quaternary Alkaloids by HPLC–DAD. *Journal of Chromatographic Science,* **48**: 441–444. https://doi.org/10.1093/chromsci/48.6.441

Chrzanowska, M. (1995). Synthesis of isoquinoline alkaloids. Total Synthesis of (±)-Stylopine. *Journal of Natural Products*, **58**(3): 401–407. https://doi.org/10.1021/np50117a008

Cos, P., Vlietinck, A. J., Berghe, D. Vanden, & Maes, L. (2006). Anti-Infective Potential of Natural Products: How to Develop a Stronger *In Vitro* "Proof-of-Concept." *Journal of Ethnopharmacology*, **106**(3): 290–302. https://doi.org/10.1016/j.jep.2006.04.003

Cowan, M. M. (1999). Plant Products as Antimicrobial Agents. *Clinical Microbiology*

Reviews, **12**(4): 564–583. https://doi.org/10.1128/cmr.12.4.564

Cragg, G. M., Kingston, D. G. I., & Newman, D. J. (2005). Anticancer Agents from Natural Products. *Taylor & Francis eBooks*. 1st Edition https://doi.org/10.1201/b11185

Dai, J., & Mumper, R. J. (2010). Plant Phenolics: Extraction, Analysis and Their Antioxidant and Anticancer Properties. *Molecules*, **15**(10): 7313–7352. https://doi.org/10.3390/molecules15107313

Dar, G. H., Koul, S. T., Naqshi, A. R., Khuroo, A. A., & Malik, A. H. (2011). A New Species of *Corydalis* DC. (Fumariaceae) from Kashmir, North-west Himalaya, India. *Taiwania*, **56**(4): 305–308. https://doi.org/10.6165/tai.2011.56(4).305

Das, R. K. (2018). Antifungal Activities and Phytochemical Screening of Two Invasive Alien Species of Nepal. *Studies in Fungi*, **3**(1): 293–301. https://doi.org/10.5943/sif/3/1/29

Dey, P., Kundu, A., Kumar, A., Gupta, M., Lee, B. M., Bhakta, T., Dash, S., & Kim, H. S. (2020). Analysis of Alkaloids (Indole Alkaloids, Isoquinoline Alkaloids, Tropane Alkaloids). *Recent Advances in Natural Products Analysis*. **2020**: 505-567. https://doi.org/10.1016/B978-0-12-816455-6.00015-9

Dias, D. A., Urban, S., & Roessner, U. (2012). A Historical Overview of Natural Products in Drug Discovery. *Metabolites*, **2**: 303–336. https://doi.org/10.3390/metabo2020303

Edeoga, H. O., Okwu, D. E., & Mbaebie, B. O. (2005). Phytochemical Constituents of Some Nigerian Medicinal Plants. *African Journal of Biotechnology*, **4**(7): 685–688. https://doi.org/10.5897/AJB2005.000-3127

Egan, P. A., Pendry, C. A., & Shrestha, S. (2024). *Papaveraceae*. Flora of Nepal On-Line Accounts. http://www.floraofnepal.org/onlineflora?wildcard=595

Elango, V., Freyer, A. J., Blasko, G., & Shamma, M. (1982). The NMR Spectra and Conformations of The Phthalideisoquinolines. *Journal of Natural Products*, **45**(5): 517–522. https://doi.org/10.1021/np50023a001

Ferri, N., Marchianò, S., Lupo, M. G., Trenti, A., Biondo, G., Castaldello, P., & Corsini, A. (2017). Geranylgeraniol Prevents the Simvastatin-Induced PCSK9 Expression: Role of The Small G Protein Rac1. *Pharmacological Research*, **122**: 96–104. https://doi.org/10.1016/j.phrs.2017.05.021

Gadir, S. A. (2012). Assessment of Bioactivity of Some Sudanese Medicinal Plants Using Brine Shrimp (*Artemia salina*) Lethality Assay. *Journal of Chemical and Pharmaceutical Research*, **4**(12): 5145–5148. http://jocpr.com/vol4-iss12-2012/JCPR-2012-4-12-5145-5148.pdf

Gairola, S., Sharma, J., & Bedi, Y. S. (2014). A Cross-Cultural Analysis of Jammu, Kashmir and Ladakh (India) Medicinal Plant Use. *Journal of Ethnopharmacology*, **155**(2): 925–986. https://doi.org/10.1016/j.jep.2014.06.029

Gross, J. H. (2017). Mass Spectrometry/ A Textbook Third Edition. *Springer,* **1040**(2).

Grothaus, P. G., Cragg, G. M., & Newman, D. J. (2010). Plant Natural Products in Anticancer Drug Discovery. *Current Organic Chemistry*, **14**(16): 1781–1791. https://doi.org/10.2174/138527210792927708

Gülçin, I. (2012). Antioxidant Activity of Food Constituents: An Overview. *Archives of Toxicology*, **86**(3): 345–391. https://doi.org/10.1007/s00204-011-0774-2

Halliwell, B., & Gutteridge, J. M. C. (1985). Free Radicals in Biology and Medicine. *Journal of Free Radicals in Biology and Medicine*, **1**(4): 331–332. https://doi.org/10.1093/acprof:oso/9780198717478.001.0001

Hamayun, M., Khan, A., Afzal, S., Mir, &, & Khan, A. (2006). Study on Traditional Knowledge and Utility of Medicinal Herbs of District Buner, NWFP, Pakistan. *Indian Journal of Traditional Knowledge*, **5**(3): 407–412. http://nopr.niscpr.res.in/handle/123456789/6930

Handa, S. S., Khanuja, S. P. S., Longo, G., & Rakesh, D. D. (2008). Extraction Technologies for Medicinal and Aromatic Plants. *Journal of Natural Products*, **5**(8): 21–40. https://perfumeclasses.com/wp-content/uploads/2019/05/Handa-S.-et-al-Extraction-Technologies-for-Medicinal-and-Aromatic-Plants.pdf

Hanwell, M. D., Curtis, D. E., Lonie, D. C., Vandermeersch, T., Zurek, E., & Hutchison, G. R. (2012). Avogadro: An Advanced Semantic Chemical Editor, Visualization, and Analysis Platform. *Journal of Cheminformatics*, **4**: 17. https://doi.org/10.1016/j.aim.2014.05.019

Harborne, J. B. (1998). Phytochemical Methods: A Guide to Modern Techniques of Plant Analysis. Chapman & Hall Pub. *London, UK*.

Harvey, A. (2000). Strategies for Discovering Drugs from Previously Unexplored Natural Products. *Drug Discovery Today*, **5**(7): 294–300. https://doi.org/10.1016/S1359-6446(00)01511-7

Huang, D., Boxin, O. U., & Prior, R. L. (2005). The Chemistry Behind Antioxidant Capacity Assays. *Journal of Agricultural and Food Chemistry*, **53**(6): 1841–1856. https://doi.org/10.1021/jf030723c

Iqbal, E., Salim, K. A., & Lim, L. B. L. (2015). Phytochemical Screening, Total Phenolics and Antioxidant Activities of Bark and Leaf Extracts of *Goniothalamus velutinus* (Airy Shaw) from Brunei Darussalam. *Journal of King Saud University - Science*, **27**: 224–232. https://doi.org/10.1016/j.jksus.2015.02.003

Iranshahy, M., Quinn, R. J., & Iranshahi, M. (2014). Biologically Active Isoquinoline Alkaloids with Drug-Like Properties from the Genus *Corydalis*. *RSC Advances*, **4**(31): 15900–15913. https://doi.org/10.1039/c3ra47944g

Islam, S., Rahi, S., Koli, H. K., Jerin, I., Sajib, S. A., Hoque, K. F., & Reza, A. (2018). Evaluation of Phytochemical, Antioxidant, Cytotoxicity and *In Vitro* Antibacterial Activity of Aqueous Extract of *Ganoderma lucidum* Cultivated in Bangladeshi Habitat. *Malaya Journal of Biosciences*, **5**(1): 1–13. https://www.researchgate.net/profile/Salek-Ahmed-Sajib/publication/326625574_Evaluation_of_phytochemical_antioxidant_cytotoxicity_and_in_vitro_antibacterial_activity_of_aqueous_extract_of_Ganoderma_lucidum_cultivated_in_Bangladeshi_habitat/links/5b599f150f7e9bc79a65e4e3/Evaluation-of-phytochemical-antioxidant-cytotoxicity-and-in-vitro-antibacterial-activity-of-aqueous-extract-of-Ganoderma-lucidum-cultivated-in-Bangladeshi-

habitat.pdf

Jahan, A., Shams, S., Ali, S., Samrana, S., Ali, A., Adhikari, A., Sajid, M., Ali, A., & Ali, H. (2021). Govaniadine Ameliorates Oxidative Stress, Inflammation, and Kupffer Cell Activation in Carbon Tetrachloride-Induced Hepatotoxicity in Rats. *ACS Omega*, **6**(4): 2462–2472. https://doi.org/10.1021/acsomega.0c02261

Jeong, E. K., Lee, S. Y., Yu, S. M., Park, N. H., Lee, H. S., Yim, Y. H., Hwang, G. S., Cheong, C., Jung, J. H., & Hong, J. (2012). Identification of Structurally Diverse Alkaloids in *Corydalis* Species by Liquid Chromatography/Electrospray Ionization Tandem Mass Spectrometry. *Rapid Communications in Mass Spectrometry*, **26**(15): 1661–1674. https://doi.org/10.1002/rcm.6272

Jha, R. N., Pandey, M. B., Singh, A. K., Singh, S., & Singh, V. P. (2009). New Alkaloids from *Corydalis* Species. *Natural Product Research*, **23**(3): 250–255. https://doi.org/10.1080/14786410801996390

Jing, L., Ma, H., Fan, P., Gao, R., & Jia, Z. (2015). Antioxidant Potential, Total Phenolic and Total Flavonoid Contents of *Rhododendron anthopogonoides* and its Protective Effect on Hypoxia-Induced Injury in PC12 Cells. *BMC Complementary and Alternative Medicine*, **15**(1): 1–12. https://doi.org/10.1186/s12906-015-0820-3

Karas, M., & Hillenkamp, F. (1988). Laser Desorption Ionization of Proteins with Molecular Masses Exceeding 10,000 Daltons. *Analytical Chemistry*, **60**(20): 2299–2301. https://doi.org/10.1021/ac00171a028

Kayani, S., Ahmad, M., Sultana, S., Khan Shinwari, Z., Zafar, M., Yaseen, G., Hussain, M., & Bibi, T. (2015). Ethnobotany of Medicinal Plants Among the Communities of Alpine and Sub-Alpine Regions of Pakistan. *Journal of Ethnopharmacology*, **164**: 186–202. https://doi.org/10.1016/j.jep.2015.02.004

Kazeem, M. I., Ogunbiyi, J. V., & Ashafa, A. O. T. (2013). *In Vitro* Studies on the Inhibition of α-Amylase and α-Glucosidase by Leaf Extracts of *Picralima*

nitida (Stapf). *Tropical Journal of Pharmaceutical Research*, **12**(5): 719–725. https://doi.org/10.4314/tjpr.v12i5.9

Khan, L. U., Khan, R. A., Khan, S., Bano, S. A., Fasim, F., & Uzair, B. (2017). Phytochemical Screening and Assessment of Pharmacological Properties of *Swertia chirayita* (Roxb. ex Fleming) Root Methanolic Extract. *International Journal of Pharmacology*, **13**(8): 1000–1009. https://doi.org/10.3923/ijp.2017.1000.1009

Khan, S. M., Page, S., Ahmad, H., Shaheen, H., Ullah, Z., Ahmad, M., & Harper, D. M. (2013). Medicinal Flora and Ethnoecological Knowledge in the Naran Valley, Western Himalaya, Pakistan. *Journal of Ethnobiology and Ethnomedicine*, **9**(1): 1–13. https://doi.org/10.1186/1746-4269-9-4

Khodorova, N. V., Shavarda, A. L., Lequart-Pillon, M., Laberche, J. C., Voitsekhovskaja, O. V., & Boitel-Conti, M. (2013). Biosynthesis of Benzylisoquinoline Alkaloids in *Corydalis bracteata*: Compartmentation and Seasonal Dynamics. *Phytochemistry*, **92**: 60–70. https://doi.org/10.1016/j.phytochem.2013.04.008

Kinghorn, A. D., Chin, Y. W., & Swanson, S. M. (2009). Discovery of Natural Product Anticancer Agents from Biodiverse Organisms. *Current Opinion in Drug Discovery and Development*, **12**(2): 189.

Kingston, D. G. I. (2011). Modern Natural Products Drug Discovery and its Relevance to Biodiversity Conservation. *Journal of Natural Products*, **74**(3): 496–511. https://doi.org/10.1021/np100550t

Klančnik, A., Piskernik, S., Jeršek, B., & Možina, S. S. (2010). Evaluation of Diffusion and Dilution Methods to Determine the Antibacterial Activity of Plant Extracts. *Journal of Microbiological Methods*, **81**(2): 121–126. https://doi.org/10.1016/j.mimet.2010.02.004

Kong, W., Wei, J., Abidi, P., Lin, M., Inaba, S., Li, C., Wang, Y., Wang, Z., Si, S., Pan, H., Wang, S., Wu, J., Wang, Y., Li, Z., Liu, J., & Jiang, J. D. (2004). Berberine is a Novel Cholesterol-Lowering Drug Working Through a Unique Mechanism

Distinct from Statins. *Nature Medicine*, **10**(12): 1344–1351. https://doi.org/10.1038/nm1135

Kostiainen, R., Kotiaho, T., Kuuranne, T., & Auriola, S. (2003). Liquid Chromatography/Atmospheric Pressure Ionization - Mass Spectrometry in Drug Metabolism Studies. *Journal of Mass Spectrometry*, **38**(4): 357–372. https://doi.org/10.1002/jms.481

Krishnaraju, A. V, Rao, T. V. N., Sundararaju, D., Vanisree, M., Tsay, H.-S., & Subbaraju, G. V. (2005). Assessment of Bioactivity of Indian Medicinal Plants Using Brine Shrimp (*Artemia salina*) Lethality Assay. *International Journal of Applied Science and Engineering*, **3**(2): 125–134. https://doi.org/https://doi.org/10.6703/IJASE.2005.3(2).125

Kumar, D., Sharma, P., Nepali, K., Mahajan, G., Mintoo, M. J., Singh, A., Singh, G., Mondhe, D. M., Singh, G., Jain, S. K., Gupta, G. K., Ntie-Kang, F., Mintoo, M. J., Mondhe, D. M., & Ntie-Kang, F. (2018). Antitumour, Acute Toxicity and Molecular Modeling Studies of 4-(pyridin-4-yl)-6-(thiophen-2-yl)pyrimidin-2(1H)-one against *Ehrlich ascites* Carcinoma and Sarcoma-180. *Heliyon*, **4**: e00661. https://doi.org/10.1016/j.heliyon.2018

Lallianrawna, S., Muthukumaran, R., Ralte, V., Gurusubramanian, G., & Kumar, N. S. (2013). Determination of Total Phenolic Content , Total Flavonoid Content and Total Antioxidant Capacity of *Ageratina adenophora* (Spreng.) King & H. Rob. *Science Vision*, **13**(4): 149–156. https://www.sciencevision.org/storage/journal-articles/February2019/zj85MiUH3g7V2sfZqbdb.pdf

Langreth, D. C., Dion, M., Rydberg, H., Schröder, E., Hyldgaard, P., & Lundqvist, B. I. (2005). Van der Waals Density Functional Theory with Applications. *International Journal of Quantum Chemistry*, **101**(5): 599–610. https://doi.org/10.1002/qua.20315

Li, H., Dong, B., Park, S. W., Lee, H. S., Chen, W., & Liu, J. (2009). Hepatocyte Nuclear Factor 1α Plays a Critical Role in PCSK9 Gene Transcription and Regulation by the Natural Hypocholesterolemic Compound Berberine. *Journal of Biological Chemistry*, **284**(42): 28885–28895.

https://doi.org/10.1074/jbc.M109.052407

Li, H. L., Zhang, W. D., Liu, R. H., Zhang, C., Han, T., Wang, X. W., Wang, X. L., Zhu, J. B., & Chen, C. L. (2006). Simultaneous Determination of Four Active Alkaloids from a Traditional Chinese Medicine *Corydalis saxicola* Bunting. (Yanhuanglian) in Plasma and Urine Samples by LC-MS-MS. *Journal of Chromatography B*, **831**: 140–146. https://doi.org/10.1016/j.jchromb.2005.11.049

Li, Y., Kong, D., Fu, Y., Sussman, M. R., & Wu, H. (2020). The Effect of Developmental and Environmental Factors on Secondary Metabolites in Medicinal Plants. *Plant Physiology and Biochemistry*, **148**: 80–89. https://doi.org/10.1016/j.plaphy.2020.01.006

Lidén, M. (2012). *Corydalis*. Flora of Nepal. http://data.rbge.org.uk/publications/FloraofNepal/library/Fumariaceae/1

Liu, B., Guo, Z. Y., Bussmann, R., Li, F. F., Li, J. Q., Hong, L. Y., & Long, C. L. (2016). Ethnobotanical Approaches of Traditional Medicine Studies in Southwest China: A Literature Review. *Journal of Ethnopharmacology*, **186**: 343–350. https://doi.org/10.1016/j.jep.2016.02.040

Liu, X., Zheng, H., Lu, R., Huang, H., Zhu, H., Yin, C., Mo, Y., Wu, J., Liu, X., Deng, M., Li, D., Cheng, B., Wu, F., Liang, Y., Guo, H., Song, H., & Su, Z. (2019). Intervening Effects of Total Alkaloids of *Corydalis saxicola* Bunting on Rats with Antibiotic-Induced Gut Microbiota Dysbiosis Based on 16s RRNA Gene Sequencing and Untargeted Metabolomics Analyses. *Frontiers in Microbiology*, **10**: 1–18. https://doi.org/10.3389/fmicb.2019.01151

Lorke, D. (1983). A New Approach to Practical Acute Toxicity Testing. *Archives of Toxicology*, **54**(4): 275–287. https://doi.org/10.1007/BF01234480

Luo, J. Z., Li, M. S., Song, X. X., Fang, Y. L., Mo, H. N., Jiang, J. C., Zhao, H. Y., & Wang, H. S. (2022). New Alkaloids and Their *In Vitro* Antitumor Activity of *Corydalis balansae*. *Fitoterapia*, **162**: 105289. https://doi.org/10.1016/j.fitote.2022.105289

Luo, T., Li, Z., Deng, X. M., Jiang, K., Liu, D., Zhang, H. H., Shi, T., Liu, L. Y., Wen, H. X., Li, Q. E., & Wang, Z. (2022). Isolation, Synthesis and Bioactivity Evaluation of Isoquinoline Alkaloids from *Corydalis Hendersonii* Hemsl. against Gastric Cancer *In Vitro* and *In Vivo*. *Bioorganic and Medicinal Chemistry*, **60**: 116705. https://doi.org/10.1016/j.bmc.2022.116705

Lupo, M. G., Macchi, C., Marchianò, S., Cristofani, R., Greco, M. F., Dall'Acqua, S., Chen, H., Sirtori, C. R., Corsini, A., Ruscica, M., & Ferri, N. (2019). Differential Effects of Red Yeast Rice, *Berberis aristata* and *Morus alba* Extracts on PCSK9 and LDL Uptake. *Nutrition, Metabolism and Cardiovascular Diseases*, **29**(11): 1245–1253. https://doi.org/10.1016/j.numecd.2019.06.001

Ma, Z. Z., Xu, W., Jensen, N. H., Roth, B. L., Liu-Chen, L. Y., & Lee, D. Y. W. (2008). Isoquinoline Aalkaloids Isolated from *Corydalis yanhusuo* and Their Binding Affinities at the Dopamine D1 Receptor. *Molecules*, **13**(9): 2303–2312. https://doi.org/10.3390/molecules13092303

Maharjan, B., Payne, D. T., Ferrarese, I., Lupo, M. G., Shrestha, L. K., Hill, J. P., Ariga, K., Rossi, I., Shrestha, S. S., Panighel, G., Shrestha, R. L. S., Sut, S., Ferri, N., & Dall'Acqua, S. (2022). Evaluation of the Effects of Natural Isoquinoline Alkaloids on Low Density Lipoprotein Receptor (LDLR) and Proprotein Convertase Subtilisin/Kexin Type 9 (PCSK9) in Hepatocytes, as New Potential Hypocholesterolemic Agents. *Bioorganic Chemistry*, **121**(February): 105686. https://doi.org/10.1016/j.bioorg.2022.105686

Majak, W., Bai, Y., & Benn, M. H. (2003). Phenolic Amides and Isoquinoline Alkaloids from *Corydalis sempervirens*. *Biochemical Systematics and Ecology*, **31**(6): 649–651. https://doi.org/10.1016/S0305-1978(02)00225-9

Manandhar, N. P. (1993). Ethnobotanical Note on Folk-Lore Remedies of Baglung District, Nepal. *Contributions to Nepalese Studies Journal*, **20**(2): 184–196.

Manandhar, S., Luitel, S., & Dahal, R. K. (2019). *In vitro* Antimicrobial Activity of Some Medicinal Plants against Human Pathogenic Bacteria. *Journal of Tropical Medicine*, **2019**(1): 1895340. https://doi.org/10.1155/2019/1895340

Manske, R. H. F. (1933). The Alkaloids of Fumaraceous Plants: III. A New Alkaloid, Bicuculline, and its Constitution. *Canadian Journal of Research*, **8**(2): 142–146. https://doi.org/10.1139/cjr33-015

Manske, R. H. F., Rodrigo, R. G. A., Maclean, D. B., Gracey, D. E. F., & Saunders, J. K. (1969). The Structure of Ochrobirine. *Canadian Journal of Chemistry*, **47**(19): 3589–3592. https://doi.org/10.22323/1.040.0029

Marques, L. M. M., Behrens, M., Kalinina, S., Rottkord, U., Adhikari, A., (S) Shrestha, R. L., Humpf, H. U., & Lopes, N. P. (2020). Govaniadine Evaluation of Cytotoxicity and Permeability in Cell Culture. *Revista Brasileira de Farmacognosia*, **30**(3): 374–380. https://doi.org/10.1007/s43450-020-00066-w

Marques, L. M. M., Callejon, D. R., Pinto, L. G., de Campos, M. L., de Oliveira, A. R. M., Vessecchi, R., Adhikari, A., Shrestha, R. L. S., Peccinini, R. G., & Lopes, N. P. (2016). Pharmacokinetic Properties, *In Vitro* Metabolism and Plasma Protein Binding of Govaniadine an Alkaloid Isolated from *Corydalis govaniana* Wall. *Journal of Pharmaceutical and Biomedical Analysis*, **131**: 464–472. https://doi.org/10.1016/j.jpba.2016.09.003

McCue, P. P., & Shetty, K. (2004). Inhibitory Effects of Rosmarinic Acid Extracts on Porcine Pancreatic Amylase *In Vitro*. *Asia Pacific Journal of Clinical Nutrition*, **13**(1): 101–106. https://apjcn.nhri.org.tw/server/APJCN/13/1/101. pdf?utm_ medium=email&utm_source=transaction

Mensor, L. L., Menezes, F. S., Leitao, G. G., Reis, A. S., dos Santos, T. C., Coube, C. S., & Leitao, S. G. (2001). Screening of Brazilian Plant Extracts for Antioxidant Activity by the Use of DPPH Free Radical Method. *Phytotherapy Research*, **15**: 127–130. https://doi.org/10.1002/ptr.687

Meyer, B. N., Ferrigni, N. R., Putnam, J. E., Jacobsen, L. B., Nichols, D. E., & McLaughlin, J. L. (1982). Brine shrimp: A Convenient General Bioassay for Active Plant Constituents. *Planta Medica*, **45**(1): 31–34. https://doi.org/10.1055/s-2007-971236

Miean, K. H., & Mohamed, S. (2001). Flavonoid (Myricetin, Quercetin, Kaempferol,

Luteolin, and Apigenin) Content of Edible Tropical Plants. *Journal of Agricultural and Food Chemistry*, **49**(6): 3106–3112. https://doi.org/10.1021/jf000892m

Mo, J., Guo, Y., Yang, Y.-S., Shen, J.-S., Jin, G.-Z., & Zhen, X. (2007). Recent Developments in Studies of L-Stepholidine and its Analogs: Chemistry, Pharmacology and Clinical Implications. *Current Medicinal Chemistry*, **14**(28): 2996–3002. https://doi.org/10.2174/092986707782794050

Muhammad, N., Shrestha, R. L., Adhikari, A., Wadood, A., Khan, H., Khan, A. Z., Maione, F., Mascolo, N., & De Feo, V. (2015). First Evidence of the Analgesic Activity of Govaniadine, an Alkaloid Isolated from *Corydalis govaniana* Wall. *Natural Product Research*, **29**(5): 430–437. https://doi.org/10.1080/14786419.2014.951933

Mukhopadhyay, S., Banerjee, S. K., Atal, C. K., Lin, L.-J., & Cordell, G. A. (1987). Alkaloids of *Corydalis govaniana*. *Journal of Natural Products*, **50**(2): 270–272. https://doi.org/10.1021/np50050a033

Mustafa, A., & Turner, C. (2011). Pressurized Liquid Extraction as a Green Approach in Food and Herbal Plants Extraction: A Review. *Analytica Chimica Acta*, **703**(1): 8–18. https://doi.org/10.1016/j.aca.2011.07.018

Ncube, N. S., Afolayan, A. J., & Okoh, A. I. (2008). Assessment Techniques of Antimicrobial Properties of Natural Compounds of Plant Origin: Current Methods and Future Trends. *African Journal of Biotechnology*, **7**(12): 1797–1806. https://doi.org/10.5897/AJB07.613

Newman, D. J., & Cragg, G. M. (2009). Microbial Antitumor Drugs: Natural Products of Microbial Origin as Anticancer Agents. *Current Opinion in Investigational Drugs*, **10**(12): 1280–1296. https://europepmc.org/article/med/19943200

Newman, D. J., & Cragg, G. M. (2016). Natural Products as Sources of New Drugs from 1981 to 2014. *Journal of Natural Products*, **79**(3): 629–661. https://doi.org/10.1021/acs.jnatprod.5b01055

Newman, D. J., & Cragg, G. M. (2020). Natural Products as Sources of New Drugs

over the Nearly Four Decades from 01/1981 to 09/2019. *Journal of Natural Products*, **83**(3): 770–803. https://doi.org/10.1021/acs.jnatprod.9b01285

Nisar, M., Shah, H., Khan, I., Fazal-Ur-Rehman, Khan, M. S., Marwat, S. K., Niazi, Z. R., & Ullah, A. (2013). Antimicrobial Potential and Phytochemical Investigation of Fixed Oil of Plant *Chenopodium ambrosioides* Linn. *Asian Journal of Chemistry*, **25**(2): 1069–1072. https://doi.org/10.14233/ajchem.2013.13439

OECD. (2022). Test guideline 425: Acute Oral Toxicity - Up-And-Down Procedure. *Guideline for Testing of Chemicals*, *December*, 26. http://www.oecd.org/termsandconditions/

Oksana, S., Marian, B., Mahendra, R., & Bo, S. H. (2012). Plant Phenolic Compounds for Food, Pharmaceutical and Cosmetics Production. *Journal of Medicinal Plants Research*, **6**(13): 2526–2539. https://doi.org/10.5897/jmpr11.1695

Olofinsan, K., Abrahamse, H., & George, B. P. (2023). Therapeutic Role of Alkaloids and Alkaloid Derivatives in Cancer Management. *Molecules,* **28**(14): 5578. https://doi.org/10.3390/molecules28145578

Olowa, L. F., & Nuñeza, O. M. (2013). Brine Shrimp Lethality Assay of the Ethanolic Extracts of Three Selected Species of Medicinal Plants from Iligan City, Philippines. *International Research Journal of Biological Sciences*, **2**(11): 74–77. https://www.isca.me/IJBS/Archive/v2/i11/12.ISCA-IRJBS-2013-177.pdf

Olson, H., Betton, G., Robinson, D., Thomas, K., Monro, A., Kolaja, G., Lilly, P., Sanders, J., Sipes, G., Bracken, W., Dorato, M., Van Deun, K., Smith, P., Berger, B., & Heller, A. (2000). Concordance of the Toxicity of Pharmaceuticals in Humans and in Animals. *Regulatory Toxicology and Pharmacology*, **32**(1): 56–67. https://doi.org/10.1006/rtph.2000.1399

Pandey, V. B., Ray, A. B., & Dasgupta, B. (1979). Minor Alkaloids of *Fumaria indica* Seeds. *Phytochemistry*, **18**(4): 695–696. https://doi.org/10.1016/S0031-9422(00)84306-X

Pant, P., Pandey, S., & Dall'Acqua, S. (2021). The Influence of Environmental

Conditions on Secondary Metabolites in Medicinal Plants: A Literature Review. *Chemistry and Biodiversity*, **18**(11): e2100345. https://doi.org/10.1002/cbdv.202100345

Parasuraman, S., Raveendran, R., & Kesavan, R. (2010). Blood Sample Collection in Small Laboratory Animals. *Journal of Pharmacology and Pharmacotherapeutics*, **1**(2): 87–93. https://doi.org/10.4103/0976-500X.72350

Parekh, J., & Chanda, S. (2010). Antibacterial and Phytochemical Studies on Twelve Species of Indian Medicinal Plants. *African Journal of Biomedical Research*, **10**(2): 175–181. https://doi.org/10.4314/ajbr.v10i2.50624

Phuyal, N., Jha, P. K., Raturi, P. P., & Rajbhandary, S. (2020). Total Phenolic, Flavonoid Contents, and Antioxidant Activities of Fruit, Seed, and Bark Extracts of *Zanthoxylum armatum* DC. *The Scientific World Journal*, **2020**: 1–7. https://doi.org/10.1155/2020/8780704

Pirillo, A., & Catapano, A. L. (2015). Berberine, a Plant Alkaloid with Lipid-and Glucose-Lowering Properties: From *In Vitro* Evidence to Clinical Studies. *Atherosclerosis*, **243**(2): 449–461. https://doi.org/10.1016/j.atherosclerosis.2015.09.032

Popova, M. E., Boeva, A. N., & Dolejs, L. (1980). Isolation and Chemistry of Alkaloids from Plants of the Papaveraceae. LXXIX. Alkaloids from *Fumaria schrammii*. *Planta Medica*, **40**(2): 156–160. https://doi.org/10.1055/s-2008-1074952

Prior, R. L., Wu, X., & Schaich, K. (2005). Standardized Methods for the Determination of Antioxidant Capacity and Phenolics in Foods and Dietary Supplements. *Journal of Agricultural and Food Chemistry*, **53**(10): 4290–4302. https://doi.org/10.1021/jf0502698

Ramakrishna, A., & Ravishankar, G. A. (2011). Influence of Abiotic Stress Signals on Secondary Metabolites in Plants. *Plant Signaling and Behavior*, **6**(11): 1720–1731. https://doi.org/10.4161/psb.6.11.17613

Ranjitkar, R., Bhandari, D. P., & Bhandari, L. (2019). Acute Toxicity Test of Ten Commercial Essential Oils of Nepalese Origin. *Journal of Plant Resources*,

17(1): 82–85. http://dpr.gov.np/wp-content/uploads/2020/07/10.-Acute-Toxicity-Test-of-Ten-Commercial-Essential-Oils.pdf

Re, R., Pellegrini, N., Proteggente, A., Pannala, A., Yang, M., & Rice-Evans, C. (1999). Antioxidant Activity Applying an Improved ABTS Radical Cation Decolorization Assay. *Free Radical Biology and Medicine*, **26**(9–10): 1231–1237. https://doi.org/10.1016/S0891-5849(98)00315-3

Reynolds, T., & Sofowora, A. (1984). Medicinal Plants and Traditional Medicine in Africa. *Kew Bulletin*, **39**(3): 667–668. https://doi.org/10.2307/4108615

Rice-Evans, C. A., Miller, N. J., & Paganga, G. (1997). Antioxidant Properties of Phenolic Compounds. *Trends in Plant Science*, **2**(4): 152–159. https://doi.org/10.1016/S1360-1385(97)01018-2

Richard, S. W., Marius, L., Noya, S., Pierre, G. I., & Germaine, N. O. O. (2011). Anti-inflammatory, analgesic and antipyretic effects of Lepidagathis anobrya Nees (Acanthaceae). *African Journal of Traditional, Complementary and Alternative Medicines*, **8**(4): https://doi.org/10.4314/ajtcam.v8i4.12

Ríos, J. L., & Recio, M. C. (2005). Medicinal Plants and Antimicrobial Activity. *Journal of Ethnopharmacology*, **100**(1–2): 80–84. https://doi.org/ 10.1016/J.JEP.2005.04.025

Sahebkar, A., Serban, M. C., Gluba-Brzózka, A., Mikhailidis, D. P., Cicero, A. F., Rysz, J., & Banach, M. (2016). Lipid-Modifying Effects of Nutraceuticals: An Evidence-Based Approach. *Nutrition*, **32**(11–12): 1179–1192. https://doi.org/10.1016/j.nut.2016.04.007

Sahni, S., Maurya, S., Jha, R. N., Pandey, V. B., & Singh, U. P. (2004). Inhibitory Effect of Two Alkaloids, (-)-Corydalmine and (-)-Isocorypalmine Isolated from *Corydalis chaerophylla* on Several Phytopathogenic Fungi. *Mycobiology*, **32**(4): 160. https://doi.org/10.4489/myco.2004.32.4.160

Sangster, A. W., & Stuart, K. L. (1965). Ultraviolet Spectra of Alkaloids. *Chemical Reviews*, **65**(1): 69–130. https://doi.org/10.1021/cr60233a003

Sarah, Q. S., Anny, F. C., & Misbahuddin, M. (2017). Brine Shrimp Lethality Assay. *Bangladesh Journal of Pharmacology*, **12**(2): 186–189. https://doi.org/10.3329/bjp.v12i2.32796

Scazzocchio, F., Cometa, M. F., Tomassini, L., & Palmery, M. (2001). Antibacterial Activity of *Hydrastis canadensis* Extract and its Major Isolated Alkaloids. *Planta Medica*, **67**(6): 561–564. https://doi.org/10.1055/s-2001-16493

Schmeller, T., Latz-Brüning, B., & Wink, M. (1997). Biochemical Activities of Berberine, Palmatine and Sanguinarine Mediating Chemical Defence Against Microorganisms and Herbivores. *Phytochemistry*, **44**(2): 257–266. https://doi.org/10.1016/S0031-9422(96)00545-6

Seger, C., Sturm, S., Strasser, E. M., Ellmerer, E., & Stuppner, H. (2004). ^{1}H and ^{13}C NMR Signal Assignment of Benzylisoquinoline Alkaloids from *Fumaria officinalis* L. (Papaveraceae). *Magnetic Resonance in Chemistry*, **42**(10): 882–886. https://doi.org/10.1002/mrc.1417

Sener, B., & Temizer, H. (1991). Chemical Studies on the Minor Isoquinoline Alkaloids from *Corydalis solida* subsp. Brachyloba. *Journal of the Chemical Society of Pakistan*, **13**(1): 63–66.

Shaheen, H., Shinwari, Z. K., Qureshi, R. A., & Ullah, Z. (2012). Indigenous Plant Resources and Their Utilization Practices in Village Populations of Kashmir Himalayas. *Pakistan Journal of Botany*, **44**(2): 739–745. http://www.pakbs.org/pjbot/PDFs/44(2)/41.pdf

Shamma, M., Moniot, J. L., Manske, R. H. F., Chan, W. K., & Nakanishi, K. (1972). Absolute Configuration of Some Spirobenzylisoquinoline Alkaloids. *Journal of the Chemical Society, Chemical Communications*, **6**: 310–311. https://doi.org/https://doi.org/10.1039/C39720000310

Sharma, V., Agarwal, A., Chaudhary, U., & Singh, M. (2013). Phytochemical Investigation of Various Extracts of Leaves and Stems of *Achyranthes aspera* Linn. *International Journal of Pharmacy and Pharmaceutical Sciences*, **5**(1): 317–320.

Shilpha, J., Satish, L., & Ramesh, M. (2018). Recent advancements in the clinical evaluation of plant-derived anticancer compounds. *Anticancer Plants: Clinical Trials and Nanotechnology,* **3**: 233–252. https://doi.org/10.1007/978-981-10-8216-0_8

Shim, H. J., Lee, J. Y., Kim, B., & Hong, J. (2013). General Fragmentations of Alkaloids in Electrospray Ionization Tandem Mass Spectrometry. *Mass Spectrometry Letters*, **4**(4): 79–82. https://doi.org/10.5478/MSL.2013.4.4.79

Shrestha, R. L., & Adhikari, A. (2017a). Anti-leshmanial Constituents from *Corydalis govaniana* Wall. *European Journal of Biotechnology and Bioscience*, **5**(5): 47–48.

Shrestha, R. L., & Adhikari, A. (2017b). Anti-oxidant Constituents from *Corydalis govaniana* Wall and *C. casimiriana* Duthie and Prain ex Prain. *Journal of Pharmacognosy and Phytochemistry*, **6**(5): 568–570.

Shrestha, R. L., & Adhikari, A. (2017c). β-Glucuronidase Inhibiting Constituents from *C. casimiriana* Duthie and Prain ex Prain and *Corydalis govaniana* Wall. *International Journal of Chemical Studies*, **5**(5): 700–701.

Shrestha, R. L., Adhikari, A., Marasini, B. P., Jha, R. N., & Choudhary, M. I. (2013). Novel Inhibitors of Urease from *Corydalis govaniana* Wall. *Phytochemistry Letters*, **6**(2): 228–231. https://doi.org/10.1016/j.phytol.2013.02.002

Shukla, R., Singh, A., & Singh, K. K. (2024). Vincristine-based nanoformulations: a preclinical and clinical studies overview. *Drug Delivery and Translational Research,* **14**(1). https://doi.org/10.1007/s13346-023-01389-6

Simoes-Pires, C., Hostettmann, K., Haouala, A., Cuendet, M., Falquet, J., Graz, B., & Christen, P. (2014). Reverse Pharmacology for Developing an Anti-Malarial Phytomedicine. The Example of *Argemone mexicana*. *International Journal for Parasitology: Drugs and Drug Resistance*, **4**(3): 338–346. https://doi.org/10.1016/j.ijpddr.2014.07.001

Singh, S., Youssouf, M., Malik, Z. A., & Bussmann, R. W. (2017). Sacred Groves: Myths, Beliefs, and Biodiversity Conservation - A Case Study from Western

Himalaya, India. *International Journal of Ecology*, **2017**: 1–12. https://doi.org/10.1155/2017/3828609

Singleton, V. L., Orthofer, R., & Lamuela-Raventós, R. M. (1999). Analysis of Total Phenols and Other Oxidation Substrates and Antioxidants by Means of Folin-Ciocalteu Reagent. *Oxidants and Antioxidants*, **299**: 152–178. https://doi.org/10.1016/j.scienta.2016.11.004

Sivakumaran, N., Samarakoon, S. R., Adhikari, A., Ediriweera, M. K., Tennekoon, K. H., Malavige, N., Thabrew, I., & Shrestha, R. L. S. (2018). Cytotoxic and Apoptotic Effects of Govaniadine Isolated from *Corydalis govaniana* Wall. Roots on Human Breast Cancer (MCF-7) Cells. *BioMed Research International*, **2018**. https://doi.org/10.1155/2018/3171348

Skehan, P., Storeng, R., Scudiero, D., Monks, A., Mcmahon, J., Vistica, D., Warren, J. T., Bokesch, H., Kenney, S., & Boyd, M. R. (1990). New Colorimetric Cytotoxicity Assay for Anticancer-Drug Screening. *Journal of the National Cancer Institute*, **82**(13): 1107–1112. https://doi.org/10.1093/jnci/82.13.1107

Snyder, L. R., Kirkland, J. J., & Dolan, J. W. (2010). Introduction to Modern Liquid Chromatography. *Wiley Online Library*. Wiley. https://doi.org/ 10.1002/9780470508183

Stroes, E. S., Thompson, P. D., Corsini, A., Vladutiu, G. D., Raal, F. J., Ray, K. K., Roden, M., Stein, E., Tokgözoɬlu, L., Nordestgaard, B. G., Bruckert, E., De Backer, G., Krauss, R. M., Laufs, U., Santos, R. D., Hegele, R. A., Hovingh, G. K., Leiter, L. A., Mach, F., … Ginsberg, H. N. (2015). Statin-Associated Muscle Symptoms: Impact on Statin Therapy - European Atherosclerosis Society Consensus Panel Statement on Assessment, Aetiology and Management. *European Heart Journal*, **36**(17): 1012–1022. https://doi.org/10.1093/ eurheartj/ehv043

Suffness, M., & Pezzuto, J. M. (1990). Assays Related to Cancer Drug Discovery. *Methods in Plant Biochemistry:Assays for Bioactivity*, **6**.

Sultana, B., Anwar, F., & Ashraf, M. (2009). Effect of Extraction Solvent/Technique

on the Antioxidant Activity of Selected Medicinal Plant Extracts. *Molecules*, **14**(6): 2167–2180. https://doi.org/10.3390/molecules14062167

Sun, L., Wang, Y., & Miao, M. (2020). Inhibition of α-Amylase by Polyphenolic Compounds: Substrate Digestion, Binding Interactions and Nutritional Intervention. *Trends in Food Science and Technology*, **104**: 190–207. https://doi.org/10.1016/j.tifs.2020.08.003

Sun, M., Liu, J., Lin, C., Miao, L., & Lin, L. (2014). Alkaloid Profiling of the Traditional Chinese Medicine *Rhizoma Corydalis* using High Performance Liquid Chromatography-Tandem Quadrupole Time-of-Flight Mass Spectrometry. *Acta Pharmaceutica Sinica B*, **4**(3): 208–216. https://doi.org/10.1016/j.apsb.2014.04.003

Sun, N., Lu, G., Yuan, B., & Yuan, B. (2006). Research Advances in *Corydalis thalictrifolia* Franch. *Traditional Chinese Drug Research and Clinical Pharmacology*, **17**: 78–80.

Suneka, S., & Manoranjan, T. (2021). Brine Shrimp Lethality Assay with Selected Medicinal Plants Extracts. *Vingnanam Journal of Science*, **16**(2): 14–17. https://doi.org/10.4038/vingnanam.v16i2.4201

Tian, B., Tian, M., & Huang, S. M. (2020). Advances in Phytochemical and Modern Pharmacological Research of *Rhizoma Corydalis*. *Pharmaceutical Biology*, **58**(1): 265–275. https://doi.org/10.1080/13880209.2020.1741651

Tian, M., Yang, C., Yang, J., Dong, H., Liu, L., Ren, Y., & Wang, Z. (2019). Ultrahigh Performance Liquid Chromatography–Electrospray Ionization Tandem Mass Spectrometry Method for Qualitative and Quantitative Analyses of Constituents of *Corydalis bungeana* Turcz Extract. *Molecules*, **24**(19): 3463. https://doi.org/10.3390/molecules24193463

Tian, Y., Zhang, C., & Guo, M. (2017). Comparative Study on Alkaloids and Their Anti-proliferative Activities from Three *Zanthoxylum species*. *BMC Complementary and Alternative Medicine*, **17**(1): 460. https://doi.org/10.1186/s12906-017-1966-y

Toporkova, V. I., Ponkratova, A. O., Whaley, A. K., Luzhanin, V. G., & Goncharov, M. U. (2022). The Use of Spectroscopic Methods for Structural Elucidation of Individual Secondary Metabolites Isolated from the Aerial Parts of *Corydalis bracteata*. *The Bulletin of the Scientific Centre for Expert Evaluation of Medicinal Products. Regulatory Research and Medicine Evaluation*, **12**(1): 57–64. https://doi.org/10.30895/1991-2919-2022-12-1-56-64

Triska, J., Uretsky, B. F., Pitt, B., & Birnbaum, Y. (2023). Closing the Digitalis Divide: Back to the Basics of Randomized Controlled Trials. *Cardiovascular Drugs and Therapy,* **37**(4): 807–813. https://doi.org/10.1007/s10557-021-07287-8

Tuli, L., Jha, R. N., Pandey, V. B., & Singh, U. P. (2001). Antifungal Activity of Chaerophylline and Berberine Hydroxide Isolated from *Corydalis* species. *Mycobiology*, **29**(2): 100–103. https://doi.org/10.1080/12298093.2001.12015769

Tundis, R., Loizzo, M. R., & Menichini, F. (2010). Natural Products as α-Amylase and α-Glucosidase Inhibitors and Their Hypoglycaemic Potential in the Treatment of Diabetes: An Update. *Mini-Reviews in Medicinal Chemistry*, **10**(4): 315–331. https://doi.org/10.2174/138955710791331007

Ur-Rahman, I., Sher, H., & Bussmann, R. W. (2019). Reference Guide on High Value Medicinal and Aromatic Plants–Sustainable Management and Cultivation Practices. *University of Swat, Pakistan*.

Vichai, V., & Kirtikara, K. (2006). Sulforhodamine B Colorimetric Assay for Cytotoxicity Screening. *Nature Protocols*, **1**(3): 1112–1116. https://doi.org/10.1038/nprot.2006.179

Virginia, D. M., Shegokar, R., & Pathak, Y. (2023). Malaria-Current Treatment Options. *Malarial Drug Delivery Systems: Advances in Treatment of Infectious Diseases,* **2023**: 71–89. https://doi.org/10.1007/978-3-031-15848-3_4

Wagner, H., & Bladt, S. (1996). Plant Drug Analysis, A Thin Layer Chromatography Atlas Second edition. *Springer*.

Wagner, H., & Ulrich-Merzenich, G. (2009). Synergy Research: Approaching a New

Generation of Phytopharmaceuticals. *Phytomedicine*, **16**(2–3): 97–110. https://doi.org/10.1016/j.phymed.2008.12.018

Waksmundzka-Hajnos, M., Sherma, J., & Kowalska, T. (2008). Thin Layer Chromatography in Phytochemistry. *Taylor & Francis eBooks*. https://doi.org/10.1201/9781420046786

Wang, J. B., & Mantsch, J. R. (2012). L-Tetrahydropalamatine: A Potential New Medication for the Treatment of Cocaine Addiction. *Future Medicinal Chemistry*, **4**(2): 177–186. https://doi.org/10.4155/fmc.11.166

Wang, L., Xia, G., Xia, H., Wei, X., Wang, Y., & Lin, S. (2023). (+)/(−)-Yanhusamides A−C, Three Pairs of Unprecedented Benzylisoquinoline-Pyrrole Hetero-Dimeric Alkaloid Enantiomers from *Corydalis yanhusuo*. *Acta Pharmaceutica Sinica B*, **13**(2): 754–764. https://doi.org/10.1016/j.apsb.2022.10.025

Wangchuk, P., Keller, P. A., Pyne, S. G., Sastraruji, T., Taweechotipatr, M., Rattanajak, R., Tonsomboon, A., & Kamchonwongpaisan, S. (2012). Phytochemical and Biological Activity Studies of the Bhutanese Medicinal Plant *Corydalis crispa*. *Natural Product Communications*, **7**(5): 575–580. https://doi.org/10.1177/1934578x1200700507

Wangchuk, P., Keller, P. A., Pyne, S. G., Willis, A. C., & Kamchonwongpaisan, S. (2012). Antimalarial Alkaloids from a Bhutanese Traditional Medicinal Plant *Corydalis dubia*. *Journal of Ethnopharmacology*, **143**(1): 310–313. https://doi.org/10.1016/j.jep.2012.06.037

Wei, X., Shen, H., Wang, L., Meng, Q., & Liu, W. (2016). Analyses of Total Alkaloid Extract of *Corydalis yanhusuo* by Comprehensive RP × RP Liquid Chromatography with pH Difference. *Journal of Analytical Methods in Chemistry*, **2016**: 1–8. https://doi.org/10.1155/2016/9752735

Welz, A., Koba, M., Kośliński, P., & Siódmiak, J. (2022). Comparison of LC-MS and LC-DAD Methods of Detecting Abused Piperazine Designer Drugs. *Journal of Clinical Medicine*, **11**(7): 1758. https://doi.org/10.3390/jcm11071758

Wikipedia contributors. (2024). Papaveraceae. *Wikipedia, the free encyclopedia*.

https://en.wikipedia.org/wiki/Papaveraceae

Wojdyło, A., Oszmiański, J., & Czemerys, R. (2007). Antioxidant Activity and Phenolic Compounds in 32 Selected Herbs. *Food Chemistry*, **105**(3): 940–949. https://doi.org/10.1016/j.foodchem.2007.04.038

Wu, J.-N. (2005). *An Illustrated Chinese Materia Medica (Vol. 59).* Oxford University Press.

Yamashita, M., & Fenn, J. B. (1984). Electrospray Ion Source. Another Variation on the Free-Jet Theme. *Journal of Physical Chemistry*, **88**(20): 4451–4459. https://doi.org/10.1021/j150664a002

Yashasvi, B. (2024). *Papaveraceae: Characters, Distribution and Types*. Biology Discussion. https://www.biologydiscussion.com/angiosperm/dicotyledons/papaveraceae-characters-distribution-and-types/47934

Yuan, H., Ma, Q., Ye, L., & Piao, G. (2016). The Traditional Medicine and Modern Medicine from Natural Products. *Molecules*, **21**: 559. https://doi.org/10.3390/molecules21050559

Zhang, B., Huang, R., Hua, J., Liang, H., Pan, Y., Dai, L., Liang, D., & Wang, H. (2016). Antitumor lignanamides from the Aerial Parts of *Corydalis saxicola*. *Phytomedicine*, **23**(13): 1599–1609. https://doi.org/10.1016/j.phymed.2016.09.006

Zhang, G. L., Rücker, G., Breitmaier, E., Nieger, M., Mayer, R., & Steinbeck, C. (1995). Alkaloids from *Dactylicapnos torulosa*. *Phytochemistry*, **40**(1): 299–305. https://doi.org/10.1016/0031-9422(95)00192-A

Zhang, Q. W., Lin, L. G., & Ye, W. C. (2018). Techniques for Extraction and Isolation of Natural Products : A Comprehensive Review. *Chinese Medicine*, **13**: 1–26. https://doi.org/10.1186/s13020-018-0177-x

Zheng, J., Zhao, Y., Lun, Q., Song, Y., Shi, S., Gu, X., Pan, B., Qu, C., Li, J., & Tu, P. (2017). *Corydalis edulis* Maxim. Promotes Insulin Secretion via the Activation of Protein Kinase Cs (PKCS) in Mice and Pancreatic β Cells. *Scientific Reports*,

7: 1–11. https://doi.org/10.1038/srep40454

Zimetti, F., Adorni, M. P., Ronda, N., Gatti, R., Bernini, F., & Favari, E. (2015). The Natural Compound Berberine Positively Affects Macrophage Functions Involved in Atherogenesis. *Nutrition, Metabolism and Cardiovascular Diseases*, **25**(2): 195–201. https://doi.org/10.1016/j.numecd.2014.08.004

APPENDICES

Appendix A: ^{1}H-NMR of bicuculline (**5**)

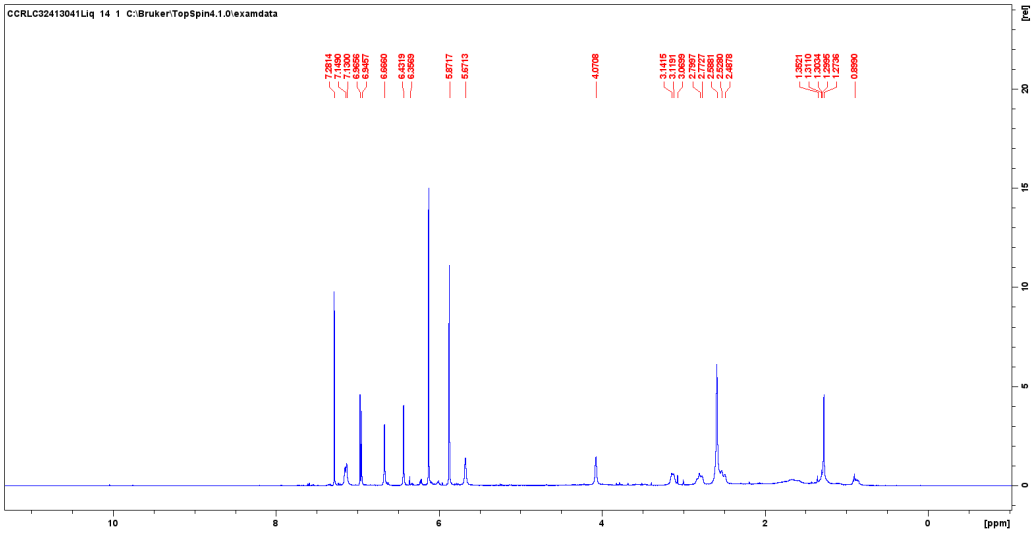

Appendix B: ^{1}H-NMR of corydalmine (**6**)

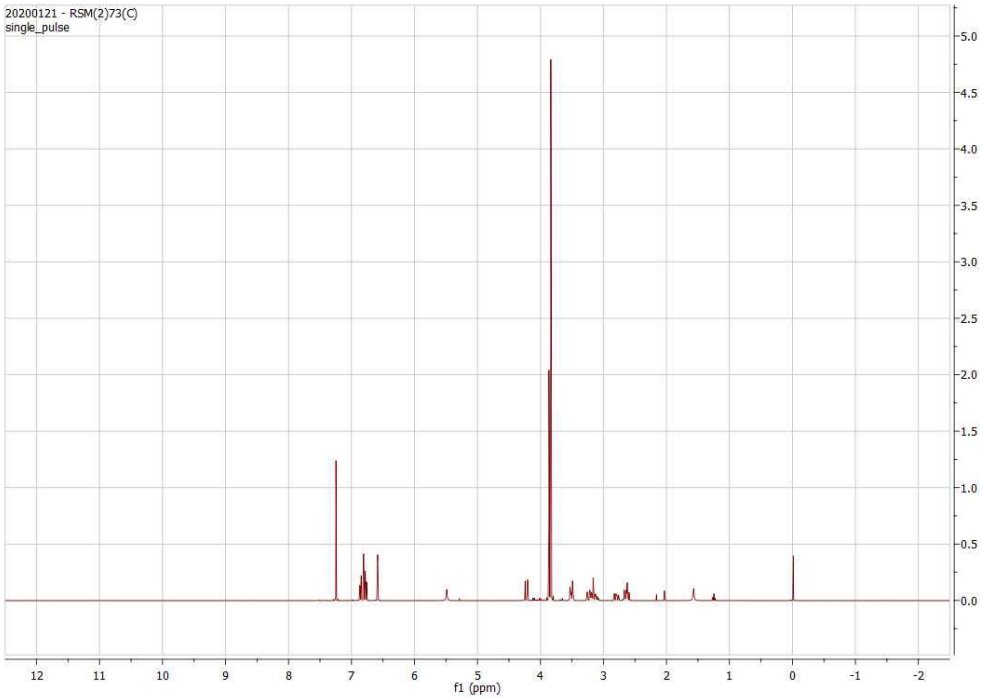

Appendix C: ^{1}H-NMR of 8-hydroxydihydrosanguinarine (**7**)

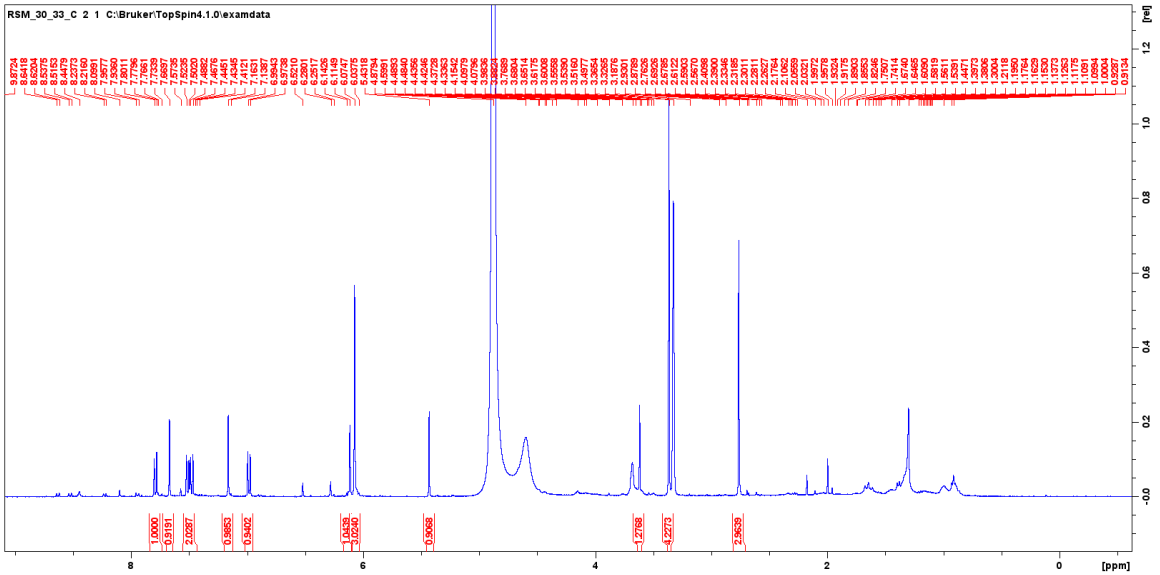

Appendix D: ^{1}H-NMR of dihydrosanguinarine (**8**)

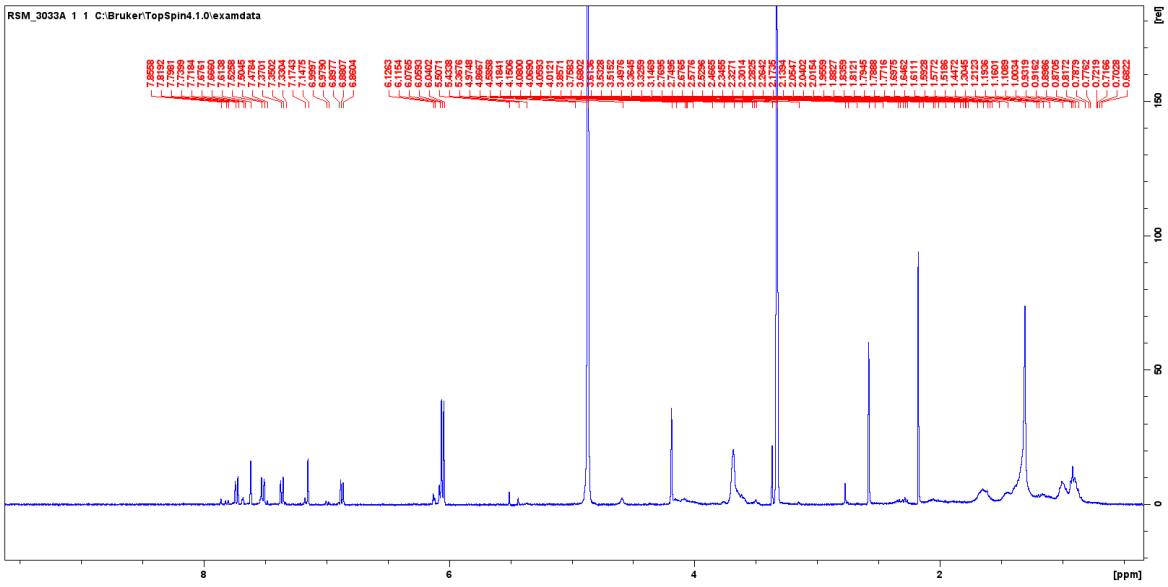

Appendix E: ^{1}H-NMR of scoulerine (**9**)

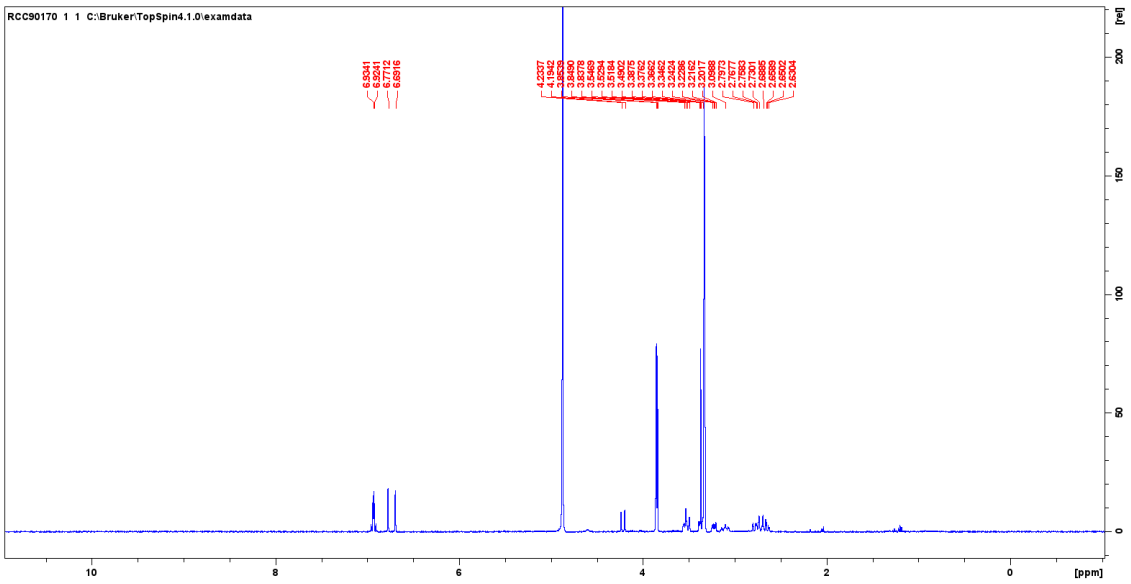

Appendix F: ^{1}H-NMR of govaniadine (**10**)

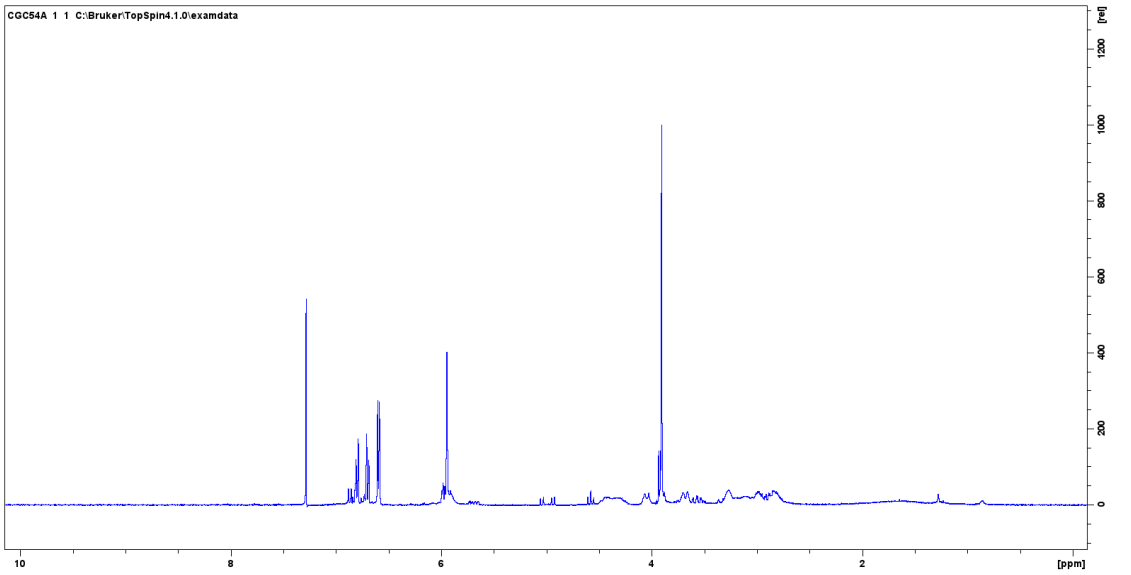

Appendix G: ^{1}H-NMR of stylopine (**11**)

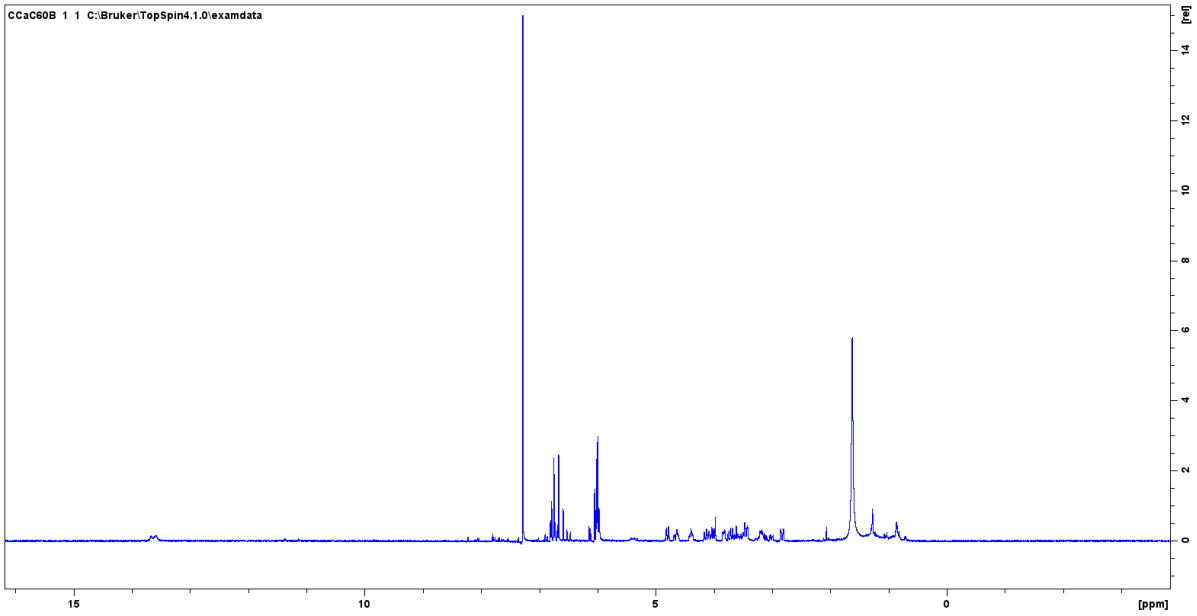

Appendix H: ^{1}H-NMR of adlumine (**12**)

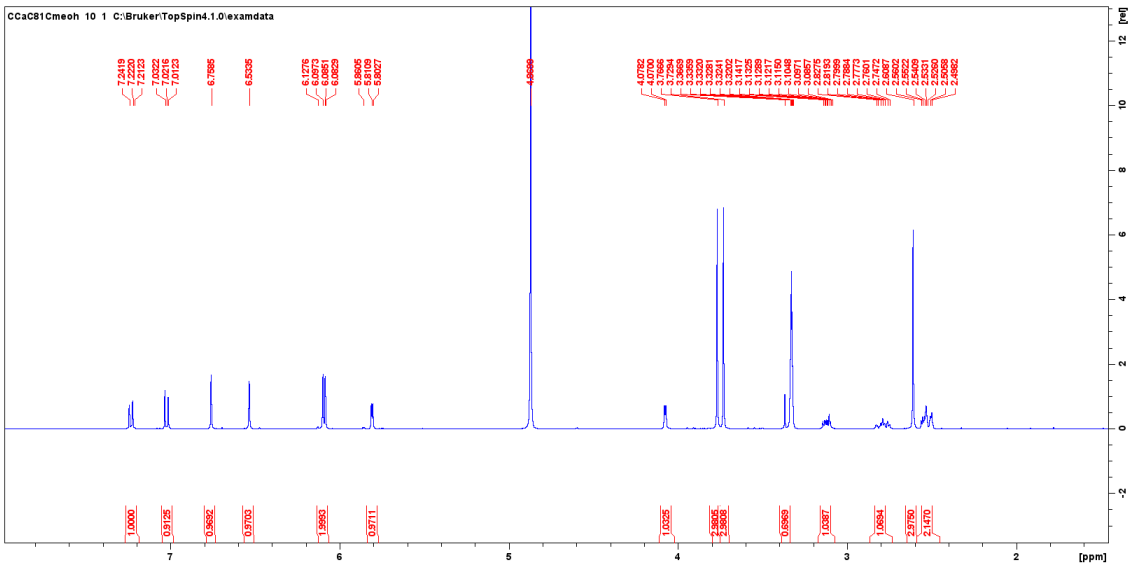

Appendix I: ^{1}H-NMR of adlumidine (**13**)

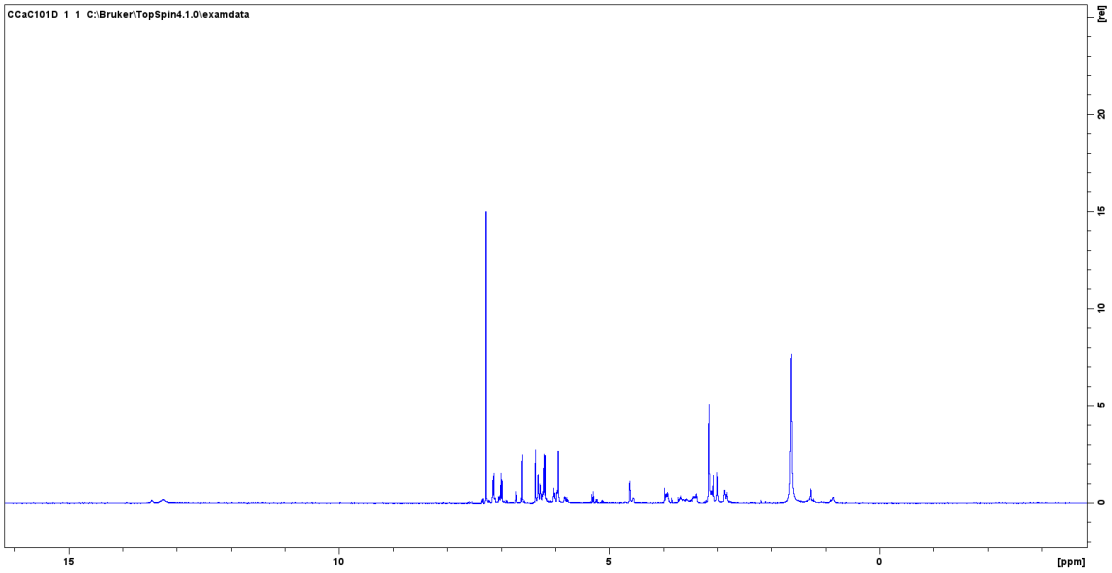

Appendix J: Antimicrobial activities of extracts of *C. chaerophylla*

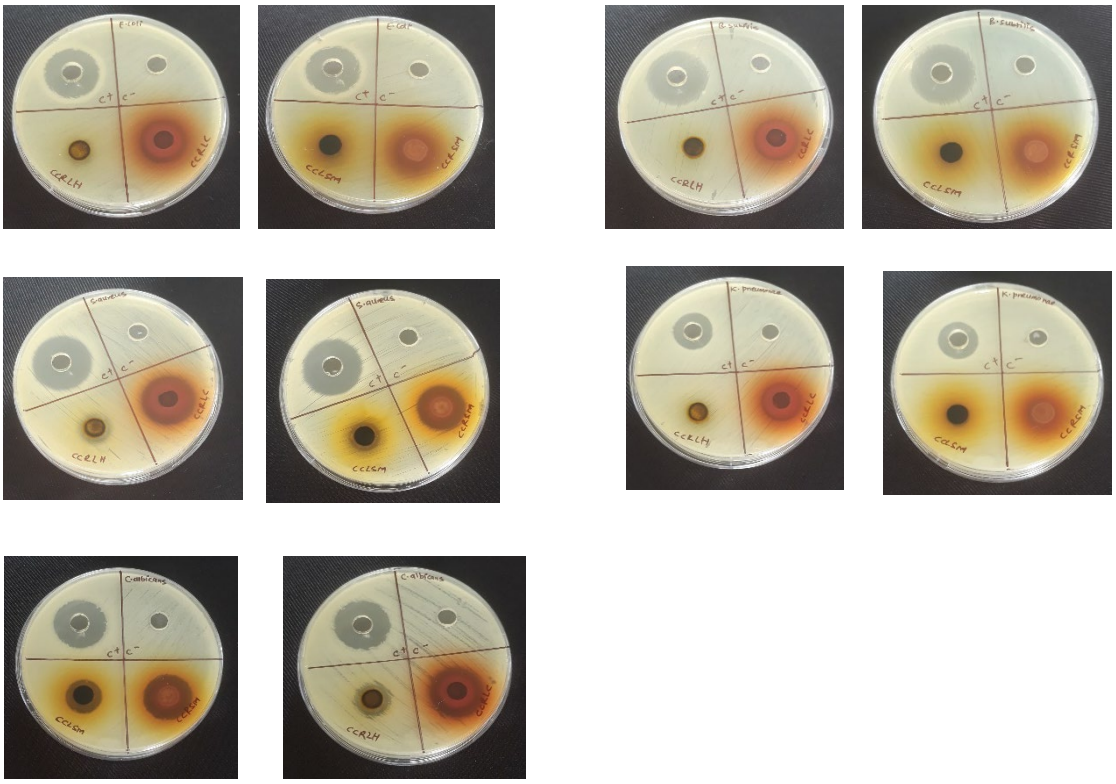

LIST OF PUBLICATIONS RESULTING FROM CURRENT STUDY

1. **Maharjan, B.,** Rossi, I., Sut, S., Shrestha, T., Shrestha, L. K., Hill, J. P., Ariga, K., Benetazzo, V., Adorni, M. P., Papotti, B., Shrestha, S. S., Shrestha, R. L. S., Ferri, N., & Dall'Acqua, S. **(2024)**. Bioactive alkaloids from Nepalese *Corydalis chaerophylla* DC acting on the regulation of PCSK9 and LDL-R *in vitro*. *Chemistry & Biodiversity*, e202401388. https://doi.org/10.1002/cbdv.202401388

2. **Maharjan, B.**, Shrestha, L. K., Hill, J. P., Ariga, K., Shrestha, S. S., Sut, S., Shrestha, R. L. S., & Dall'Acqua, S. **(2023)**. Chemical Characterization of *Corydalis chaerophylla* DC Extracts and Preliminary Evaluation of Their *in vitro* and *in vivo* Biological Properties. *Chemistry & Biodiversity*, **20(12)**, e202301209. https://doi.org/10.1002/cbdv.202301209

3. **Maharjan, B.**, Payne, D. T., Ferrarese, I., Lupo, M. G., Shrestha, L. K., Hill, J. P., Ariga, K., Rossi, I., Shrestha, S. S., Panighel, G., Shrestha, R. L. S., Sut, S., Ferri, N., & Dall'Acqua, S. **(2022)**. Evaluation of the effects of natural isoquinoline alkaloids on low density lipoprotein receptor (LDLR) and proprotein convertase subtilisin/kexin type 9 (PCSK9) in hepatocytes, as new potential hypocholesterolemic agents. *Bioorganic Chemistry*, **121**, 105686. https://doi.org/10.1016/j.bioorg.2022.105686

4. **Maharjan, B.**, Shrestha, T., Bharati, S., Dhital, S., Neupane, P., Parajuli, N., Marasini, B. P., Subin, J. A., Shrestha, R. L. S. Molecular Docking and Simulation Studies of the Inhibition of Human Pancreatic α-Amylase from *Corydalis chaerophylla* D.C., Moroccan Journal of Chemistry, Under Review.

OTHER LIST OF PUBLICATIONS

1. Shrestha, R.L.S., Neupane, P., Dhital, S., Parajuli, N., **Maharjan, B.**, Shrestha, T., Bharati, S., Marasini, B. P., Subin, J. A. **(2024)**. Inhibitory Effects of Phytochemicals of Spices on Human Monoamine Oxidase B through Molecular Docking, Molecular Dynamics Simulation, and DFT Study. *Discover Chemistry.*

2. Shrestha, R.L.S., Parajuli, N., Neupane, P., Dhital, S., **Maharjan, B.**, Shrestha, T., Bharati, S., Marasini, B.P., Subin, J. A. **(2024)**. A Computational Approach of Anti-diabetic Potential Evaluation of Flower and Seed of *Nyctanthes arbor tristis* Linn. *Turkish Computational and Theoretical Chemistry*, 9(1), 1-18. https://doi.org/10.33435/tcandtc.1487560.

3. Thanait, P., Dhital, S., Parajuli, N., Poudel, M., Shrestha, T., Bharati, S., **Maharjan, B.**, Marasini, B. P., Subin, J. A., & Shrestha, R.L.S. **(2024)**. α-Glucosidase Inhibitory Activity of Compounds from the Essential Oil of *Leucas lavandulifolia* Sm.: Insights from GC-MS Analysis and Molecular Docking Studies. *Asian Journal of Chemical Sciences*, 14(4), 47-66. https://doi.org/10.9734/ajocs/2024/v14i4317

4. Shrestha, R.L.S., Neupane, P., Dhital, S., Parajuli, N., **Maharjan, B.**, Shrestha, T., Bharati, S., Marasini, B.P., Subin, J. A. **(2024)**. Bioactive Molecules Against Malarial Dihydroorotate Dehydrogenase: An *in silico* Approach, *Moroccan Journal of Chemistry*, 12(4), 1742-1769. https://doi.org/10.48317/IMIST.PRSM/morjchem-v12i4.48008

5. Tamang, A., Parajuli, N., Poudel, M., M.C., S., Shrestha, A., Shrestha, T., Bharati, S., **Maharjan, B.**, Bhattarai, D. P., Marasini, B. P., Subin, J. A., Shrestha, R. L. S. **(2024)**, GC-MS Analysis, Oral Toxicity Evaluation, and Molecular Docking Studies of *Ocimum tenuiflorum* L. Essential Oil: Exploring its Anti-Diabetic Potential through PPARδ Activation, 5 (1): 49-58

6. Dhital, S., Parajuli, N., Poudel, M., Shrestha, T., Bharati, S., **Maharjan, B.**, Marasini, B. P., Subin J. A., & Shrestha, R.L.S. **(2024)**. Spatial and Energetic Stability Assessment of the Adducts of Phytocompounds of *Piper longum* L.

with α-amylase by Computational Approach, *Biointerface Research in Applied Chemistry*.

7. Tamang, A., Bhusal, D., Parajuli, N., Dhital, S., Poudel, M., Shrestha, T., Bharati, S., **Maharjan, B.**, Subin, J. A., Marasini, B. P., & Shrestha, R.L.S. **(2024)**. Chemical Analysis and Biological Studies of Leaf Extracts of Smallanthus sonchifolius (Poepp.) H. Rob. with an *In-silico* Assessment of GC-MS Identified Compounds. *South Asian Research Journal of Natural Products*, 7(3), 279–297. Retrieved from https://journalsarjnp.com/index.php/SARJNP/article/view/161

8. Poudel, M., Parajuli, N., Khanal, S., Gosain, B., Shakhakarmi, K., Bharati, S., **Maharjan, B.**, Shrestha, T., Subin, J. A., Shrestha, R.L.S., & Marasini, B. P. **(2024)**. Exploration of Antioxidant, Antibacterial, and Alpha-glucosidase Inhibition Potential of *Cirsium verutum* (D. Don) Spreng Extracts: *In vitro* and *in silico* Approach. *Asian Journal of Applied Chemistry Research*, 15(4), 55-70.

9. Karki, H., Parajuli, N., Thapa, A., Pokharel, A., Yadav, R. K., Dhital, S., Shrestha, T., Bharati, S., **Maharjan, B.**, Bhattarai, D. P., & Shrestha, R. L. S. **(2024)**. Phytochemical, Antibacterial, Antioxidant, and Toxicity Analysis of Chloroform Extract of *Aegle marmelos* L. Correa Leaf. *South Asian Research Journal of Natural Products*, 7(2), 135-144.

10. Panta, R., Dhital, S., Budha, R., Parajuli, N., Neupane, P., Shrestha, T., Bharati, S., **Maharjan, B.**, Bhattarai, D.P., & Shrestha, R. L. S. **(2024)**. Evaluation of TPC, TFC, and Antioxidant Activity of Extracts of *Piper longum* L. *Asian Journal of Applied Chemistry Research*, 15(2), 17-23.

11. Paudel, N., Rai, M., Adhikari, S., Thapa, A., Bharati, S., **Maharjan, B.**, Shrestha, R. L. S., & Singh, A. V. (**2024**). Green extraction, phytochemical profiling, and biological evaluation of *Dysphania ambrosioides*: an *in silico* and *in vitro* medicinal investigation. *Journal of Herbs, Spices & Medicinal Plants*, 30(2), 97-114.

12. Shrestha, R. L. S., Panta, R., **Maharjan, B.**, Shrestha, T., Bharati, S., Dhital, S., Neupane, P., Parajuli, N., Marasini, B.P. & Subin, J. A. (**2024**). Molecular docking and ADMET prediction of compounds from *Piper longum* L. Detected

by GC-MS analysis in diabetes management. *Moroccan Journal of Chemistry*, 12(2), 776-798.

13. Shrestha, R. L. S., Neupane, P., Dhital, S., Parajuli, N., **Maharjan, B.**, Shrestha, T., Bharati, S., Marasini, B.P. & Adhikari, S. J. **(2024)**. Selected phytochemicals as potent acetylcholinesterase inhibitors: An *in silico* prediction. *Journal of the Serbian Chemical Society*.

14. Shrestha, R. L. S., **Maharjan, B.**, Shrestha, T., Marasini, B. P., & Subin, J. A. (**2024**). Geometrical and thermodynamic stability of govaniadine scaffold adducts with dopamine receptor D1. *Results in Chemistry*, 7, 101363.

15. Thapa, A., **Maharjan, B.**, Bharati, S., Shrestha, T., Homagai, P. L., Bhattarai, D. P., & Shrestha, R. L. S. (**2024**). Chemical Composition, Antibacterial, Antioxidant, and Cytotoxicity Activities of Essential Oil of Leaf of *Ageratina adenophora* (Spreng.) RM King and H. Rob. *Journal of Nepal Chemical Society*, 44(1), 173-182.

16. Neupane, P., Dhital, S., Parajuli, N., Shrestha, T., Bharati, S., **Maharjan, B.**, Adhikari Subin, J. & Shrestha, R. L. S. (**2023**). Exploration of Anti-Diabetic Potential of *Rubus ellipticus* Smith through Molecular Docking, Molecular Dynamics Simulation, and MMPBSA Calculation. *Journal of Nepal Physical Society*, 9(2), 95-105.

17. Budha, R., **Maharjan, B.**, Panta, R., Bharati, S., Shrestha, T., Homagai, P. L., Bhattarai, D.P. & Shrestha, R. L. S. (**2023**). Evaluation of Chemical Constituents and Antioxidant Activity of Extracts of *Nardostachys jatamansi* (D. Don) DC. *Amrit Research Journal*, 4(1), 30-39.

18. Pokharel, A., Thapa, A., Karki, H., Yadav, R. K., Bharati, S., Shrestha, T., Homagai, P. L., **Maharjan, B.**, & Shrestha, R. L. (**2023**). Chemical and biological analysis of extracts of *Acorus calamus* L. *Journal of Nepal Chemical Society*, 43(2), 151–158. https://doi.org/10.3126/jncs.v43i2.53813

19. Thapa, A., Pokharel, A., Karki, H., Yadav, R. K., Paudel, N., Bharati, S., Shrestha, T., **Maharjan, B.**, Karanjit, S., & Shrestha, R. L. (**2022**). Phytochemical Analysis, Cytotoxicity, Antibacterial and Antioxidant Activities

of Extracts of Leaf of *Ageratina adenophora* (Spreng.). *Amrit Research Journal*, 3(01), 84–93. https://doi.org/10.3126/arj.v3i01.50500

20. Chaudhary, R., **Maharjan, B.**, Bharati, S., Shrestha, T., Mishra, P. K., Karanjit, S., Bhattarai, D. P., Homagai, P. L., & Shrestha, R. L. **(2021)**. Phytochemical Screening, GC-MS Analysis and Biological Activities of Extracts of *Artemisia vulgaris* Linn. *Amrit Research Journal*, 2(01), 83–92. https://doi.org/10.3126/arj.v2i01.40743

21. D.C., S., **Maharjan B.**, Shrestha, T., Bharati, S., Gautam, S.D. & Shrestha, R. L. **(2020).** GC-MS analysis, Antibacterial, Brine Shrimp Lethality Analysis and Antioxidant Study of *Trachyspermum ammi* (L.) Sprague. *Amrit Research Journal,* 1(01), 45-50, https://doi.org/10.3126/arj.v1i1.32452

22. Manandhar, S., **Maharjan, B.**, & Shrestha, R. L. **(2019)**. Antioxidant, antibacterial and GC-MS analysis of methanolic extract of *Azadirachta indica* Juss. *The Pharma Innovation Journal*, 8(12), 178-180.

23. Miya, T., **Maharjan, B.**, Shrestha, T., & Shrestha, R. L. **(2019)**. Phytochemical Screening, GC-MS Analysis and Biological Activity Analysis of *Vitex negundo* Linn. *International Journal of Medicine & Biomedical Sciences*, 2, 50-53.

24. Bharati, S., **Maharjan, B.**, Shrestha, T., & Jha, R.N. **(2019)**. GC-MS, FTIR and Biological Activities of Extracts of *Centella asiatica*. *International Journal of Medicine & Biomedical Sciences*, 2, 54-58.

25. Shrestha, R. L., Gautam, S. D., Shrestha, S., & **Maharjan, B. (2018)**. GC-MS analysis and Antibacterial activity of *Nardostachys jatamansi* (D.Don) DC. *International Journal of Pharmaceutical Science and Research.* 3(1), 9-11.

26. Shrestha, R. L., Gautam, S. D., & **Maharjan, B. (2017)**. GC-MS Analysis, and Antioxidant Activity of *Foeniculum vulgare* Mill. *Journal of Nepal Chemical Society*, 37, 6-10.

27. Shrestha, R. L., Gautam, S. D., & **Maharjan, B. (2017)**. GC-MS Analysis, Antibacterial Activity and Brine Shrimp Lethality Analysis of *Anacardium occidentale* Linn. *Journal of Nepal Chemical Society*, 36, 108-113.

ORAL AND POSTER PRESENTATION IN SEMINAR/CONFERENCE AND TRAININGS/WORKSHOPS

1. Poster Presentation in "5th International Conference Kathmandu Symposia on Advanced Materials KaSAM-2024" organized by Nepal Polymer Institute and Far-Western University, IOE, Tribhuvan University held at Park Village Hotel, Budhanilkantha, Kathmandu, Nepal during October 22-24, 2024.

2. Participation and Completion of a 6 days Workshop on "Fusing Ancient Practices with Scientific Drug Design by Computational Approach" organized by Kathmandu Valley School & College at Syuchatar Bridge, Kalanki, Kathmandu during May 23-28, 2024.

3. Participation as Researcher in Scientific Workshop "To Enhance the Academic Quality of Teachr/Faculty" organized by Amrit Campus, Tribhuvan University held at Amrit Campus, Thamel, Kathmandu, Nepal during May 21-23, 2024.

4. Poster Presentation in PhD Festival 2023 organized by Institute of Science and Technology, Tribhuvan University held at Kirtipur, Kathmandu during October 9-10, 2023.

5. Oral Presentation in "International Chemical Congress (ICC-2023)" organized by Nepal Chemical Society in association with Central Department of Chemistry, Tribhuvan University, held at Park Village Hotel, Budhanilkantha, Kathmandu, Nepal during May 25-27, 2023.

6. Oral Presentation in "9th National Conference on Science and Technology" organized by Nepal Academy of Science and Technology (NAST), held at NAST, Khumaltar, Lalitpur, Nepal during June 26-28, 2022.

7. Oral Presentation in "8th Asian Conference on Colloid and Interface Science, ACCIS 2019" organized by Asian Society for Colloid and Surface Science (ASCASS), held at Pulchowk Campus, Institute of Engineering, Tribhuvan University, Lalitpur, Kathmandu, Nepal during September 24-27, 2019.

AWARDS AND FELLOWSHIPS

1. UGC PhD Fellowship and Research Support, Award No. PhD-75/76-S&T-6

2. Internship Award by International Center for Materials Nanoarchitectonics (WPI-MANA), National Institute for Materials Science (NIMS) from January 6 to 28, 2020.

3. Open Access publishing facilitation by Universita degli Studi di Padova, as part of the Wiley-CRUI-CARE agreement.

FIELD AND LABORATORY IMAGES


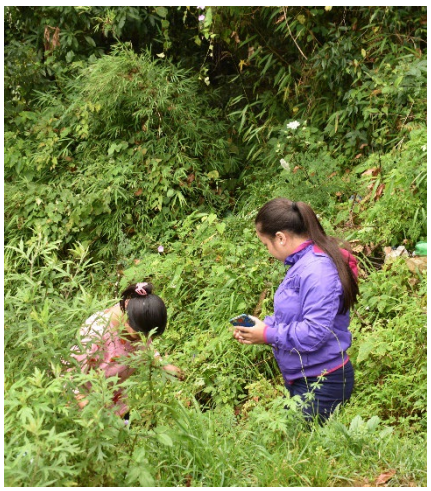




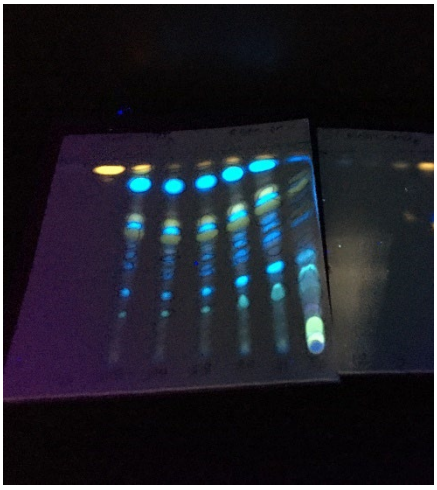

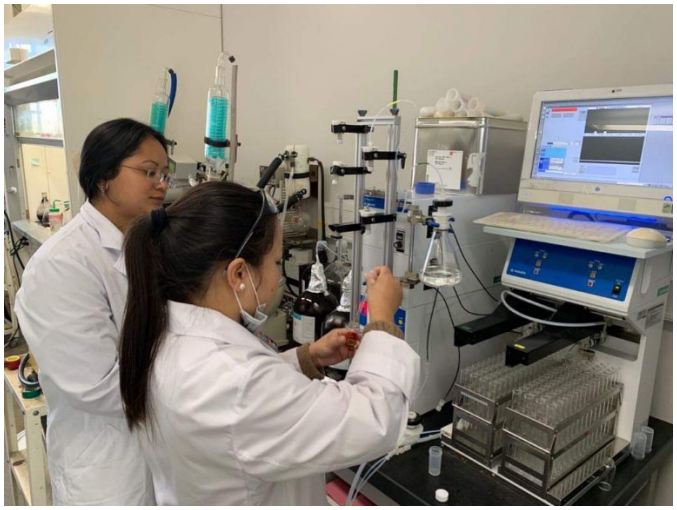

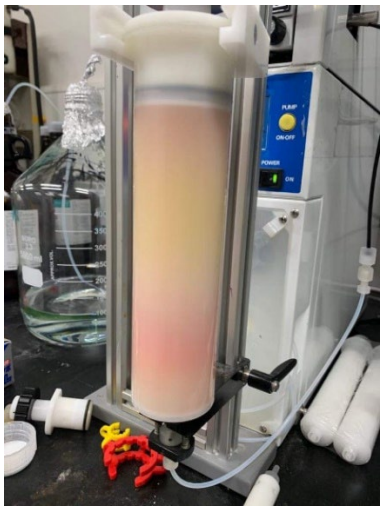

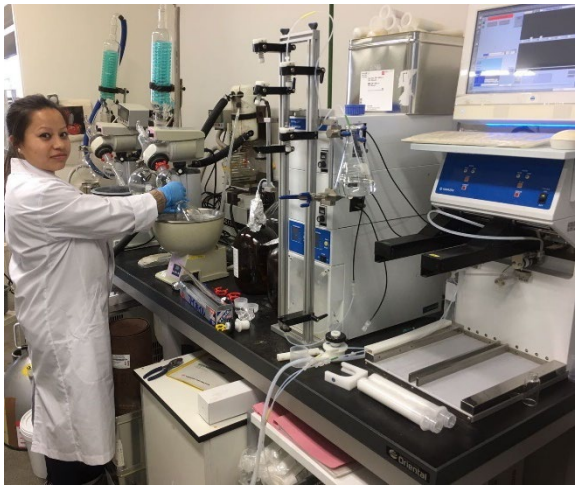

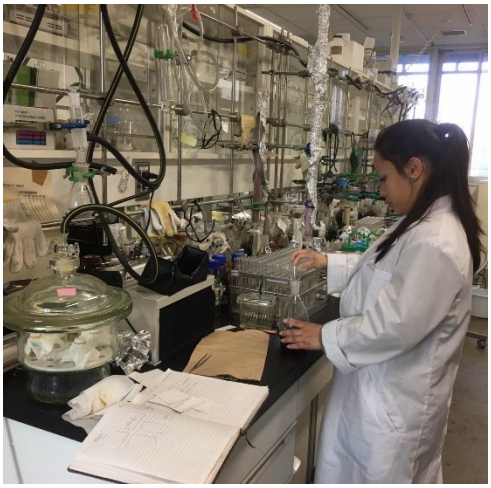

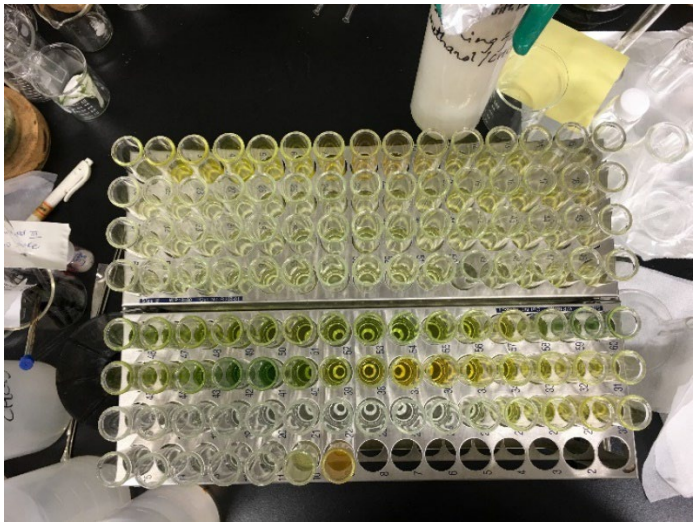

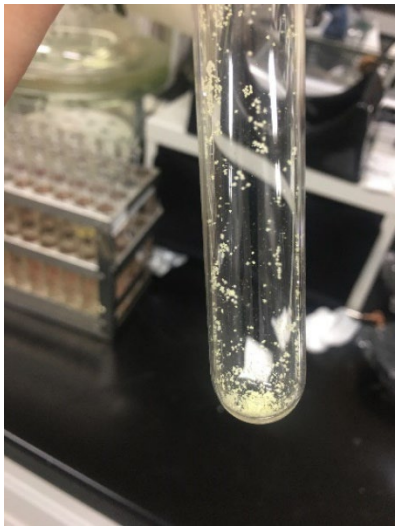

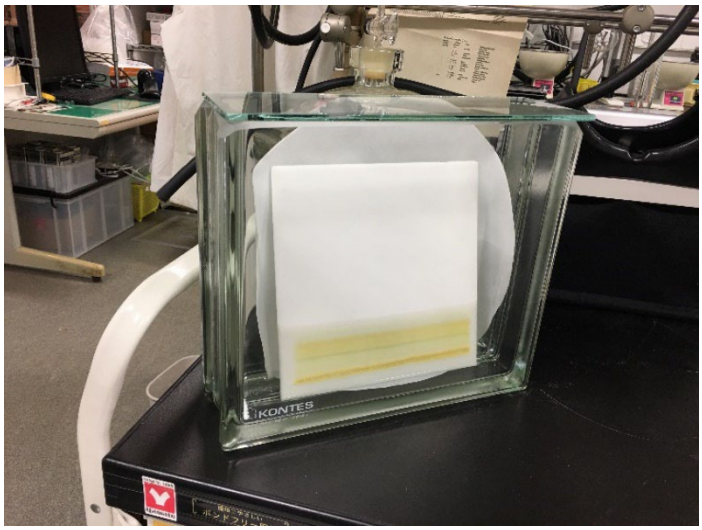
KONTES

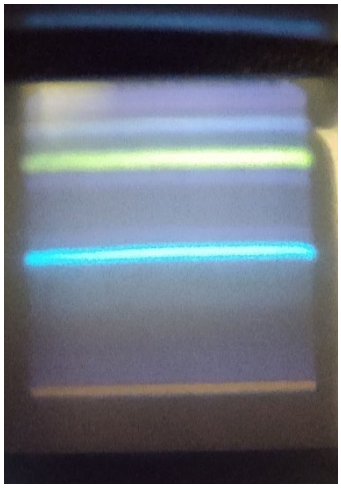

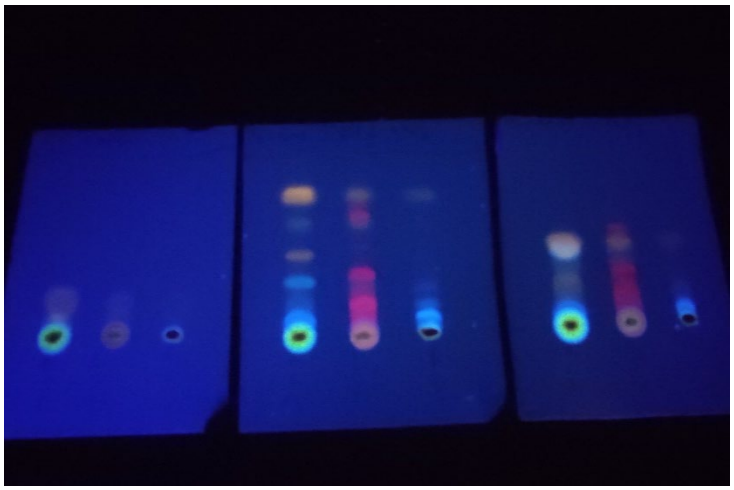

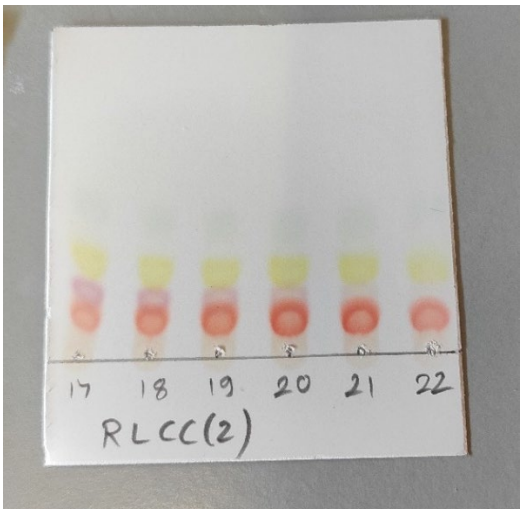
17 18 19 20 21 22
RLCC(2)

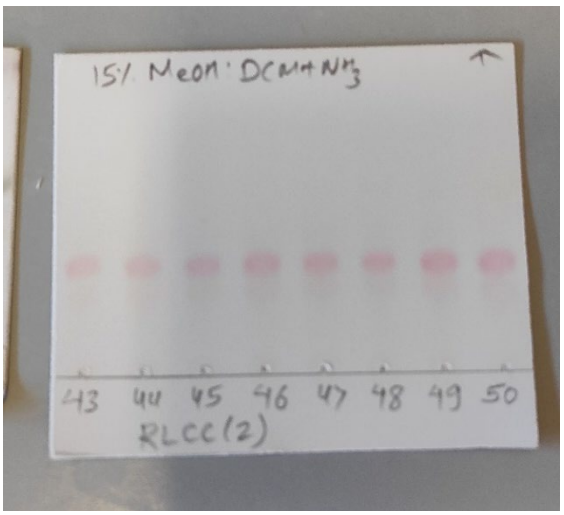
15% MeOH · DCM + NH3
43 44 45 46 47 48 49 50
RLCC(2)

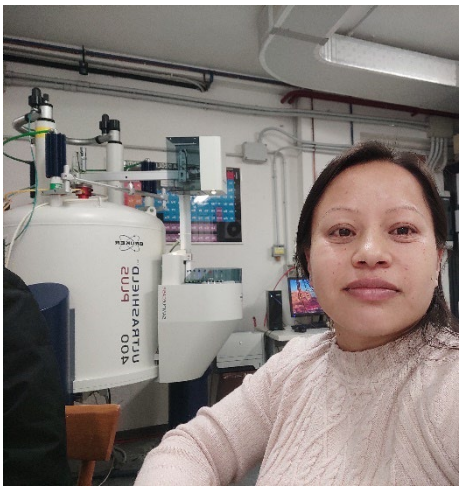


ACCIS 2019
The 8th Asian Conference on Colloid
& Interface Science

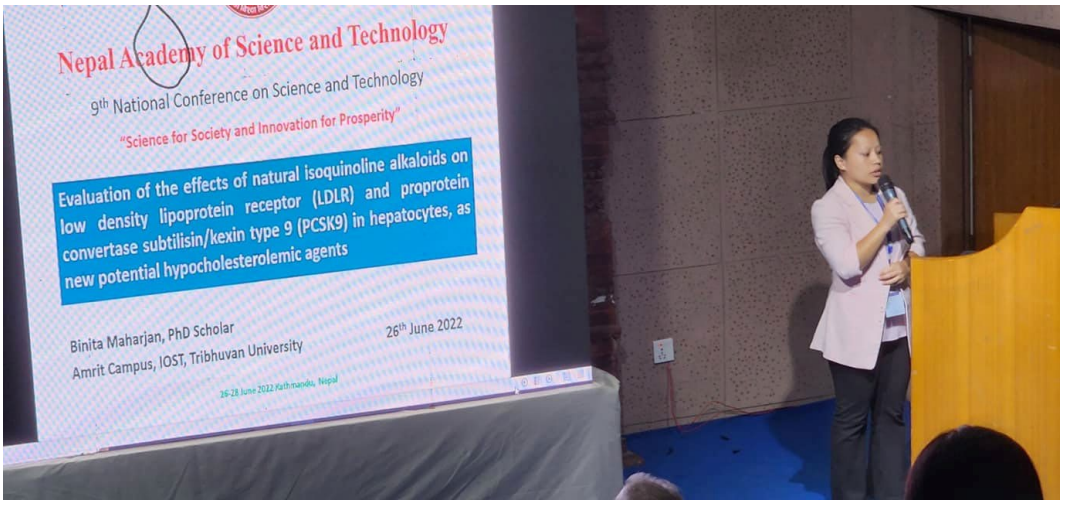
Nepal Academy of Science and Technology
9th National Conference on Science and Technology
"Science for Society and Innovation for Prosperity"
Evaluation of the effects of natural isoquinoline alkaloids on low density lipoprotein receptor (LDLR) and proprotein convertase subtilisin/kexin type 9 (PCSK9) in hepatocytes, as new potential hypocholesterolemic agents
Binita Maharjan, PhD Scholar
Amrit Campus, IOST, Tribhuvan University
26th June 2022


International Chemical Congress (ICC-2023)
Chemistry for Sustainable Development
Park Village Hotel | Kathmandu, Nepal
Nepal Chemical Society
International Chemical Congress (ICC-2023)
USAID

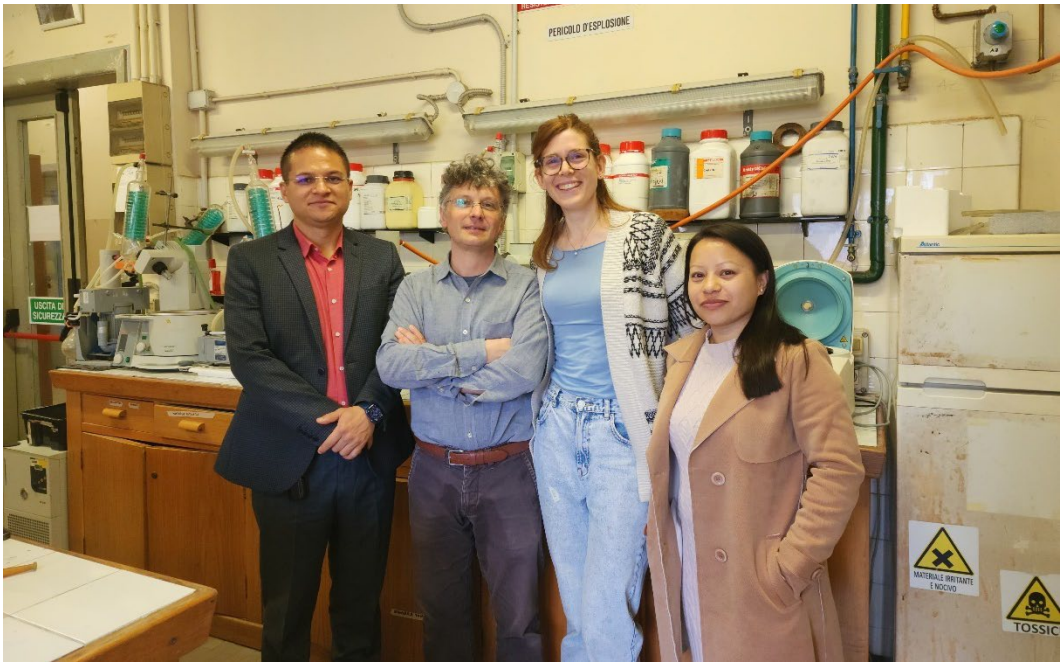
PERICOLO D'ESPLOSIONE
USCITA DI SICUREZZ
MATERIALE IRRITANTE E NOCIVO
TOSSIC

The 8th Asian Conference on Colloid & Interface Science (ACCIS 2019)
Sept. 24-27, Kathmandu, Nepal

ASCASS

CERTIFICATE OF APPRECIATION

This certificate is presented to

Binita Maharjan

(Volunteer)

in recognition of his outstanding contribution to
The 8th Asian Conference on Colloid & Interface Science (ACCIS 2019)
organized by the **Asian Society for Colloid and Surface Science (ASCASS)**
held in Pulchowk Campus, Institute of Engineering, Tribhuvan University, Lalitpur, Kathmandu, Nepal.

Dr. Lok Kumar Shrestha
Chairperson (ACCIS 2019)

September 27, 2019

Prof. Dr. Toyoko Imae
President (ASCASS)

Nepal Academy of Science and Technology (NAST)

CERTIFICATE OF PARTICIPATION

Awarded to

BINITA MAHARJAN

for Presentation in Oral / Poster / Participation in the
9th National Conference on Science and Technology
June 26-28,2022 (Asar 12-14, 2079)
Khumaltar, Lalitpur, Nepal

Ms. Luna Vajra
Chief, Promotion Division

Prof. Dr. Mahesh K. Adhikari
Secretary

Dr. Sunil Babu Shrestha
Vice Chancellor

International Chemical Congress (ICC-2023)

Chemistry for Sustainable Development

May 25-27, 2023 | Kathmandu, Nepal

Organized by

Nepal Chemical Society

in association with

Central Department of Chemistry

Tribhuvan University

Certificate of Participation

This is to certified that

Prof./Dr./Mr./Ms. .....Binita Maharjan.....

.....

has participated and delivered oral lecture in International Chemical Congress (ICC-2023) held in Park Village Hotel, Kathmandu, Nepal during May 25-27, 2023.

Dr. Surendra K. Gautam	**Dr. Mahesh K. Joshi**	**Prof. Dr. Jagadeesh Bhattrai**
Conference Convener	Conference Secretary	Conference Co-convener
(President NCS)	(General Secretary NCS)	(HoD, CDC, TU)

Date: May 27, 2023

Scientific Workshop
Ascol

CERTIFICATE

This certificate is presented to

. . . BINITA . MAHARJAN . . . . . .

for prarticipant as External-Internal Expert, PhD- Mphil Researcher, Volunter, Participant in **Scientific Workshop** "**To Enhance the Academic Quality of Teacher/Faculty** organized by Amrit Campus, Thamel, Kathmandu ,Nepal, **Conducted during May 21-23, 2024.**

Asst. Prof. Chandradip Kumar Yadav	Prof. Dr. Jagadeesh Bhattarai	Asso. Prof. Dr. Lok Bahadur Baral
Program Co-ordinator	President, Nepal Chemical Society	Campus Chief

CERTIFICATE OF PARTICIPATION AND COMPLETION

Presented to
BINITA MAHARJAN

from
Department of Chemistry, Amrit Campus, TU

on
May 28, 2024

For a 6 days workshop on
Fusing Ancient Practices with Scientific Drug Design by Computational Approach

May 23-28, 2024 (Jestha 10 - 15, 2081)

Kathmandu Valley School & College
Syuchatar Bridge, Kalanki, Kathmandu

JUBILANT COLLEGE

Dr. Subin Adhikari	Dr. Bishnu Prasad Marasini	Assoc. Prof. Dr. Surendra Kumar Gautam	Dr. Swagat Shrestha
Senior Scientist, SRTN	Senior Scientist	Asst. Dean, IOST, TU	Assoc. Prof. of Amrit Campus, TU
Workshop Expert	NHRC	Chief Guest	Program Chairperson